NOTE TO USERS

This reproduction is the best copy available.

UMI®

Design of Functionalized Cyclic Aryl Ethers and Alkenes and their Subsequent Ring-opening Polymerization

by

Leslie J. May

A Thesis

Submitted to the Faculty of Graduate Studies

in Partial Fulfillment of the Requirements

for the Degree of

Master's of Science

In Chemistry

Department of Chemistry

The University of Manitoba

Winnipeg, Manitoba

© June 2001

National Library of Canada
Acquisitions and Bibliographic Services
395 Wellington Street
Ottawa ON K1A 0N4
Canada

Bibliothèque nationale du Canada
Acquisitions et services bibliographiques
395, rue Wellington
Ottawa ON K1A 0N4
Canada

Your file Votre référence

Our file Notre référence

The author has granted a non-exclusive licence allowing the National Library of Canada to reproduce, loan, distribute or sell copies of this thesis in microform, paper or electronic formats.

The author retains ownership of the copyright in this thesis. Neither the thesis nor substantial extracts from it may be printed or otherwise reproduced without the author's permission.

L'auteur a accordé une licence non exclusive permettant à la Bibliothèque nationale du Canada de reproduire, prêter, distribuer ou vendre des copies de cette thèse sous la forme de microfiche/film, de reproduction sur papier ou sur format électronique.

L'auteur conserve la propriété du droit d'auteur qui protège cette thèse. Ni la thèse ni des extraits substantiels de celle-ci ne doivent être imprimés ou autrement reproduits sans son autorisation.

0-612-62792-6

Canada

THE UNIVERSITY OF MANITOBA

FACULTY OF GRADUATE STUDIES

*****

COPYRIGHT PERMISSION PAGE

Design of Functionalized Cyclic Aryl Ethers and Alkenes and their Subsequent Ring-opening Polymerization

BY

Leslie J. May

A Thesis/Practicum submitted to the Faculty of Graduate Studies of The University of Manitoba in partial fulfillment of the requirements of the degree of

Master of Science

LESLIE J. MAY ©2001

Permission has been granted to the Library of The University of Manitoba to lend or sell copies of this thesis/practicum, to the National Library of Canada to microfilm this thesis and to lend or sell copies of the film, and to Dissertations Abstracts International to publish an abstract of this thesis/practicum.

The author reserves other publication rights, and neither this thesis/practicum nor extensive extracts from it may be printed or otherwise reproduced without the author's written permission.

Abstract

The ring-opening polymerization of a variety of cyclic and bicyclic monomers that were prepared via nucleophilic aromatic substitution reactions mediated by the cyclopentadienyliron moiety was explored. The ability to design structurally different monomers using this approach, allowed for the isolation of polymeric materials with different chemical and physical properties. It has been well established that organoiron complexes containing an assortment of functionalities can be prepared using this methodology. A variety of asymmetric cyclic aryl ethers were prepared following reaction of diiron complexes with a dinucleophile. Following cleavage of the metal moieties, the aromatic macrocycles were converted to the corresponding insoluble polyaromatic ethers via ring-opening polymerization in the presence of an anionic initiator. The ring-opening metathesis polymerization of a series of bicyclo[2.2.1]heptenes was also investigated. Two classes of polynorbornenes containing cationic iron moieties within their side chains were synthesized using organoiron chemistry, and subsequently polymerized in the presence of ruthenium-based catalyst. The resulting organometallic polynorbornenes, with terminal or lateral side chains displayed excellent solubility and thermal stability.

Acknowledgments

Numerous people have contributed support, advice and help throughout the duration of my M. Sc. program, and I would like to take this opportunity to thank a special group of them. To attempt to appropriately thank my supervisor, Dr. Alaa S. Abd-El-Aziz for all of his efforts throughout the duration of my M. Sc. program is impossible. He has provided me with the opportunity to advance my skills as a researcher, teacher and group member. Each of these factors, as well as his continued support and guidance have allowed me to develop a sense of confidence in myself that will help me in my future endeavors, and for this I am truly grateful.

Each member of the Abd-El-Aziz research group, either past or present have assisted my studies and research in some manner. I would like to extend special thanks to Andrea Edel and Shelly Buhay for their insightful leadership on various research projects. Erin Todd, Jeff Hurd and Wes Budakowski are also acknowledged for all of the countless hours of hard work towards the success of this project and this manuscript they have contributed. All of your support and help over the last few years has meant a great deal to me. I would also like to thank Basil Elmayergi for his assistance with some of the work.

To my family and friends who have supported and advised me throughout my entire academic career, I appreciate it more than you will ever know. I know I could not have accomplished all I have without the support of The Girls, my mom and sister, all of them have stuck by me through the last few years, and I love them for that!

Contents

Abstract i

Acknowledgements ii

List of Figures v

List of Tables vii

List of Equations ix

Abbreviations x

1.0 Ring-opening Polymerization of Cyclic Monomers

1.1 Introduction 1
1.2 The Use of Organoiron Complexes in Monomer and Polymer Synthesis 12
1.3 Monomer and Polymer Characterization Techniques 19
1.3.1 Spectroscopic Analysis 21
1.3.2 Molecular Weight Determination 28
1.3.3 Thermal Analysis 31

2.0 Aromatic Macrocycle Syntheses and Polymerization

2.1 Introduction 34

2.2 Established Synthetic Routes to Aromatic Macrocycles 38
2.2.1 Nucleophilic Aromatic Substitution Reactions 40
2.2.2 Catalyzed Macrocyclization Reactions 49
2.2.3 Metal-mediated Nucleophilic Substitution Reactions 53

2.3 Ring-opening Polymerizations 57

2.4 Results and Discussion 61
2.4.1 Ring Closure Reactions 61
2.4.2 Isolation of Cyclic Aryl Ethers 65
2.4.3 Ring-opening Polymerization of Cyclic Aryl Ethers 78

2.5 Summary 79

2.6 Experimental
2.6.1 General Methods 81
2.6.2 Starting Materials 81
2.6.3 Ring Closure Reactions 81

2.6.4 Isolation of Organic Cyclic Monomers 82
2.6.5 Ring-opening Polymerizations of Aromatic Macrocycles 82

3.0 Preparation of Polynorbornenes Containing Cationic Iron Moieties

3.1 Preparation of Polynorbornenes with Modified Side Chains 83

3.2 Results and Discussion 94
3.2.1 Synthesis of Norbornenes Containing One $CpFe^+$ Moiety
3.2.1.1 Preparation of Monometallic Starting Complexes 95
3.2.1.2 Preparation of Norbornenes Containing One $CpFe^+$ moiety 102
3.2.2 Synthesis of Norbornenes Containing Two $CpFe^+$ moieties
3.2.2.1 Synthesis of Bimetallic Starting Materials 123
3.2.2.2 Preparation of Norbornenes Containing Two $CpFe^+$ moieties 131
3.2.3 Synthesis of Polynorbornenes with Organoiron Side Chains 146

3.3 Summary 161

3.4 Experimental
3.4.1 General Methods 171
3.4.2 Starting Materials 171
3.4.3 Synthesis of Monometallic and Bimetallic Starting Materials 172
3.4.4 Isolation of Organoiron Monomers 173
3.4.5 Preparation of Substituted Polynorbornenes 174

4.0 References 176

Appendices A and B 186

List of Figures

1.1	Examples of ROMP and olefin disproportion	9
1.2	Different tacticities observed in polymers	20
1.3	Energy levels for a nucleus with $I = \pm ½$	22
1.4	(I) FID signal of t_1; (II) 2-D FT; (III) Contours on the diagonal of a 2-D plot	26
1.5	Analysis of the HH COSY NMR of geraniol	27
1.6	Analysis of the CH COSY NMR of geraniol	27
1.7	GPC instrumentation	28
1.8	Separation of large and small polymer chains using GPC	29
1.9	A representative example of a DSC thermogram	32
1.10	A representative example of a TGA thermogram	33
2.1	Mixture of products obtained from macrocyclization reactions	40
2.2	Mechanism for amine-catalyzed hydrolysis-condensation reaction	52
2.3	Examples of ring-opening polymerizations of aromatic macrocycles	59
2.4	Thermograms showing conversion of cyclic monomer to linear polymer	60
2.5	^{1}H NMR spectrum of macrocycle **5a** and corresponding linear oligomers	64
2.6	Isolated cyclic aryl ethers (**6a-d**)	65
2.7	^{1}H NMR spectrum of macrocycle **6a**	69
2.8	^{13}C NMR spectrum of macrocycle **6a**	70
2.9	Molecular structure of macrocycle **6a**	71
2.10	Molecular structure of macrocycle **6b**	72
2.11	ROP of macrocycle **6b**	79
2.12	DSC thermogram of macrocycle **6b** and its corresponding linear polymer	80

3.1	Some norbornene monomers polymerized using Schrock's catalyst	85
3.2	Polynorbornenes substituted with terminal or lateral side chains	91
3.3	^{1}H NMR spectrum of complex **3e**	98
3.4	^{13}C NMR spectrum of complex **3e**	99
3.5	^{13}C NMR spectra for complex **3a** and monomer **5a**	107
3.6	HH COSY NMR spectrum for monomer **5a**	108
3.7	Proton assignments for the *endo* isomer of monomer **5a**	109
3.8	Proton assignments for the *endo* isomer of monomer **5a**	110
3.9	Proton assignments for the *exo* isomer of monomer **5a**	111
3.10	Proton assignments for the *exo* isomer of monomer **5a**	112
3.11	CH COSY NMR spectrum for monomer **5a**	114
3.12	Identification of the olefinic carbons and hydrogens of monomer **5a**	115
3.13	Identification of H_{7s}, H_{7a} and C_7 of monomer **5a**	116
3.14	^{1}H NMR spectrum of complex **7**	126
3.15	^{13}C NMR spectrum of complex **7**	128
3.16	HH COSY NMR spectrum for monomer **13a**	135
3.17	Proton assignments for the *endo* isomer of monomer **13a**	136
3.18	Proton assignments for the *exo* isomer of monomer **13a**	139
3.19	^{1}H NMR spectra for monomer **5a** and polymer **14a**	149
3.20	^{1}H NMR spectra for polymers **15a** and **17a**	156
3.21	TGA thermogram of polymers **14a** and **16a**	162
3.22	TGA thermogram of polymers **14a** and **15d**	163
3.23	DSC thermogram of polymers **17a**, **17b** and **17d**	164

List of Tables

2.1	^{1}H NMR, Yield, IR and MS data for macrocycles **6a-d**	73
2.2	^{13}C NMR data for cyclic aryl ethers **6a-d**	75
2.3	Selected torsion angles (Deg) for macrocycle **6a**	77
3.1	Yield, IR and elemental analysis data for monometallic complexes **3c-e**	100
3.2	^{1}H NMR data for monometallic complexes **3c-e**	100
3.3	^{13}C NMR data for monometallic complexes **3c-e**	101
3.4	Yield, IR and elemental analysis data for monomers **5a-e**	117
3.5	^{1}H NMR data for monomers **5a-e**	118
3.6	^{1}H NMR data for monomers **5a-e**	120
3.7	^{13}C NMR data for monomers **5a-e**	121
3.8	Yield, IR and elemental analysis data for complexes **7** and **8**	129
3.9	^{1}H NMR data for complexes **7** and **8**	129
3.10	^{13}C NMR data for complexes **7** and **8**	130
3.11	Yield, IR and elemental analysis data for bimetallic monomers **10**, **11** and **13a-c**	140
3.12	^{1}H NMR data for bimetallic monomers **10**, **11** and **13a-c**	141
3.13	^{1}H NMR data for bimetallic monomers **10**, **11** and **13a-c**	143
3.14	^{13}C NMR data for bimetallic monomers **10**, **11** and **13a-c**	144
3.15	Yield and IR data for organoiron polymers **14a-e**	150
3.16	^{1}H NMR data for monometallic polymers **14a-e**	151
3.17	Yield and IR data for bimetallic polymers **15a-e**	152
3.18	^{1}H NMR data for bimetallic polymers **15a-e**	153
3.19	IR and ^{1}H NMR data for polynorbornenes **16a-e**	157

3.20 IR and ^{1}H NMR data for polynorbornenes **17a-e** 158

3.21 GPC data for polynorbornenes **14a-e** and **16a-e** 165

3.22 GPC data for polynorbornenes **15a-e** and **17a-e** 166

3.23 TGA data for monometallic polymers **14a-e** 167

3.24 TGA data for bimetallic polymers **15a-e** 168

3.25 TGA and DSC data for polynorbornenes **16a-e** 169

3.26 TGA and DSC data for polynorbornenes **17a-e** 170

List of Equations

1.1	Condensation polymerization	2
1.2	Addition polymerization	2
1.3	ROP of cyclic phosphazene	3
1.4	ROP of cyclic aryl ether ketone	7
1.5	ROMP of cyclic alkene	7
1.6	Deuterium experiment used to prove metathesis of double bonds	10
1.7	Number-average molecular weight (Mn)	30
1.8	Weight-average molecular weight (Mw)	30
2.1	Intramolecular versus intermolecular reactions	38

Abbreviations

APT	Attached proton test
AROP	Anionic ring-opening polymerization
ArC	Quaternary aromatic carbon
ArCH	Aromatic carbon
ArH	Aromatic hydrogen
BF_4	Tetrafluoroborate
BPh_4	Tetraphenylborate
CH COSY	Heteronuclear correlation spectroscopy
$Cr(CO)_3$	Chromium tricarbonyl
Cp	Cyclopentadienyl ring
$CpFe^+$	Cyclopentadienyliron
$CpFe^+ArC$	Quaternary aromatic carbon of a cyclopentadienyliron-complexed ring
$CpFe^+ArCH$	Aromatic carbon of a cyclopentadienyliron-complexed ring
$CpFe^+ArH$	Aromatic hydrogen of a cyclopentadienyliron-complexed ring
$CpRu^+$	Cyclopentadienylruthenium
CROP	Cationic ring-opening polymerization
CsF	Cesium fluoride
Cy	Cyclohexane
DCC	Dicyclohexylcarbodiimide
DMAc	Dimethylacetamide
DMF	Dimethylformamide
DMAP	4-(Dimethylamino)pyridine
DME	1,2-Dimethoxyethane
DP	Degree of polymerization
DSC	Differential scanning calorimetry
DMSO	Dimethyl sulfoxide
emr	Electromagnetic radiation
FID	Free induction decay
FT	Fourier transformation
FT-IR	Fourier transformation-infrared spectroscopy
GPC	Gel permeation chromatography
hν	Photolysis
HH COSY	Homonuclear correlation spectroscopy
IR	Infrared
J	Coupling constant

K_2CO_3	Potassium carbonate
$Mn^+(CO)_3$	Manganese tricarbonyl
Mn	Number-average molecular weight
Mw	Weight-average molecular weight
n	*Endo* isomer
NH_4PF_6	Ammonium hexafluorophosphate
NMR	Nuclear Magnetic Resonance
PF_6^-	Hexafluorophosphate anion
p-HD	Pseudo-high dilution
ppm	Parts per million
rf	Radio frequency
R.T.	Room temperature
ROMP	Ring-opening metathesis polymerization
ROP	Ring-opening polymerization
S_NAr	Nucleophilic aromatic substitution
T_c	Crystallization temperature
T_g	Glass transition temperature
T_m	Melt temperature
TBAB	Tetrabutylammonium bromide
TGA	Thermogravimetric analysis
THF	Tetrahydrofuran
x	*Exo* isomer

1.0 Ring-opening Polymerization of Cyclic Monomers

1.1 Introduction

Natural and synthetic polymers have been used in everyday applications for hundreds of years. Naturally occurring materials, such as starch, cotton and proteins were some of the first known polymeric materials.[1-3] Although synthetic polymers were first synthesized in the late 1800's, they were not correctly identified until the mid 1950's.[1-3] In the nineteenth century, organic chemists began to find residual organic materials at the bottom of their reaction flasks, which could not be characterized due to their insolubility. Unfortunately, this "sticky gunk" was classified as unwanted side products, and was usually discarded. During the late nineteenth and early twentieth century, Ostwald discovered that these products were important materials that displayed properties similar to inorganic colloids, such as soap micelles.[2] Thus, he classified these materials as organic colloids, although they were in fact polymers. These synthetic materials were not correctly classified until the 1920's, when Staudinger introduced his *Macromolecular Hypothesis*, which stated that certain types of organic colloids were actually composed of long-chain molecules that consisted of repeating units.[2] Staudinger continued to work in the area of synthetic polymers, and was awarded the Nobel Prize in chemistry in 1953 for his hypothesis, which is the basis for polymer science.

Shortly after Staudinger's hypothesis, another polymer chemist, Carothers, stated that polymeric materials could be divided into two classes based on the compositional differences between the polymeric species and its corresponding monomer.[1] The first class is condensation polymers, which are formed via the reaction of polyfunctional monomers with the elimination of a small molecule such as water or hydrochloric acid

(Equation 1.1). Some of the functional groups that result from this type of reaction are amides, esters and siloxanes. Addition polymers are the second class of materials, which are generally formed via conversion of a carbon-carbon double bond to a single bond within the structure of the monomer (Equation 1.2). In contrast to condensation polymers, addition polymers are prepared without the loss of a small molecule and the chemical structure of the resulting polymers and their corresponding monomers are very similar.

Condensation Polymerization

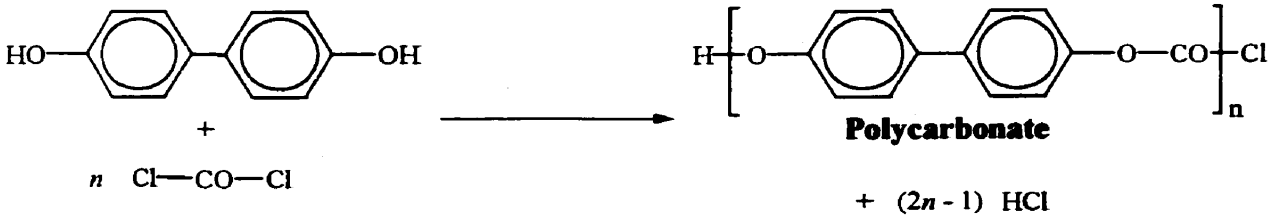

Equation 1.1: Condensation polymerization.

Addition Polymerization



Equation 1.2: Addition polymerization.

Another type of reaction that plays an important role in the production of polymeric materials is ring opening polymerization (ROP).[1,4] The first example of this type of polymerization was the ring opening of cyclic phosphazene monomers to give the

corresponding linear inorganic polymers (Equation 1.3).[4] Unlike addition polymerization, ROP is a thermodynamically driven process involving the reshuffling of bonds, which does not require an exothermic driving force such as the conversion of multiple bonds to single bonds to proceed. However, the two processes are similar in that no small molecules are formed during the polymerizations, as is observed in the formation of condensation polymers. The three polymerization process are alike as each method can be a "living" process.[4,5] In a "living" system, the initiation step of the polymerization is much faster than the propagation steps, such that each molecule of the initiator becomes associated with a growing polymer chain. As well, the propagation steps must occur at faster rates than the termination of the polymerization so that all monomer molecules are consumed by growing polymer chains. The ability to create a "living" polymerization system is important because it allows for control of the microstructure and molecular weight of the resulting polymeric materials.[1-5]

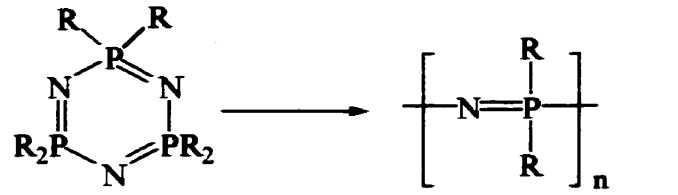

Poly(organophosphazene)

Equation 1.3: ROP of cyclic phosphazene.

The thermodynamic factors (ΔH, ΔS, ΔG) that determine if the ring opening of a cyclic monomer will occur depend on the relative stability of the linear polymer in comparison to its corresponding monomer.[1,3] ROP of all organic macrocycles except 6-

membered rings are thermodynamically favored, with the likelihood of polymerization occurring in the following order; 3,4 > 8 > 5,7 >> 6. The possibility of ring opening the cyclic molecules is a direct result of the ring strains associated with the compounds. The ROP of 6-membered organic rings is not usually observed, as there is little to no ring strain associated with the monomers, thus, there is no driving force for the polymerization.[1] Smaller ring sizes primarily exhibit angle ring strain, which results from the distortion of the ring atoms' bond angles from their normal geometries. Conformational ring strain is found in larger ring molecules. Monomers with 5- or 7-members suffer from torsional strain due to the eclipsed conformations of adjacent ring atoms, whereas, rings with 8- or more members have transannular strain because of repulsive interactions between the hydrogens or substituents attached to ring atoms.[1]

There are numerous pathways available for ring-opening polymerization, three of the most common being cationic, anionic and metathesis. The initiation and propagation processes in cationic ring-opening polymerization (CROP) can proceed via one of three routes.[1,4] In the first, an electrophilic initiator opens a cyclic monomer to produce a linear chain that contains an electrophilic end group. Propagation of the system proceeds via the ring opening of another cyclic monomer using this newly formed electrophilic species and continues until termination of the polymerization process occurs (**I** in Scheme 1.1). In the second type of CROP, initiation of the system occurs prior to the opening of the monomeric ring. As illustrated in **II** of Scheme 1.1, coordination of the electrophilic catalyst to a nucleophilic atom within the cyclic monomer produces a positively charged cyclic species. This cationic ring is then opened via reaction with another equivalent of monomer to give a new initiating species. Propagation of the system involves the

subsequent addition of new monomers to the growing chain via the methodology described above. In the third type of CROP, initiation of a cyclic monomer occurs via the protonation of a nucleophilic ring atom in the presence of a cationic species. The activated monomer then reacts with a neutral species to produce a growing polymer chain and the original positive species. The positively charged species then reacts with another equivalent of monomer, forming a cationic macrocycle that can undergo subsequent reaction with the growing end of the polymeric chain until the polymerization reaction is terminated (**III** in Scheme 1.1).

I

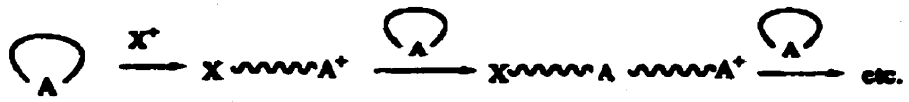

II

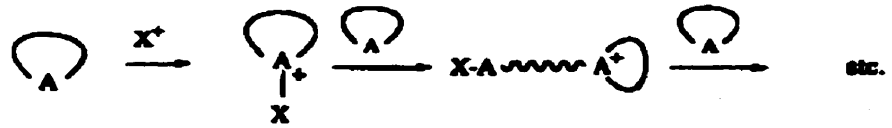

III

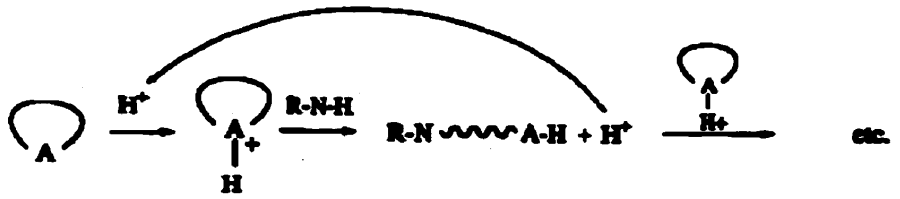

Scheme 1.1: Cationic ring-opening polymerization mechanisms.

The principles of anionic ring-opening polymerization (AROP) are very similar to those of cationic ring-opening.[4] That is, the formation of an activated species can occur prior to or following the ring opening of a cyclic monomer (Scheme 1.2). The major difference in the two ROP mechanisms is that a nucleophilic, not an electrophilic initiator is employed in the anionic polymerizations.[4]

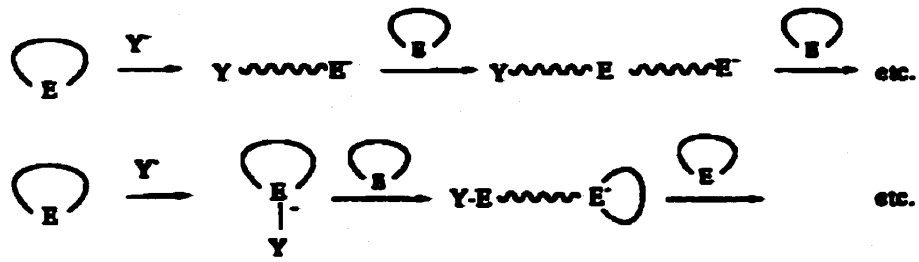

Scheme 1.2: Anionic ring-opening polymerization mechanisms.

Cationic and anionic ROP of various cyclic monomers have found wide applications in the industrial preparation of polymeric materials. For example, poly(ethylene oxide) and polycaprolactam are two materials that are industrially prepared using ROP.[1,4] In the last decade, the anionic ROP of aromatic macrocycles has been investigated as a route for the preparation of engineering thermoplastics on an industrial scale (Equation 1.4). The processability of these materials using traditional methodologies suffers from the low solubility and high melt viscosities of the resulting polymers, which can make the production of high molecular weight materials difficult.[6] The use of cyclic monomers is advantageous because the cycles exhibit low melt viscosities, which facilitates their processing. Furthermore, the polymerizations do not require solvents to proceed and do not yield volatile byproducts.[7]

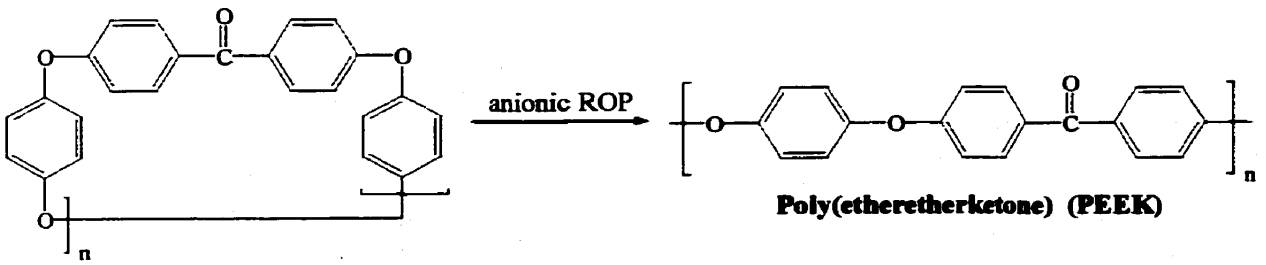

Equation 1.4: ROP of cyclic aryl ether ketone.

One of the most well-known classes of ring-opening polymerization is ring-opening metathesis polymerization (ROMP). The word "metathesis" refers to the interchanging of carbon atoms between a pair of double bonds.[8] ROMP involves the opening of a carbon-carbon double bond in a strained cyclic olefin in the presence of a metathesis catalyst, which leads to the formation of an unsaturated polymer (Equation 1.5).[8,9]

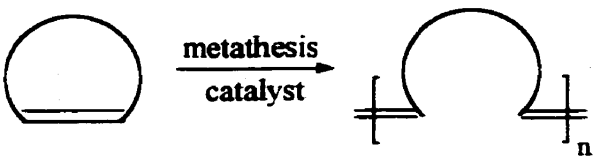

Equation 1.5: ROMP of cyclic alkene.

Of the three ROP examples presented, metathesis polymerization is the newest route, having only been discovered in the late 1950's. Eleuterio was the first to report the ring-opening polymerization of a series of cyclic olefins in the presence of a heterogeneous catalyst system in 1957.[8-11] He reported the polymerization of bicyclo[2.2.1]hept-2-ene (norbornene) using a catalyst containing 7.5% molybdenum oxide (MoO_3) deposited on γ-alumina (γ-Al_2O_3), which had been reduced with hydrogen, and activated in the

presence of lithium aluminum hydride. Three years later, Truett and coworkers conducted further studies on the polymerization of norbornene, and found that in the presence of a $(C_7H_{15})_4AlLi/TiCl_4$ catalytic system, polymeric materials could be obtained via metathesis or vinyl polymerization (Scheme 1.3).[9,12] In cases where metathesis conditions were employed, polynorbornene was isolated, whereas, if conditions for vinyl polymerizations were applied, a saturated polymer was obtained as a result of the addition of double bonds within the monomer species.

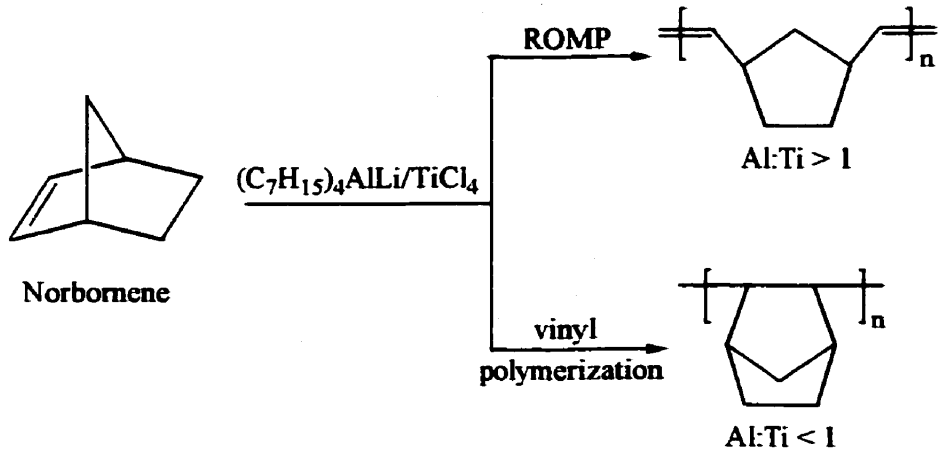

Scheme 1.3: Comparison of metathesis and vinyl polymerization of norbornene.

In the 1960's, the idea of breaking a double bond during a polymerization reaction was not widely accepted, as all other polymerization processes involved cleavage of single bonds or the opening of the π-component of a double bond.[11,13] Thus, it was proposed that the polymerization of a cyclic olefin occurred via cleavage of the σ-bond adjacent to the double bond in the monomer. This theory was generally accepted until

1967, when Calderon illustrated that the polymerization of olefins and olefin "disproportion" reactions were two aspects of the same process, namely olefin metathesis, and that they could be performed using the same catalytic system (Figure 1.1).[8,13] He showed that $WCl_6/EtAlCl_2/EtOH$ (1/4/1) could not only polymerize cyclooctene but also disproportionate pent-2-ene. As well, he demonstrated that the reaction of but-2-ene and but-2-ene-d_8 lead to the formation of a single alkene product, but-2-ene-d_4 (Equation 1.6). This provided indisputable proof that olefin metathesis occurred via cleavage of the double bond within the olefin, and not through σ-bond cleavage as was previously believed.[8]

Olefin Disproportion

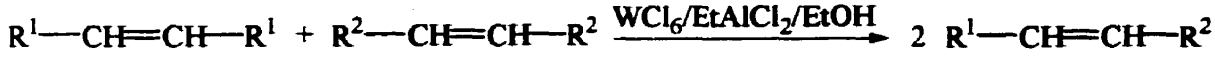

ROMP

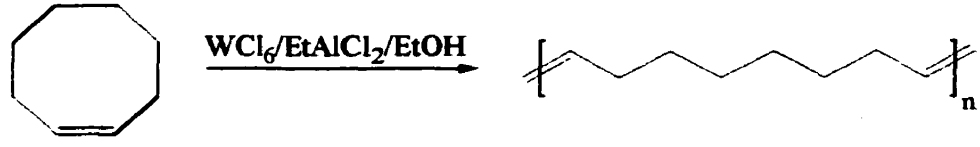

Figure 1.1: Examples of ROMP and olefin disproportion.

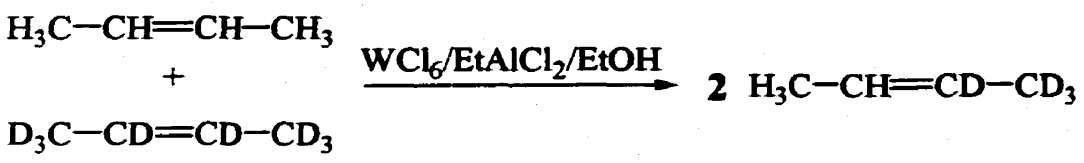

Equation 1.6: Deuterium experiment used to prove metathesis of double bonds.

The role of the metathesis catalysts in the ROMP of cyclic olefins has been investigated extensively. The reactivity and use of numerous heterogeneous and homogeneous transition metal-based catalysts have been studied. Carbene-metal catalysts based on molybdenum, tungsten, rhenium and ruthenium have been shown to be the most effective.[8,9] In 1970, a metal-carbene/metallacyclobutane mechanism was first proposed, in which a reaction between a metal-carbon double bond and an olefin resulted in the formation of a metallacyclobutane.[4] As an example, the ROMP mechanism of norbornene is shown in Scheme 1.4. The initial step involves the electrophilic attack of the metal center on the olefin, resulting in the reversible formation of a weak adduct (I), which is subsequently converted to a metallacyclobutane ring (II). The metallacyclobutane ring then cleaves leading to the formation of a cyclopentane ring that contains an olefin at one end and a reactive metal-carbene species at the other (III). Propagation occurs when a second monomer reacts with the active metal-carbene center, again forming a metallacyclobutane species that opens via the same methodology, to give a dimer functionalized with a metal-carbene end group (IV). This propagation step continues until all monomer has been consumed or a termination step is employed.[8]

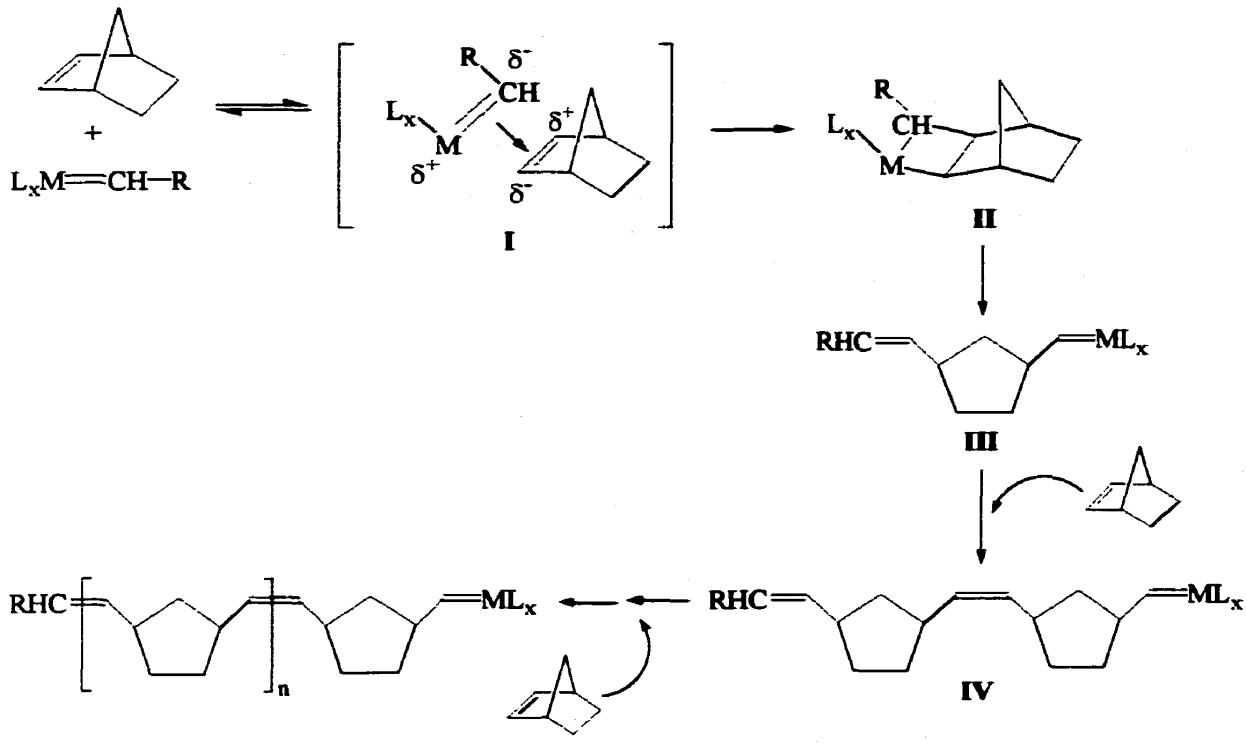

Scheme 1.4: Mechanism for the ROMP of norbornene.

Carbene-type catalysts are useful for the polymerization of olefins because unlike heterogeneous catalysts, which commonly require a co-catalyst to facilitate polymerization, metal-carbene systems have single active sites that are very reactive towards alkenes.[4,8] These defined reactive sites, allow for accurate definition and control over the polymerization processes, which enables polymer chemists to manipulate the microstructure and the molecular weight of the resulting polymers. As well, certain metal-carbene catalysts commonly produce "living" systems, which provides the opportunity to form high molecular weight homo- and block co-polymers.[8,11]

1.2 The Use of Organoiron Complexes in Monomer and Polymer Synthesis

The incorporation of aromatic ether linkages into small and large molecules is of interest due to the important properties these units impart onto the resulting materials. Oligomeric aryl ethers are commonly used as lubricants, while the corresponding polymers have found use as engineering thermoplastics as a result of their excellent thermal stability and resistance to chemical and radiation damage.[14,15]

Traditionally, aryl ether linkages are prepared via Ulmann ether or nucleophilic aromatic substitution (S_NAr) reactions. Ulmann ether synthesis involves the coupling of a halogenated arene with a phenoxide salt at elevated temperatures (100-300°C) in the presence of a copper-based catalyst (Scheme 1.5).[15,16] This reaction has been employed in the preparation of both oligomeric and polymeric materials, however, drawbacks to this methodology include the harsh reaction conditions, the presence of side products and low product yields.

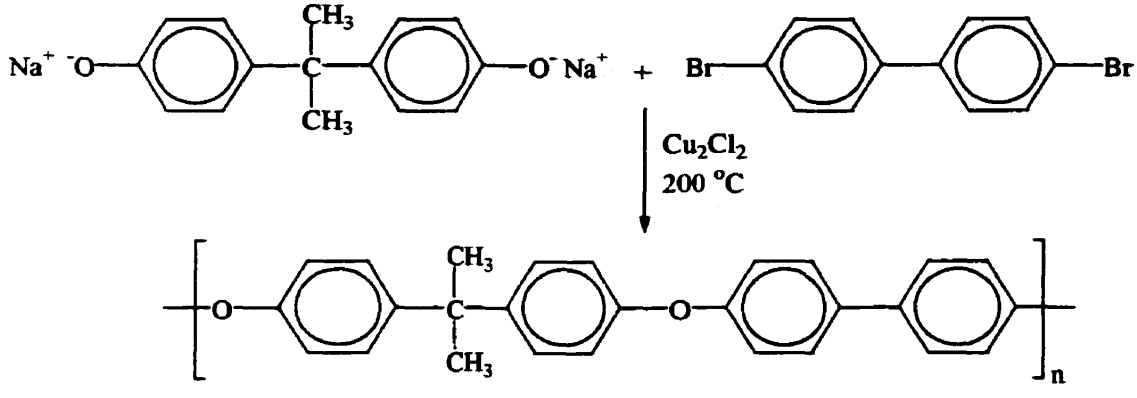

Scheme 1.5: Ulmann ether synthesis of polyaromatic ethers.

Nucleophilic aromatic substitution (S_NAr) involves the reaction of a haloarene with an alkoxide at elevated temperatures (200°C) in the presence of an appropriate base (Scheme 1.6).[1,6,15,17-21] The reaction requires that one or more electron-withdrawing groups be present on the halogenated arene to activate the aromatic ring towards substitution. In organic synthesis, functionalities such as nitro or sulfonyl groups are commonly employed. The good product yields and wide range of nucleophilic reagents that can be employed in this reaction have made this synthetic route popular in the production of polyaromatic ethers.[1,6] However, the reaction conditions needed to prepare the substitution products are harsh and removal of the electron-withdrawing substituents once the final product is obtained may require additional synthetic steps.[22,23]

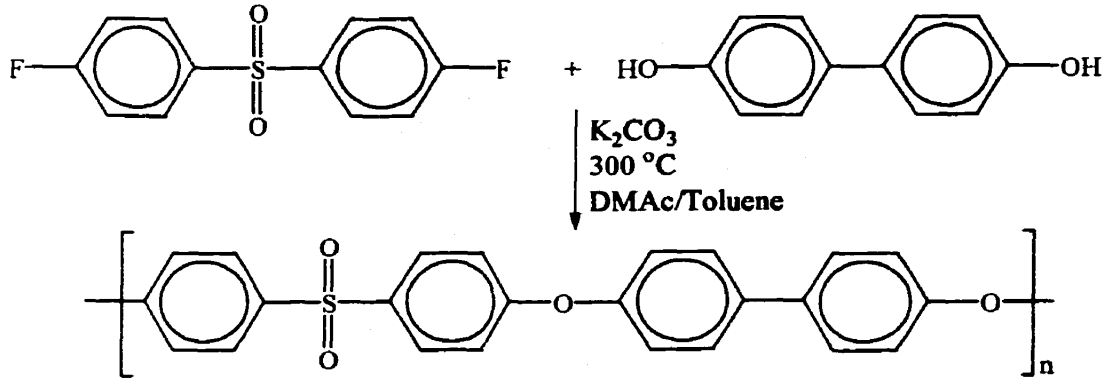

Scheme 1.6: Preparation of a polyaromatic ether via nucleophilic substitution.

The complexation of haloarenes to metallic moieties such as chromium tricarbonyl [$Cr(CO)_3$], cyclopentadienyliron [$CpFe^+$], cyclopentadienylruthenium [$CpRu^+$] and manganese tricarbonyl [$Mn^+(CO)_3$] provides an alternative route to the preparation of nucleophilic aromatic substitution products.[24,25] The electron-withdrawing abilities of the metallic moieties are sufficient enough that synthetic reactions can occur

under milder conditions than the traditional organic routes. It has been found that the $CpFe^+$ moiety has an electron-withdrawing effect similar to that of *o*- and *p*-nitro groups combined.[26] The extent of the activation of the arene towards nucleophilic attack depends on the nature of the metal moiety π-coordinated to it. Kinetic studies have shown that the activity increases in the order of: $Cr(CO)_3 \ll CpRu^+ \cong CpFe^+ < Mn^+(CO)_3$.[26-28]

Substitution reactions mediated by the cyclopentadienyliron ($CpFe^+$) moiety have led to the preparation of numerous oligomeric and polymeric species.[14,29-44] The advantages of this metal moiety over others stems from its chemical versatility, low cost and low toxicity.[14,34] Furthermore, the resulting organoiron products are obtained in excellent yields, and isolation of their organic analogues can be accomplished by cleavage of the metal moiety via photolysis, pyrolysis, or electrolysis.[32] In 1957, Coffield and coworkers were the first to report the preparation of an arene coordinated to the $CpFe^+$ moiety via reaction of cyclopentadienyliron dicarbonyl chloride and mesitylene.[45,46] Unfortunately, this methodology suffered from low product yields, and the small number of complexed arenes that could be prepared. Six years later, Nesmeyanov and coworkers reported the synthesis of $CpFe^+$-complexed arenes via a ligand exchange reaction of one of the cyclopentadienyl rings of ferrocene for a substituted benzene.[47,48] The reaction was carried out in the presence of a Lewis acid catalyst, such as aluminum chloride, and aluminum powder, which prevented the oxidation of the iron center to the ferricinium cation. This new methodology was versatile enough to allow for the synthesis of numerous alkyl-, aryl- and halobenzenes (Scheme 1.7).[47-52]

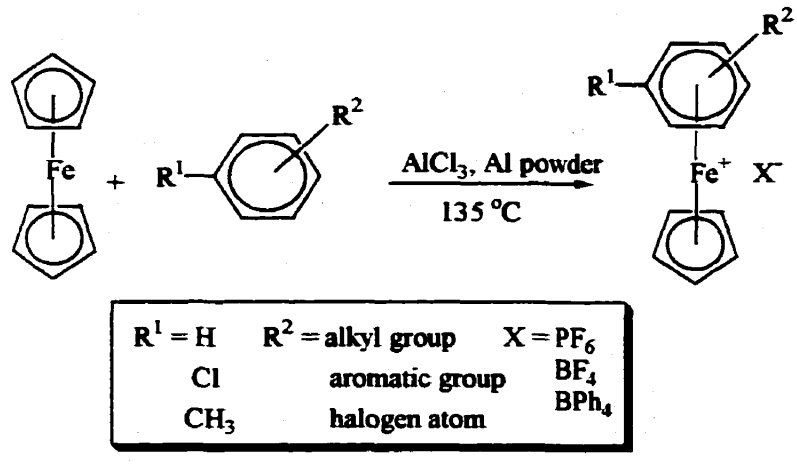

Scheme 1.7: Synthesis of $CpFe^{+}$-complexed arenes via a ligand exchange reaction.

As shown in Scheme 1.7, the cationic products, η^6-arene- η^5-cyclopentadienlyiron complexes are isolated as their hexafluorophosphate, tetrafluoroborate or tetraphenylborate salts. It has been found that the type of substituents on the aromatic ring greatly affects the yields of the ligand exchange reactions.[48] For example, reactions involving benzenes containing electron-withdrawing substituents give lower product yields than those with arenes containing electron-donating groups. This has been attributed to the deactivation of the Lewis acid catalyst in the presence of electron-withdrawing functionalities.[48]

Nesmeyanov carried out the first nucleophilic aromatic substitution reactions of η^6-chlorobenzene- η^5-cyclopentadienlyiron complex in 1967.[53] Since this time, these organoiron complexes have been used as starting reagents in various metal-mediated reactions. Aromatic ether complexes of varying lengths have been prepared via a stepwise synthesis that involves successive S_NAr reactions.[34] As illustrated in Scheme 1.8, by adjusting the molar ratio of complexed arene to dinucleophile, organoiron

complexes were prepared that contained either terminal chlorine atoms (2:1 molar ratio) or hydroxyl groups (1:5 molar ratio). Subsequent S_NAr reactions with these complexes allowed for the construction of several organoiron species, which were each comprised of a different number of complexed and uncomplexed aromatic rings. In one case, a polyaromatic ether complex was prepared using this methodology that contained 35 pendent metal moieties within its structure (Scheme 1.9).[34]

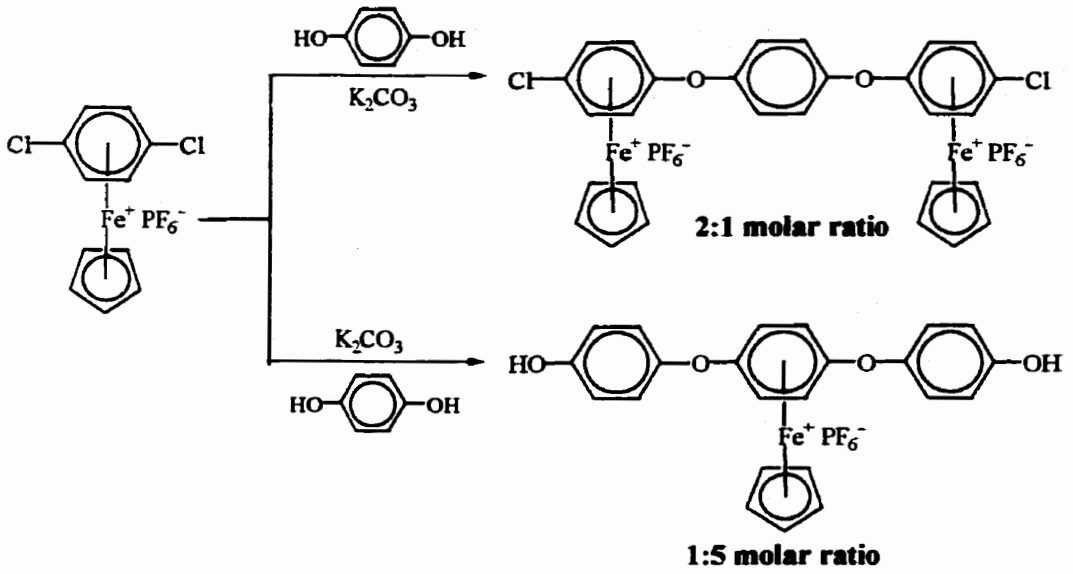

Scheme 1.8: Preparation of organoiron complexes containing different end groups.

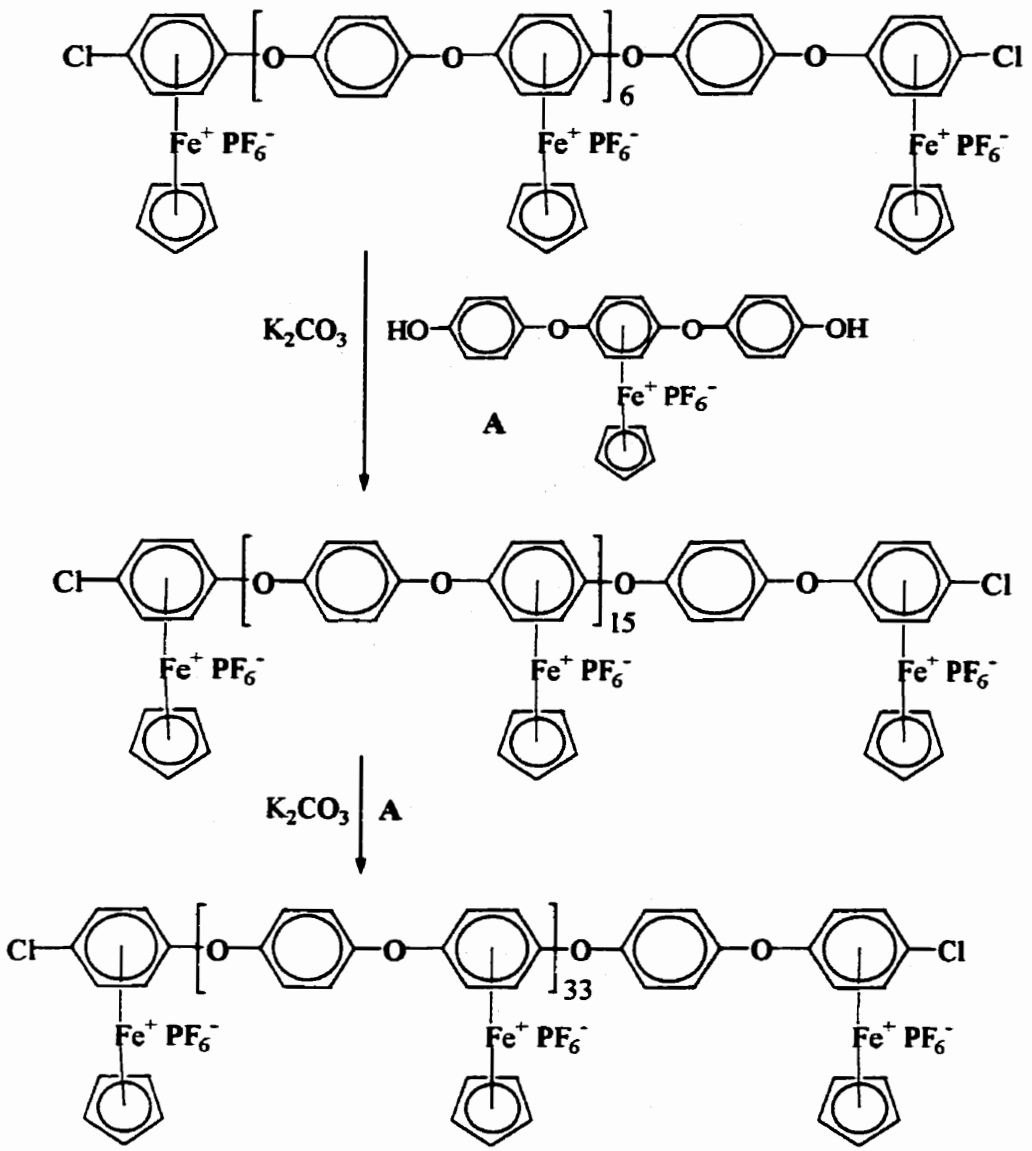

Scheme 1.9: Stepwise approach to polyaromatic ethers.

These stepwise reactions demonstrate the control this methodology allows over the design of the resulting organometallic product, which has found use in the synthesis of numerous organoiron monomers.[32,34-42,44] Pearson and coworkers have prepared monomers suitable for polycondensation reactions using S_NAr chemistry (Scheme

1.10).[41,42] Selective substitution of one of the chlorine atoms of η^6-1-4-dichlorobenzene-η^5-cyclopentadienlyiron complex with methyl-4-hydroxybenzoate yielded a monometallic product containing a terminal chlorine atom (**I**). Reaction of this complex with hydroquinone, followed by demetallation and conversion of the ester to its corresponding acid yielded a compound containing a hydroxyl group at one end and a carboxylic acid group at the other (**II**). Polycondensation reaction of this monomer lead to the isolation of the corresponding poly(aromatic ether ketone) (**III**).

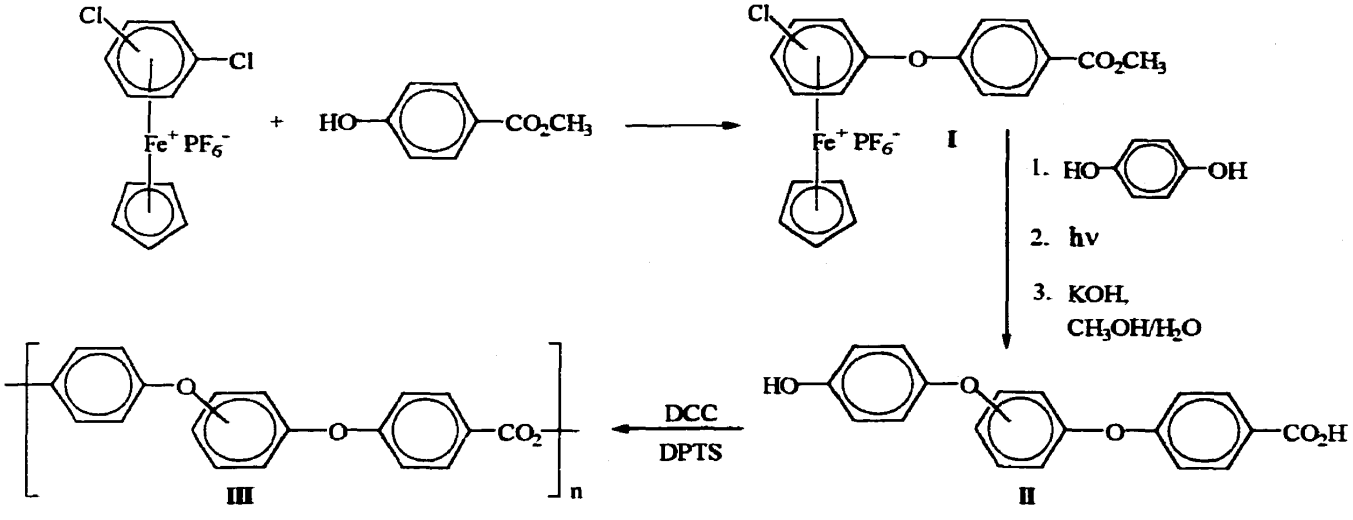

Scheme 1.10: Preparation of monomeric units using $CpFe^+$-mediated S_NAr.

Polyaromatic ethers complexed to $CpFe^+$ have also been prepared in one step S_NAr reactions.[35,36] Reaction of a dichloroarene complex and an oxygen-containing dinucleophile at high concentration, led to the isolation of numerous organometallic polyaromatic ethers (Scheme 1.11). The versatility of this methodology also allowed for the incorporation of amines and thioethers into the polymer backbones via the use of alternative dinucleophiles in the polymerization reactions. These organometallic

polymers displayed increased solubility relative to their organic counterparts due to the presence of the pendent metallic moieties, which may prove useful in the processing of these rigid polymeric materials.[36]

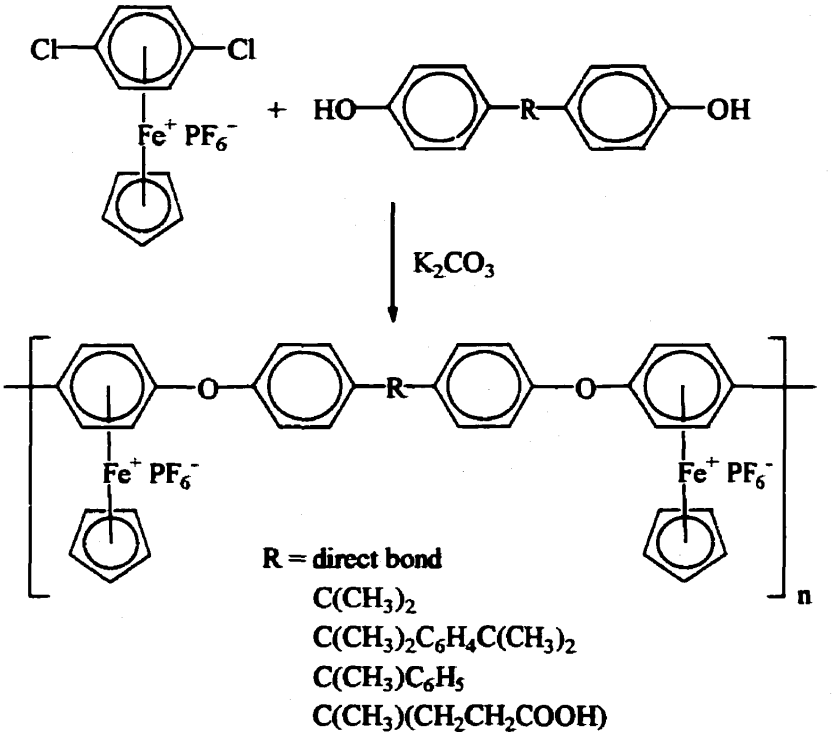

Scheme 1.11: Polyaromatic ethers prepared via S_NAr polymerization reactions.

1.3 Monomer and Polymer Characterization Techniques

A number of techniques are commonly used to study the physical and chemical properties of monomeric and polymeric materials. Spectroscopic techniques that are used for the characterization of monomers in synthetic chemistry can also be used for the structural identification of macromolecules. For example, nuclear magnetic resonance (NMR) and Fourier transform-infrared (FT-IR) spectroscopy can be used to determine the chemical nature of the repeat unit, as well as the microstructure and tacticity of a

polymer.[1] For example, the substituents attached to a polymer backbone can exist in ordered or regular forms, as observed in syndiotactic and isotactic polymers, or in a random nature, as seen in atactic polymer samples (Figure 1.2).[1]

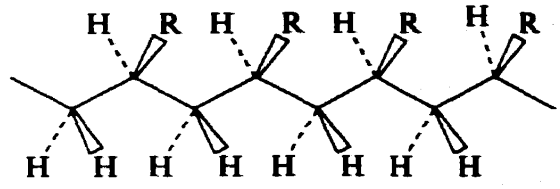

Isotactic

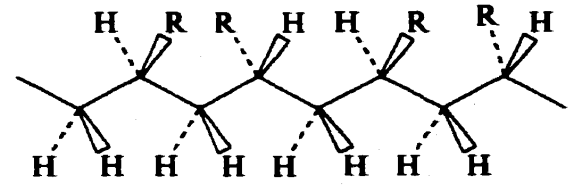

Syndiotactic

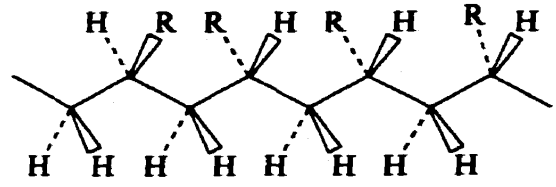

Atactic

Figure 1.2: Different tacticities observed in polymer structures.

The molecular weight of a polymer sample can be determined using a variety of techniques including size exclusion chromatography, viscometry, mass spectrometry and spectroscopic techniques.[1,2] Size exclusion chromatography, also known as gel permeation chromatography (GPC), is one of the most popular methods. The principles of the technique are similar to those of liquid chromatography, that is different components of a sample can be separated and individually analyzed after being subjected to the technique.[54] In GPC, the molecular weights of polymer samples are obtained and used to determine the number of repeating units within the structure. Knowing the

molecular weight of a polymer is important as it directly influences the properties and uses of the material.[1-3]

The thermal properties of a polymeric sample can be determined using differential scanning calorimetry (DSC) and thermal gravimetric analysis (TGA).[1-3,54] DSC investigates the molecular motion of polymer chains, as well as the different phase changes the material can undergo at different temperatures. TGA is used to determine the thermal stability of a polymer by monitoring the weight of the sample as a function of increasing temperature. The thermal information obtained using these techniques is important for determining the types of applications polymeric materials can be used in.

1.3.1 Spectroscopic Analysis

Spectroscopy is the study of the interaction (absorption or transmittance) of electromagnetic radiation (emr) with molecules or atoms.[55] Nuclear magnetic resonance (NMR) and infrared (IR) are two of the most common spectroscopic techniques used to determine the structural composition of a sample. IR spectroscopy is based on the principle that bonds and functional groups within a molecule produce unique absorption bands when irradiated with emr.[54,55] Within a given molecule, covalent bonds are continuously vibrating through either stretching or bending modes. When the molecule is exposed to IR-frequency emr, it absorbs the light and the bonds within it are excited to higher vibrational levels. This results in numerous absorption bands, which are plotted as a function of wavenumber ($1/\lambda$) to give an IR spectrum representative of that molecule. The reason why different functional groups produce distinctive absorption bands is because each type of bond requires a specific amount of energy to be excited, and thus, only IR radiation with energy equal to this value will be able to promote the

transition.[54,55] It is for this reason that the IR spectrum of a molecule is commonly referred to as its "fingerprint".

NMR spectroscopy provides information about the structure of a molecule by examining the population of different energy states that isotopes of an atom exhibit when subjected to a magnetic field.[54,55] Various nuclei can be studied using NMR, of which ^{1}H, ^{13}C, ^{19}F and ^{31}P are the most common. Each nucleus has various degenerate spin states associated with it, which become separated when exposed to a magnetic field. A particular nucleus has (2I+1) spin states, where I is the spin quantum number of that nucleus. In the case of ^{1}H and ^{13}C, the spin quantum number equals ½, thus each atom has two different energy states (m) when exposed to a magnetic field, m = + ½ and m = - ½ (Figure 1.3).[54]

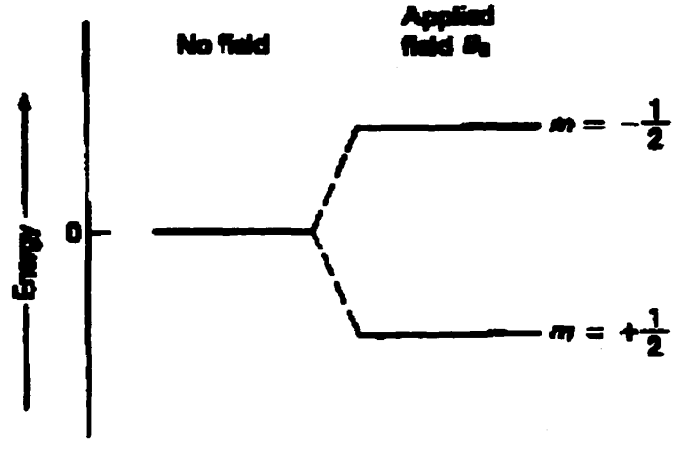

Figure 1.3: Energy levels for a nucleus with I = ± ½.

In some nuclei, the positive charge associated with them spin about their nuclear axes, thus creating a magnetic dipole along the axis whose magnitude is represented as a magnetic moment (μ).[55] Most of the nuclei reside in the lower energy state (m = + ½), where their magnetic moments are aligned in the same direction as the external magnetic

field.[54] When the sample is briefly pulsed with emr in the radio-frequency (rf) region, the nuclei absorb energy that is equal to the difference between the two energy states, m = + ½ and m = - ½. This causes an excitation of some of the nuclei to the higher energy state (m = - ½). The excited nuclei then return to the lowest energy state, during which time a free induction decay (FID) signal, which is a time domain spectrum is recorded by the spectrometer.[56] This cycle of pulsing the sample with emr and then recording the FID signal is repeated numerous times in order to improve the signal-to-noise ratio of the resulting spectrum.[54] The FID signal is then converted using Fourier transformation (FT), and the NMR spectrum is obtained as a plot of absorption versus frequency or chemical shift (δ = frequency/magnetic field strength). Nuclei of the same atom may absorb emr of different energies as a result of their local environments, and thus chemical shift values are unique to nuclei of different functional groups. As well, nuclei of two different atoms will absorb energy at different frequencies, allowing for the independent study of individual atoms.[54,55]

The conventional NMR spectra of some molecules can be very complex, and thus two-dimensional NMR techniques can be employed to aid in the assignment of their spectra. Two common 2-D NMR techniques are homo- and heteronuclear correlation spectroscopy. Homonuclear correlation spectroscopy (HH COSY) experiments are useful because they provide information regarding the connectivity of hydrogen atoms within a molecule, while heteronuclear correlation spectroscopy (CH COSY) indicates which hydrogens are attached to which carbon atoms in a molecule.[56,57] In contrast to 1-D NMR spectra, 2-D NMR spectra are functions of two time variables. The first time variable t_1, is the time period between rf-emr pulses, whereas, the second time variable t_2,

represents the "real time" period necessary to acquire the FID signal.[57] Fourier transformation of every set of data points within the total FID signal results in a 2-D signal, where the amplitude of the stacked peaks increases to a maximum value and then decreases, as seen in **II** of Figure 1.4. This maximum value represents the center of the contours on the diagonal of a 2-D plot (Figure 1.4).[56]

To analyze a 2-D spectrum, correlations between the nuclei must first be identified. For example, Figure 1.5 represents the HH COSY NMR spectrum of geraniol (**1.2**), a terpene obtained from roses. The 2D-FT signals are represented along the diagonal as a series of contours. Adjacent to the diagonal there are other contours known as crosspeaks. These crosspeaks represent the connectivities existing between the hydrogen atoms in the compound.[56] To analyze the spectrum (Figure 1.5), a horizontal line is drawn from the center of a crosspeak to the diagonal, where it intercepted a contour (Hydrogen 6). A second line from the same crosspeak is then drawn vertically towards the diagonal, until it comes into contact with a second contour (Hydrogen 5). When arranged in this pattern, the two contours in the diagonal are said to be correlated or coupled with each other.[56] This process is carried out for the remaining contours in the spectrum, allowing for the determination of all the proton-proton (H-H) connectivities.

Analysis of the CH COSY NMR spectrum of geraniol was carried out in a similar manner (Figure 1.6). In this spectrum, the 1-D plot of the ^{1}H NMR is found on the y-axis, while the 1-D plot of the ^{13}C NMR is along the x-axis. Each contour in this 2-D plot represents a correlation between a carbon and hydrogen atom in the molecule. Connectivities between these atoms are obtained by drawing a vertical line from a contour to a peak in the ^{13}C NMR spectrum (Carbon 1), followed by a horizontal line

from the same contour to a peak in the ^{1}H NMR spectrum (Hydrogen 1).[56] As in the analysis of the HH COSY NMR spectrum, this technique is performed until all C-H connectivities are identified. Combining the information obtained from both 2-D NMR plots provides sufficient information to assign both the ^{1}H NMR and ^{13}C NMR spectrum of the molecule.[56,57]

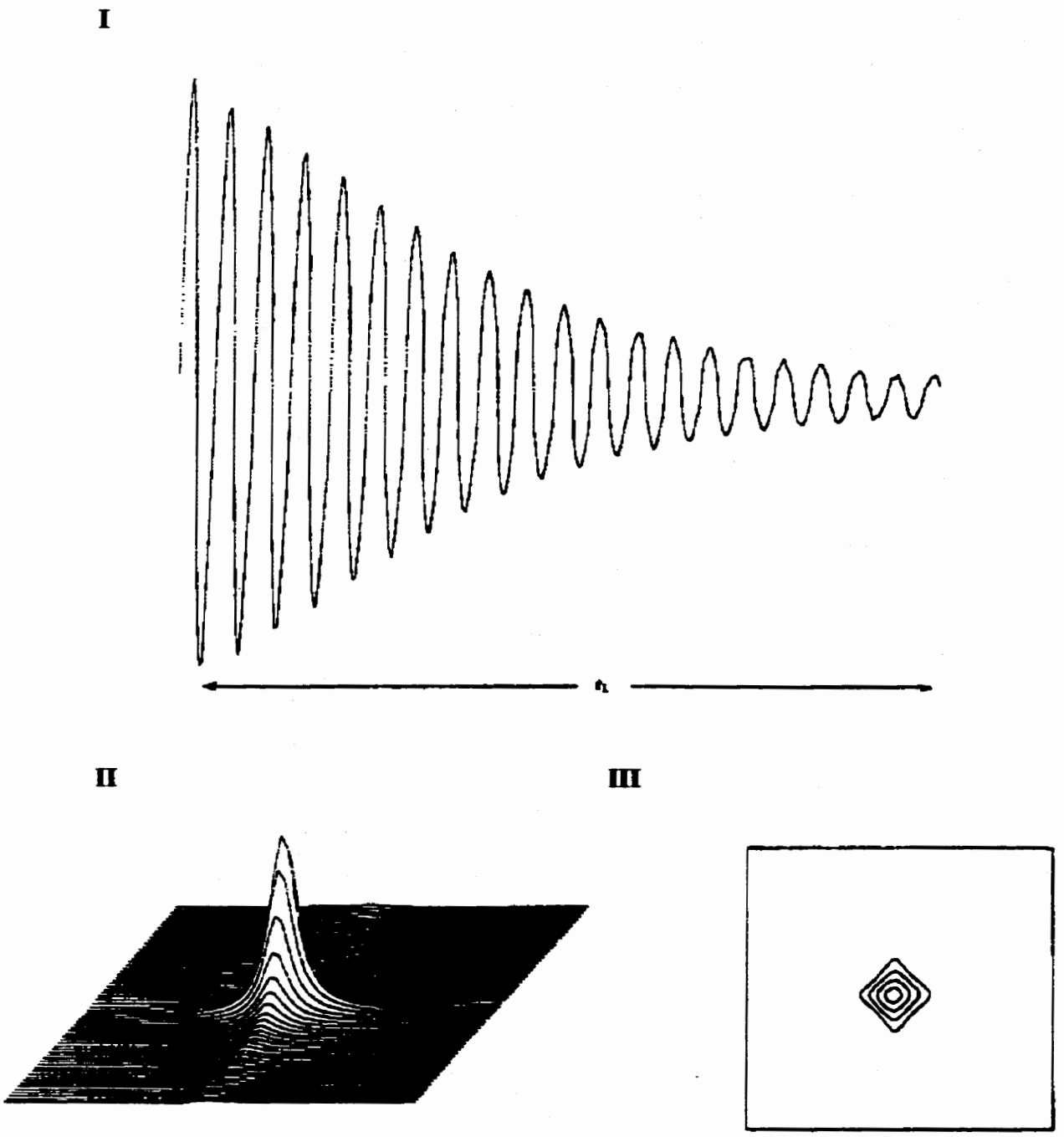

Figure 1.4: (I) FID signal of t_1; (II) 2-D FT; (III) Contours on the diagonal of a 2-D plot.

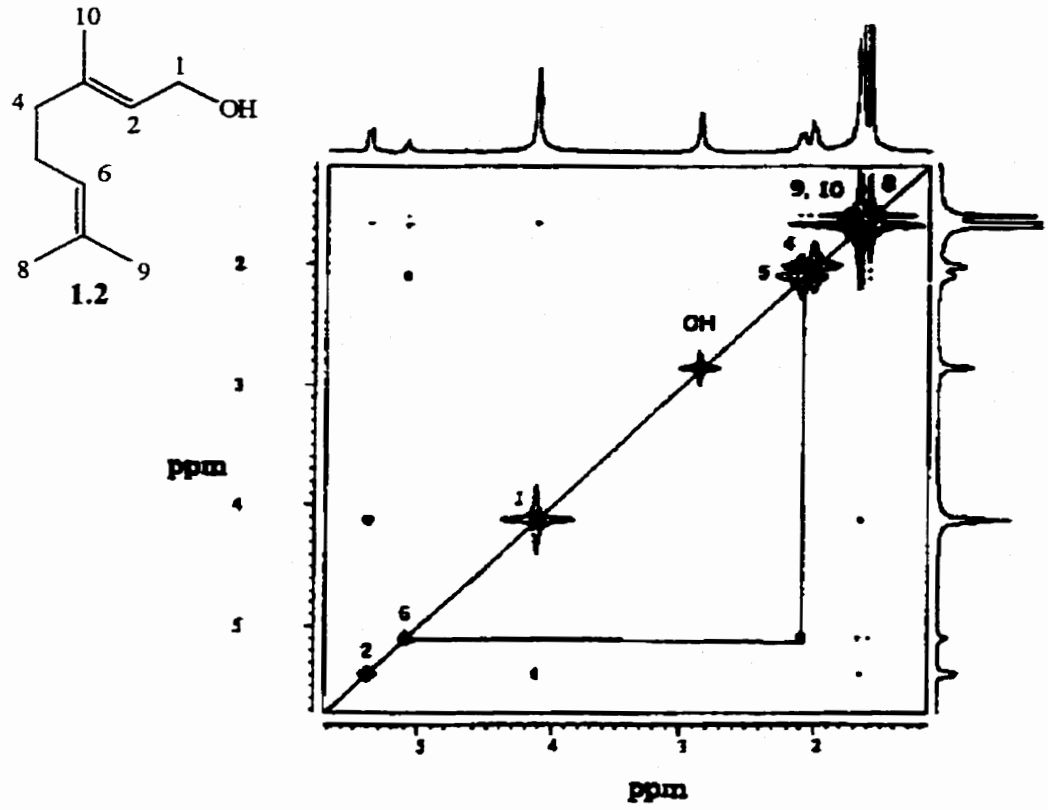

Figure 1.5: Analysis of the HH COSY NMR of geraniol.

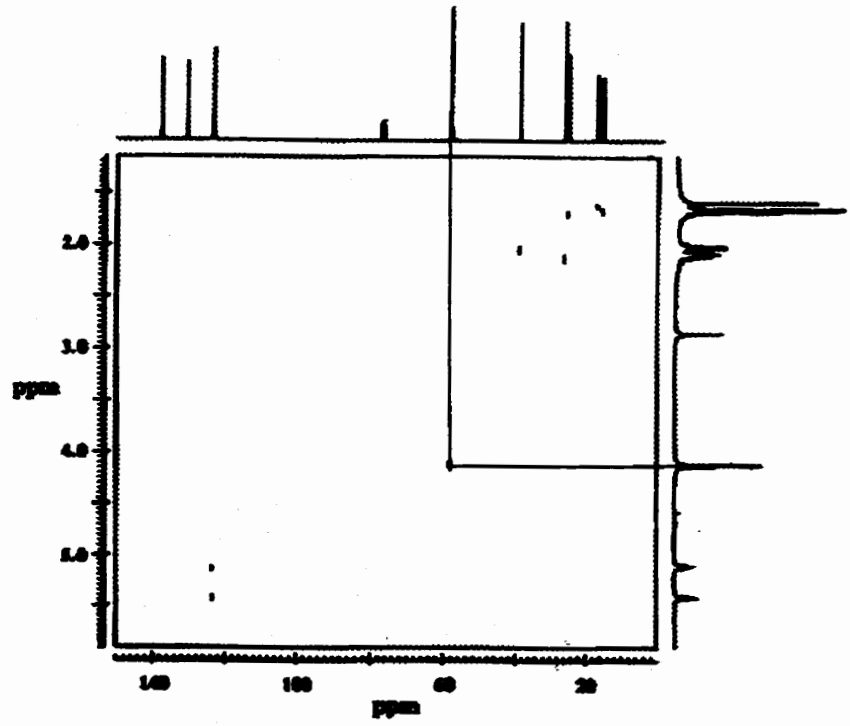

Figure 1.6: Analysis of the CH COSY NMR of geraniol.

1.3.2 Molecular Weight Determination

Determining the exact molecular weight of a polymer sample is more complex than for simple molecules because not all polymer chains within a given sample are the same size, therefore, average molecular weights are determined.[1-3] Gel permeation chromatography (GPC) is one method used to determine the molecular weights and the degree of polymerization (DP) of polymer samples. As mentioned earlier, the principles of GPC are similar to those of liquid chromatography, this also applies to the instrumentation used in the technique as seen in Figure 1.7. In a typical GPC experiment, a polymer sample is dissolved in the same solvent that serves as the mobile phase and is then injected into the system via syringe. The mobile phase is responsible for the movement of the sample components through the GPC column, where separation occurs, and on to the detector where each component is analyzed.

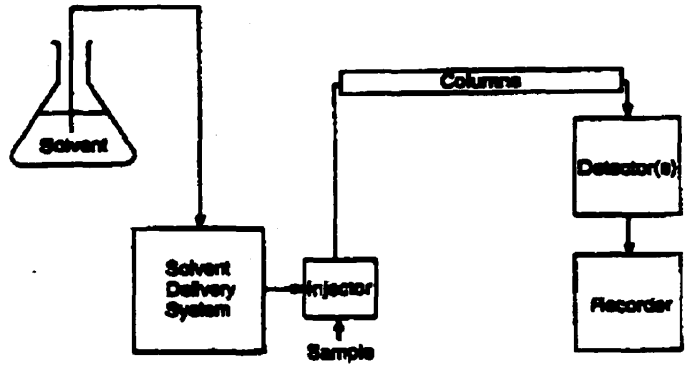

Figure 1.7: GPC instrumentation.

The separation of the individual components of a polymer sample is a direct result of the interaction of the polymer chains with the stationary phase of the column, which consists of a porous gel made up of crosslinked polymer particles.[1-3] As the sample is

moved through the column (**A** and **B** in Figure 1.8), smaller polymer chains are able to enter the pores of the stationary phase, and thus spend a longer time in the column than their larger counterparts, which pass through the column with little to no interaction with the stationary phase. This is known as the size exclusion effect.[2] These interactions result in different retention times for the polymer molecules, with the larger polymer chains emerging from the column prior to the smaller ones (**C** and **D** in Figure 1.8). When compared to the retention times of standard polymeric materials analyzed by the same column, the average molecular weights of the polymer molecules can be determined.

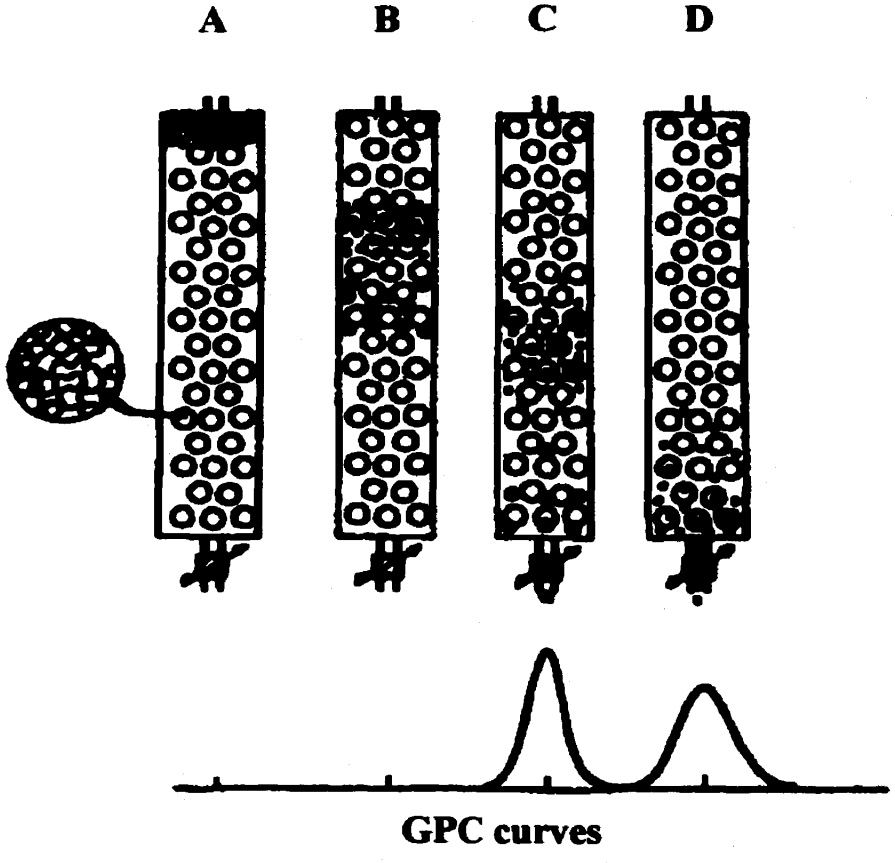

Figure 1.8: Separation of large and small polymer chains using GPC.

GPC calculates various molecular weights for a single polymer sample, including the number-average molecular weight (Mn) and the weight-average molecular weight (Mw). The number-average molecular weight of a sample is based on the number of polymer chains of a given molecular weight. Mn represents the weight fraction (N_xM_x) of a polymer chain relative to the total number of polymer species in the sample (N_x) (Equation 1.7).[1-3] Alternatively, the weight-average molecular weight is based on the mass of the species present ($N_xM_x^2$) relative to the weight-fraction (N_xM_x) of each polymer chain in the sample (Equation 1.8).[1-3] It has been found that Mw is biased to heavier polymer molecules within a sample, as they will possess larger weight-fractions than the smaller chains. As well, because each polymer chain contributes equally to the value of Mn, regardless of its molecular weight, Mn is almost always a smaller value than Mw.[1,3]

$$Mn = \frac{\Sigma NxMx}{\Sigma Nx}$$

Equation 1.7

$$Mw = \frac{\Sigma NxMx^2}{\Sigma NxMx}$$

Equation 1.8

Using the two calculated molecular weights described above, the polydispersity index (PDI) of a polymer sample can be determined. The PDI of a sample is the ratio of Mw/Mn and represents the range of molecular weights of the various polymer chains.[1-3] The weight-average molecular weight (Mw) can also be used to determine the degree of polymerization (DP) of a sample by dividing it by the formula weight of one polymer repeat unit. It is important to determine the DP of a sample because it represents the number of repeating units (n) within a polymer's structure.[1-3]

1.3.3 Thermal Analysis

The thermal properties of polymer samples are commonly studied using differential scanning calorimetry (DSC) and thermogravimetric analysis (TGA). Synthetic polymers can consist of both crystalline and amorphous regions. The crystalline regions of a polymer are those where the polymer chains are aligned in an ordered fashion, which arise when the chains posses high stereoregularity and contain little or no branching.[1,3] In contrast, the amorphous regions of a polymer are a result of random ordering of the polymer chains. DSC is used to determine the temperature at which phase changes of these regions occur. These phase transitions are observed as changes in the heat flow or heat capacity of the sample as a function of temperature.[54]

In a typical DSC thermogram of a sample, three types of phase transformations can be observed; the glass transition temperature (T_g), the crystallization temperature (T_c) and the melt temperature (T_m) (Figure 1.9). Below the T_g of a sample, the amorphous regions are in a brittle or glassy state where all molecular motions of the polymer chains are restricted to short vibrations and rotations.[1-3] As the sample is heated above its T_g, these disordered regions become soft and rubbery, which allows for more conformational freedom of the polymer chains. The temperature at which this transformation of the amorphous states occurs is denoted the T_g of the polymeric sample. After this phase transformation, the amorphous domains in the material can vibrate and flow freely. If a sample is then further heated, the chains within the amorphous regions may become ordered, resembling the chains in the crystalline areas of the polymer. The temperature at which this phase transformation occurs is referred to as the T_c of a polymer. It is important to note that not all amorphous regions can gain enough energy to become

crystalline, thus, a T_c is not always observed.[1-3] Finally, the T_m of a sample is the temperature at which the crystalline regions of the polymer undergo melting. Above this temperature, the sample is commonly referred to as being "in the melt". Analogous to the T_c of a sample, if there are no crystalline regions in the polymer, no T_m is observed. Likewise, if the polymer sample is 100% crystalline, that is there are no amorphous regions within it, no T_g will be observed in the DSC thermogram.[1-3]

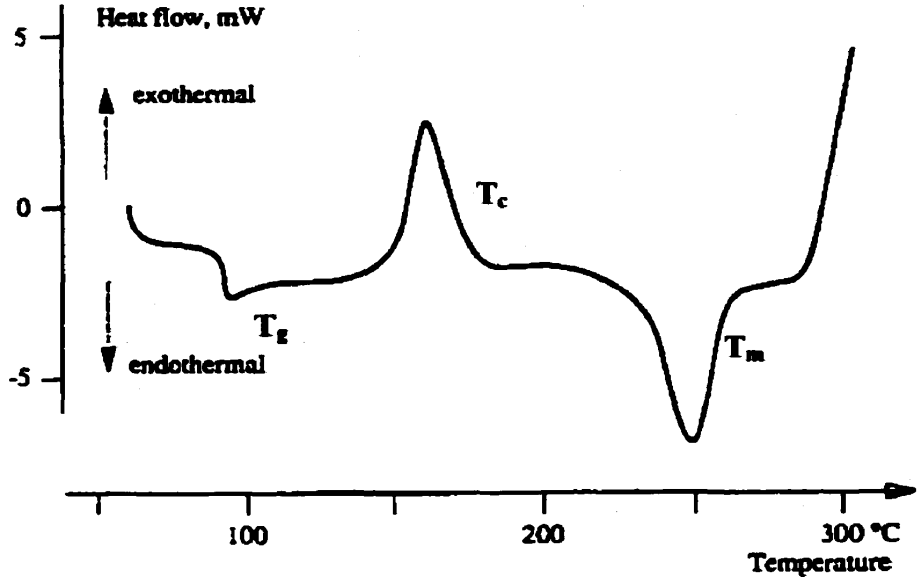

Figure 1.9: A representative example of a DSC thermogram.

Thermogravimetric analysis (TGA) is another technique used to determine the thermal properties of polymeric materials. TGA determines the thermal stability of a polymer by continuously monitoring the weight of a sample as a function of increasing temperature.[3,54] The decomposition temperature of a polymeric sample is observed as a weight loss step in the TGA thermogram, which is a plot of sample weight versus temperature (Figure 1.10). Knowing the decomposition temperature of a polymer is

important as it influences the types of applications the material can be used in. For example, polyaromatic ethers, which are commonly used in high temperature applications do not begin to decompose until temperatures above 500°C.[1.15]

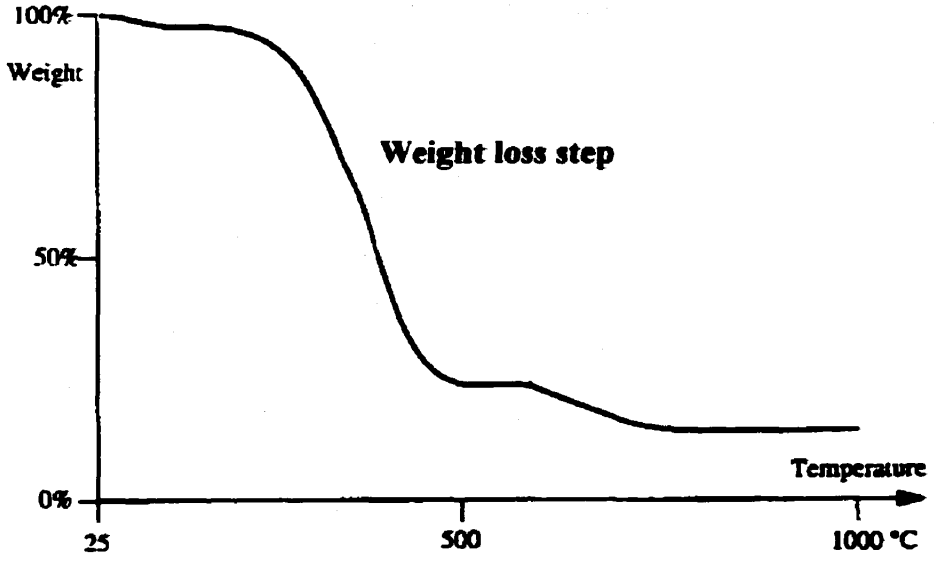

Figure 1.10: A representative example of a TGA thermogram.

2.0 Aromatic Macrocycle Syntheses and Polymerization

2.1 Introduction

Pedersen's discovery of crown ethers (**2.1**) and their ability to form guest-host complexes with cationic species, initiated a large scale study into the preparation and properties of macrocyclic compounds.[58-61] Since his findings in the 1960's, others have made remarkable contributions to the area of supramolecular chemistry, which is a discipline involving the study of chemical species that are more complex than molecules themselves.[61] For example, Cram's extensive work on spherands (**2.2**), as well as his introduction of the class name "cavitands" for organic compounds that contain enforced cavities capable of accommodating a guest molecule, were important to the growth of this area of chemistry.[62,63] Lehn expanded the applications of macrocyclic compounds by his introduction of cryptands (**2.3**), which are three-dimensional structures containing two intramolecular cavities capable of forming complexes with guest molecules.[61,64] All three scientists were recognized for their remarkable efforts in the advancement of supramolecular chemistry when awarded with the Nobel Prize in chemistry in 1988.

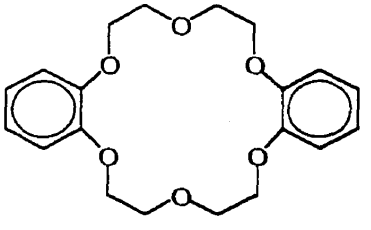

2.1

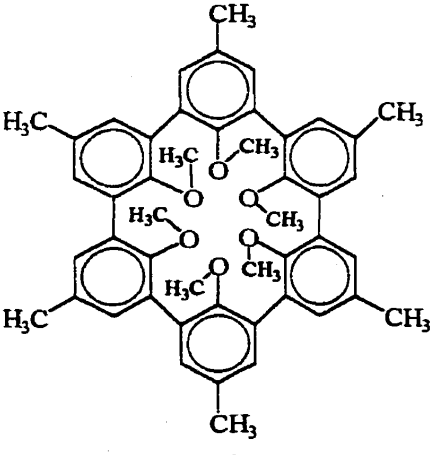

2.2

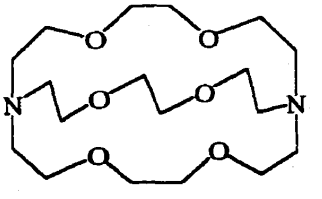

2.3

A summary of the different synthetic routes used in the preparation of macrocyclic compounds is outlined in Scheme 2.1. The first ring closure route involves the cyclization of an asymmetric monomer functionalized with two chemically different end groups. The second illustrates the capping of an elongated symmetric monomer with a small molecule, while the third shows condensation reactions involving either two or four monomers (symmetric or asymmetric).[60] While various routes to the synthesis of macrocycles containing aliphatic linkages have been established, few synthetic methodologies for the preparation of fully aromatic macrocycles have been developed.

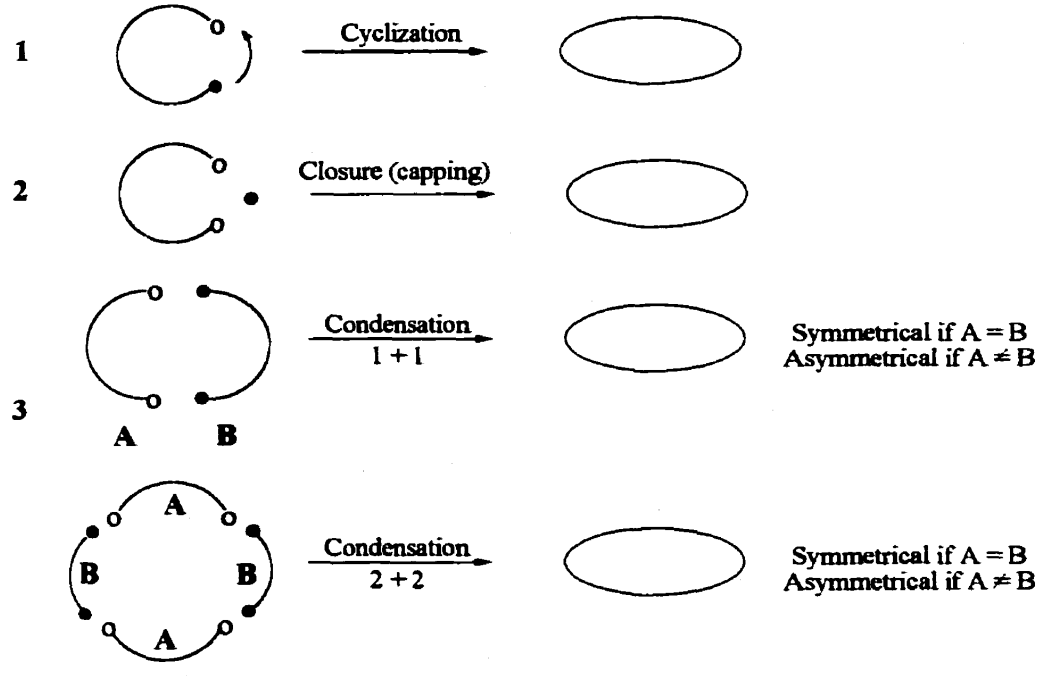

Scheme 2.1: Ring closure routes.

Some of the first reports detailing the synthesis of aromatic macrocycles began to appear in the 1970's.[65-67] Kime and coworkers were among the first to outline the

synthesis and binding properties of fully aromatic macrocycles. They prepared cyclic aryl ethers via the reaction of aromatic diphenols with *o*-dibromobenzene (Scheme 2.2).[65] Unfortunately, they found that in contrast to aliphatic-based macrocycles, the aromatic products did not form guest-host complexes with cationic metals as a result of their structural rigidity and the decreased basicity of the oxygen donor atoms within the cycles. This discovery somewhat hindered the advancement of the syntheses of aromatic macrocycles, as guest-host chemistry was a popular aspect of macrocyclic compounds.

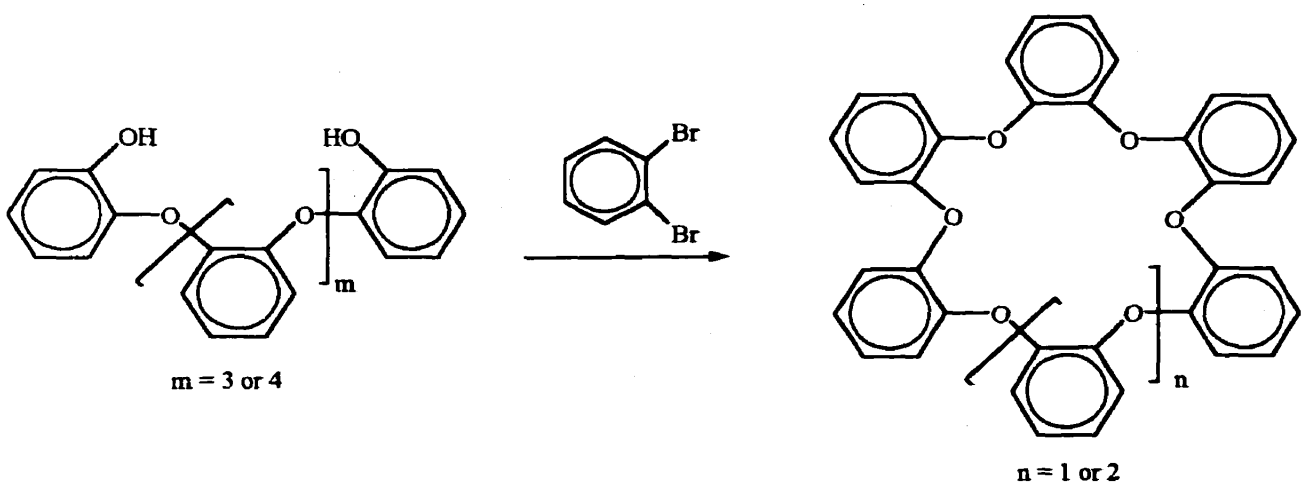

Scheme 2.2: Two of the first examples of fully aromatic macrocycles.

Aside from the binding properties of aromatic macrocycles, other groups were interested in these highly strained molecules for their importance to conformational studies of aromatic compounds.[66,67] In the early 1970's, Montaudo and coworkers prepared a series of cyclic aryl sulfides by reacting 1,3- and 1,4-benzenedithiol with 1,3-dichloro-4,6-dinitrobenezene in the presence of NaOH (Scheme 2.3).[66] The resulting aromatic sulfides were analyzed to determine the conformational preference of these types of molecules. It was found that these rigid compounds possessed interesting

structural and spectroscopic properties, as determined using NMR and molecular modeling.[66]

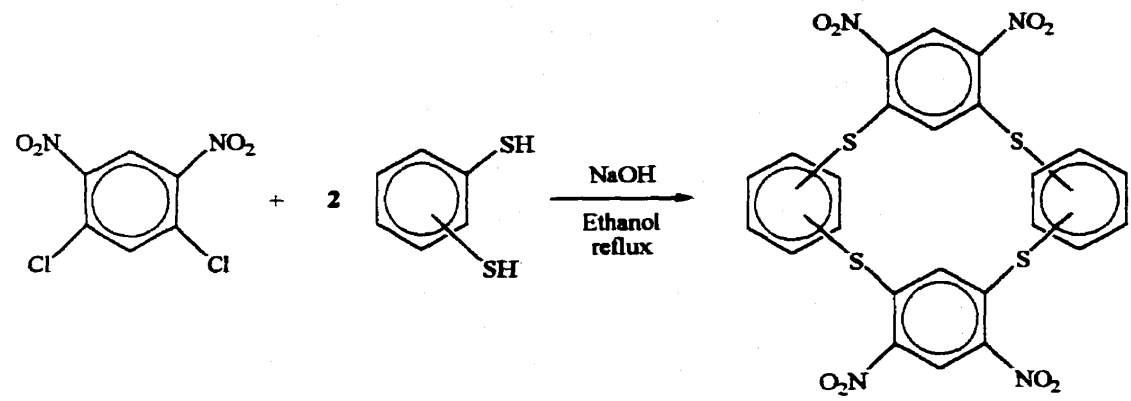

Scheme 2.3: Preparation of cyclic aryl sulfides for conformational studies.

In the last decade, investigations into cyclic aryl compounds have escalated due to the interesting properties they possess such as rigidity, thermal and chemical stability and reduced conformational freedom.[7,68-72] These properties have allowed for their use as high temperature catalysts, as molecular recognition systems or as building blocks in supramolecular chemistry.[7,68-72] One of the most popular application of cyclic aryl compounds is as monomers in ring opening polymerizations (ROP) to yield high performance engineering thermoplastics. The use of cyclic monomers is advantageous because the cycles exhibit low melt viscosity, which facilitates their processing. As well, the polymerizations give out little or no heat, do not require solvents to proceed and do not yield volatile byproducts.[7,68-72]

2.2 Established Synthetic Routes to Aromatic Macrocycles

All of the synthetic routes available for the preparation of high molecular weight polymers such as polycondensation, metal-mediated coupling and nucleophilic aromatic substitution can also be applied to the preparation of macrocyclic products. This is possible because both the intramolecular process of cyclization and the intermolecular process of polymerization have equal probability of occurring, depending on reaction conditions and monomer structure (Equation 2.1). For macrocyclization purposes, experimental factors must be chosen such that the intramolecular reaction is favored over the polymerization process.[60]

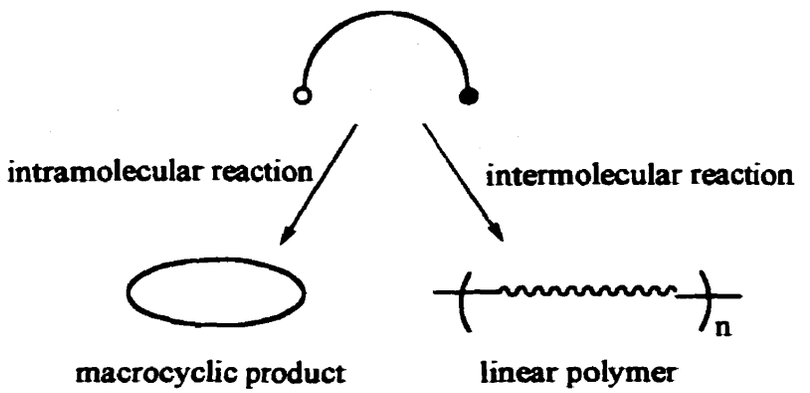

Equation 2.1: Intramolecular versus intermolecular reactions.

Pseudo high-dilution (p-HD) conditions have been developed to minimize the amount of linear product formed during macrocyclization reactions.[73] These conditions follow the principle that if the concentrations of the functional end groups of the reactants are kept low, and if the reaction that yields the cyclized product is fast, the intramolecular reaction will be favored over the intermolecular one. Since dilute reaction solutions would yield very little product overall, an "influxion" procedure has been developed that

meets the low concentration requirement, while still yielding large amounts of products. This process involves the slow addition of reactants over a long period of time into a reaction flask containing a large volume of solvent. Thus, the concentration of the species directly involved in the cyclization reactions are kept at a minimum, promoting cyclization, while the overall yield of the products is high because there are ample amounts of starting reagents used.[73] A typical macrocyclization reaction carried out using these conditions involves addition of the reactants over an 8 hour period into a mixture of refluxing solvents containing an appropriate base or catalyst, such that the final concentration of the reaction mixture is below 40 mM. The reaction is then allowed to proceed for an additional 24 hours, after which time the products are isolated.[7]

Macrocyclization reactions commonly yield a mixture of cyclic products of various sizes, as well as linear oligomers and polymers (Figure 2.1). In general, the formation of the 1 + 1 macrocyclic product is most favored, and is obtained in high yields if the ring strain of the resulting cycle is low. However, due to the rigidity associated with aromatic macrocycles, a complex mixture is generally obtained following the macrocyclization reactions.[74] It has been found that the single-sized cycles can be separated from the linear oligomers based on their differences in solubility. From the above explanations, it is easy to see that the synthetic preparation of macrocyclic products is a challenging one, as a single product is difficult to obtain at the end of a reaction.

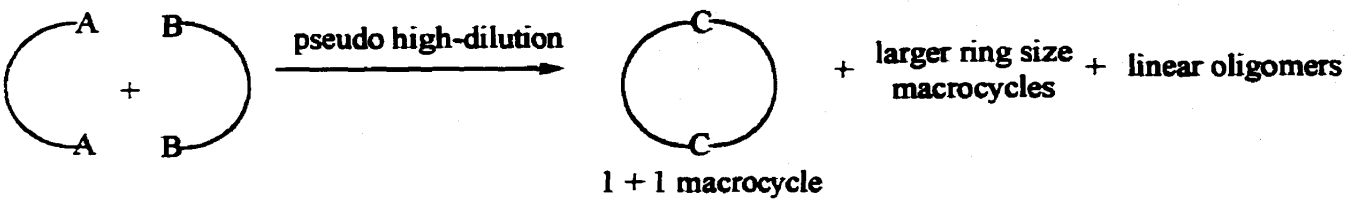

Figure 2.1: Mixture of products obtained from macrocyclization reactions.

2.2.1 Nucleophilic Aromatic Substitution Reactions

One of the most popular methodologies employed to prepare macrocyclic compounds is nucleophilic aromatic substitution (S_NAr). There are two available routes in this type of methodology; the first, and most popular is the AA + BB approach (Scheme 2.4).[7] This process involves reaction between an equimolar amount of two symmetric monomers; one functionalized with two terminal nucleophilic groups, and the other with two appropriate leaving groups, usually fluorine atoms. Initially, displacement of one of the leaving groups occurs, resulting in the formation of a linear oligomer containing a nucleophilic group at one end and a halogen atom at the other. At this point in the synthesis, there are two competing reactions; macrocyclization to form the desired product and polymerization to form the linear analogue. By using pseudo high-dilution (p-HD) conditions, the polymerization process is suppressed, and formation of the macrocyclic product is favored.

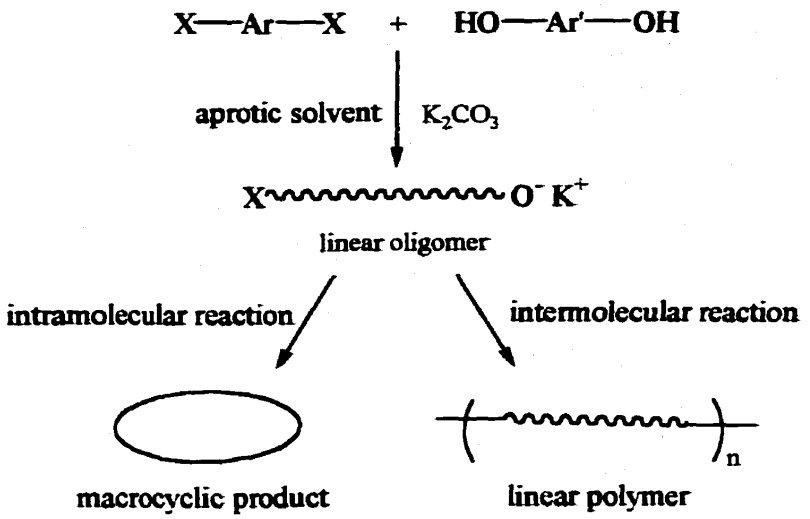

Scheme 2.4: AA+BB S_NAr methodology.

The second S_NAr synthetic route is denoted the AB approach (Scheme 2.5).[7] Here, an asymmetrical monomer functionalized with two different end groups is first prepared, and then subjected to p-HD conditions to yield the macrocyclic product. This approach is advantageous relative to the AA + BB approach because it eliminates the need to stoichiometrically balance the amount of starting reagents used in the reaction, however, the same two competing reactions observed in the AA + BB synthesis are also present in this methodological approach. Thus, appropriate reaction conditions must be used to obtain the cyclized product instead of the corresponding polymer.

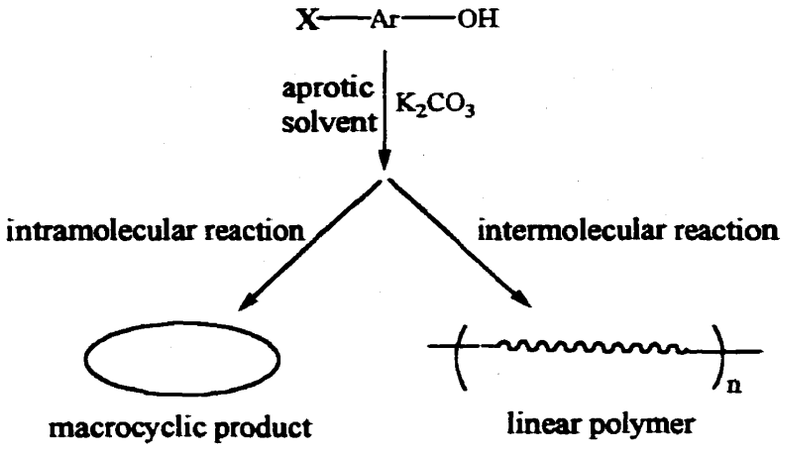

Scheme 2.5: AB S_NAr methodology.

Dow Chemical Co. and General Electric are two manufacturers that have largely contributed to the investigation into the preparation and ring opening polymerization (ROP) of aromatic macrocycles.[68,75-82] Dow Chemical has played a large role in this area, using both the AA + BB and the AB approach for the synthesis of cyclic aryl ether sulfones (Scheme 2.6). A typical AA + BB experiment involved the simultaneous addition of bis(4-fluorophenyl) sulfone and 4-hydroxyphenyl sulfone into refluxing DMAc/toluene containing K_2CO_3 over a 60 hour time period.[68,75] After addition was complete, the reaction was allowed to reflux for an additional 2 days. The asymmetric reagent used in the AB approach was first prepared via the reaction of 4-fluorophenylsulfonyl chloride and diphenyl carbonate, and then subjected to cyclization.[68,76] Using the AA + BB approach, it was found that macrocycles with even ring sizes of four and greater were obtained, whereas with the AB approach, both even- and odd-membered rings containing three or more units were isolated. In each of the

approaches, the smallest sized macrocycle was the dominant product in the mixtures obtained.

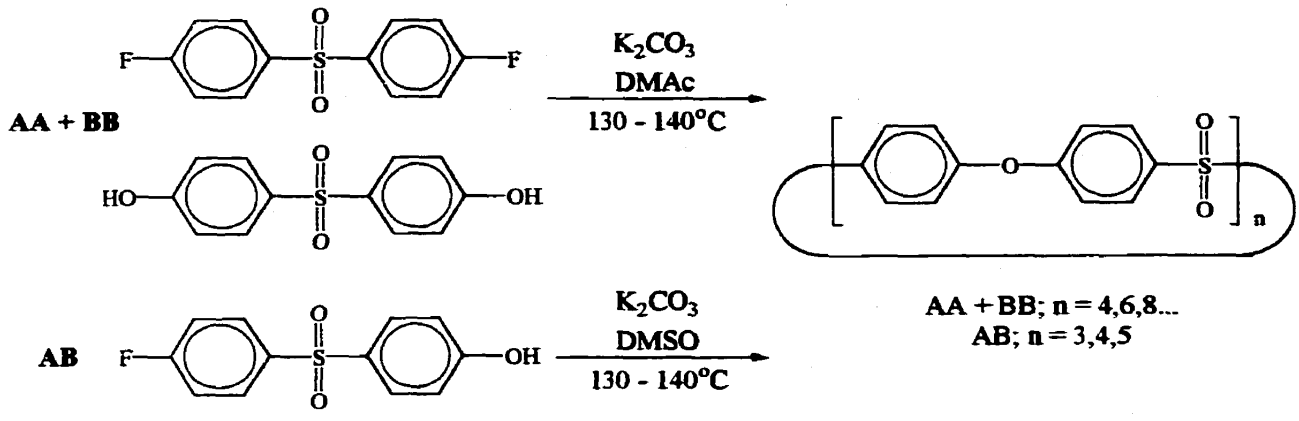

Scheme 2.6: Synthesis of cyclic aryl ether sulfones via AA + BB or AB approach.

General Electric is another company that has contributed to the early development of aromatic macrocycles.[77-82] Initial work involved the use of starting materials with "bent" conformations that favored the formation of cyclic products relative to their linear analogues. For example, numerous aromatic/aliphatic mixed macrocycles were prepared by reacting 2,2',3,3'-tetrahydro-3,3,3',3'-tetramethyl-1,1'-spiro[1-indene]-6,6'-diol (SBI) (I) with various halogenated aromatic reagents (Scheme 2.7).[77] Using this preorganizational approach, mixtures of cyclooligomers with varying ring sizes were obtained in yields ranging from 40-52%. These were adequate yields considering the reactions were carried out using conventional polymerization conditions, with the final concentration of the reactants being as high as 67 mM.[7] This value is much higher than the maximum suggested concentration of 40 mM for reactions carried out using p-HD conditions.[7]

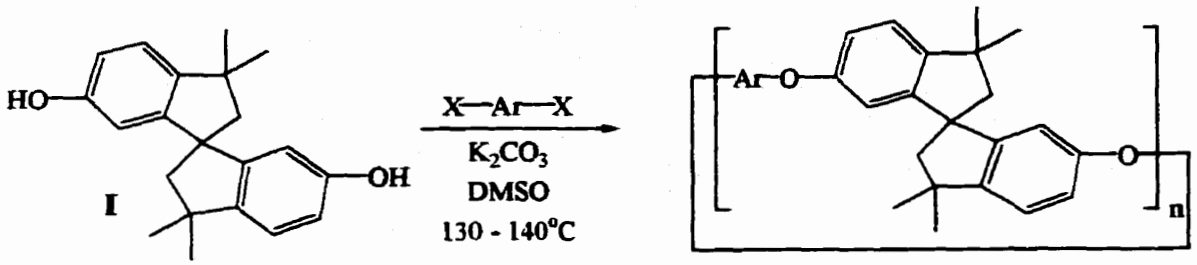

Ar	X	Cyclic Yields
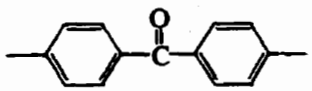	F	47 %
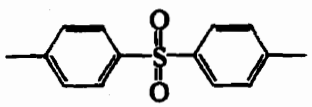	F	45 %
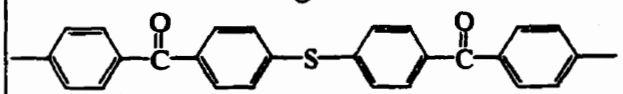	F	48 %
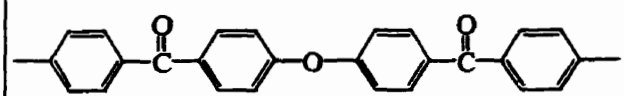	F	40 %
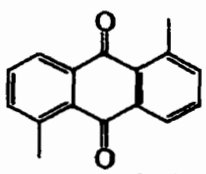	Cl	52 %

Scheme 2.7: Preorganizational approach to aliphatic/aromatic macrocycles.

In addition to large corporations, independent researchers have also studied the use of S_NAr chemistry for the preparation of cyclic aryl ethers. Hay and coworkers have performed numerous studies on the synthesis, characterization and ROP of a number of aromatic macrocycles.[7,83-94] The cyclic aryl ethers were generally prepared via S_NAr reactions under p-HD conditions to give mixtures that contained even and odd numbered cycles. Single-sized cycles could be isolated based on the differences in solubility of the cycles relative to the linear oligomers. Hay also prepared an interesting series of

macrocyclic products containing diphenylacetylene moieties.[7,83] To synthesize these macrocycles, nucleophilic substitution of various difluoro compounds with the potassium salt of 3,3'-dihydroxydiphenylacetylene were carried out under p-HD conditions as shown in Scheme 2.8. The incorporation of acetylene units into the macrocycles was of interest for the preparation of cross-linked polymers, following the initial ring opening polymerization of the cyclic products.

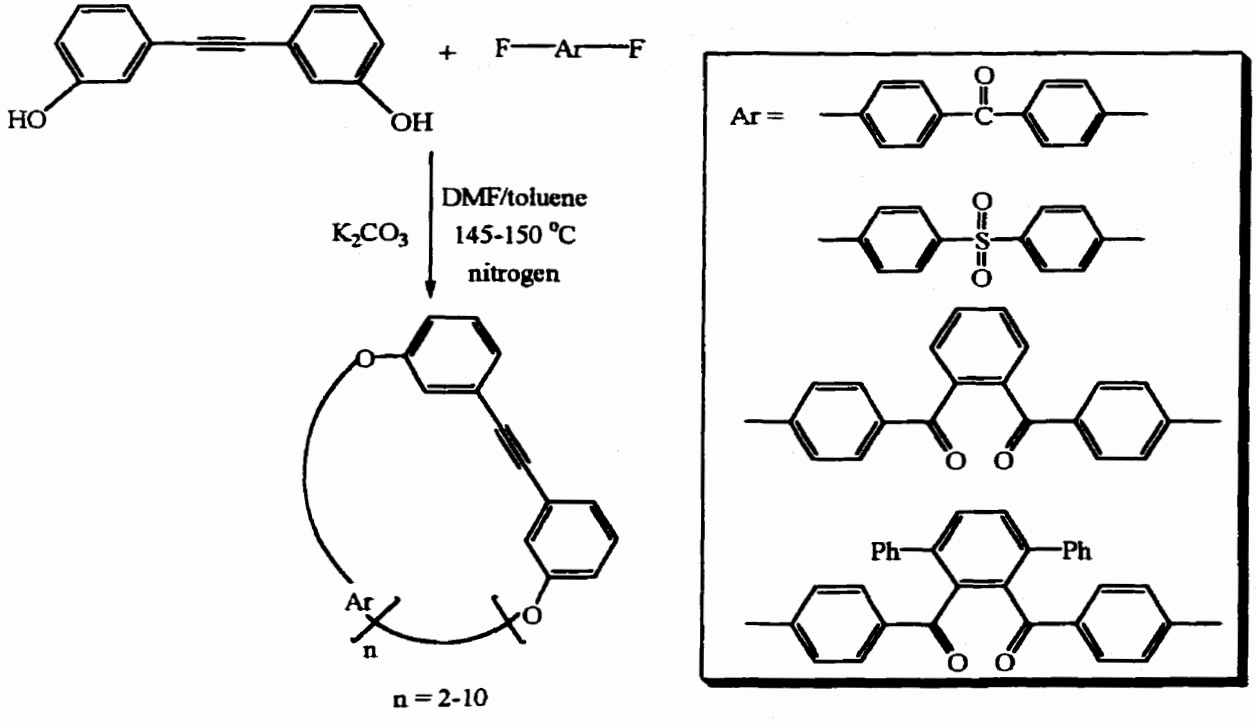

Scheme 2.8: Synthesis of aromatic macrocycles containing acetylene moieties.

Cyclic aryl thioether sulfones have also been prepared via S_NAr chemistry. Colquhoun and coworkers prepared macrocyclic sulfones via S_NAr of 4,4'-dichlorodiphenyl sulfone with 4,4'-sulfonylbis(thiophenol) under p-HD conditions, as illustrated in Scheme 2.9.[95,96] The mixtures formed by the substitution reactions should have had even-numbered cycles (dimer, tetramer, etc.), as an AA + BB approach was

used, however, cycles made up of odd numbers of units were also formed. It was concluded that these odd numbered cycles formed as a result of redistribution or back-biting during the substitution reactions.[96] In a subsequent communication, Colquhoun and coworkers reported the conversion of the cyclic aryl thioether sulfones to their all-sulfone analogues via oxidation reactions using hydrogen peroxide (Scheme 2.9).[97] The cyclic aryl sulfones may find use as new monomers for ROP, or as π-electron deficient receptors in guest-host chemistry due to the strong electron withdrawing ability of the sulfonyl groups.

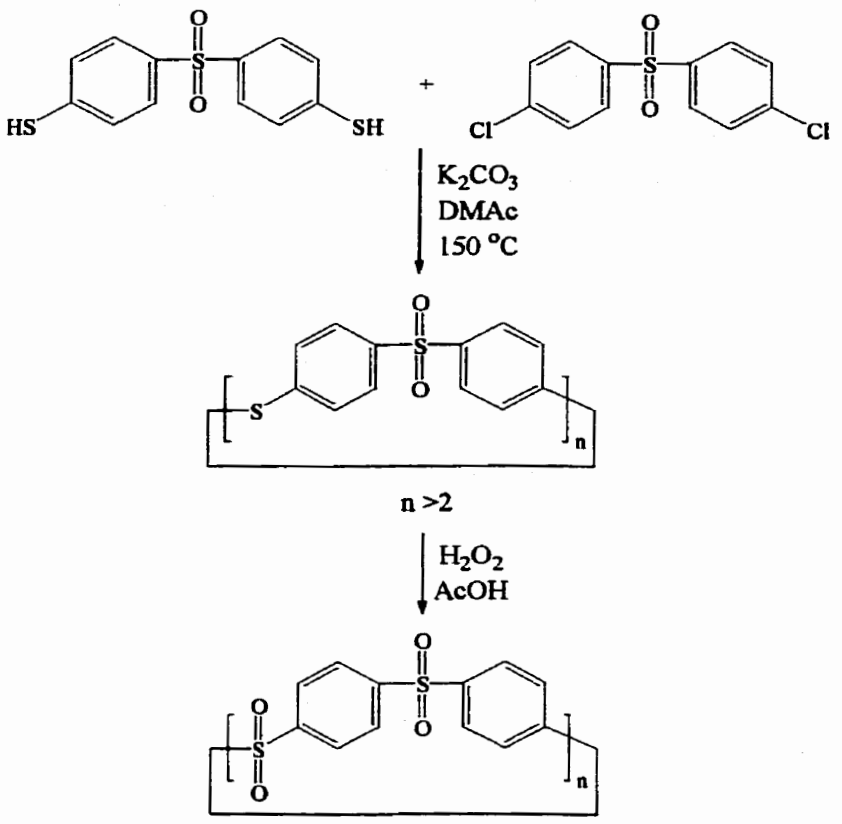

Scheme 2.9: Preparation of cyclic aryl sulfones.

Thus far, all of the cyclization reactions discussed have resulted in the formation of a complex mixture of macrocycles of various sizes and their corresponding linear

oligomers. This is beneficial for ring opening polymerization (ROP) experiments because the melt temperature of the mixture is generally lower than that of the single-sized macrocycles, however, it is disadvantageous because it may be difficult to remove small amounts of unwanted linear oligomers from the mixture. As well, the study and control of the ROP process is difficult when dealing with a mixture of cyclic products. Thus, Gibson and coworkers have investigated the preparation and characterization of single-sized macrocycles via nucleophilic substitution reactions.[74,97,98] It is known that the formation of the 1 + 1 cyclic product (dimer) is most favored, however, the rigid nature of aromatic macrocycles can discourage the cyclization of short linear units.[74] To amend this problem, Gibson has proposed that macrocyclization of long, linear precursors would reduce the ring strain associated with the resulting cyclic product, and thus give the 1 + 1 macrocycle in high yields. Numerous elongated biphenols were prepared via the mulitstep synthetic strategy outlined in Scheme 2.10. As an example, protection of one of the hydroxyl groups of bisphenol A was achieved by reaction with benzyl bromide, to give compound **1**. Subsequent reaction of **1** with 4-chlorophenyl sulfone yielded the benzyl ether capped sulfone, which was then subjected to palladium catalyzed hydrogenation to remove the protecting groups to give the elongated biphenyl oligomer terminated with two hydroxyl groups (**2**).

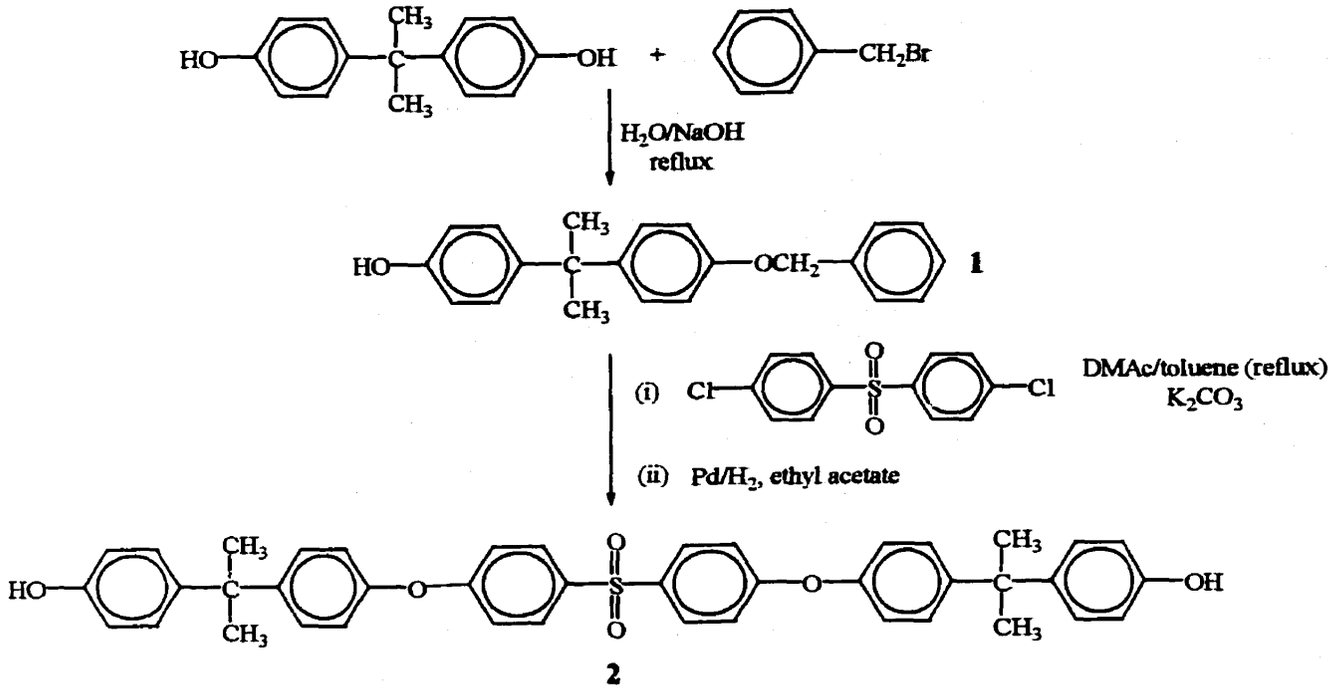

Scheme 2.10: Synthesis of elongated monomers for the preparation of aromatic macrocycles.

Single-sized macrocycles were then prepared via S_NAr reactions of halogenated aromatic compounds with the elongated monomers under pseudo high-dilution conditions (Scheme 2.11). The resulting dimers contained 35-55 atoms within their cyclic structures, and were isolated in yields ranging from 21-83%. The melt temperatures of these macrocycles were comparable to those of the complex mixtures obtained by others due to the asymmetry associated with them.[7,74]

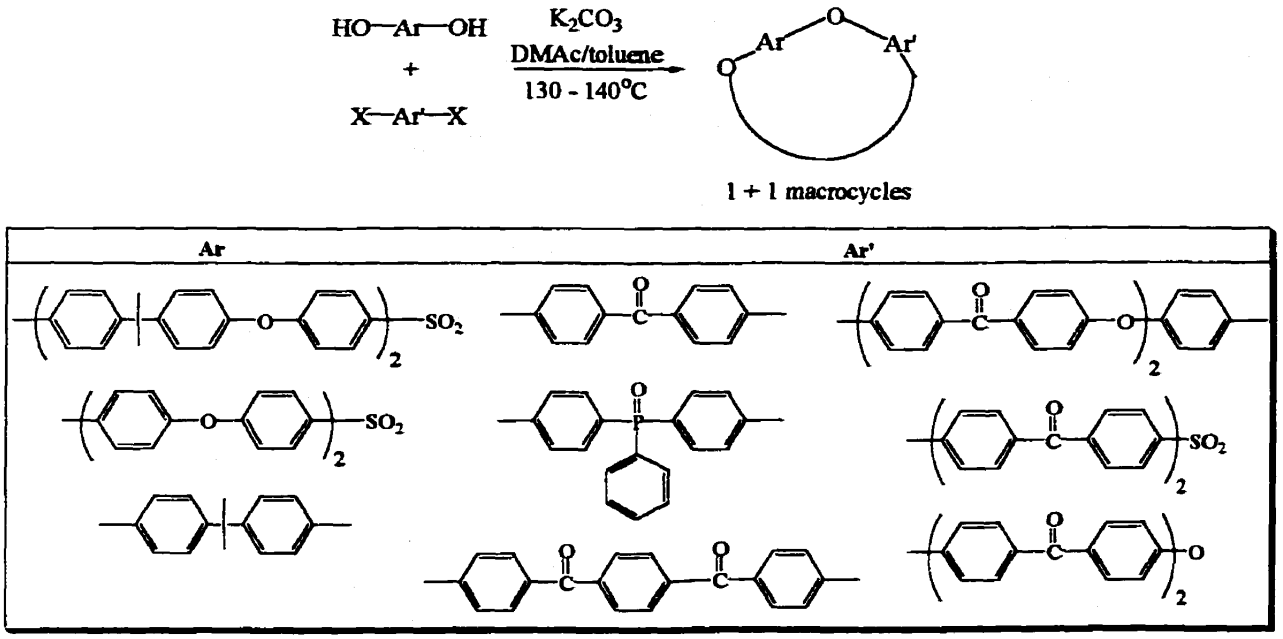

Scheme 2.11: Elongated oligomers approach to the synthesis of aromatic macrocycles.

2.2.2 Catalyzed-Macrocyclization Reactions

In 1990, Colquhoun and coworkers reported the preparation of cyclic aryl ethers using nickel(0)-promoted coupling of aryl halides under p-HD conditions.[99] The chlorobenzoyl-terminated precursor (**2**) of the aromatic macrocycle was prepared via Friedel-Crafts acylation of a linear unit containing terminal benzenes (**1**) with 4-chlorobenzoyl chloride in the presence of aluminum chloride (Scheme 2.12). The macrocyclic product was subsequently formed by Ni(0)-catalyzed coupling of the terminal aryl halides, and isolated in 40% yield. A single crystal of the cyclic aryl ether was obtained, and it was found that the biaryl units were extremely distorted relative to their normal conformation due to the rigidity of the macrocycle. This single-sized cycle

was subjected to ROP in the presence of an anionic initiator to yield the corresponding linear poly(ether ketone), resulting in one of the first examples of successful ROP of a fully aromatic macrocycle.[99]

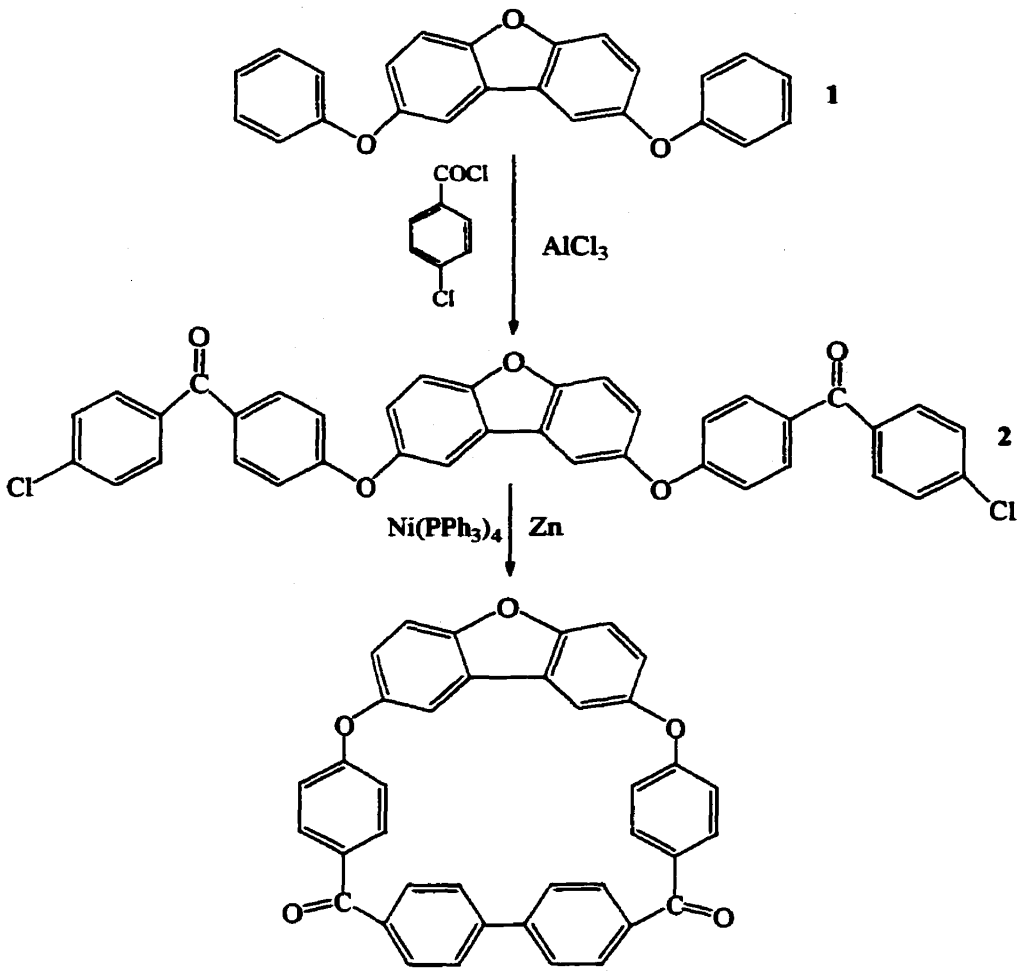

Scheme 2.12: Ni(0)-catalyzed coupling in the preparation of aromatic macrocycles.

Researchers at General Electric have investigated the preparation of aromatic macrocycles containing carbonate functionalities via an amine-catalyzed hydrolysis/condensation reaction.[79-82] This synthetic strategy involved the initial formation of bisphenol A bis(chloroformate) via the phosgenation of bisphenol A,

followed by the cyclization of the linear oligomers in the presence of triethylamine and aqueous sodium hydroxide (Scheme 2.13).

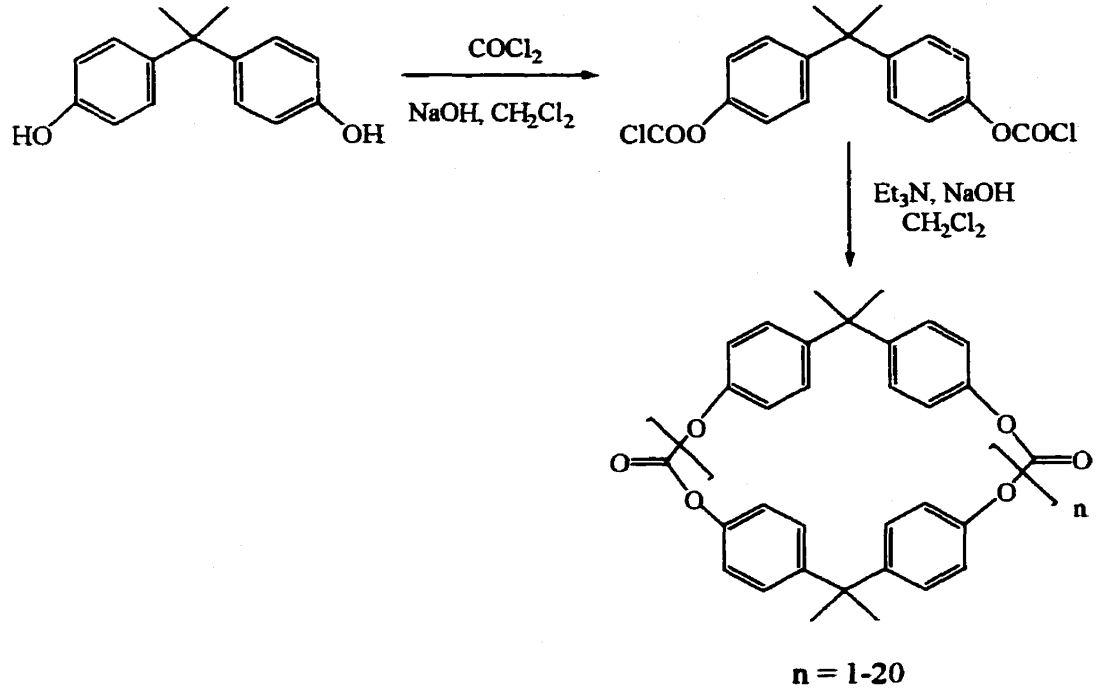

Scheme 2.13: Preparation of mixed aliphatic/aromatic macrocycles.

It was found that the cyclization reactions were dependent on the nature of the acylammonium salt formed from the monosubstitution of bisphenol A bis(chloroformate) with triethylamine.[80] The acylammonium salt could undergo a variety of reactions leading to the formation of either the desired macrocycle products or linear analogues. The synthetic pathway leading to the formation of the cyclic products is shown in Figure 2.2. The acylammonium salt (1) underwent hydrolysis to yield a chloroformate-phenoxide intermediate (2), which could then follow one of two routes, both eventually leading to the formation of the macrocyclic products. The first route involved reaction of

2 with another equivalent of triethylamine to form an acylammonium-phenoxide salt (3), which then underwent cyclization to give the macrocycle. The alternative route involved the condensation of 2 with another molecule of the acylammonium salt (1) to yield a bis(chloroformate) (4), which could be further reacted to yield macrocyclic products or linear oligomers. Any linear oligomers could be reacted in the manner described above, leading to the formation of larger-sized macrocycles.[80]

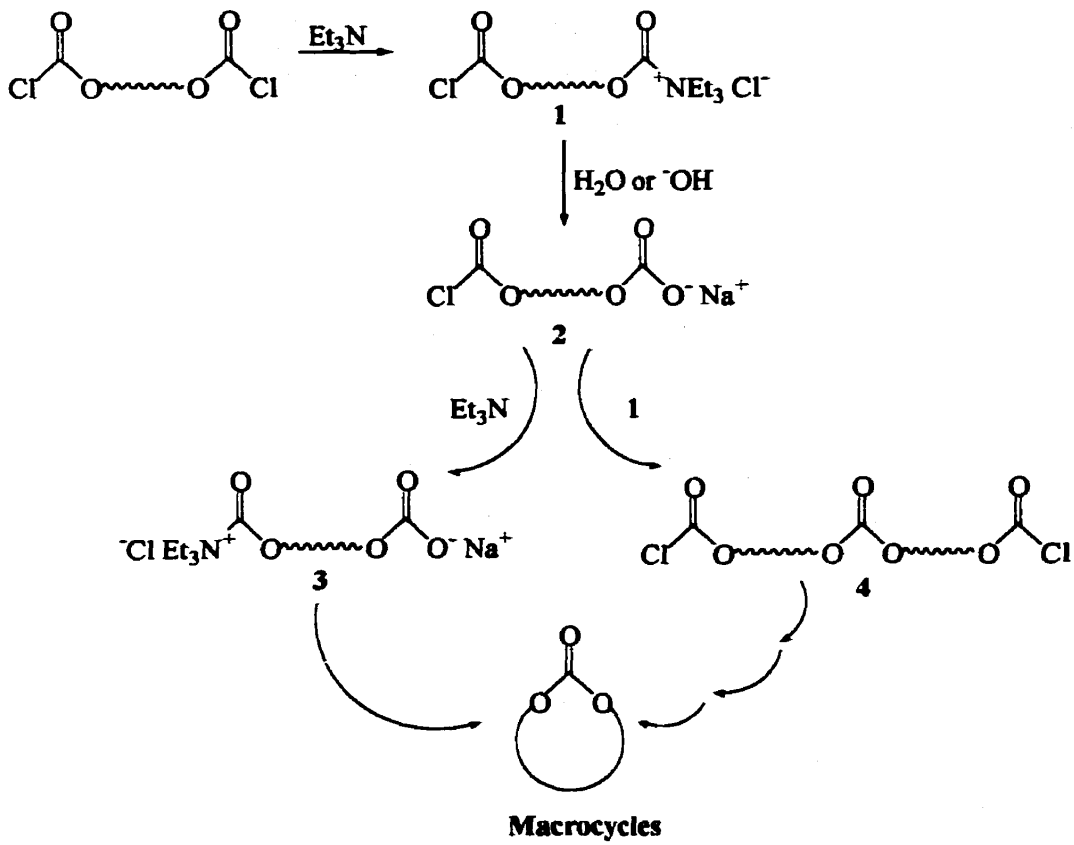

Figure 2.2: Mechanism for amine-catalyzed hydrolysis-condensation reaction.

As illustrated by Figure 2.2, a mixture of cyclic products was obtained, and while the overall yield exceeded 90%, the cyclic dimer (n = 2) was obtained in low yields of 5-

10%. This was attributed to the ring strain associated with this smaller-sized macrocycle, making its formation less favored compared to the larger-sized cyclic products.[80]

2.2.3 Metal-mediated Nucleophilic Substitution Reactions

The use of organometallic reagents in the preparation of macrocyclic products is an area that has received little attention. To date, metal-mediated nucleophilic aromatic substitutions facilitated by pendent chromiumtricarbonyl ($Cr(CO)_3$),[100,101] cyclopentadienylruthenium ($CpRu^+$)[102-104] and cyclopentadienyliron ($CpFe^+$)[105,106] moieties have been utilized in macrocyclization reactions. These reactions are accomplished by the initial π-coordination of a metallic moiety to a dichloroarene, followed by reaction of this complex with a dinucleophile. The strong electron-withdrawing capability of the metal allows these reactions to proceed without the presence of any other electron-withdrawing groups.[24]

Baldoli and coworkers published one of the earliest reports detailing metal-mediated macrocyclization reactions.[100] They reported the preparation of dibenzo-18-crown-6 via substitution of (η^6-1,2-dichlorobenzene)tricarbonylchromium with the sodium salt of diethylene glycol (Scheme 2.14). The $Cr(CO)_3$-complexed macrocycle was not isolated from the reaction mixture but was oxidatively demetallated *in situ* with iodine and crystallized from acetone to give the organic macrocycle in 30% yield. A drawback to this method was that a phase transfer catalyst, tetrabutylammonium bromide (TBAB) was needed for the reaction to proceed successfully.

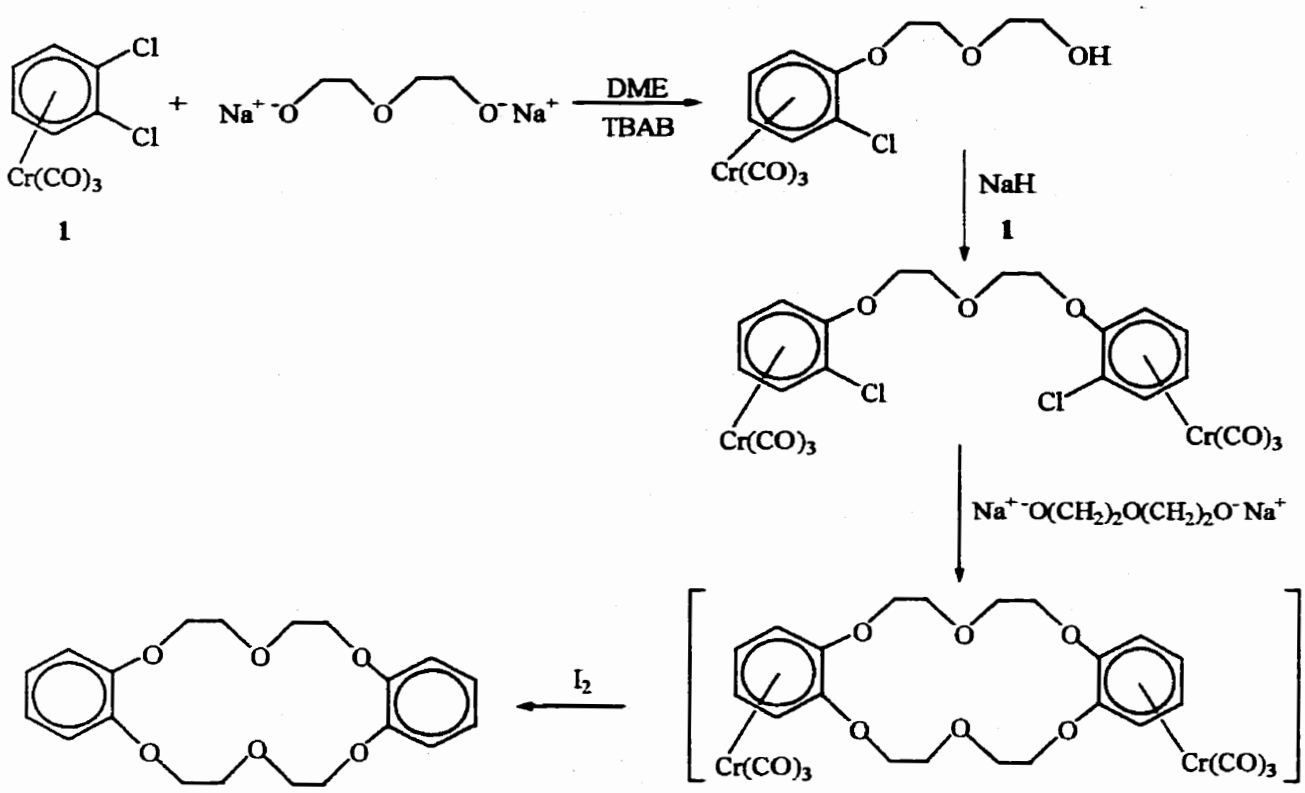

Scheme 2.14: $Cr(CO)_3$-mediated synthesis of dibenzo-18-crown-6.

Prior to this report, other chromium tricarbonyl-complexed macrocycles had been prepared, however, the metal moiety was not directly involved in the cyclization reaction but simply complexed to the macrocycle products.[101] This was achieved via the ligand exchange reactions of chromium hexacarbonyl and an appropriate crown ether in a refluxing solution of isooctane for 10 days. The resulting organometallic macrocycles were isolated in modest yields of 30%. In recent years, these chromium-complexed macrocycles (**2.4**) have found applications as molecular sensors for the complexation of alkali metal cations.[107]

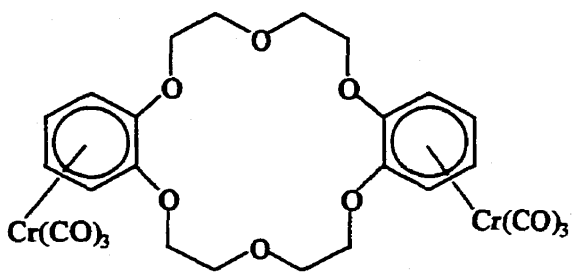

$Cr(CO)_3$(benzo[18]crown-6)

2.4

Reports utilizing temporary complexation of cyclopentadienylruthenium or cyclopentadienyliron moieties to assist in the formation of macrocycles via nucleophilic substitution reactions have surfaced in the last five years.[102-104] Janetka and coworkers have explored a route to the preparation of cyclic biphenyl ether peptides in which the cyclopentadienylruthenium moiety was used to activate chlorinated arenes towards substitution reactions (Scheme 2.15).[103,104] They prepared a linear tripeptide containing a terminal $CpRu^+$-complexed chlorobenzene at one end and a terminal phenoxy group at the other (**1**), which readily underwent intramolecular cyclization to yield the organometallic macrocycle (**2**) in good yields (58-66%). The favored cyclization of the macrocyclic product was attributed to the intramolecular preorganization of the electron-poor π-complexed aromatic ring and the electron-rich phenol ring in the linear precursor. The desired cyclic peptide was then obtained by decomplexation of the metallic moiety from the macrocycle via photolytic techniques.[103,104]

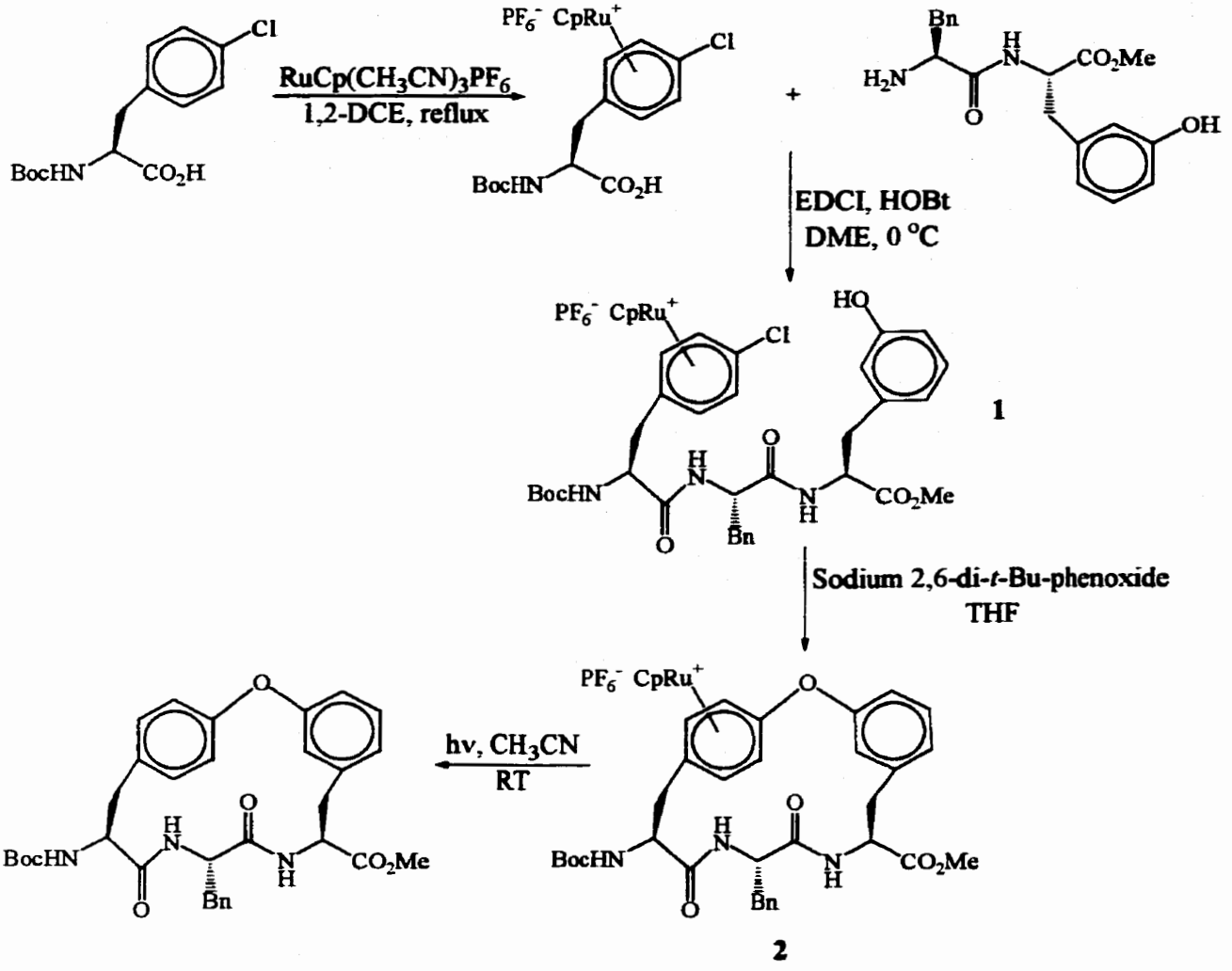

Scheme 2.15: Use of organoruthenium chemistry in the synthesis of macrocycles.

Meanwhile, Comba and coworkers made use of cyclopentadienyliron-mediated S_NAr reactions for the preparation of tetrathiamacrocycles, which are sulfur derivatives of crown ethers.[105] As illustrated below, η^6-1,2-dichlorobenzene-η^5-cyclopentadienyliron hexafluorophosphate was reacted with 3,7-dithianonane-1,9-dithiol at 60 °C for 24 hours to give the organic thiamacrocycle in 30% yield (Scheme 2.16). The organometallic

macrocycle was not isolated but demetallated *in situ*, as Comba and coworkers were interested only in the organic derivatives, as the binding properties of the oxygenated derivatives (crown ethers) are well-known.

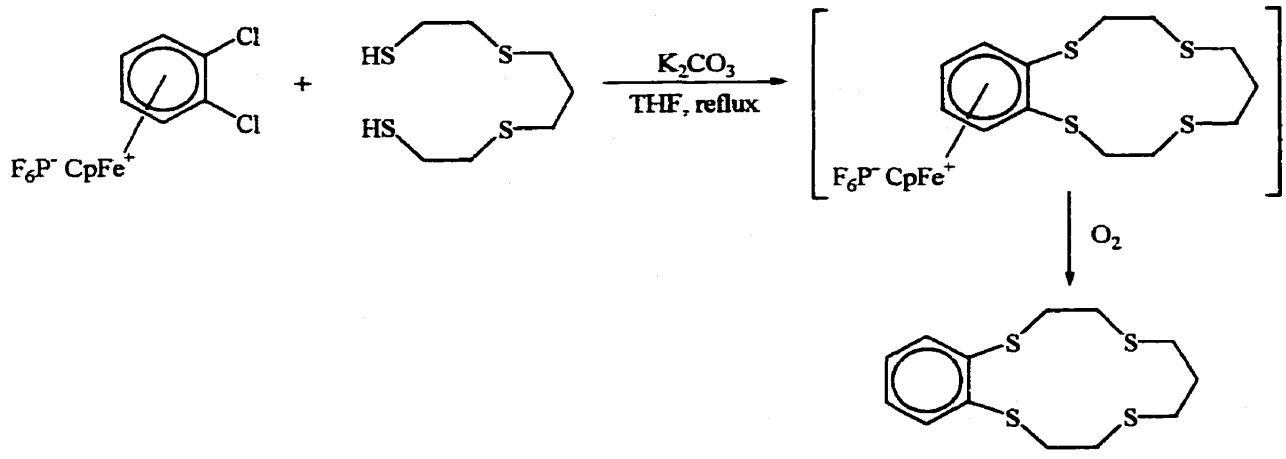

Scheme 2.16: Macrocycles prepared via $CpFe^+$-mediated S_NAr reactions.

2.3 Ring-opening Polymerizations

Engineering thermoplastics such as poly(aromatic ethers), poly(aromatic sulfones), poly(phenylenesulfide) and poly(etheretherketone) are industrially important as a result of their high thermal stability and excellent resistance to chemical solvents.[14,40] These polymers are usually synthesized via step-growth condensation polymerizations, where chain ends react together resulting in the loss of a small molecule such as water or sodium chloride.[1,3] Unfortunately, the processability of these polymers is hindered due to their high melt viscosity and low solubility in common organic solvents. In recent years, the ring-opening polymerization (ROP) of cyclic monomers has been employed for the production of thermally stable polymers.[7,68-71] The appeal to this methodology arises

from the inherent low melt viscosities of the cyclic monomers combined with the ability to control their ROP in the melt, without the release of harmful byproducts.

The ROP of macrocycles is an entropically-driven process in which an equilibrium between the breaking of linkages in the cycles and the re-forming of bonds to generate the polymeric species is achieved at high concentrations, as these are generally solvent-free reactions.[71] Overall, the process involves the reorganizing of bonds and linkages, thus no heat or volatiles are given off, and the molecular weight of the end product is determined by the number of cycles present at the beginning of the reaction. The low viscosities of the cyclic monomers are also an attractive feature because they allow the polymers to be processed using shape-forming methods such as reinforced reaction injection molding or various coating processes.[7,71] In contrast, the processing of polymers prepared using traditional condensation reactions is more difficult as a result of their high melt viscosities.

Generally, ROP of the cyclic precursors has been accomplished in the melt at temperatures above 300 °C using anionic initiators such as 4-hydroxybenzophenone (KOPhBz), potassium carbonate (K_2CO_3) and cesium fluoride (CsF) (Figure 2.3). As well, the ROP of cyclic aryl ether thioethers has also been accomplished in the melt via a free-radical process in the presence of elemental sulfur or a disulfide initiator (Figure 2.3).[7]

The bond in the cycle that breaks depends on the functionalities present within its structure. For example, in cyclic aryl ethers, it has been found that cleavage of the ring occurs at the etheric oxygen.[7,68,71] In cyclic aryl ether ketones, Colquhoun and others have demonstrated that ether linkages activated by *para* carbonyl groups are susceptible

to nucleophilic attack by initiators.[99,108] The same *p*-activation of a sulfide linkage was also observed in the ROP of cyclic aryl thioether ketones in the presence of a phenoxide initiator.[69]

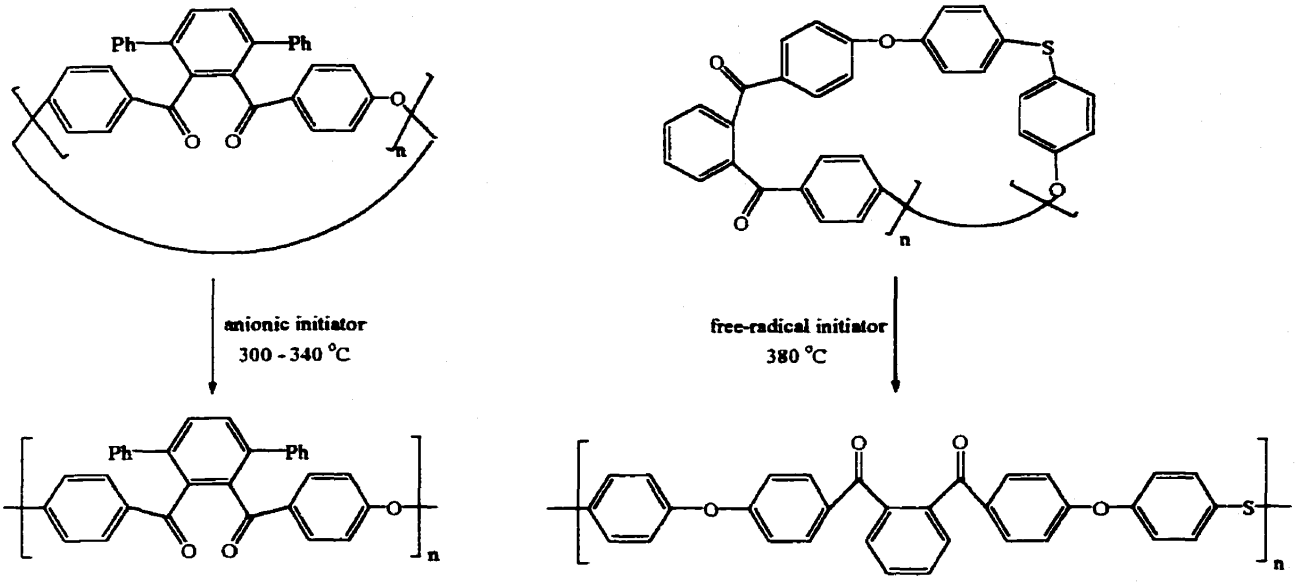

Figure 2.3: Examples of ring-opening polymerizations of aromatic macrocycles.

Differential scanning calorimetry (DSC) is a useful tool for analyzing the ROP of macrocycles.[69,108] For example, the conversion of cyclic products into their corresponding linear polymers can be followed using DSC, as illustrated in Figure 2.4.[69] The first heating scan (a) shows a sharp endothermic peak in the range of 300-350°C, which represents the melt temperature (T_m) of the pure cyclic precursor. Prior to the polymerization of a sample, the T_m must be known, as the reaction must be carried out above this temperature. The second curve in the thermogram is the T_m of the macrocycle in the presence of an initiator (2 wt%). Once heated above the T_m, the macrocycle opens in the presence of the initiator and polymerization of the cycles occurs. The final heating scan (c), is of the linear polymer produced directly following ROP of the macrocycle. It

can be seen that the T_m of the macrocycle is absent in this scan, indicating that all macrocycle molecules have been converted to polymer species, and a new endothermic peak has appeared at 110°C. This peak is the glass transition temperature (T_g) of the resulting linear polymer.[69]

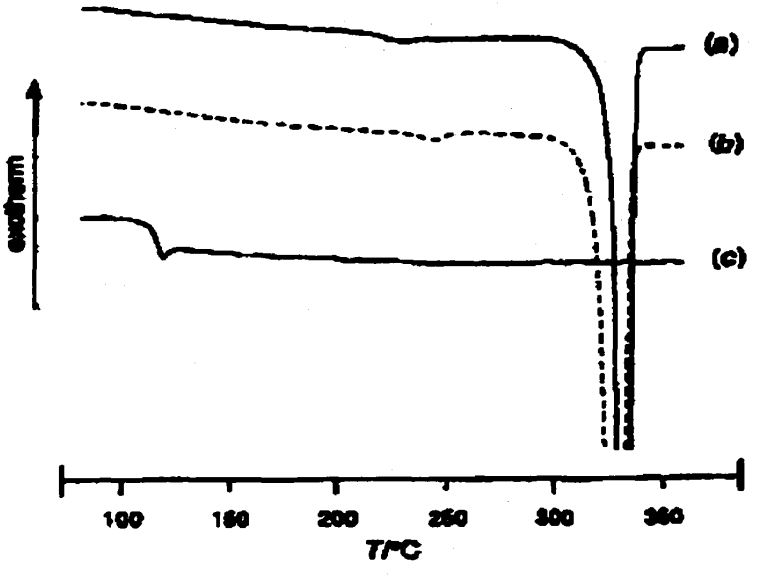

Figure 2.4: Thermograms showing the conversion of cyclic monomer to linear polymer.

2.4 Results and Discussion

Numerous oligomeric and polymeric species have been successfully prepared via nucleophilic substitution reactions facilitated by the cyclopentadienyliron ($CpFe^+$) moiety.[14,29-44] This organoiron methodology utilizes mild reaction conditions, and the resulting organoiron complexes can be obtained in excellent yields. It has been shown that using $CpFe^+$-mediated S_NAr reactions, diiron complexes containing two chlorine atoms can be isolated.[34] Using these complexes, asymmetric cyclic compounds were prepared following ring closure reactions with 4,4'-biphenol. Once the metallated macrocycles were formed, removal of the metal was accomplished using photolytic techniques. The resulting organic macrocycles were subsequently subjected to ROP to yield thermally stable polyaromatic ethers.

2.4.1 Ring Closure Reactions

It has been determined that various factors such as reaction concentration and time, as well as the reactivity and structure of the reactants can be manipulated to promote the intramolecular ring closure of aromatic macrocycles over the intermolecular formation of linear oligomers.[73,74] The reactants used in the macrocyclization reactions were chosen to minimize the ring strain of the resulting aromatic macrocycles to permit ring closure, while still maintaining the rigidity of the compounds, which allows for their ring-opening polymerization.[7,74] For these reasons, *meta*-dichlorobenzene complex rather than the *ortho*- or *para*-substituted complexes were used to form the reactants. The starting bimetallic species (**3a-d**) had been previously prepared using $CpFe^+$-mediated substitution reactions, and their structures fully characterized (Scheme 2.17).[109]

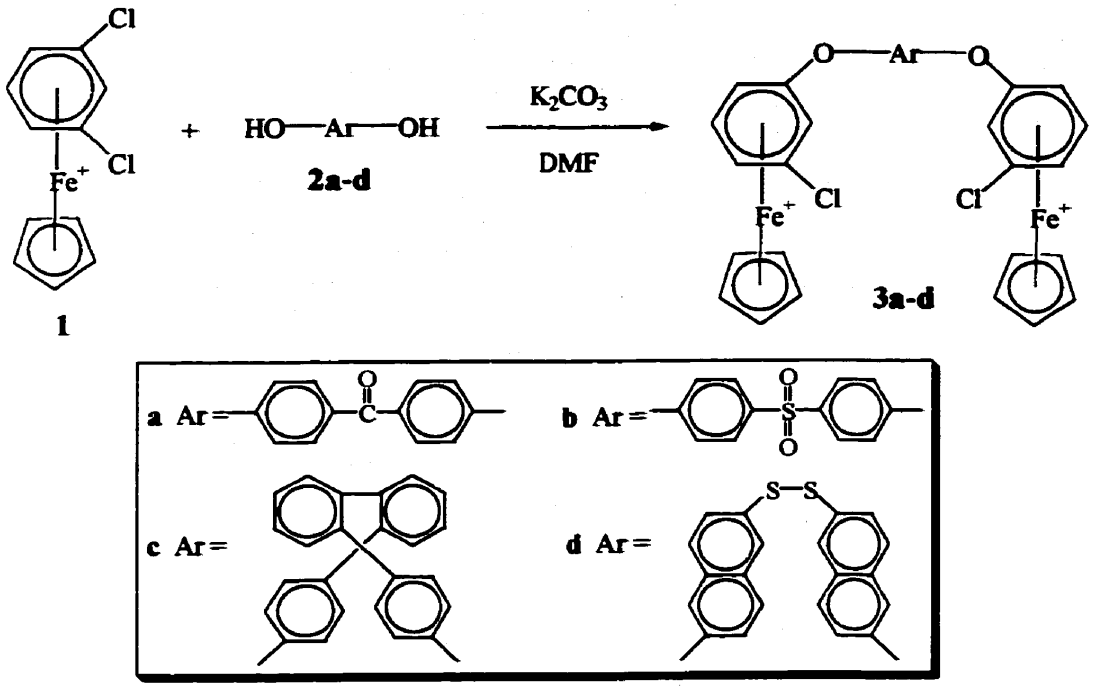

Scheme 2.17: Preparation of starting bimetallic complexes (3a-d).

Ring closure reactions via nucleophilic substitution using an AA + BB approach were achieved by reacting an equimolar amount of 4,4'-biphenol (**4**) with a diiron complex (**3a-d**) in the presence of a weak base (Scheme 2.18). This reaction yielded mixtures of the metallated macrocycles (**5a-d**) and linear oligomers. NMR was used to determine that complete reaction of the starting materials had taken place. Overall, an increase in the complexity of the spectra was observed following the ring closure reactions (Figure 2.5). The Cp resonances of the macrocyclization products shifted upfield (δ 5.15-5.36 ppm) relative to the peaks in the starting complexes' spectra (δ 5.33-5.41 ppm), due to the formation of the aromatic ether linkages upon displacement of the chloro groups. The formation of linear oligomers during the ring closure reactions was supported based on the appearance of phenolic proton resonances (δ 8.5 ppm) in the ^{1}H NMR spectra, as well as the appearance of more than one resonance for the Cp protons.

MS data further supported the isolation of a mixture of products following the ring closure reactions as molecular ion peaks and fragmentation patterns were observed for both macrocycles and linear oligomers. Analysis of the mass spectra also showed that the only cyclized product that formed during the reactions was the 1 + 1 macrocycle. This is in contrast to other S_NAr approaches, which usually lead to the formation of various sized macrocycles when pseudo-high dilution conditions are employed.[7]

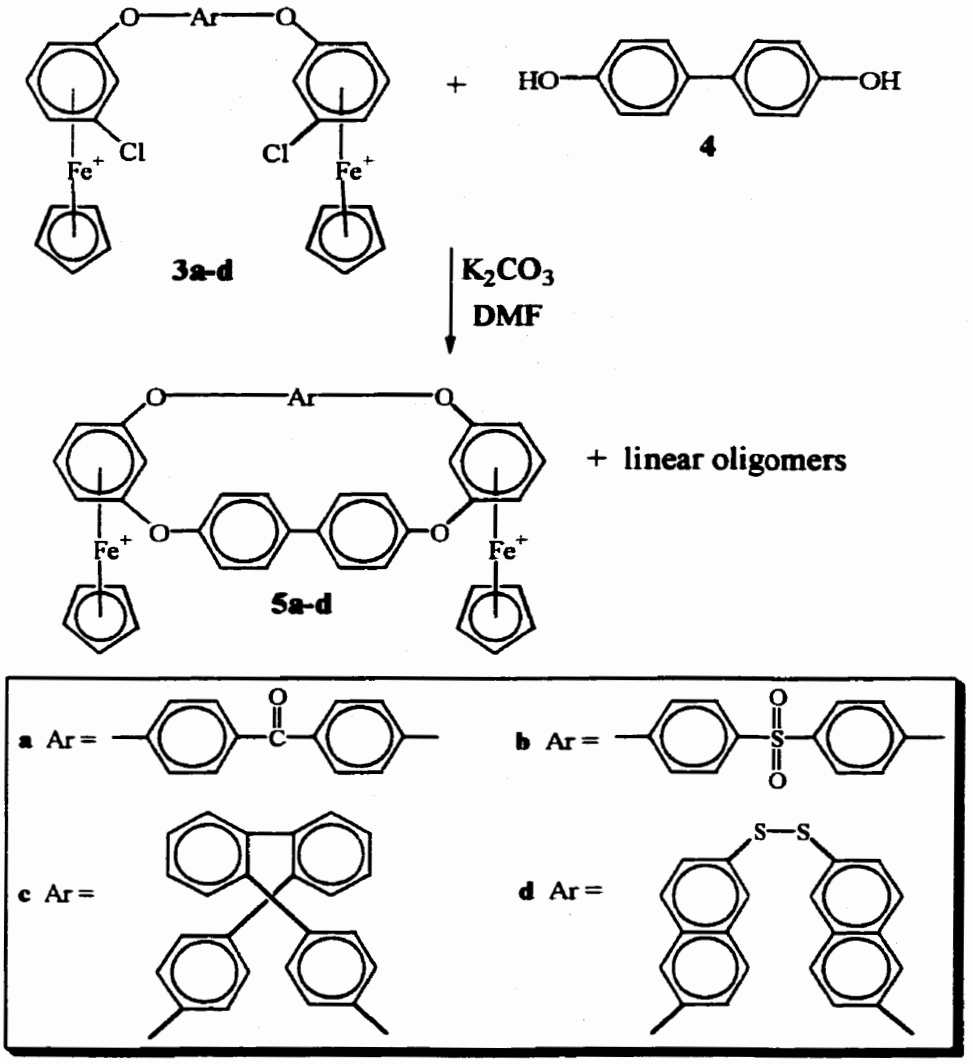

Scheme 2.18: Aromatic macrocycles (**5a-d**) prepared via $CpFe^+$-mediated S_NAr.

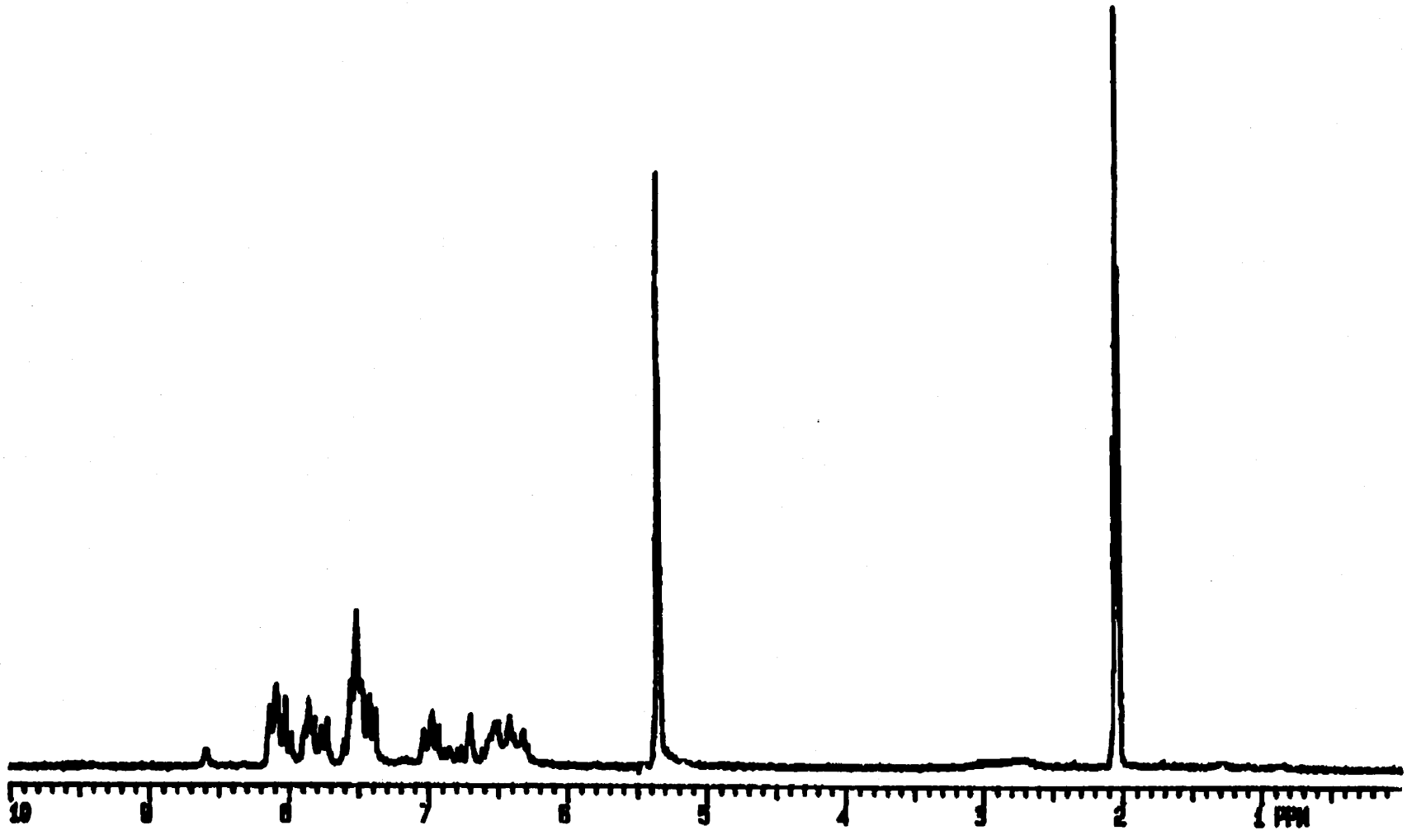

Figure 2.5: ^{1}H NMR spectrum of macrocycle **5a** and corresponding linear oligomers.

2.4.2 Isolation of Cyclic Aryl Ethers

Cleavage of the metal moieties from the macrocycles **5a-d** was accomplished using photolytic techniques to yield mixtures of the organic macrocycles and their linear oligomers. Isolation of the macrocyclic dimers from the mixtures was achieved via column chromatography (Figure 2.6). The rigid cyclic aryl ethers (**6a-d**) were obtained in yields ranging from 30-68%, and were characterized using NMR, IR and MS (Tables 2.1 and 2.2).

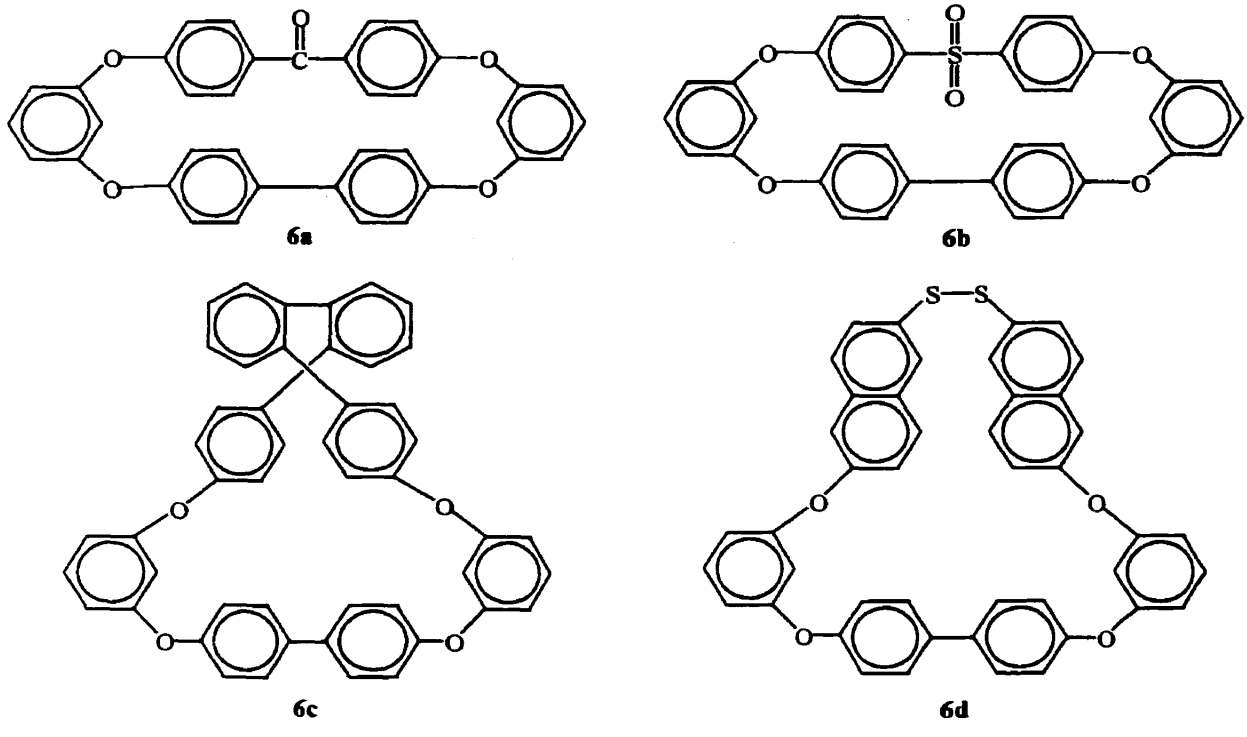

Figure 2.6: Isolated cyclic aryl ethers (**6a-d**).

The ^{1}H NMR spectrum of cyclic aryl ether **6b** is displayed in Figure 2.7, as a representative example of the macrocycles obtained. Based on the structure of the macrocycle, it was anticipated that all of the peaks in the spectrum would appear in the downfield region around 7 ppm, however, a triplet was observed at 6.17 ppm. This

resonance represented the two aromatic inner-ring protons (Ha) of the macrocycle (**2.6**).

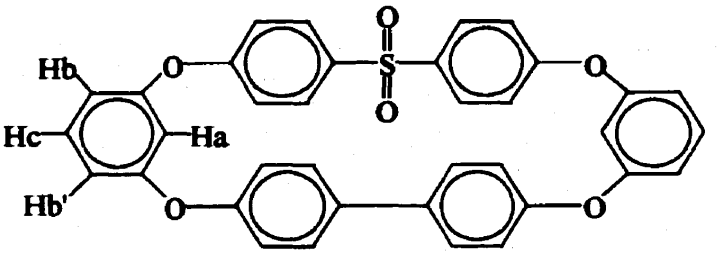

2.6

These protons appeared as a triplet due to long-range coupling with the two nonequivalent protons on the *meta*-substituted aromatic rings (Hb and Hb'). As well, the peak resonated at a much higher field than the other aromatic protons within the molecule due to the shielding cones they resided in, which were caused by the two adjacent *para*-substituted aromatic rings (**2.7**).[110,111] These shielding cones were a direct result of the structural conformation of the macrocycle, which was suggested to be saddle-shaped (**2.8**).[66,110,111] The saddle-shaped conformation of the macrocycle caused an anisotropic shielding of the Ha protons, which resulted in their appearance upfield in the ^{1}H NMR spectra. The remainder of the aromatic protons (ArH) appeared between 6.80 and 7.80 ppm in the spectrum (Figure 2.7).

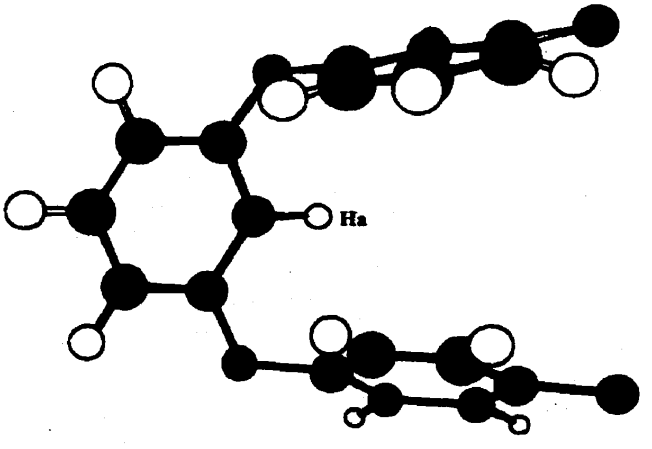

2.7

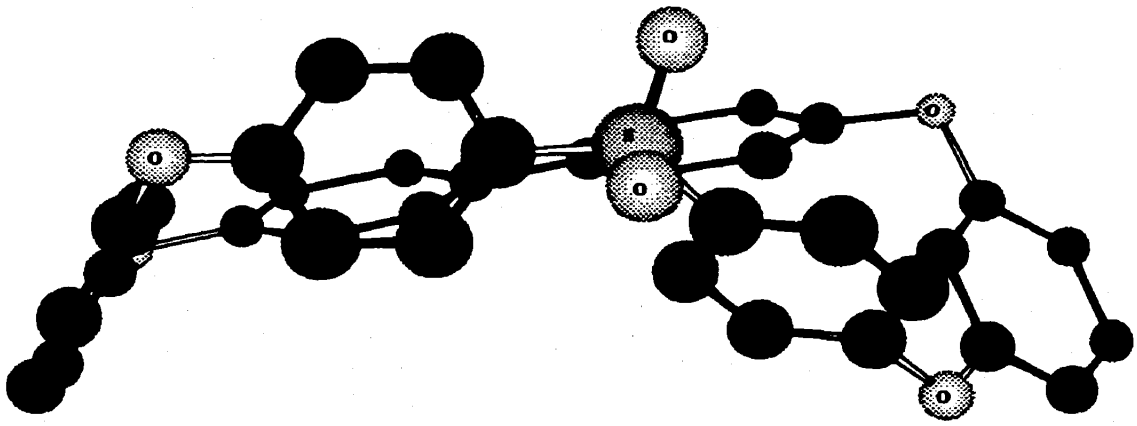

2.8

Analyses of the 13C NMR spectra were also instrumental in determining successful isolation of the cyclic aryl ethers. These spectra were recorded as decoupled attached proton tests (ATP). In this type of ^{13}C NMR experiment, all carbon atoms in the molecule are represented by a single peak, where quaternary and methylene carbons appear in an upward direction, and methine and methyl carbons point downwards. The ^{13}C NMR spectrum for **6b** is shown in Figure 2.8. The symmetric nature of macrocycle **6b** resulted in a relatively simple ^{13}C NMR spectrum. The aromatic carbons (ArCH) appeared as eight downward-pointing peaks in the range of 108-132 ppm, while the 6 nonequivalent quaternary aromatic carbons (ArC) appeared as six peaks pointing upwards between 135 and 162 ppm, two of which resonated at very close chemical shifts (δ 135.47 and 135.62 ppm).

Single-crystal X-ray structures of two of the cyclic aryl ethers (**6a** and **6b**) were obtained, providing conclusive proof that cyclic dimers were formed during the macrocyclization reactions. The crystallographic data, including bond angles and bond

lengths, as well as the structural refinement for two of the cyclic aryl ethers are listed in Appendices 2.1 and 2.2. The molecular structures of **6a** and **6b** are shown in Figures 2.9 and 2.10, respectively. It has previously been demonstrated that the structural rigidity associated with aromatic macrocycles can cause numerous distortions in the conformations and bond angles of the linkages within the rings.[99,112-114] For example, it has been found that biaryl linkages within aromatic macrocycles possess a remarkable degree of flexibility, which is not usually expected of this nominally rigid unit.[99,115] An observable twist of the rings within the normally planar biaryl unit can been seen in the crystal structure of **6a** in Figure 2.9, illustrating the flexibility of this unit. Furthermore, distortions of the bond angles of the diaryl units adjacent to the carbonyl in the macrocycle were observed. These linkages adopted a conformation such that one aromatic ring lied in the plane of the C-O-C bridge (average torsion angles 23°), while the second ring lied at a slightly higher angle relative to the plane (average torsion angles 36°).[112] This arrangement led to an enlargement of the theoretically trigonal bond angles of these linkages, C(13)-C(14)-O(2)=125.1° and C(22)-C(21)-O(2)=123.3°. Selected torsion angles for the molecular structure of macrocycle **6a** are listed in Table 2.3.

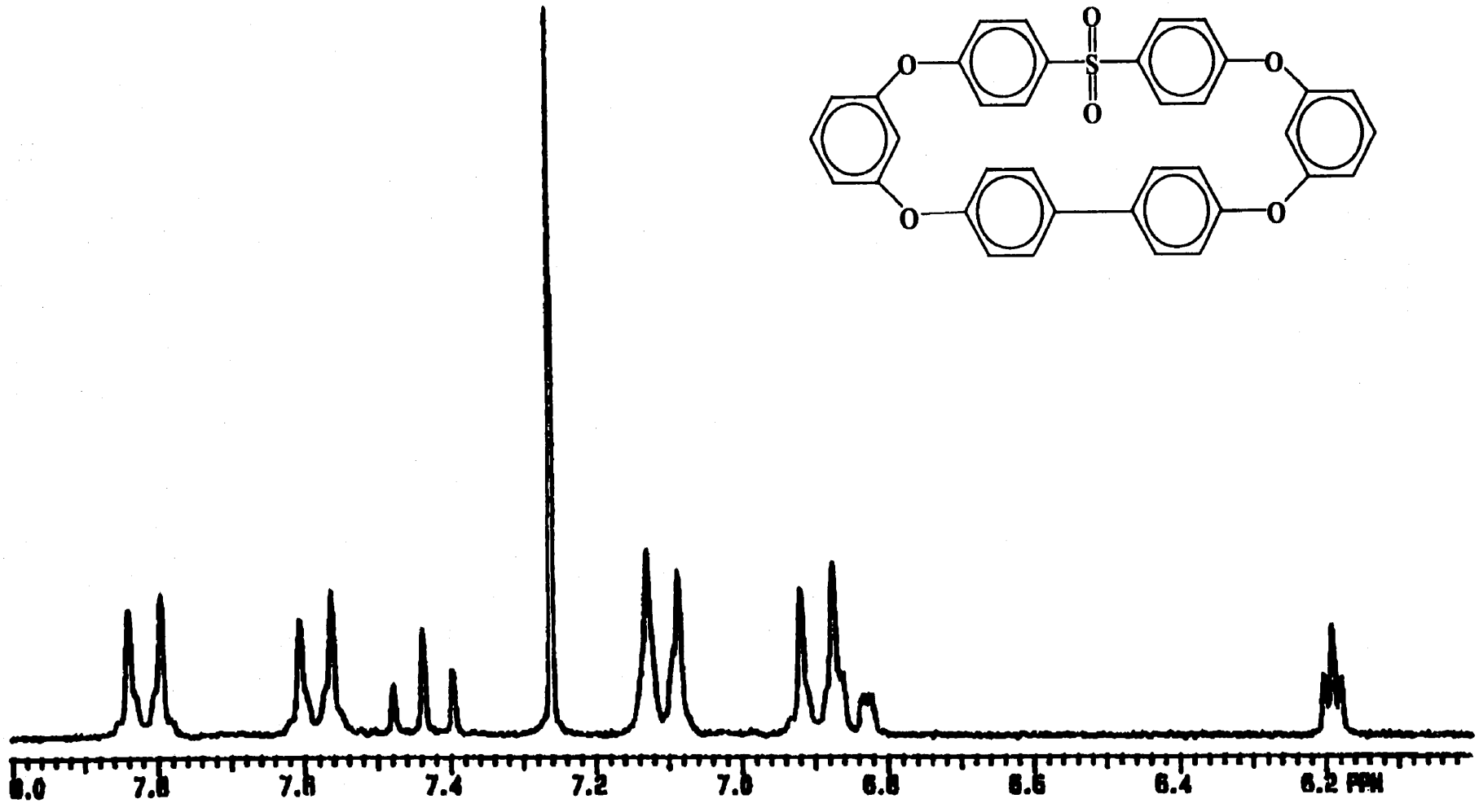

Figure 2.7: ^{1}H NMR spectrum of macrocycle **6b**.

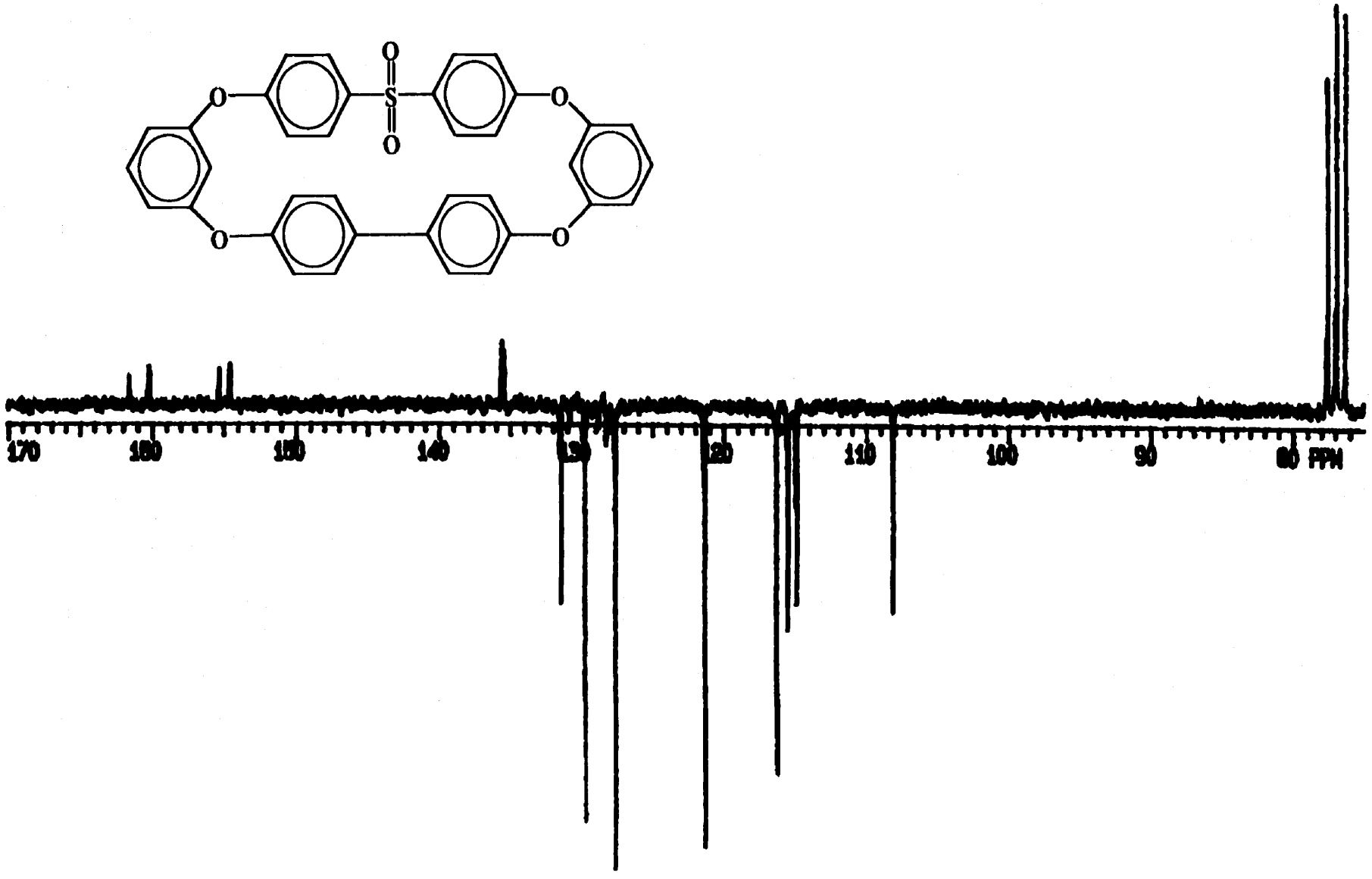

Figure 2.8: ^{13}C NMR spectrum of macrocycle **6b**.

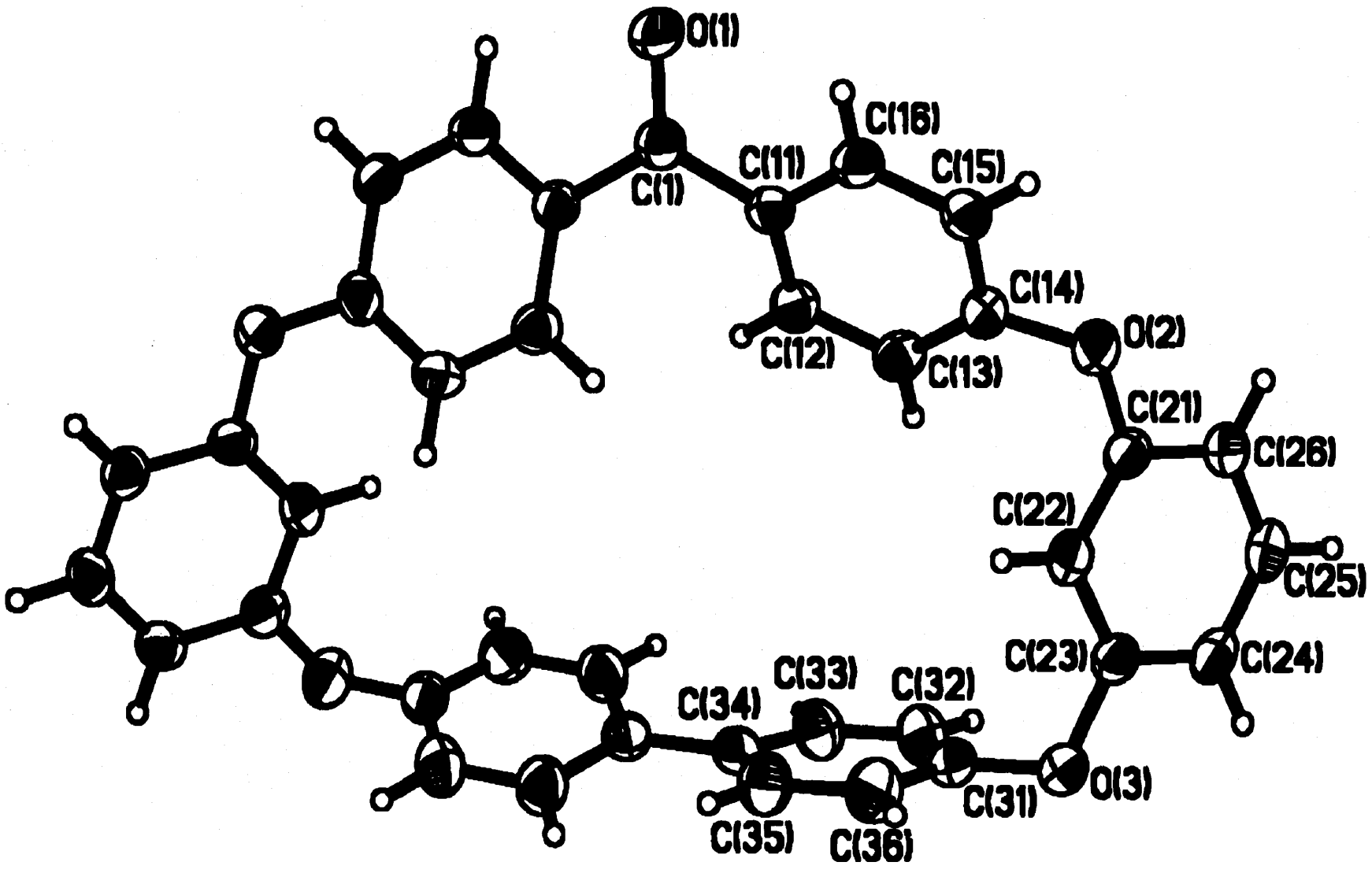

Figure 2.9: Molecular structure of macrocycle **6a**.

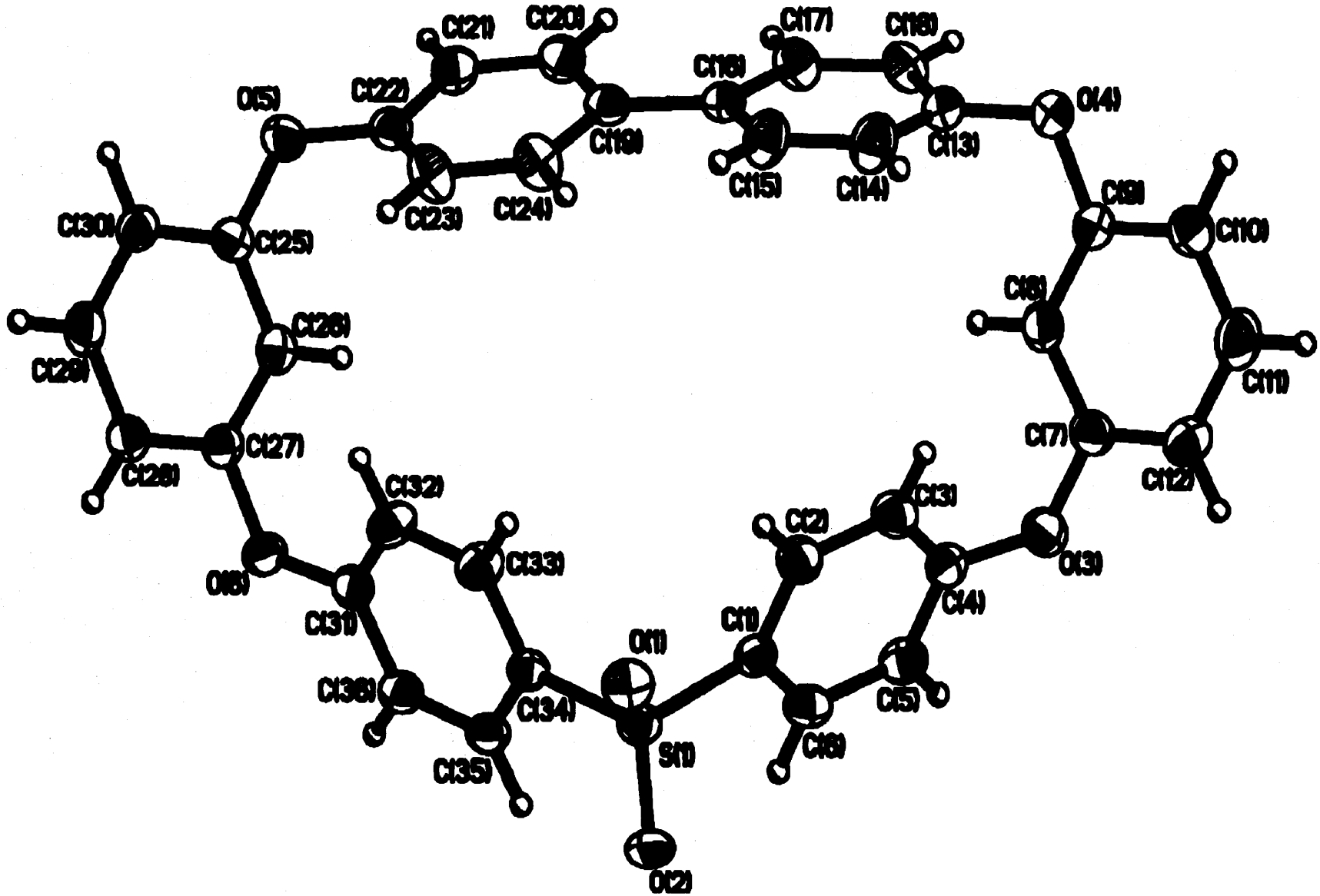

Figure 2.10: Molecular structure of macrocycle **6b**.

Table 2.1a: ^{1}H NMR, Yield, IR and MS data for macrocycles **6a** and **6b**.

MACROCYCLE	PRODUCT YIELD	ArH	IR ABSORBANCIES (cm^{-1})	MS DATA M^+ (m/z)
6a	0.0823 g (30%)	6.21 (t, J = 2.30, 2H) 6.87 (m, 2H) 6.92 (m, 2H) 6.96 (d, J = 8.71, 4H) 7.03 (d, J = 8.67, 4H) 7.38 (t, J = 8.10, 2H) 7.43 (d, J = 8.71, 4H) 7.59 (d, J = 8.75, 4H)	--- (CO)	548
6b	0.0906 g (31%)	6.17 (t, J = 2.24, 2H) 6.80-6.81 (m, 2H) 6.88 (d, J = 8.99, 4H) 7.09 (d, J = 8.46, 6H) 7.42 (t, J = 8.14, 2H) 7.56 (d, J = 8.17, 4H) 7.80 (d, J = 8.92, 4H)	1216 (SO_2)	584

Note: --- Denotes data not obtained.
NMR spectra recorded at 200 MHz.

Table 2.1b: ^{1}H NMR, Yield, IR and MS data for cyclic aryl ethers **6c** and **6d**.

MACROCYCLE	PRODUCT YIELD	ArH	IR ABSORBANCIES (cm^{-1})	MS DATA M^{+} (m/z)
6c	0.2328 g (68%)	6.12 (t, *J* = 2.3, 2H) 6.71 (d, *J* = 8.8, 5H) 6.79 (d, *J* = 2.0, 1H) 6.84 (d, *J* = 2.2, 1H) 6.88 (d, *J* = 2.3, 1H) 6.94 (d, *J* = 8.8, 4H) 7.00 (br. s, 1H) 7.06 (d, *J* = 8.7, 5H) 7.14 (d, *J* = 1.8, 1H) 7.25-7.38 (m, 7H) 7.58 (d, *J* = 8.7, 2H) 7.73 (d, *J* = 7.7, 2H)	---	684
6d	0.0822 g (24%)	6.35 (t, *J* = 2.14, 2H) 6.93 (d, *J* = 8.79, 5H) 6.99 (d, *J* = 2.32 Hz, 2H) 7.10 (d, *J* = 2.48, 1H) 7.14 (d, *J* = 2.49, 2H) 7.19 (d, *J* = 2.28, 2H) 7.33 (d, *J* = 8.52, 4H) 7.42 (t, *J* = 8.17, 2H) 7.58 (br. s, 4H) 7.62 (d, *J* = 8.87, 2H) 7.88 (br. s, 2H)	---	684

Note: --- Denotes data not obtained.
NMR spectra recorded at 200 MHz.

Table 2.2a: ^{13}C NMR data for cyclic aryl ethers **6a** and **6b**.

MACROCYCLE	quaternary ArC	ArCH	OTHERS
6a	132.68 136.51 156.43 156.86 159.31 160.07	106.69 113.72 114.14 118.25 121.04 128.19 131.06 131.63	182.85 (CO)
6b	135.47 135.62 154.55 155.30 160.27 161.63	108.10 114.97 115.55 116.34 121.39 127.65 129.80 131.51	---

Note: NMR spectra recorded at 50 MHz.

Table 2.2b: ^{13}C NMR data for cyclic aryl ethers **6c** and **6d**.

MACROCYCLE	quaternary ArC	ArCH	OTHERS
6c	136.26 139.78 139.85 152.20 154.58 156.35 158.16 160.04	105.79 112.88 112.97 119.24 120.21 120.29 121.40 125.53 127.53 127.78 127.83 128.83 129.42 130.69	64.41*
6d	130.16 132.41 133.35 135.54 154.84 155.78 157.60 158.09	107.61 113.90 115.14 115.23 118.76 119.88 125.63 125.84 128.15 129.37 131.14	---

Note: NMR spectra recorded at 50 MHz.
* Denotes a quaternary carbon.

Table 2.3: Selected torsion angles (Deg) for macrocycle **6a**.

C(1)-C(11)-C(12)-C(13)	175.18 (11)	C(31)-O(3)-C(23)-C(22)	47.75 (17)
C(21)-O(2)-C(14)-C(13)	-23.3 (2)	C(21)-C(22)-C(23)-O(3)	178.89 (12)
C(21)-O(2)-C(14)-C(13)	161.17 (12)	O(3)-C(23)-C(24)-C(25)	-178.93 (12)
C(21)-O(2)-C(14)-C(15)	-174.12 (12)	O(2)-C(21)-C(26)-C(25)	173.72 (12)
O(2)-C(14)-C(15)-C(16)	174.19 (12)	C(23)-O(3)-C(31)-C(36)	-114.24 (14)
C(1)-C(11)-C(16)-C(15)	-175.97 (11)	C(23)-O(3)-C(31)-C(32)	68.19 (16)
C(14)-O(2)-C(21)-C(22)	-36.9 (2)	O(3)-C(31)-C(32)-C(33)	-179.90 (13)
C(14)-O(2)-C(21)-C(26)	148.81 (12)	C(32)-C(33)-C(34)-C(34)#1	175.39 (11)
O(2)-C(21)-C(22)-C(23)	-174.59 (12)	C(34)#1-C(34)-C(35)-C(36)	-175.66 (11)
C(31)-O(3)-C(23)-C(24)	-135.22 (13)	O(3)-C(31)-C(36)-C(35)	179.62 (12)

2.4.3 Ring-opening Polymerization of Cyclic Aryl Ethers

The ring-opening polymerization (ROP) of the cyclic aryl ethers was achieved above the melt temperature (T_m) of the macrocycles in the presence of a nucleophilic initiator. In comparison to traditional routes used to prepare polyaromatic ethers, ROP is advantageous because it is a solventless process that does not result in the release of harmful byproducts.[7] Prior to polymerization, the T_m values of the macrocycles were determined using differential scanning calorimetry (DSC). It was found that the cycles were highly crystalline materials that underwent melting at temperatures above 350°C.

As an example, ROP of macrocycle **6b** was carried out in the presence of K_2CO_3 for one hour at 350°C (Figure 2.11). Following polymerization of the macrocycle, an insoluble material was obtained that could not be analyzed using NMR spectroscopy or gel permeation chromatography (GPC). Therefore, DSC, a technique independent of sample solubility was employed for analysis of the polymer sample. The DSC thermograms for the macrocycle and the corresponding polymer are shown in Figure 2.12. The DSC curve for **6b** exhibited only one peak at 329°C, corresponding to the T_m of the macrocycle. In comparison, three peaks were observed in the polymer's thermogram (Figure 2.12). The endothermic peak at 92°C, represented the glass transition temperature (T_g) of the polymer. The appearance of this peak in the polymer's DSC curve, as well as the absence of the T_m peak of the macrocycle, indicated that successful opening of the cyclic monomer had occurred. Two other peaks were seen in the polymer's thermogram, one at 130°C, which represented the crystallization temperature (T_c) of the polymer, and another at 282°C for the melting of the crystalline regions of the sample.

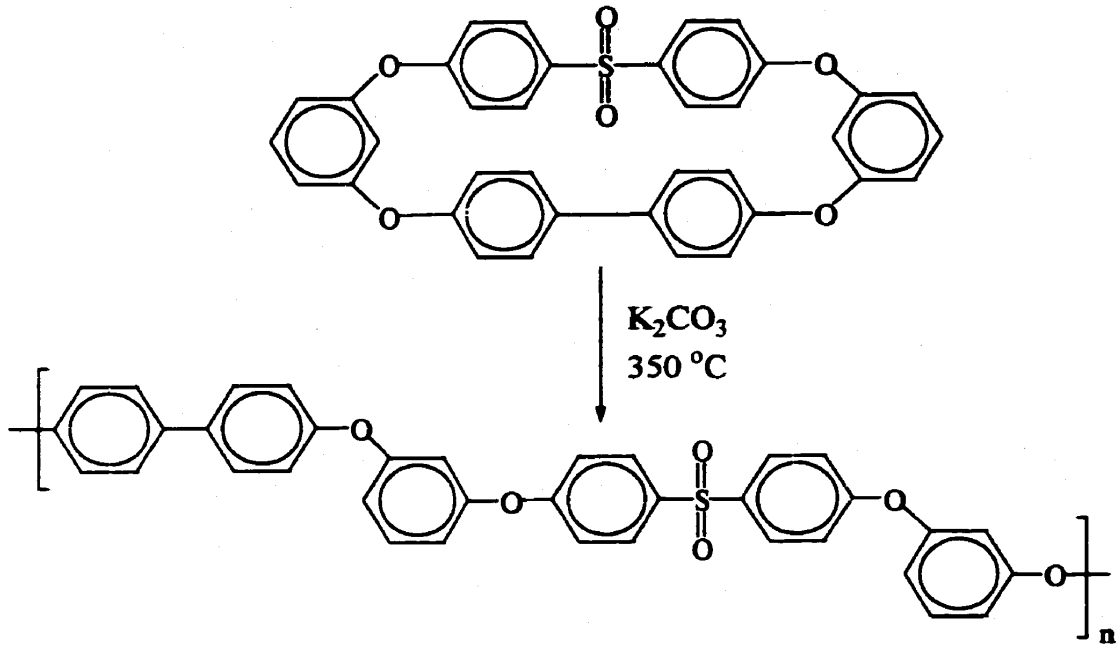

Figure 2.11: ROP of macrocycle **6b**.

2.5 Summary

This work illustrated the first examples of cyclic aryl ethers prepared via cyclopentadienyliron-mediated nucleophilic substitution reactions. Using well-established organoiron methodology, diiron species containing terminal chlorine atoms were prepared and then subjected to ring closure reactions with 4,4'-biphenyl, which yielded mixtures of the 1 + 1 metallated macrocycles and their corresponding linear oligomers. Following photolytic demetallation and purification, cyclic aryl ethers were isolated and characterized using spectroscopic techniques, MS and single-crystal X-ray crystallography. Ring-opening polymerization of these aromatic macrocycles was accomplished in the presence of a nucleophilic initiator at temperatures above 350°C to give insoluble polyaromatic ethers.

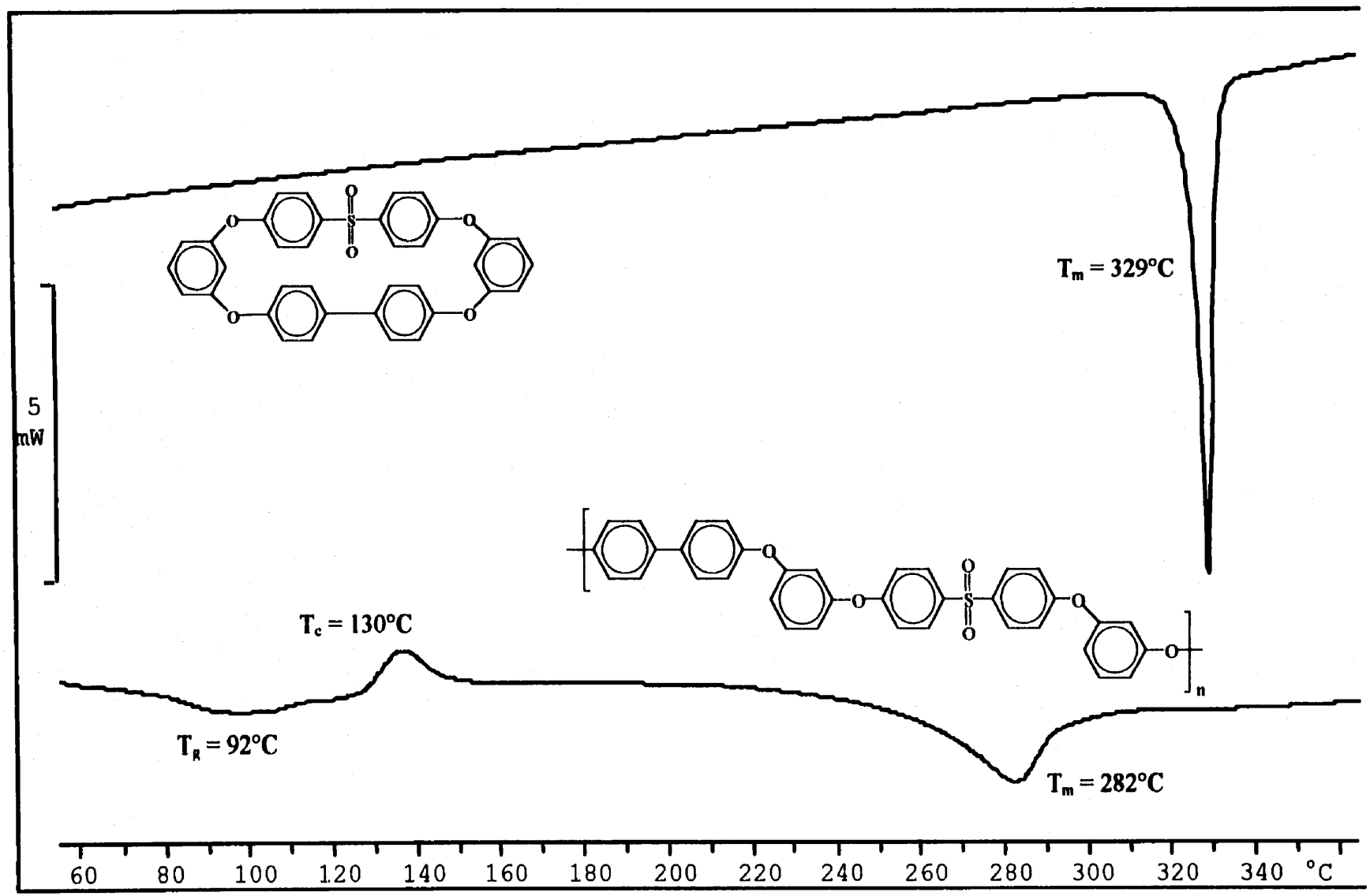

Figure 2.12: DSC thermogram of macrocycle **6b** and its corresponding linear polymer.

2.6 Experimental

2.6.1 General Methods

^{1}H and ^{13}C NMR spectra were recorded at 200 and 50 MHz, respectively, on a Varian Gemini 200 NMR spectrometer with chemical shifts referenced to the solvent residues and coupling constants reported in hertz. Infrared spectra were recorded on a Bomem, Hartmann & Braun FT-IR spectrophotometer using NaCl plates. EI-mass spectra were recorded on a Hewlett-Packard 5890 Series II mass spectrometer, by use of a direct injection probe. Signal positions are given in *m/z* units. Differential scanning calorimetry was performed on a Mettler DSC821^{e} at heating rates of 20°C/min under nitrogen (50 mL/min), with all transition temperatures reported at the midpoint. The X-ray crystallography for the aromatic macrocycles was preformed at St. Mary's University in Nova Scotia.

2.6.2 Starting Materials

Ammonium hexafluorophosphate, *m*-dichlorobenzene, 4-hydroxyphenyl sulfone, 4,4'-dihydroxybenzophenone, 4,4'-(9-fluorenylidene)diphenol, 6-hydroxy-2-naphthyl disulphide and 4,4'-biphenol were all commercially available. All solvents (reagent grade) were used without further purification, except hexane, which was dried over $CaCl_2$, distilled and stored over 4-Å sieves. The bimetallic complexes (**3a-d**) were prepared according to previously reported methodologies.[14]

2.6.3 Ring Closure Reactions

In a 50 mL round bottom flask, the appropriate bimetallic complex (**3a-d**) (0.5 mmol) and 4,4'-biphenol (0.5 mmol, 0.0931 g) were combined with K_2CO_3 (2.5 mmol, 0.3455 g) and 10 mL of DMF. The resulting red-brown solution was then stirred under a

nitrogen atmosphere for 20 h at room temperature. The yellow-brown solution was then poured into 10% (v/v) HCl, to which NH_4PF_6 was added. This caused the precipitation of the product as a yellow solid, which was collected by suction filtration, washed with several portions of distilled water and allowed to dry. After this time, a small amount of diethyl ether was used to wash any remaining nucleophile from the product.

2.6.4 Isolation of Organic Cyclic Monomers (6a-d)

In a 50 mL centrifuge tube, the metallated macrocycle (**5a-d**) (0.5 mmol) was dissolved in 40 mL of a 3:1 mixture of dichloromethane:acetonitrile. The solution was then irradiated with UV light (254 mn) for 6 hours, after which time the solvent was removed under reduced pressure. The residue was dissolved in chloroform, washed with several portions of distilled water, dried over $MgSO_4$, gravity filtered and the solvent removed using a rotary evaporator. The photolysis products were separated via column chromatography using a silica gel column. Ferrocene was first eluted from the column using hexane, followed by the isolation of the cyclic aryl ethers using chloroform as the mobile phase.

2.6.5 Ring-opening Polymerization of Aromatic Macrocycles

In a test tube, the aromatic macrocycle and K_2CO_3 (2% wt.) were combined and placed under a nitrogen atmosphere. The tube was then heated to 350°C using a sand bath and allowed to react for 1 hour. The resulting polymers were grey-black solids that were insoluble in common organic solvents.

3.0 Preparation of Polynorbornenes Containing Cationic Iron Moieties

3.1 ROMP of Bicyclo[2.2.1]hept-2-enes

The first article describing the ring-opening metathesis polymerization (ROMP) of bicyclo[2.2.1]hept-2-ene (norbornene) was reported by Truett in 1960.[12] He was able to prepare polynorbornenes using lithium aluminum tetraheptyl and titanium tetrachloride as the metathesis catalyst/co-catalyst system. At the time, this method of polymerization was termed "coordination polymerization", as it was believed that the reaction involved successive steps of coordination of the catalyst to the double bond, followed by cleavage of an adjacent single bond (Scheme 3.1).[12] It wasn't until a decade later, when Calderon proved metathesis of a double bond was possible, that the correct mechanism for ROMP of a cyclic or acyclic olefin was determined (Scheme 1.4).

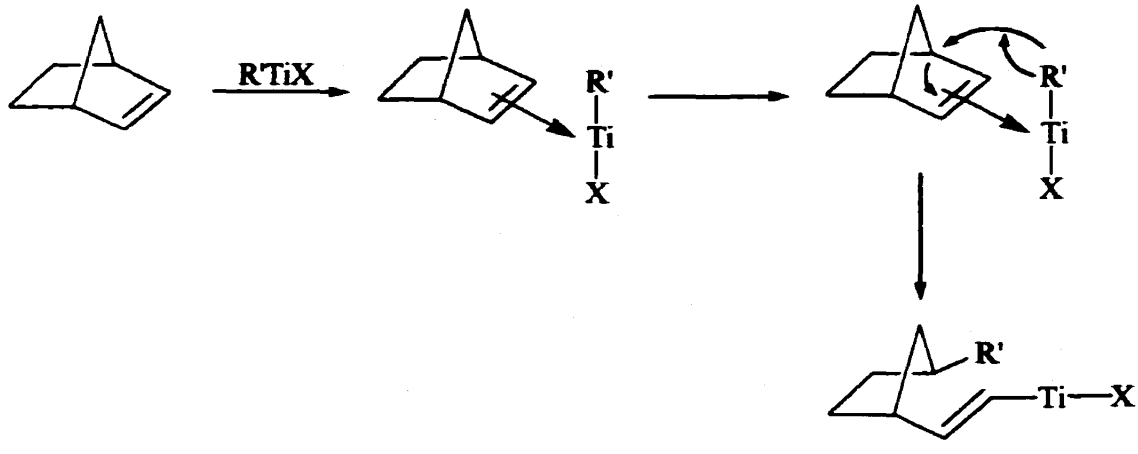

Scheme 3.1: Coordination polymerization mechanism.

There are a wide variety of catalytic systems that are able to initiate the ROMP of alkenes.[8] Initial work in the area involved the use of catalysts that required additional components (co-catalysts) in order to acquire sufficient activity to polymerize an olefin.

These systems were usually heterogeneous, which made defining the specific catalytic site responsible for activating the polymerizations difficult.[8] Well-defined, highly active metal-carbene complexes have since replaced these "first generation" catalysts. Metal-carbene catalysts contain a single active site that controls the polymerization process, allowing for accurate determination of the ROMP mechanism, as well as the formation of living systems.[8]

To date, two types of metal-carbene complexes that have received a great deal of attention are those based on molybdenum and ruthenium. Schrock and coworkers introduced a molybdenum alkylidene complex, Mo(CH-*t*-Bu)(N-2,6-C_6H_3-*i*-Pr_2)(O-*i*-Bu)$_2$ in the mid 1980's that was shown to be very active in the polymerization of bicyclic olefins (**3.1**).[116-118] He later found that the reactivity of the catalyst towards carbon-carbon double bonds could be altered by varying the nature of the alkoxide ligands attached to the metal center.[118] Since this discovery, Schrock has successfully polymerized a wide variety of functionalized norbornene monomers using this molybdenum alkylidene catalyst (Figure 3.1).[117-122]

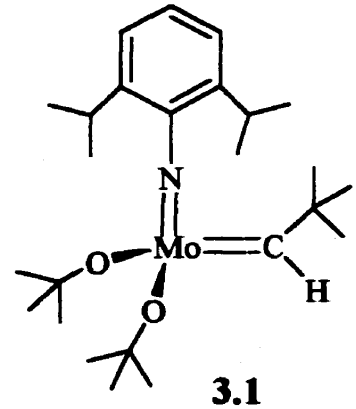

3.1

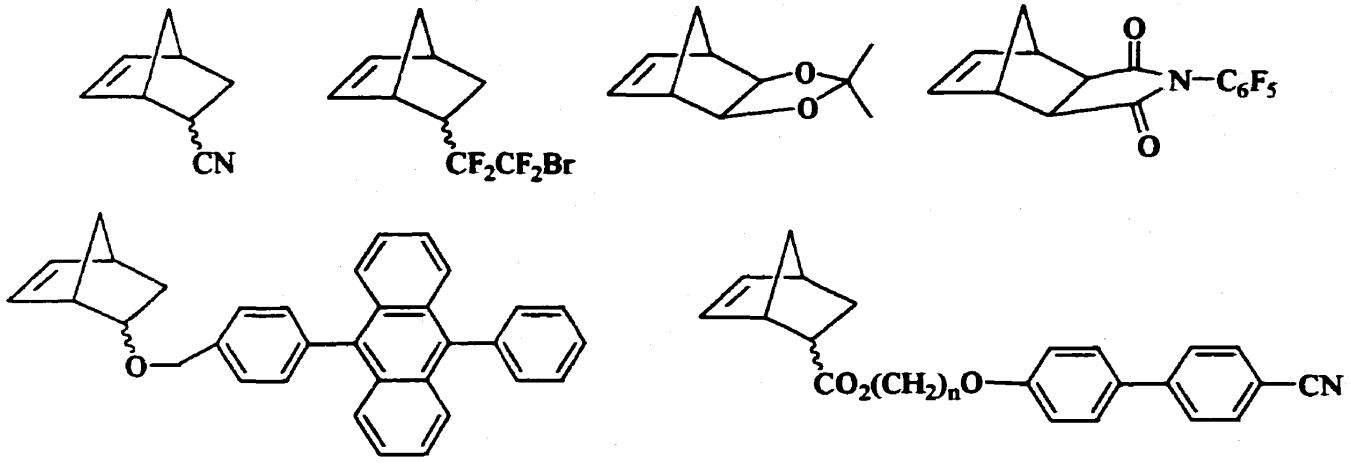

Figure 3.1: Some norbornene monomers polymerized using Schrock's catalyst.

ROMP of highly strained cycloalkenes using ruthenium-based metathesis catalysts has been known for quite some time. $RuCl_3 \cdot 3H_2O$ was first used to polymerize cyclobutene and norbornene in alcoholic and aqueous solutions in 1964.[8,9] The ability of this late transition metal catalyst to polymerize cycloolefins in protic environments, as well its ability to be recycled for use in subsequent reactions, lead to its application in industrial polymerizations.[8,9,11] For example, polynorbornene has been prepared industrially under the name Norsorex since 1976 using $RuCl_3 \cdot 3H_2O$ in a butanol/HCl solvent system. The resulting polymer is an amorphous powder with a molecular weight exceeding 2 million g/mol.[9] This ruthenium-based system has also been employed in the polymerization of norbornene derivatives such as 7-oxanorbornenes (Scheme 3.2).[123,124]

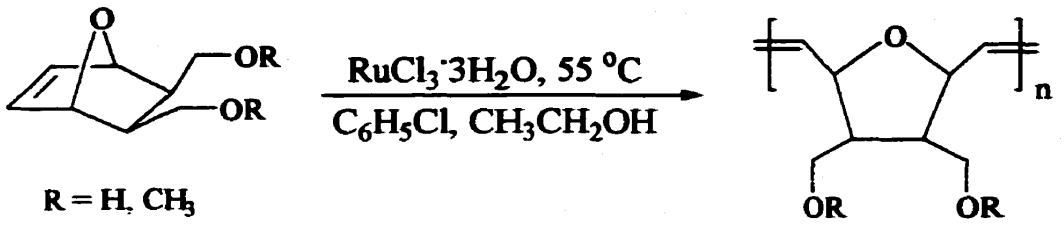

R = H, CH_3

Scheme 3.2: Polymerization of 7-oxanorbornenes using $RuCl_3$.

Investigations into the preparation of more reactive ruthenium-based catalysts that required less harsh polymerization conditions, and could result in the preparation of living systems, began in the mid 1980's. The first ruthenium-carbene metathesis catalysts (**3.2**) that were introduced displayed good metathesis activity and functional group tolerance.[125,126] However, their syntheses required numerous steps, and their initiation rates in the ROMP of cyclic olefins were very slow, leading to the formation of polymers with wide polydispersity indicies.

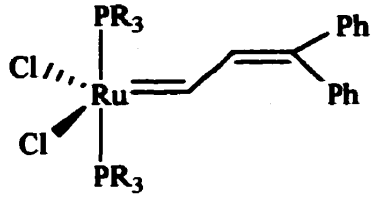

R = Ph, Cy

3.2

In 1995, Grubbs and coworkers introduced a new series of ruthenium-carbene catalysts, which were prepared by altering the source of the carbene from 3,3-diphenylcyclopropene to diazoalkanes (Scheme 3.3).[127] These new ruthenium benzylidene catalysts showed greater metathesis activity than the previous systems as a result of rapid initiation of the monomers. As well, they displayed excellent functional group tolerance and chemical stability in air and protic environments.[128]

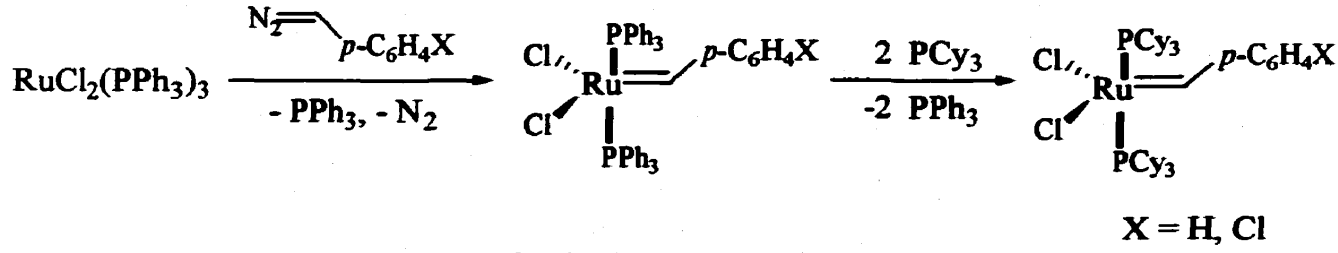

Scheme 3.3: Synthesis of ruthenium benzylidene ROMP catalysts.

Since the development of highly tolerant, stable metathesis catalysts, the polymerization of a wide variety of norbornene monomers has been investigated. Of all the bicycloalkenes, norbornene has received the most attention due to its facile ROMP, which arises because of the high ring strain associated with the monomer.[8] As well, norbornene and its derivatives are readily available, or may be easily synthesized via Diels-Alder reactions of cyclopentadiene and substituted ethylenes, thus providing the opportunity to prepare a wide variety of substituted monomers (Scheme 3.4).[9]

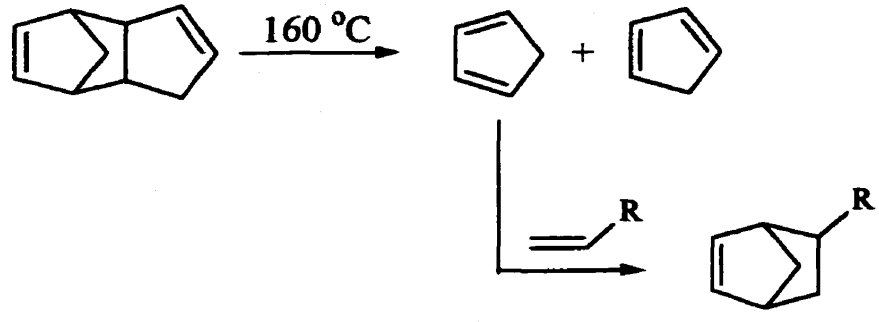

Scheme 3.4: Preparation of norbornene monomers via Diels-Alder reactions.

The preparation of various functionalized polynorbornenes is of interest due to the varying properties the polymers may exhibit. For example, polynorbornenes have been prepared that possess light-emitting properties, which are useful in the field of

electrooptics.[122,129-131] Traditionally, these electroluminescent (EL) devices have been based on inorganic or small organic materials, however, polymer-based systems are more attractive as they are more easily processed and offer greater surface areas.[129] As a representative example, the polymerization of a norbornene monomer functionalized with (*tert*-butylphenyl)-*p*-biphenyloxadiazole was achieved using Schrock's catalyst (Scheme 3.5). The resulting polymer was cast as a film and incorporated into an EL device. The optical spectrum of the material was obtained, and based on the results it was concluded that the system could be used as a blue-light-emitting device.[129]

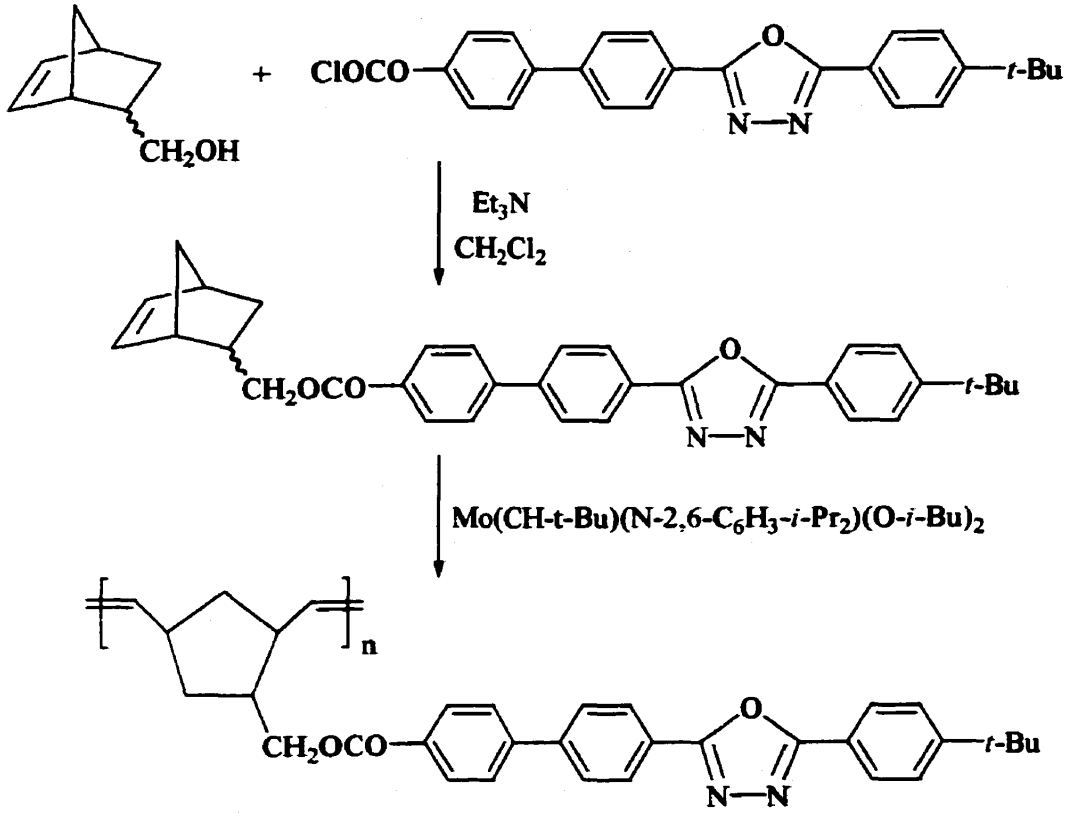

Scheme 3.5: Synthesis of blue-light-emitting polynorbornene.

Various biological polymers based on polynorbornene have been synthesized using Grubbs' catalyst.[132-134] Several years ago, polynorbornenes functionalized with carbohydrates were prepared to facilitate studies into the biological interactions of carbohydrates and proteins.[132] These types of biopolymers are traditionally prepared using radical polymerization techniques, which suffer from lack of control over molecular weights and molecular weight distributions of the polymers. ROMP in the presence of a ruthenium benzylidene catalyst offers the advantages of a living system, which overcomes the disadvantages of the traditional polymerization methodologies. More recently, oligopeptide-substituted polynorbornenes (**3.3**) were prepared that were capable of mediating cell adhesion, which is an important feature in the treatment of diseases such as cancer.[133,134] Again the advantages of using a ruthenium-carbene ROMP catalyst, including the living nature of the polymers and control over the molecular weights were important features of these polymerizations.

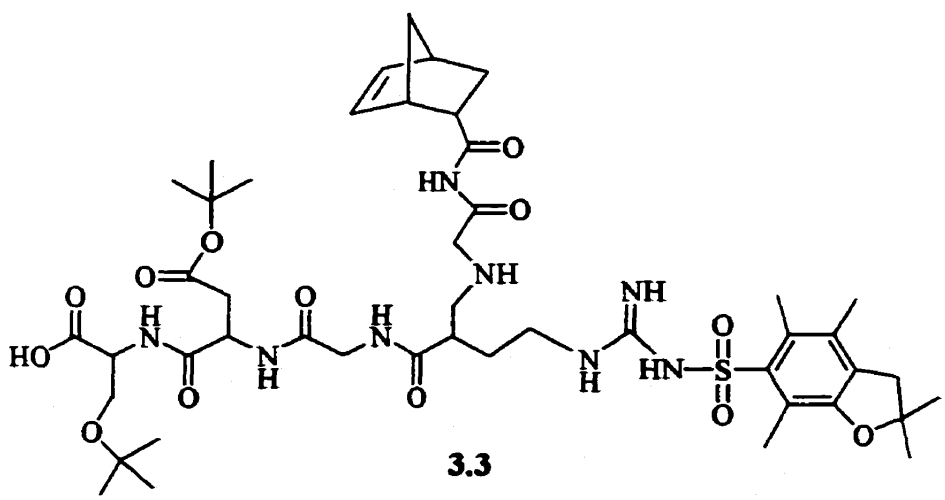

3.3

Numerous side chain liquid crystalline polymers (SCLCP) based on polynorbornenes have been prepared in the last decade because of the facile substitution and polymerization of the monomers.[8,135-142] To be classified as a SCLCP, the polymer must be of high molecular weight, while still exhibiting the liquid crystalline behavior of a low mass molecule.[142] This is achieved by designing polymeric materials that contain flexible side chains (spacers) that terminate in rigid groups (mesogens) (**3.4**).[1] LC polynorbornenes are classified as one of two types: those whose repeating unit contain a single side chain, and those whose repeating unit is substituted with two side chains. Furthermore, the polynorbornenes substituted with one side chain can be arranged such that the side chain is positioned in a terminal or lateral manner relative to the polymer backbone (Figure 3.2).[141-144]

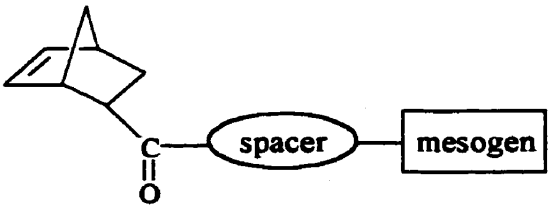

3.4

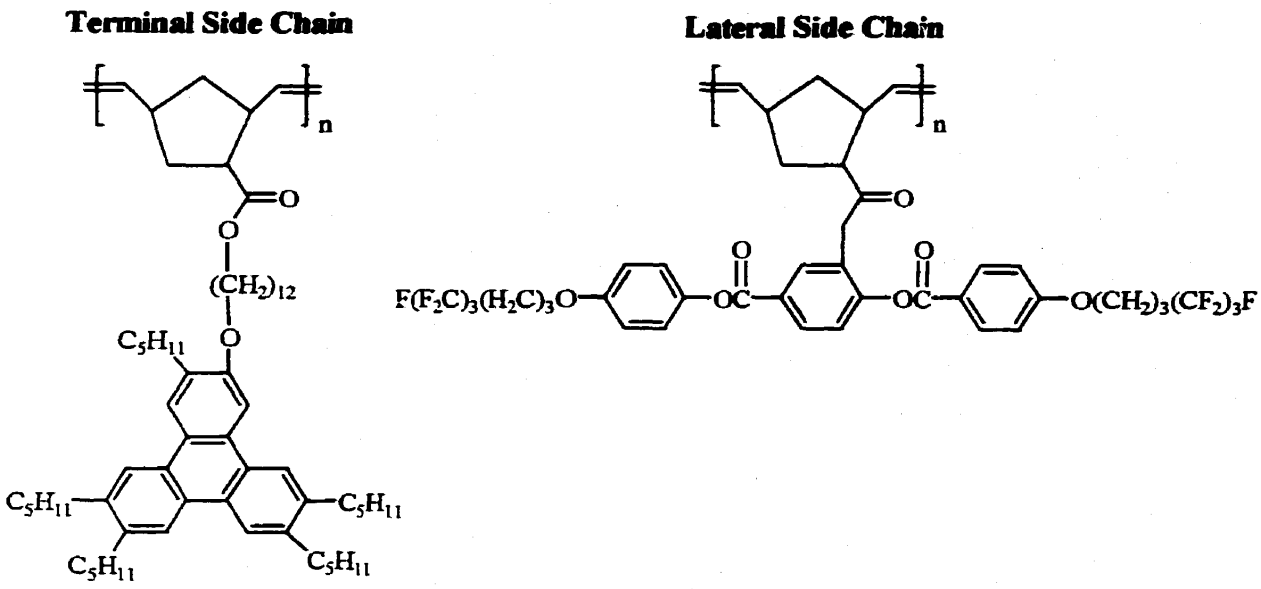

Figure 3.2: Polynorbornenes substituted with terminal or lateral side chains.

Polynorbornenes functionalized with inorganic or organometallic units have also been prepared.[145-148] Schrock and coworkers have presented two routes for the synthesis of electrochemically-active polynorbornenes (Scheme 3.6).[145,146] In the first, polynorbornenes containing pendent ferrocenyl moieties in their side chains were prepared by polymerizing norbornene monomers substituted with the organoiron group (**I** in Scheme 3.6). In the second synthetic method, polynorbornenes end-capped with ferrocenyl groups were isolated by polymerizing norbornenes with molybdenum alkylidene catalysts containing ferrocene ligands (**II** in Scheme 3.6). All of the ferrocene-containing materials displayed redox-active properties, and were used in the preparation of modified electrode surfaces.[146]

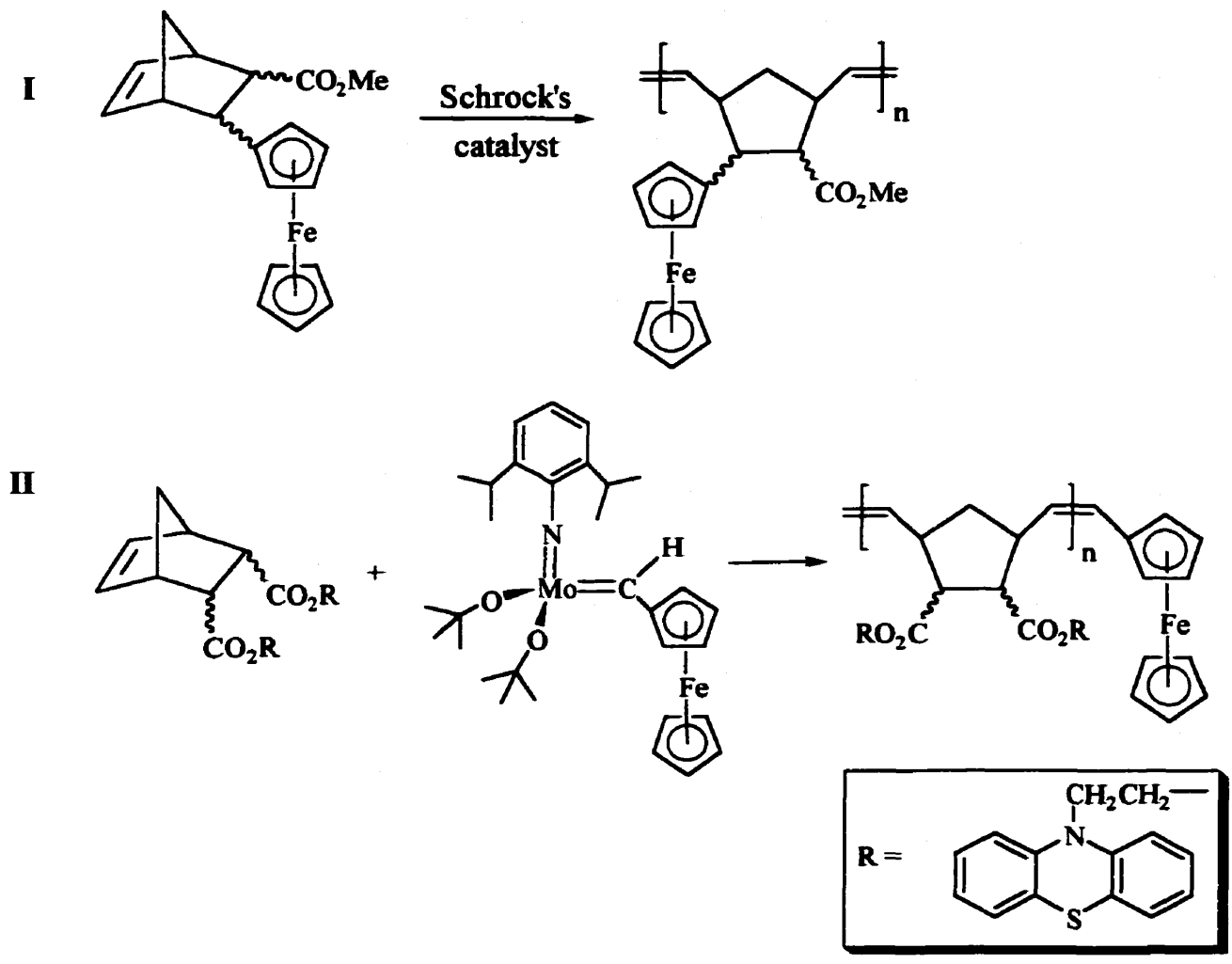

Scheme 3.6: Two synthetic routes towards ferrocene functionalized polynorbornenes.

Recently, Allcock and coworkers reported the first example of phosphazene-functionalized polynorbornenes.[147,148] Polymers containing phosphazene functionalities are of interest due to the fire resistant properties associated with phosphorus and nitrogen containing materials. As illustrated in Scheme 3.7, numerous phosphazenes were synthesized according to Allcock's established methodology, and then substituted with 5-norbornene-2-methanol in the presence of sodium hydride. The functionalized

polynorbornenes were then prepared using Grubbs' catalyst to give polymeric materials that displayed high char yields above 450°C, which was attributed to the fire resistant properties of the phosphazene ring.[147]

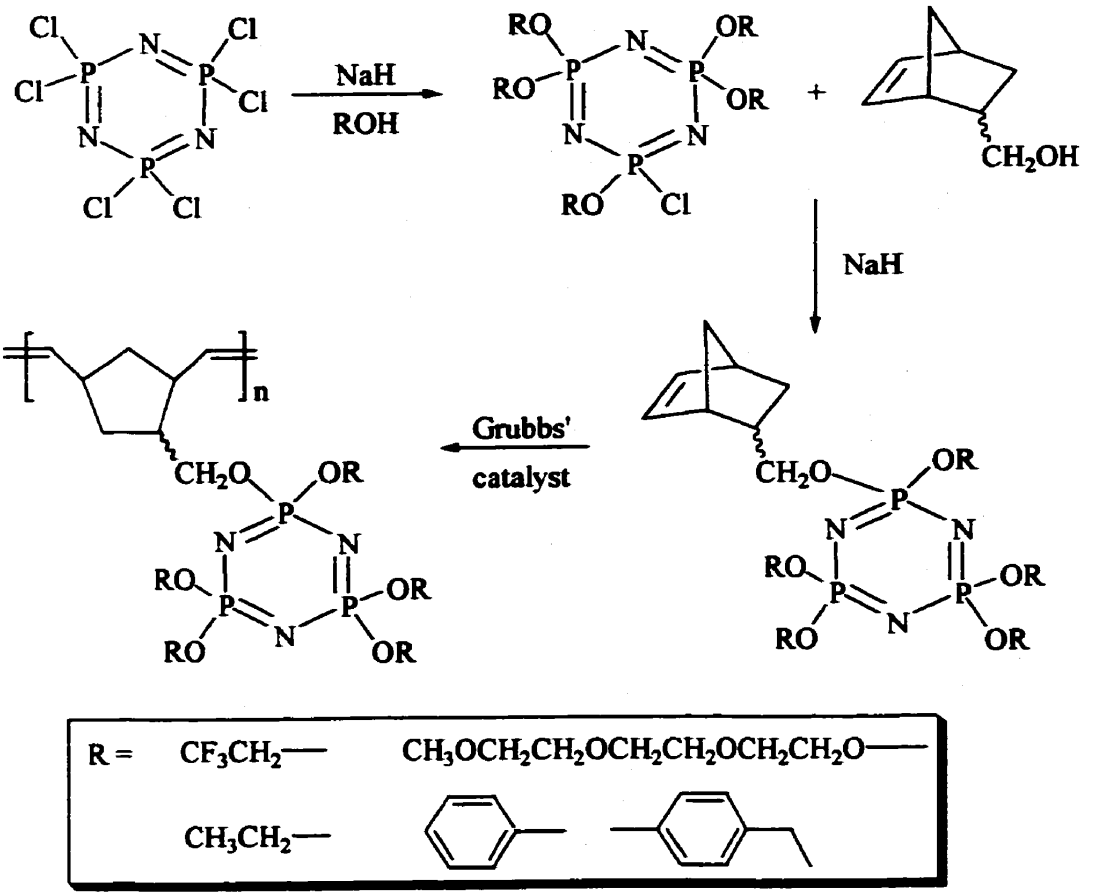

Scheme 3.7: Fire retardant phosphazene containing polynorbornenes.

3.2 Results and Discussion

The preparation of organometallic polymers has received a great deal of attention in the last decade as a result of the properties that metals impart to the resulting polymeric species.[149-152] For example, polymeric materials containing cationic cyclopentadienyliron ($CpFe^+$) moieties have demonstrated increased solubility relative to their organic counterparts.[36] As well, it has been established that $CpFe^+$-complexes of polyarenes exhibit redox properties that could allow for their potential use as redox systems, electrocatalysts or modified electrodes.[153,154] These appealing chemical and physical properties have lead to a study into the preparation of polynorbornenes substituted with side chains containing cationic cyclopentadienyliron moieties.

Using metal-mediated nucleophilic aromatic substitution reactions, a series of organoiron complexes were prepared and subsequently coupled to norbornene units. The resulting metallated monomers were polymerized via ring-opening metathesis routes using a ruthenium-based catalyst to give polynorbornenes with cyclopentadienyliron-complexed side chains. The structures of the monomers and polymers were characterized by spectroscopic techniques and elemental analysis. The molecular weights of the polynorbornenes were calculated using gel permeation chromatography (GPC), and their thermal properties were investigated using differential scanning calorimetry (DSC) and thermogravimetric analysis (TGA).

3.2.1 Synthesis of Norbornenes Containing One $CpFe^+$ Moiety

3.2.1.1 Preparation of Monometallic Starting Complexes

Taking advantage of the exceptional electron-withdrawing ability of the $CpFe^+$ moiety, numerous monometallic organoiron complexes (**3a-e**) were prepared via nucleophilic aromatic substitution (S_NAr) reactions of η^6-chlorobenzene-η^5-cyclopentadienyliron hexafluorophosphate (**1a**) or η^6-4-chlorotoluene-η^5-cyclopentadienyliron hexafluorophosphate (**1b**) with various phenolic dinucleophiles (**2a-c**) (Scheme 3.8). Under the conditions employed, reaction of only one of the phenolic ends of the dinucleophiles was achieved, leaving a free hydroxyl group in the resulting organoiron complexes that could undergo further reaction. These complexes were obtained in excellent yields (81-97%), and were characterized using NMR, FT-IR and CH elemental analysis (Tables 3.1-3.3).

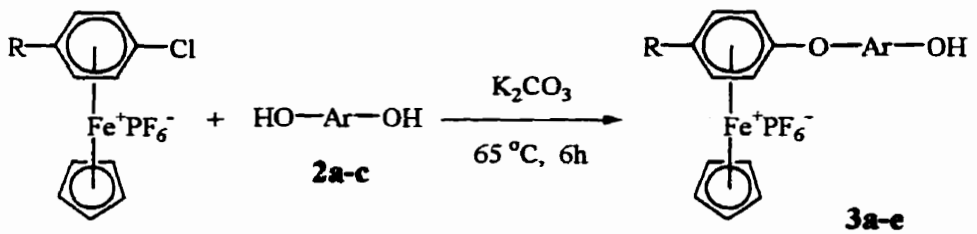

1a; R = H
1b; R = CH_3

Complex	R	Ar	Complex	R	Ar
3a	H	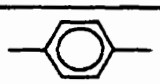	**3d**	CH_3	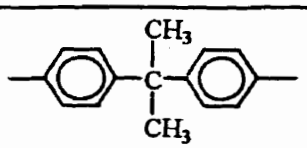
3b	CH_3	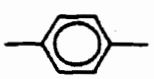			
3c	H	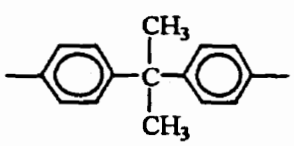	**3e**	H	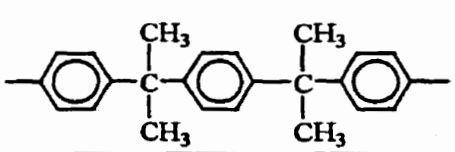

Scheme 3.8: Synthesis of monometallic starting complexes **3a-e**.

The ^{1}H NMR and ^{13}C NMR spectra of complex **3e** can be seen in Figures 3.3 and 3.4, respectively, as representative examples of the spectra for the complexes prepared. The asymmetric nature of this complex resulted in the appearance of two singlets in the ^{1}H NMR spectrum for the 12 methyl protons of the two isopropylidene groups at 1.62 and 1.69 ppm (Figure 3.3). The intense singlet at 5.22 ppm was due to the 5 cyclopentadienyl protons of the metal moiety. This singlet had shifted upfield relative to its chemical shift in the ^{1}H NMR spectrum of the starting material (5.31 ppm), as the group attached to the complexed aromatic ring changed from an electron-withdrawing chlorine atom to an electron-donating etheric bond. The 5 complexed aromatic protons appeared as one doublet and two triplets in the range of 6.26-6.43 ppm, which is a splitting pattern characteristic of monosubstituted rings. The protons alpha to the ether bridge appeared as a doublet at 6.30 ppm, while the protons beta and gamma to the ether linkage appeared as triplets at 6.43 and 6.26 ppm, respectively. The uncomplexed aromatic protons resonated downfield in the spectrum relative to the complexed aromatic proton resonances. Doublets at 6.73 and 7.08 ppm represented the aromatic protons of the terminal phenolic ring, while the protons of the uncomplexed aromatic ring attached to the metallated aromatic ring via the ether linkage, appeared as doublets at 7.24 and 7.42 ppm. The 4 aromatic protons of the ring encompassed by the two isopropylidene groups appeared as an intense singlet with a chemical shift of 7.17 ppm. The final peak in the ^{1}H NMR spectrum of complex **3e** was a broad singlet at 8.13 ppm, which represented the hydrogen of the terminal hydroxyl group. The presence of the free hydroxyl groups within all of the complexes was further confirmed upon IR analyses of the samples.

The ^{13}C NMR of complex **3e** is seen in Figure 3.4. Peaks representing the two isolated isopropylidene groups were observed at 30.90 (CH_3), 31.01 (CH_3), 41.90 (quat. C) and 42.49 (quat. C). The four peaks in the range of 77.05-87.15 ppm corresponded to the monosubstituted complexed aromatic ring and the Cp moiety, with the single quaternary aromatic carbon of the complexed ring resonating at 133.90 ppm. Each of the six sets of uncomplexed aromatic carbons appeared as individual peaks between 115.24 and 129.45 ppm, as they were all inequivalent due to the asymmetric nature of the complex. The same pattern was observed for the quaternary carbons of the uncomplexed aromatic rings, which appeared as six peaks in the range of 141.83-155.33 ppm.

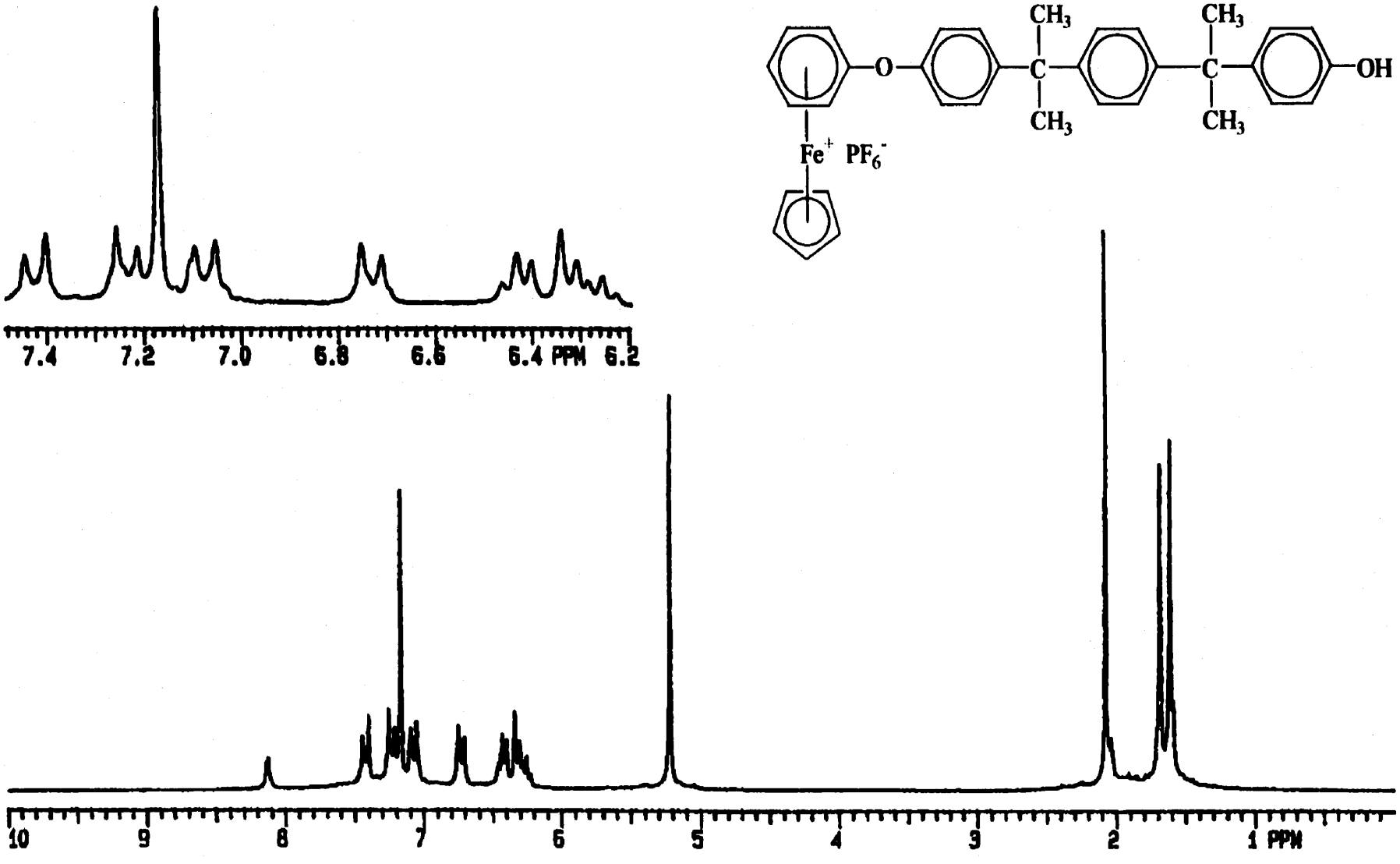

Figure 3.3: ^{1}H NMR spectrum of complex **3e**.

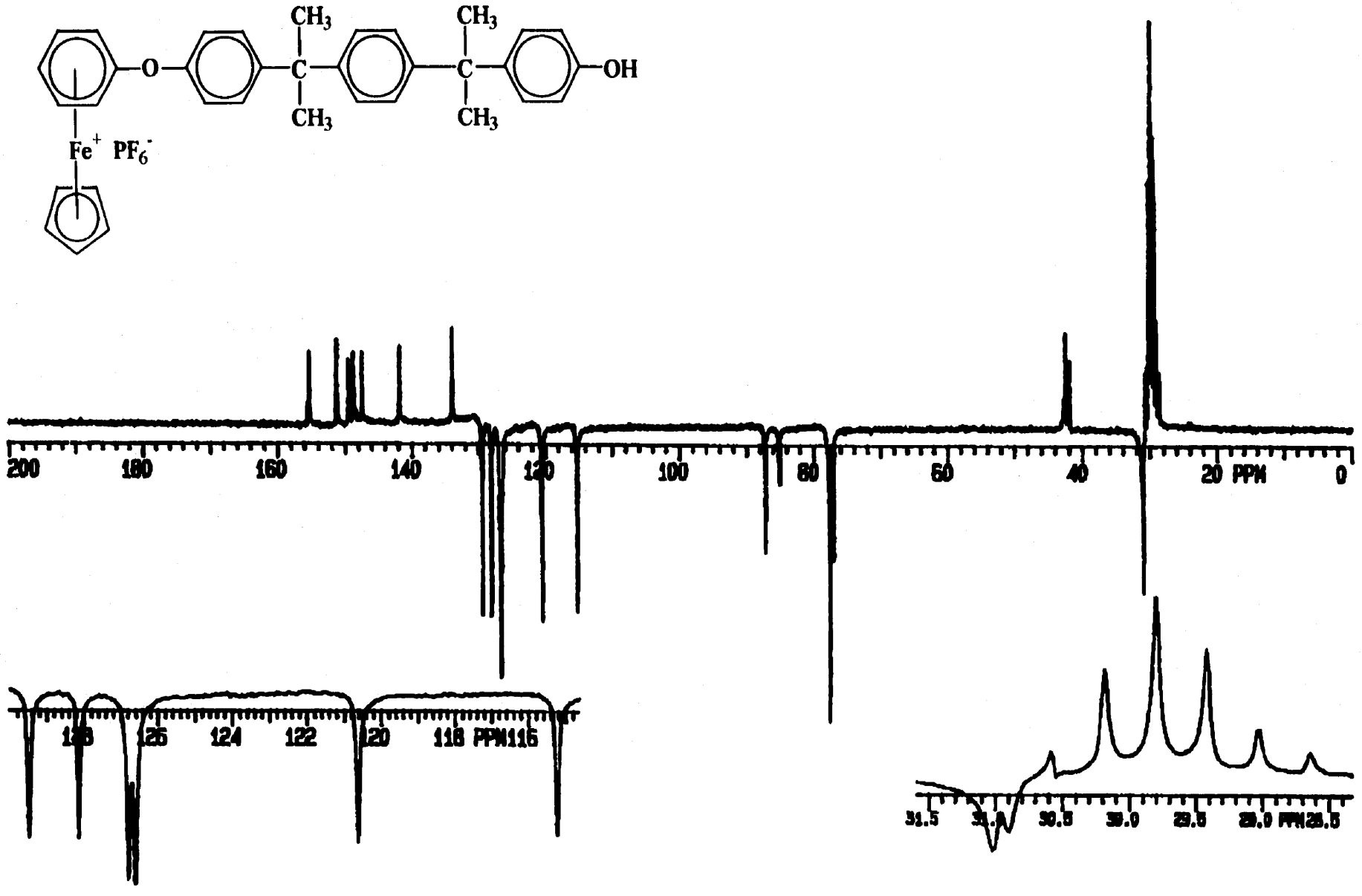

Figure 3.4: ^{13}C NMR spectrum of complex **3e**.

Table 3.1: Yield, IR and elemental analysis data for monometallic complexes **3a-c**.

COMPLEX	PRODUCT YIELD	IR ABSORBANCES (cm^{-1})	CH ANALYSIS CALCULATED	CH ANALYSIS FOUND
3c	1.1064 g (97%)	3405 (OH)	C, 54.76; H, 4.42	C, 54.39; H, 4.69
3d	1.1064 g (95%)	3389 (OH)	C, 55.50; H, 4.66	C, 54.97; H, 4.95
3e	1.3174 g (96%)	3318 (OH)	C, 61.06; H, 5.12	C, 60.82; H, 5.04

Table 3.2: ^{1}H NMR data for monometallic complexes **3c-e**.

	δ (ppm) in acetone-d_6				
COMPLEX	OH	ArH	$CpFe^+$-ArH	Cp	CH_3
3c	8.20 (s, 1H)	6.77 (d, 2H, J = 7.62) 7.11 (d, 2H, J = 7.70) 7.24 (d, 2H, J = 7.41) 7.42 (d, 2H, J = 7.61)	6.26-6.34 (m, 3H) 6.41-6.44 (m, 2H)	5.22 (s, 5H)	1.67 (s, 6H)
3d	8.17 (s, 1H)	6.77 (d, 2H, *J* = 7.77) 7.11 (d, 2H, *J* = 7.77) 7.19 (d, 2H, *J* = 8.35) 7.39 (d, 2H, *J* = 8.34)	6.27 (dd, 4H, *J* = 14.28; 6.23)	5.16 (s, 5H)	1.66 (s, 6H) 2.45 (s, 3H)
3e	8.13 (s, 1H)	6.73 (d, 2H, *J* = 8.43) 7.08 (d, 2H, *J* = 8.42) 7.17 (s, 4H) 7.24 (d, 2H, *J* = 8.50) 7.42 (d, 2H, *J* = 8.43)	6.26 (t, 1H, *J* =5.72) 6.30 (d, 2H, *J* =6.59) 6.43 (t, 2H, *J* =6.09)	5.22 (s, 5H)	1.62 (s, 6H) 1.69 (s, 6H)

Note: NMR spectra recorded at 200 MHz.
Coupling constants reported in hertz.

Table 3.3: ^{13}C NMR data for monometallic complexes **3c-e**.

δ (ppm) in acetone-d_6						
COMPLEX	quaternary ArC	ArCH	quaternary $CpFe^+$- ArC	$CpFe^+$-ArCH	Cp	OTHERS
3c	141.61 150.11 151.28 155.73	115.54 120.73 128.32 129.56	134.22	77.20 85.37 87.46	77.76	31.13 (CH_3) 42.39*
3d	141.50 149.99 151.51 155.72	115.38 120.55 128.21 129.45	100.99 133.14	76.50 87.41	78.08	9.53 (CH_3) 31.02 (CH_3) 42.29*
3e	141.83 147.36 148.72 149.39 151.15 155.33	115.24 120.58 126.59 126.76 128.11 129.45	133.90	77.05 85.06 87.15	77.54	30.90 (CH_3) 31.01 (CH_3) 41.90* 42.49*

Note: NMR spectra recorded at 50 MHz.
* Denotes a quaternary carbon.

3.2.1.2 Preparation of Norbornenes Containing One $CpFe^+$ moiety

The strategic syntheses of organoiron complexes containing terminal hydroxyl groups allowed for the incorporation of cyclopentadienyliron-complexed units into norbornene monomers. This was accomplished via condensation reactions of organoiron complexes **3a-e** with *exo,endo*-5-norbornene-2-carboxylic acid (**4**), to give the corresponding metallated monomers (**5a-e**) as mixtures of their *exo* and *endo* isomers (Scheme 3.9). These monomeric units were isolated in good yields ranging from 79 to 95%, and characterized using NMR, FT-IR and CH analysis (Tables 3.4-3.7).

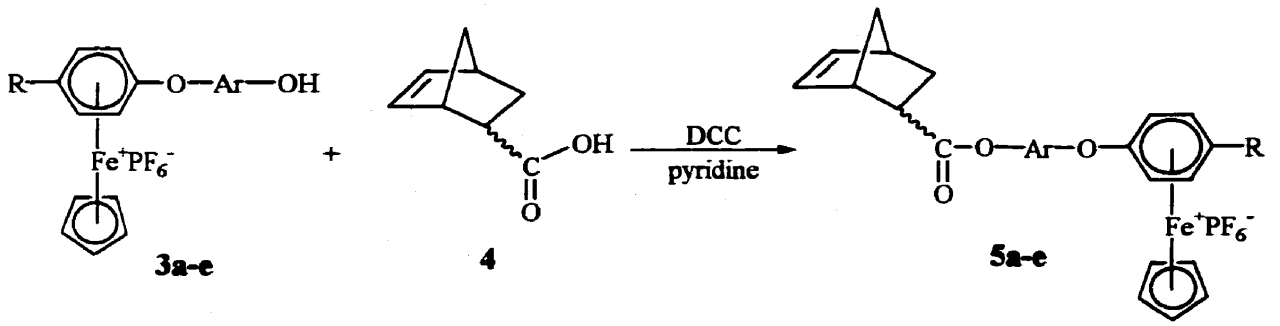

Complex	R	Ar	Complex	R	Ar
5a	H	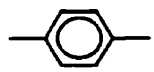	**5d**	CH_3	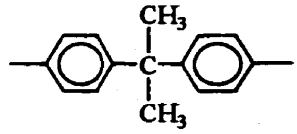
5b	CH_3				
5c	H	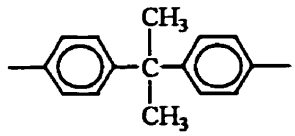	**5e**	H	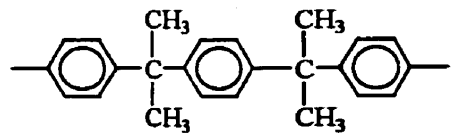

Scheme 3.9: Preparation of monometallic norbornenes **5a-e**.

NMR and IR spectroscopy were important tools in the identification of the structures of the organoiron monomers. For example, the FT-IR spectra of the monomers lacked the broad peak in the range of 3318-3550 cm^{-1}, which represented the free hydroxyl group in the spectra of the organoiron starting complexes. The spectra for the metallated monomers showed peaks in the range of 1748-1754 cm^{-1} that corresponded to the carbonyl group of the ester linkage formed upon condensation of the starting complexes with the norbornene units. Another set of peaks between 700 and 740 cm^{-1} were observed for the out-of-plane bending vibrations of the *cis* olefinic bond in the norbornenes.[155]

Comparison of the NMR spectra of the starting organoiron complexes and the new complexed-monomers also provided evidence that the condensation reactions had proceeded successfully. Figure 3.5 shows a comparison of the ^{13}C NMR spectra of complex **3a** and its corresponding monomer, **5a**. Evaluation of the two spectra revealed new peaks in the upfield region of the monomer's spectrum that corresponded to the saturated carbons of the norbornene unit. As well, there were four peaks between 133 and 139 ppm that represented the olefinic carbons of the norbornene monomer. It is important to note that the monomers were mixtures of their *exo* (*x*) and *endo* (*n*) isomers, and as such, there were two peaks in the spectra for every carbon of the norbornene ring. Thus, it was expected that four peaks would be observed for the two olefinic carbons, one pair corresponding to the *exo* isomer (δ 132.96 and δ 138.94 ppm) and another for the *endo* isomer (δ 136.64 and δ 138.79 ppm). The final set of new peaks present in the ^{13}C NMR spectrum of the monomer were those at 173.34 and 174.99 ppm, which represented the carbons of the carbonyl group within the newly formed ester linkage. It is also

interesting to note that an upfield shift of the resonance for the quaternary aromatic carbon attached to the hydroxy group in **3a** (δ 156.70 ppm) occurred in the monomer's spectrum (δ 151.23 ppm). In contrast, a downfield shift of the quaternary carbon *para* to the ester linkage in the monomer, relative to its position in the hydroxyl starting material, was observed (**3a** = δ 145.99 ppm, **5a** = δ 150.00 ppm). These shifts were a direct result of the formation of the ester linkage between the norbornene unit and the pendent aromatic side chain.

Since the monomers existed as a mixture of their *exo* and *endo* isomers, full assignment of their one-dimensional NMR spectra was difficult, and thus, two-dimensional NMR was needed to fully identify their structures. As an example, the homonuclear correlation spectroscopy (HH COSY) NMR spectrum for monomer **5a** is shown in Figure 3.6. Peaks representing the uncomplexed aromatic protons appeared downfield in the spectrum between 7.2 and 7.5 ppm, whereas the complexed aromatic protons appeared at higher field in the range of 6.3-6.5 ppm. The olefinic protons of the norbornene unit were found downfield relative to the aliphatic norbornene protons in the range of 6.12-6.26 ppm. The intense singlet at 5.25 ppm in the spectrum represented the cyclopentadienyl protons of the metallic moiety. The remaining norbornene protons resonated between 1.39-3.38 ppm, and were assigned based on the characteristic coupling observed for bicyclo[2.2.1]hept-2-ene systems.[156-163]

For the identification of the *endo* isomer, assignment of the olefinic resonances was required so that their connectivities with ring protons at higher fields could be utilized. As seen in Figure 3.7, H_6 and H_5 were easily identified as a result of their strong coupling with each other, as well as their expected couplings with the bridgehead protons

H_1 and H_4, respectively. Each appeared in the spectrum as a doublet of doublets, with H_5 resonating at 6.26 ppm ($J_{5,6}$ = 5.48 Hz and $J_{4,5}$ = 2.93 Hz) and H_6 appearing further upfield at 6.12 ppm ($J_{5,6}$ = 5.48 Hz and $J_{1,6}$ = 2.58 Hz). H_1 (δ 3.38 ppm) and H_4 (δ 2.97 ppm) appeared as broad singlets in the NMR spectrum, and aside from their couplings with H_6 and H_5, they also displayed weak long-range coupling with each other, which helped to confirm their identities (Figure 3.8). The multiplet resonating between 3.33-3.36 ppm was assigned to H_2 based on its connectivity with H_1, as well as H_{3x} and H_{3n}, as illustrated in Figure 3.8. Confirmation of the assignment of the H_3 protons (H_{3x} = m, δ 2.03-2.06 ppm; H_{3n} = m, δ 1.39-1.52 ppm) was obtained based on the characteristic strong coupling they demonstrated with each other ($J_{3x,3n}$ = 11-13 Hz), as well as their connectivity with H_4.[157,163] The bridge protons, H_{7a} and H_{7s} also showed strong coupling with each other ($J_{7a,7s}$ = 8.40 Hz), and were assigned to the multiplet at 1.39-1.52 ppm (H_{7a}) and the doublet resonating at 1.58 ppm (H_{7s}).

The protons of the *exo* isomer were identified using the methodology described above. The two olefinic protons H_6 and H_5 were assigned to the multiplet resonating between 6.20 and 6.23 ppm. Their characteristic couplings with the two bridgehead protons were then used to assign H_1 to the broad singlet at 3.24 ppm, and H_4 to the broad singlet appearing at 3.17 ppm (Figure 3.9). In the *endo* isomer, H_2 was assigned based on its connectivity with H_1, however, this coupling is not observed in the *exo* isomer.[157,163] Thus, H_2 was found following the identification of the H_3 protons. As shown in Figure 3.10, H_{3x} (m, δ 2.03-2.06 ppm) was identified via its coupling with the bridgehead proton H_4, however, H_{3n} could not be found using H_4 as there is no observable coupling for these protons within the *exo* isomer.[157,163] Using the characteristic strong coupling of the two

H_3 protons, as well as their coupling with H_2, H_{3n} was found to resonate within the multiplet between 1.39-1.52 ppm, and H_2 was assigned to the doublet of doublets at 2.52 ppm ($J_{2,3x}$ = 8.57 Hz and $J_{2,3n}$ = 2.52 Hz). Finally, both H_7 protons were assigned to the multiplet between 1.39 and 1.52 ppm.

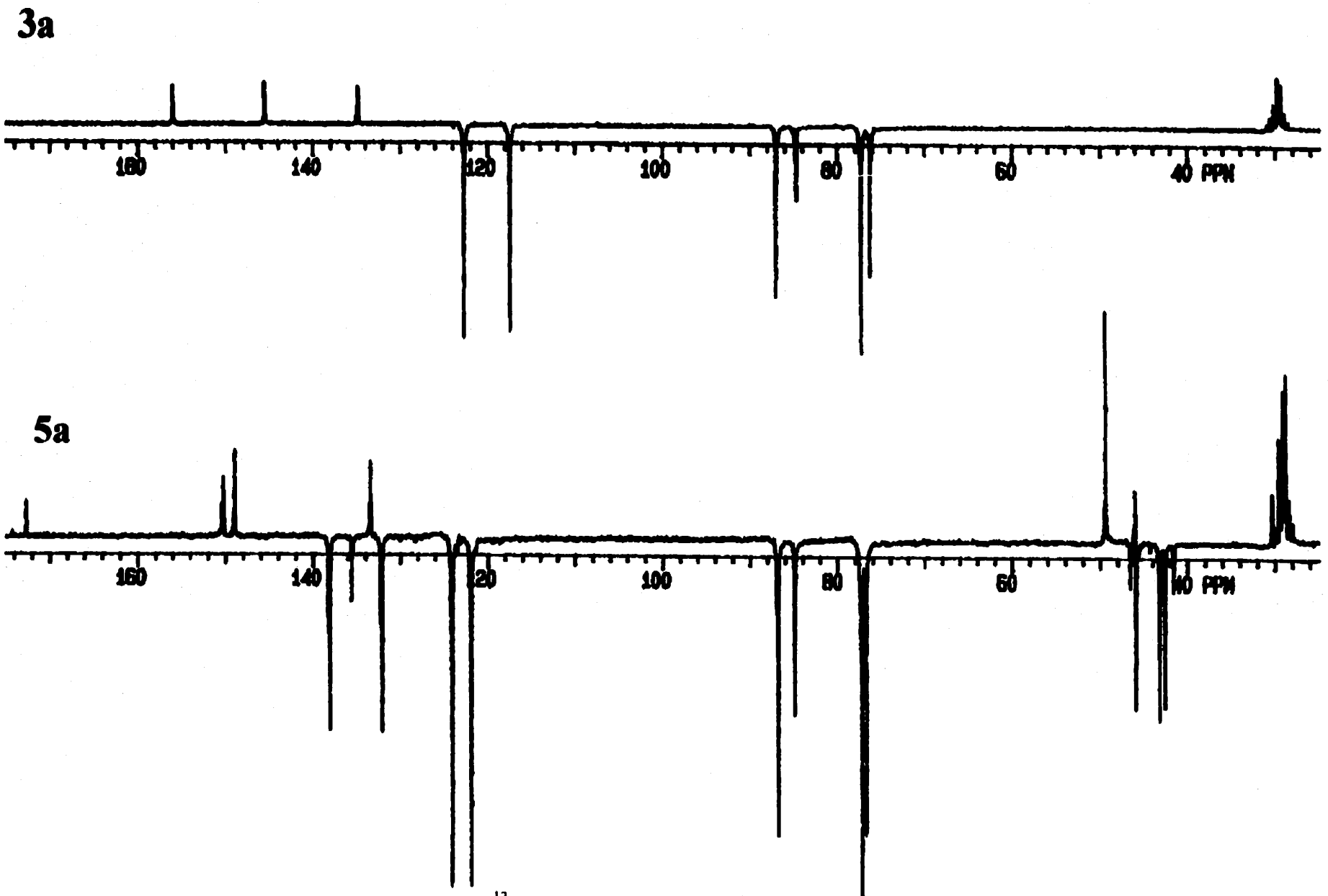

Figure 3.5: ^{13}C NMR spectra for complex **3a** and monomer **5a**.

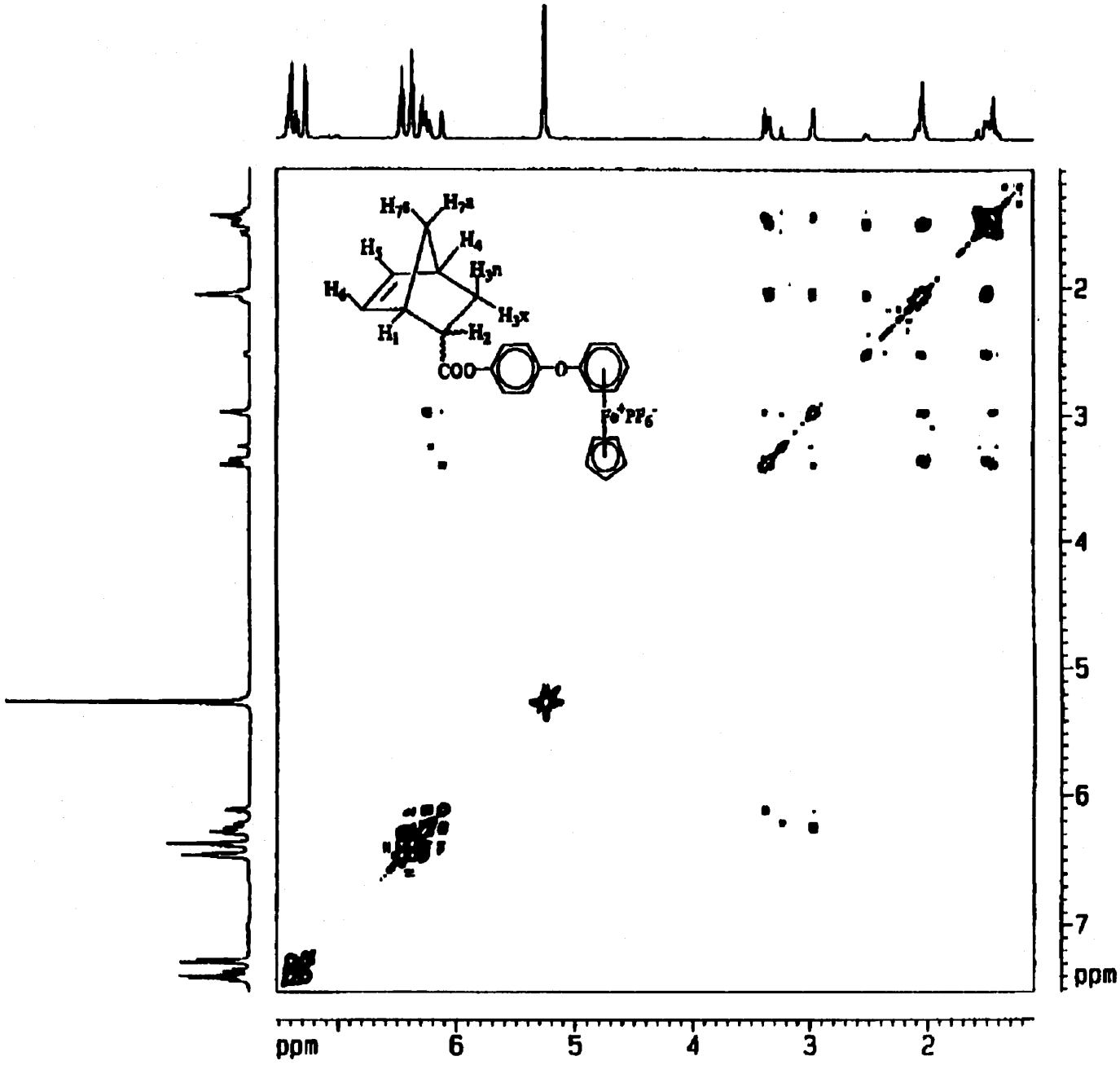

Figure 3.6: HH COSY NMR spectrum for monomer **5a**.

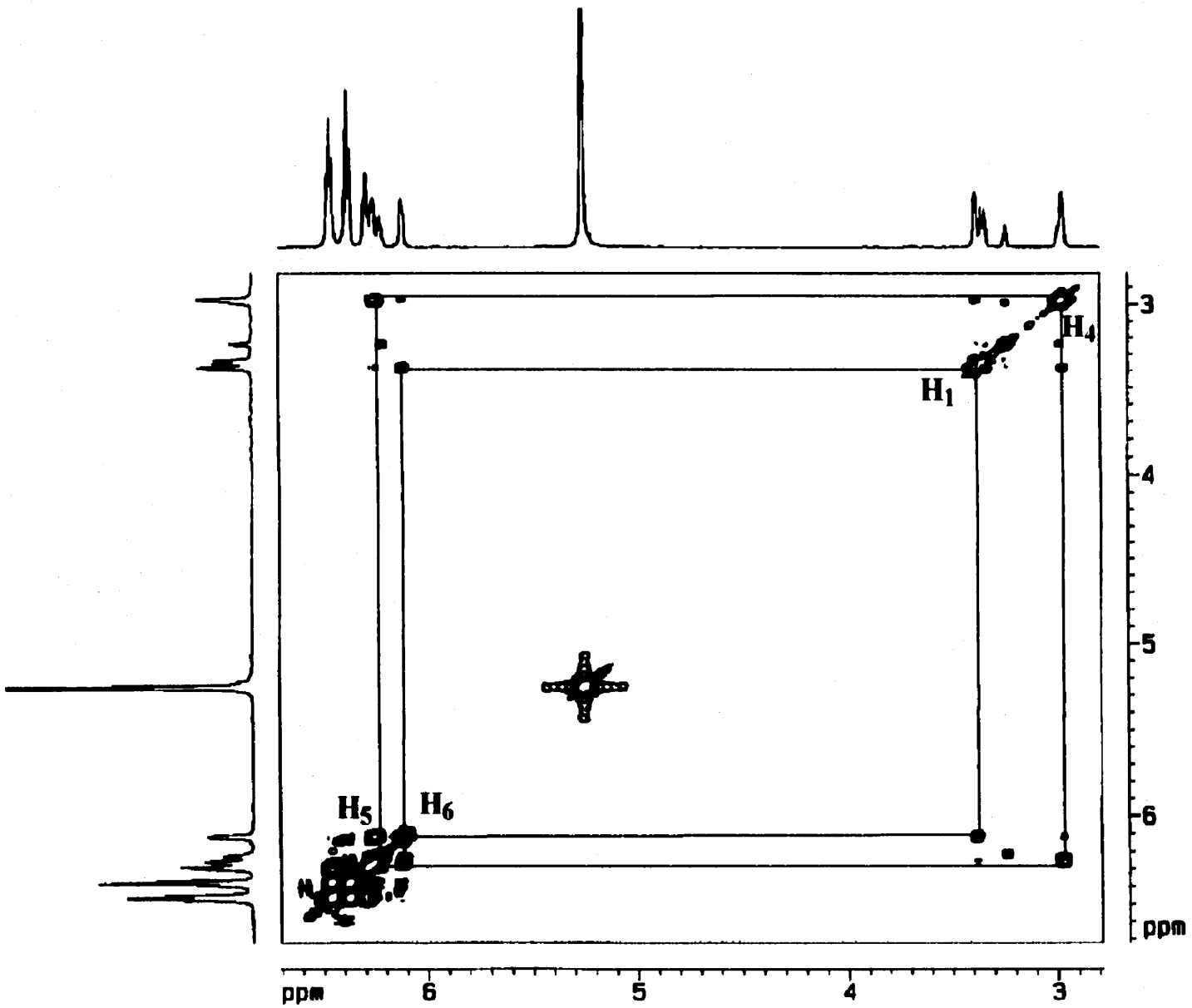

Figure 3.7: Proton assignments for the *endo* isomer of monomer **5a**.

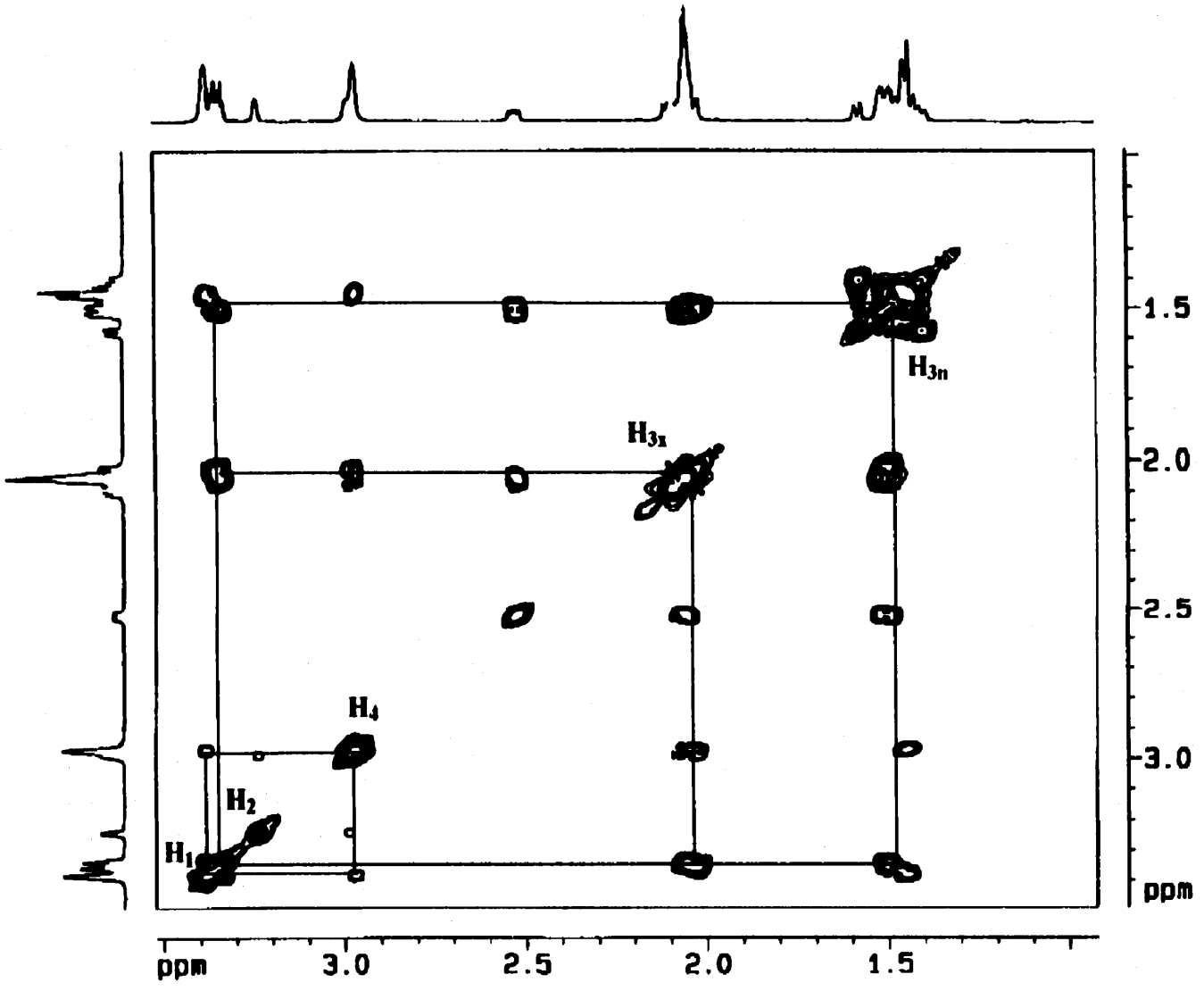

Figure 3.8: Proton assignments for the *endo* isomer of monomer **5a**.

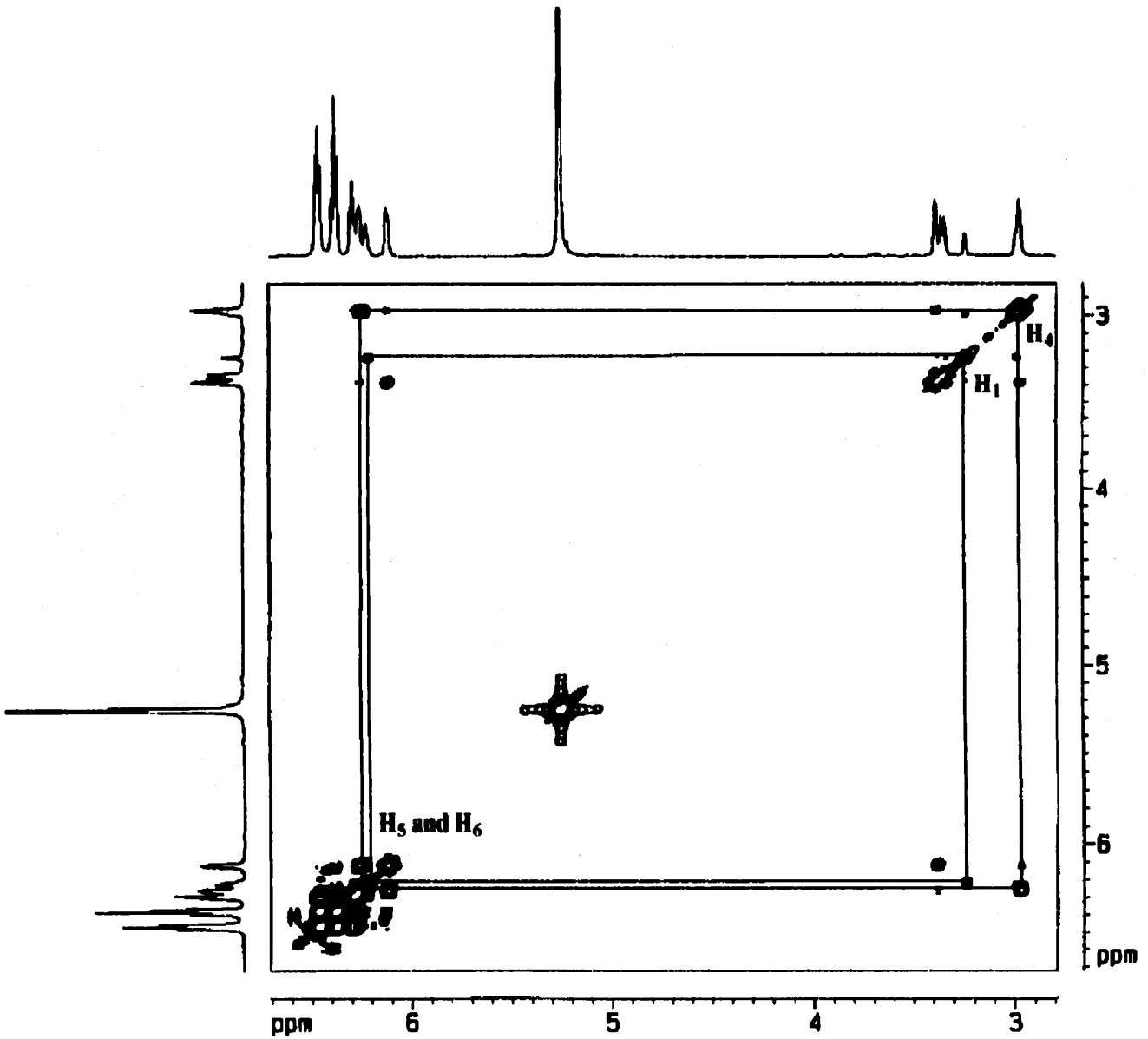

Figure 3.9: Proton assignments for the *exo* isomer of monomer **5a**.

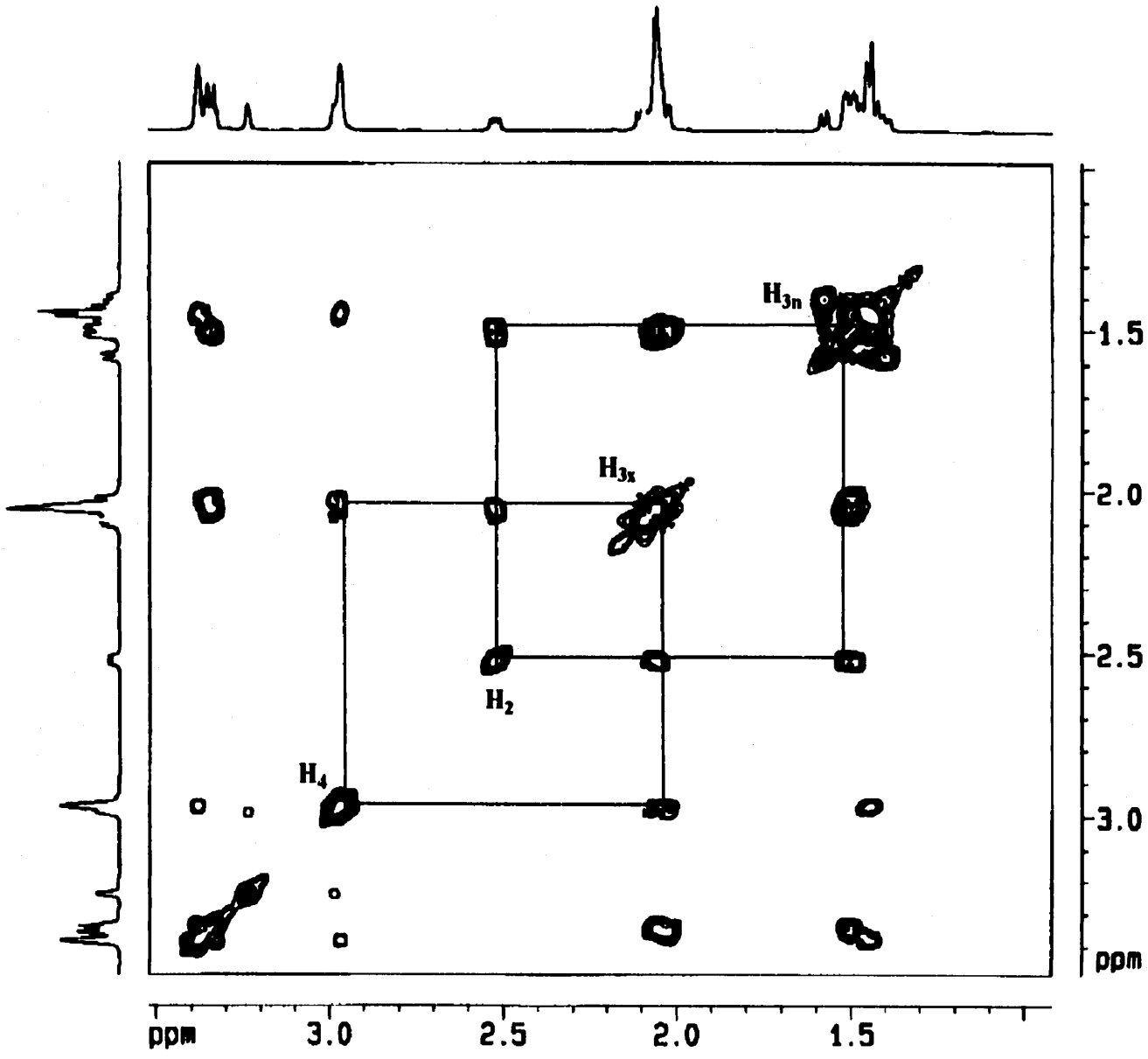

Figure 3.10: Proton assignments for the *exo* isomer of monomer **5a**.

Following analysis of the monomers' HH COSY NMR spectra, the heteronuclear correlation spectroscopy (CH COSY) NMR spectra were analyzed to provide confirmation of the proton assignments (Figure 3.11). As shown in Figure 3.12, correct assignment of the olefinic protons was confirmed as $C_6(n)$ and $C_5(n)$ correlated with the two doublets of doublets within the ^1H NMR spectrum. As well, the olefinic carbons of the *exo* isomer ($C_6(x)$ and $C_5(x)$) were found within the multiplet resonating between 6.20 and 6.23 ppm (Figure 3.12). Other correlations of interest were those of H_{7a} and H_{7s} with C_7, as well as H_{3x} and H_{3n} with C_3. As illustrated in Figure 3.13, the resonances in the ^1H NMR spectrum that were assigned to H_{7a} and H_{7s} of the *exo* isomer (m, δ 1.39-1.52 ppm) displayed connectivity with a single peak in the ^{13}C NMR spectrum (δ 50.21 ppm). This indicated that both of these protons were attached to the same carbon. As expected, this pattern was also observed for the two H_7 protons of the *endo* isomer (Figure 3.13) and both H_3 protons of each isomer.

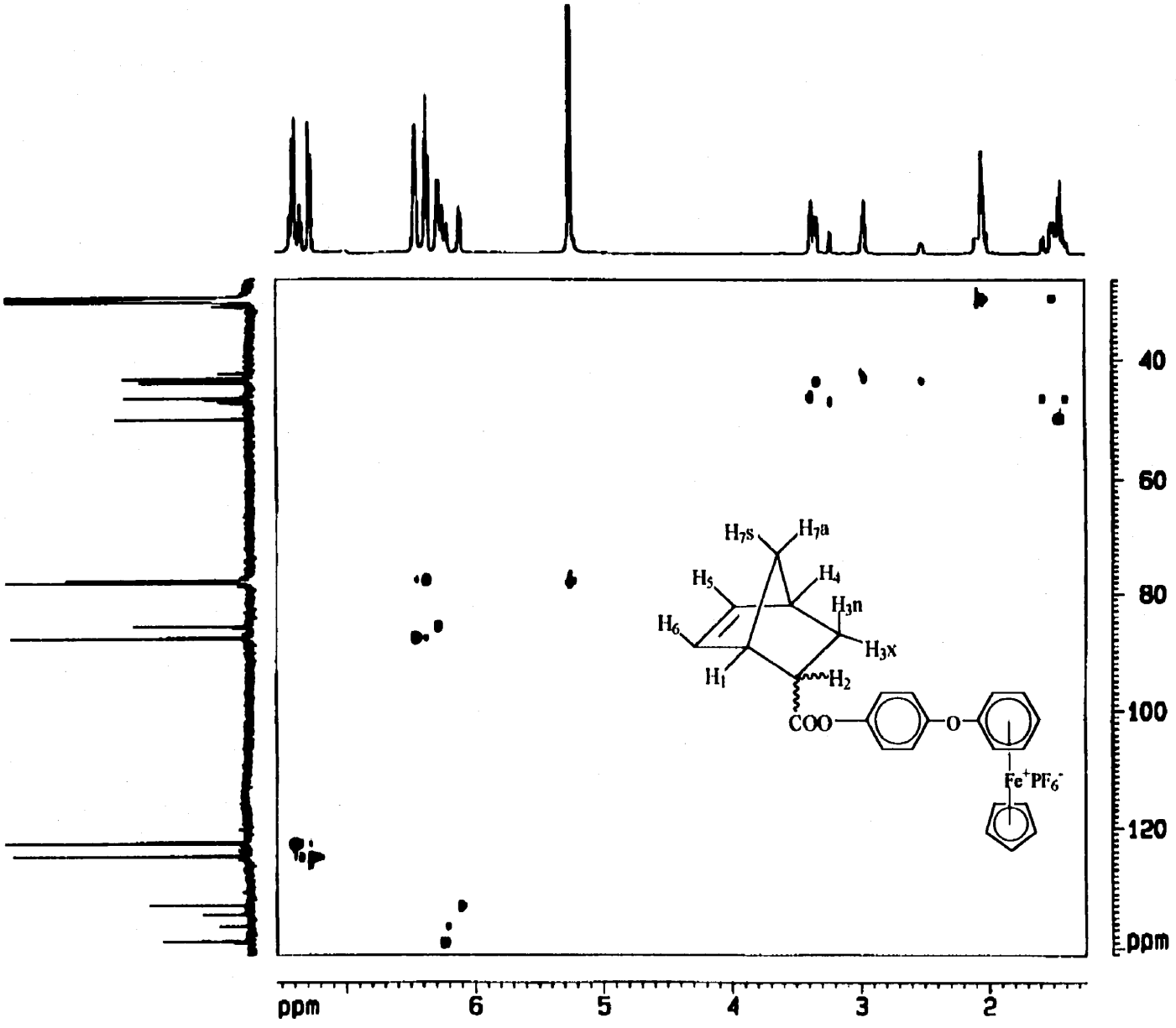

Figure 3.11: CH COSY NMR of monomer **5a**.

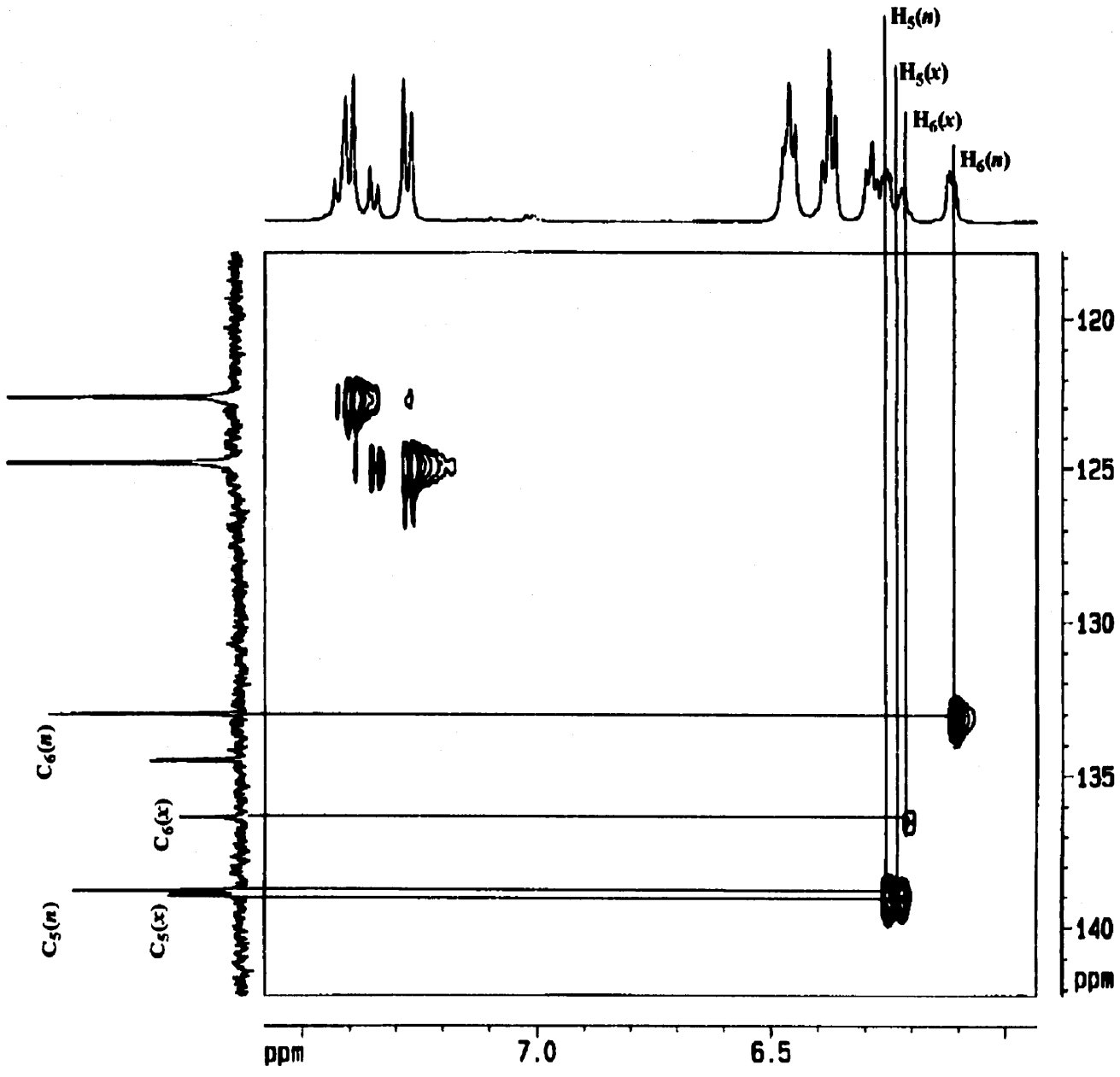

Figure 3.12: Identification of the olefinic carbons and hydrogens of monomer **5a**.

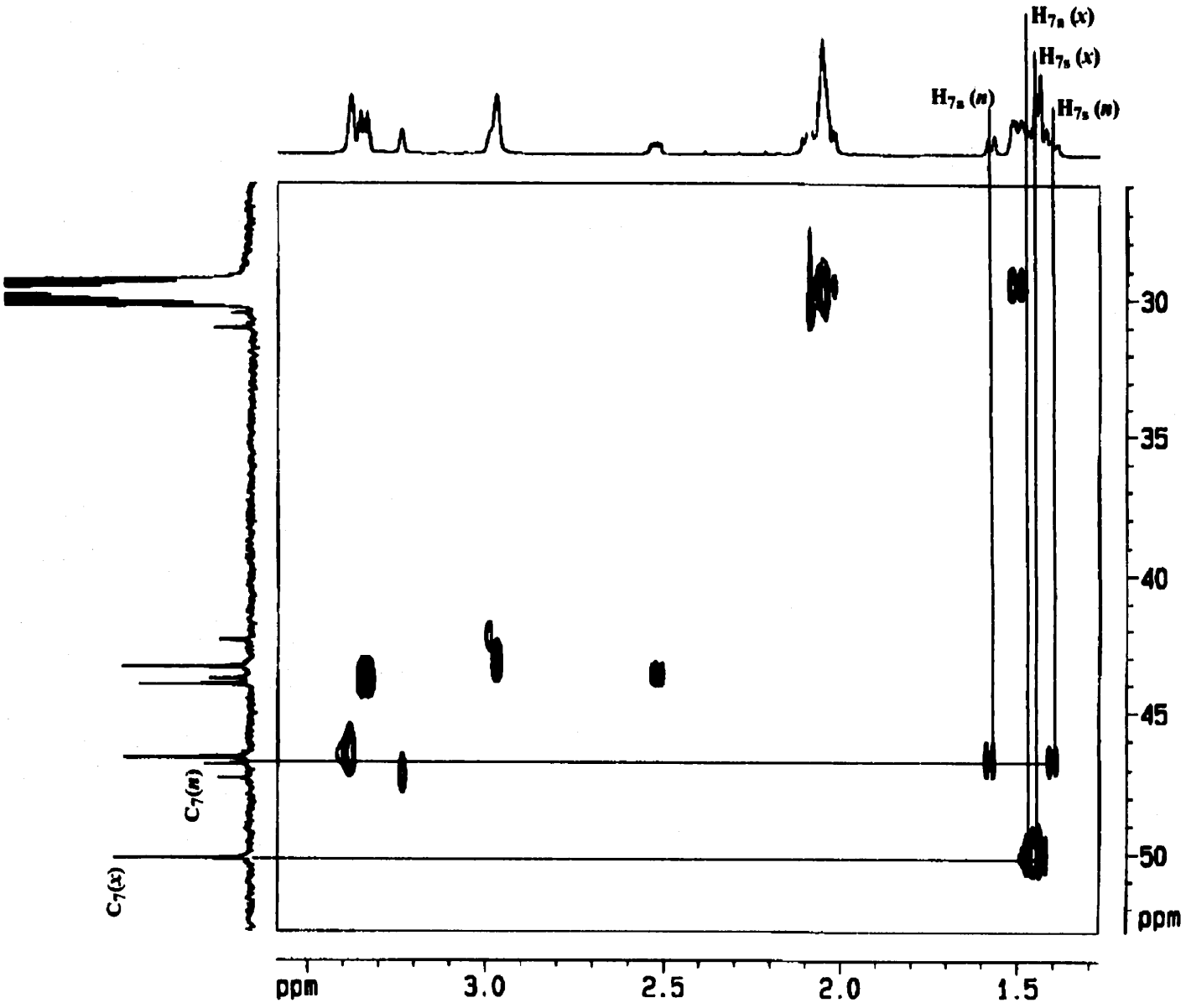

Figure 3.13: Identification of H_{7s}, H_{7a} and C_7 of monomer **5a**.

Table 3.4: Yield, IR and elemental analysis data for monometallic monomers **5a-e**.

MONOMER	PRODUCT YIELD	IR ABSORBANCES (cm^{-1})	CH ANALYSIS CALCULATED	CH ANALYSIS FOUND
5a	1.0873 g (95%)	1754 (CO) 703, 736 (*cis* =C-H out-of-plane)	C, 52.47; H, 4.05	C, 52.77; H, 4.25
5b	1.0788 g (92%)	1748 (CO) 717, 738 (*cis* =C-H out-of-plane)	C, 53.26; H, 4.30	---
5c	1.1737 g (85%)	1749 (CO) 703, 737 (*cis* =C-H out-of-plane)	C, 59.15; H, 4.82	---
5d	1.2399 g (88%)	1750 (CO) 715, 737 (*cis* =C-H out-of-plane)	C, 59.67; H, 5.01	C, 59.69; H, 5.19
5e	1.2291 g (79%)	1750 (CO) 703, 737 (*cis* =C-H out-of-plane)	C, 63.87; H, 5.36	C, 63.61; H, 5.47

Note: --- Denotes that CH analysis was not obtained.

Table 3.5a: ^{1}H NMR data for monometallic monomers **5a-c**.

δ (ppm) in acetone-d_6										
MONOMER		H_1	H_2	H_{3x}	H_{3n}	H_4	H_5	H_6	H_{7a}	H_{7s}
5a~	*endo*	3.38 (br s)	3.33-3.36 (m)	2.03-2.06 (m)	1.39-1.52 (m)	2.97 (br s)	6.26 (dd) $J_{5,6}$ = 5.48 $J_{4,5}$ = 2.93	6.12 (dd) $J_{5,6}$ = 5.48 $J_{1,6}$ = 2.58	1.39-1.52 (m)	1.58 (d) $J_{7a,7s}$ = 8.40
	exo	3.24 (br s)	2.52 (dd) $J_{2,3x}$ = 8.57 $J_{2,3n}$ = 2.52	2.03-2.06 (m)	1.39-1.52 (m)	3.17 (br s)	6.20-6.23 (m)	6.20-6.23 (m)	1.39-1.52 (m)	1.39-1.52 (m)
5b	*endo*	3.37 (br s)	3.29-3.33 (m)	1.93-1.99 (m)	1.36-1.53 (m)	2.96 (br s)	6.22-6.27 (m)	6.08-6.11 (m)	1.36-1.53 (m)	1.58 (m)
	exo	3.22 (br s)	2.54-2.69 (m)	1.93-1.99 (m)	1.36-1.53 (m)	2.96 (br s)	6.22-6.27 (m)	6.22-6.27 (m)	1.36-1.53 (m)	1.36-1.53 (m)
5c	*endo*	3.33 (br s)	3.24-3.31 (m)	1.86-2.00 (m)	1.33-1.53 (m)	2.94 (br s)	6.20-6.23 (m)	6.07 (dd) $J_{5,6}$ = 5.54 $J_{1,6}$ = 2.60	1.33-1.53 (m)	1.57 (br s)
	exo	3.19 (br s)	2.47 (dd) $J_{2,3x}$ = 9.12 $J_{2,3n}$ = 4.14	1.86-2.00 (m)	1.33-1.53 (m)	2.94 (br s)	6.20-6.23 (m)	6.20-6.23 (m)	1.33-1.53 (m)	1.33-1.53 (m)

Note: NMR spectra recorded at 500 (~) and 200 MHz.
Coupling constants reported in hertz.

Table 3.5b: ^{1}H NMR data for monometallic monomers **5d-e**.

MONOMER		δ (ppm) in acetone-d_6								
		H_1	H_2	H_{3x}	H_{3n}	H_4	H_5	H_6	H_{7a}	H_{7s}
5d	*endo*	3.32 (br s)	3.24-3.30 (m)	1.91-1.97 (m)	1.34-1.51 (m)	2.93 (br s)	6.20-6.23 (m)	6.07 (dd) $J_{5,6}$ = 5.68 $J_{1,6}$ = 2.67	1.34-1.51 (m)	1.57 (br s)
	exo	3.19 (br s)	---	1.91-1.97 (m)	1.34-1.51 (m)	2.93 (br s)	6.20-6.23 (m)	6.20-6.23 (m)	1.34-1.51 (m)	1.34-1.51 (m)
5e~	*endo*	3.33 (br s)	3.26-3.29 (m)	1.96-2.03 (m)	1.36-1.48 (m)	2.93 (br s)	6.19-6.22 (m)	6.07 (dd) $J_{5,6}$ = 5.18 $J_{1,6}$ = 2.33	1.36-1.48 (m)	1.55 (d) $J_{7a,7s}$ = 8.50
	exo	3.19 (br s)	2.46 (dd) $J_{2,3x}$ = 8.45 $J_{2,3n}$ = 4.10	1.96-2.03 (m)	1.36-1.48 (m)	2.95 (br s)	6.19-6.22 (m)	6.19-6.22 (m)	1.36-1.48 (m)	1.36-1.48 (m)

Note: NMR spectra recorded at 500 (~) and 200 MHz.
Coupling constants reported in hertz.
--- Denotes a hidden peak.

Table 3.6: ^{1}H NMR data for monometallic monomers **5a-e**.

δ (ppm) in acetone-d_6				
MONOMER	ArH	$CpFe^+$-ArH	Cp	CH_3
5a~	7.27 (d, 2H, *J* = 8.80) 7.35 (d, 1H, *J* = 8.80) 7.39-7.45 (m, 1H)	6.29 (t, 1H, *J* = 5.88) 6.37 (d, 2H, *J* = 6.37) 6.45 (t, 2H, *J* = 6.35)	5.25 (s, 5H)	---
5b	7.25 (d, 2H, *J* = 8.87) 7.35-7.40 (m, 2H)	6.33 (dd, 4H, *J* = 13.55, *J* = 6.96)	5.21 (s, 5H)	2.48 (s, 3H)
5c	6.98 (d, 1H, *J* = 8.50) 7.04 (d, 1H, *J* = 8.45) 7.24-7.35 (m, 4H) 7.42 (d, 1H, *J* = 2.12) 7.43 (d, 1H, *J* = 2.19)	6.27 (t, 1H, *J* = 5.90) 6.34 (d, 2H, *J* = 6.60) 6.45 (d, 2H, *J* = 6.19)	5.24 (s, 5H)	1.72 (s, 3H) 1.73 (s, 3H)
5d	7.00 (d, 1H, *J* = 8.71) 7.07 (d, 1H, *J* = 8.71) 7.21-7.34 (m, 4H) 7.40 (d, 1H, *J* = 2.16) 7.44 (d, 1H, *J* = 2.18)	6.30 (dd, 4H, *J* = 14.24, *J* = 6.92)	5.18 (s, 5H)	1.71 (br s, 6H) 2.47 (s, 3H)
5e~	6.98 (d, 1H, *J* = 8.50) 7.04 (d, 1H, *J* = 8.45) 7.20 (br d, 2H, *J* = 3.70) 7.23-7.30 (m, 6H) 7.43 (d, 2H, *J* = 8.45)	6.26 (t, 1H, *J* = 5.88) 6.33 (d, 2H, *J* = 6.45) 6.43 (d, 2H, *J* = 6.23)	5.22 (s, 5H)	1.67 (s, 3H) 1.68 (s, 3H) 1.70 (s, 6H)

Note: NMR spectra recorded at 500 (~) and 200 MHz.
Coupling constants reported in hertz.

Table 3.7a: ^{13}C NMR data for monometallic complexes **5a-c**.

MONOMER		δ (ppm) in acetone-d_6											
		C_1	C_2	C_3	C_4	C_5	C_6	C_7	Cp	$CpFe^+$-ArCH	ArCH	CO	OTHERS
5a~	*endo*	46.65	44.04	29.49	43.39	138.79	136.64	46.87	78.07	77.77 85.85 87.80 134.49*	122.61 124.81 150.00* 151.23*	173.34 174.99	--
	exo	47.35	43.83	29.80	42.42	138.94	132.96	50.21					
5b	*endo*	45.51	42.78	28.64	42.20	137.80	131.83	45.81	77.27	75.63 86.47 100.26* 131.94*	121.44 123.73 148.51* 150.21*	172.46 174.03	18.70 (CH_3)
	exo	46.12	42.57	30.02	41.23	137.80	135.22	49.12					
5c	*endo*	46.32	43.64	29.41	43.03	138.47	132.67	46.59	77.19	77.19 85.25 87.33 134.05*	121.80 121.86 128.17 129.52 147.93* 149.22* 149.56* 151.36*	173.28 174.87	30.93 (CH_3) 42.75*
	exo	46.99	43.44	30.17	42.05	138.59	136.05	49.94					

Note: NMR spectra recorded at 125 (~) and 50 MHz.
* Denotes a quaternary carbon.

Table 3.7b: ^{13}C NMR data for monometallic complexes **5d-e**.

δ (ppm) in acetone-d_6													
MONOMER		C_1	C_2	C_3	C_4	C_5	C_6	C_7	Cp	$CpFe^+$-ArCH	ArCH	CO	OTHERS
5d	*endo*	46.36	43.67	29.43	43.07	138.50	132.70	46.63	78.08	76.47 87.34 100.96* 133.00*	120.71 121.88 128.19 129.50 147.80* 149.14* 149.62* 151.64*	173.32 174.94	19.54 (CH_3) 30.95 (CH_3) 42.79*
	exo	47.04	43.48	30.18	42.09	138.54	136.08	49.96					
5e~	*endo*	46.67	44.08	29.49	43.42	138.69	134.57	46.89	78.08	77.82 85.76 87.85 133.05*	121.01 121.96 127.19 127.24 128.99 130.68 148.22* 148.72* 148.82* 148.91* 149.98* 152.00*	173.43 175.09	31.10 (CH_3) 31.17 (CH_3) 42.87* 43.06*
	exo	47.40	43.89	29.80	42.44	138.93	136.43	50.23					

Note: NMR spectra recorded at 125 (~) and 50 MHz.
* Denotes a quaternary carbon.

3.2.2 Synthesis of Norbornenes Containing Two $CpFe^+$ Moieties

3.2.2.1 Synthesis of Bimetallic Starting Materials

Metal-mediated nucleophilic aromatic substitution reactions were also utilized in the preparation of starting complexes that contained two cyclopentadienyliron moieties. As seen in Scheme 3.10, bimetallic complexes **7** and **8** were prepared via the reaction of complexed chloroarenes (**1a**, **1c**) with 4,4'-bis(4-hydroxyphenyl)valeric acid (**6**). When η^6-chlorobenzene-η^5-cyclopentadienyliron hexafluorophosphate (**1a**) was used in the reaction, the resulting diiron species (**7**) was terminated with unsubstituted complexed aromatic rings. However, if η^6-1,4-dichlorobenzene-η^5-cyclopentadienyliron hexafluorophosphate (**1c**) was employed, a bimetallic complex functionalized with terminal chloro groups was isolated (**8**). As well, heat was required for successful reaction of the chlorobenzene complex with the dinucleophile, while the reaction involving the dichlorobenzene complex could be carried out at room temperature. Thus, the second chloro group on **1c** not only facilitated the substitution reaction such that it could be carried out at room temperature, its presence in the resulting bimetallic complex (**8**) allowed for further extension of the aromatic linkage via subsequent S_NAr reactions.

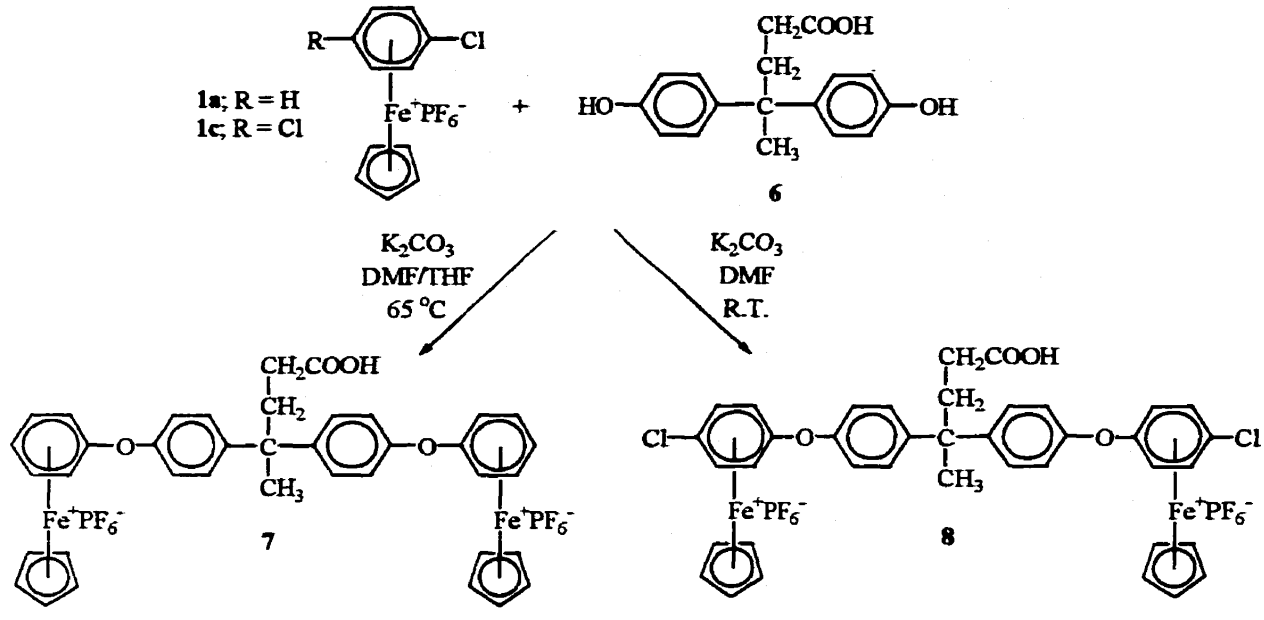

Scheme 3.10: Synthesis of bimetallic starting complexes **7** and **8**.

Complexes **7** and **8** were isolated as yellow solids in good yields (82 and 86%, respectively) and characterized using NMR, FT-IR and CH analysis (Tables 3.8-3.10). The upfield regions of the ^{1}H NMR spectra of both complexes were very similar. The methyl protons appeared as single resonances between 1.75 and 1.76 ppm, while the methylene protons appeared as two multiplets in each spectrum, one in the range of 2.12-2.22 ppm, and the other between 2.40 and 2.58 ppm. As the structures of the bimetallic complexes were symmetric, the Cp protons of both complexes appeared as single resonances with chemical shifts of approximately 5.3 ppm in the spectra. These singlets had shifted upfield relative to those of the chloroarene starting materials (δ 5.44 ppm), as the chloro groups within the starting complexes (**1a** and **1c**) had been replaced by etheric linkages in the bimetallic species (**7** and **8**). The complexed aromatic protons appeared in

the spectra between 6.30 and 6.80 ppm, while the uncomplexed aromatic protons resonated in the range of 7.33-7.49 ppm. The ^{1}H NMR spectrum of complex 7 is shown in Figure 3.14 as a representative example.

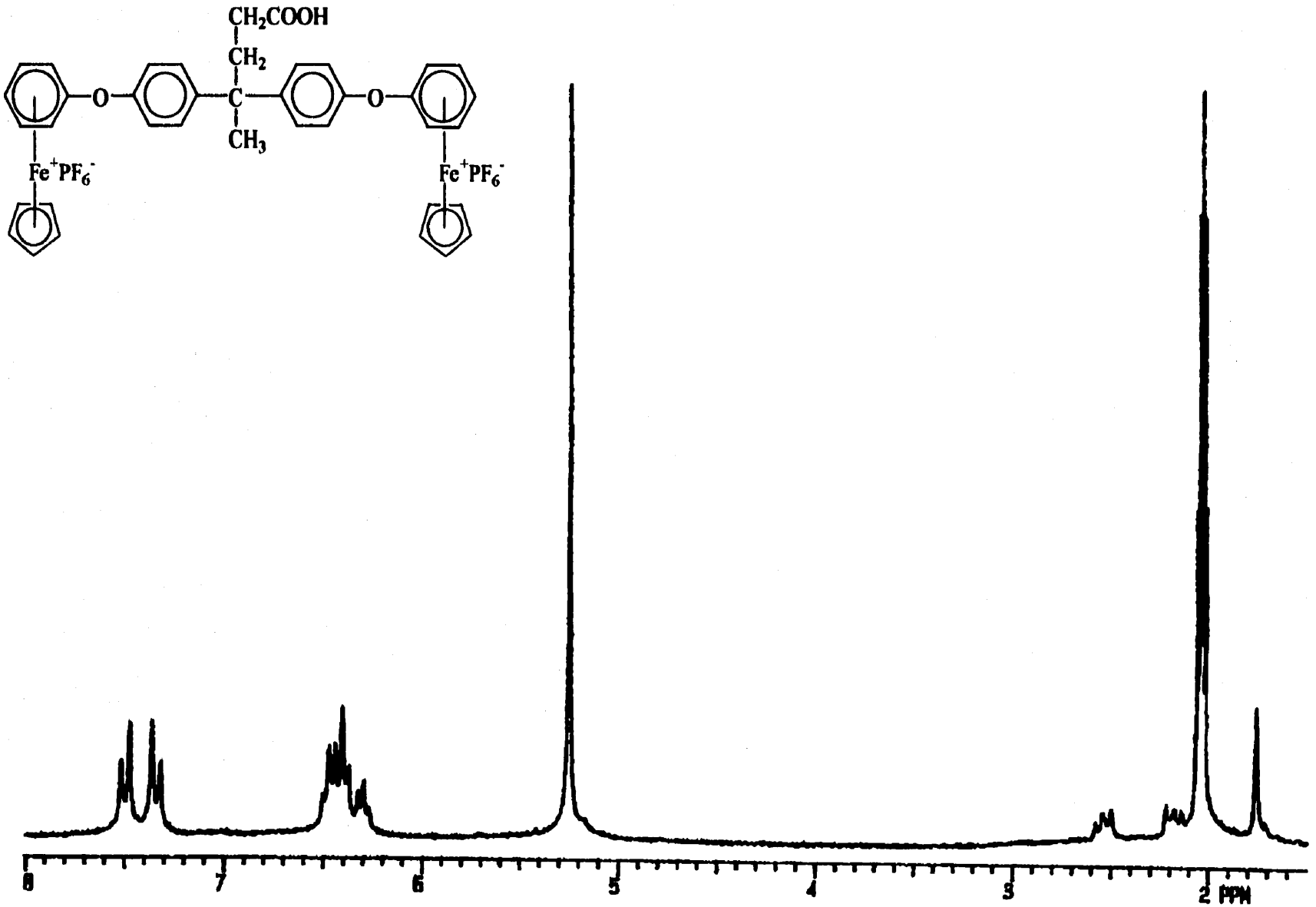

Figure 3.14: ^{1}H NMR spectrum of complex 7.

As anticipated, the ^{13}C NMR spectra of the diiron complexes also revealed some similarities. It was found that the methyl carbons in complexes 7 and 8 resonated at almost identical chemical shifts of 27.75 ppm and 27.76 ppm, respectively, while the methylene and aliphatic quaternary carbons within the aliphatic spacer of the two complexes were found between 30 and 46 ppm. The carbons of the Cp moieties were represented by a single resonance around 80 ppm in the two spectra, again illustrating the symmetric nature of these complexes.

Dissimilarities between the two spectra arose upon analysis of the complexed aromatic regions of the ^{13}C NMR spectra. For example, complex 7 displayed three complexed aromatic carbons between 77 and 88 ppm, and one complexed aromatic quaternary carbon at 134.27 ppm. In contrast, complex 8 showed two complexed aromatic carbons (δ 77.05 and δ 87.76 ppm) and two peaks at 104.68 and 133.74 ppm, representing its quaternary complexed aromatic carbons. These spectral differences were a direct result of the different substitution patterns of the complexed aromatic rings within the bimetallic structures.

The uncomplexed aromatic regions of the two spectra were essentially identical, as the aromatic bridge within each of the complexes was the same. It was found that the two uncomplexed aromatic carbons resonated at approximately 121 and 130 ppm within each of the spectra, while the uncomplexed quaternary aromatic carbons were identified at chemical shifts near 147 and 151 ppm. The carbonyl carbon of each complex appeared around 170 ppm. The ^{13}C NMR spectrum of complex 7 can be found in Figure 3.15.

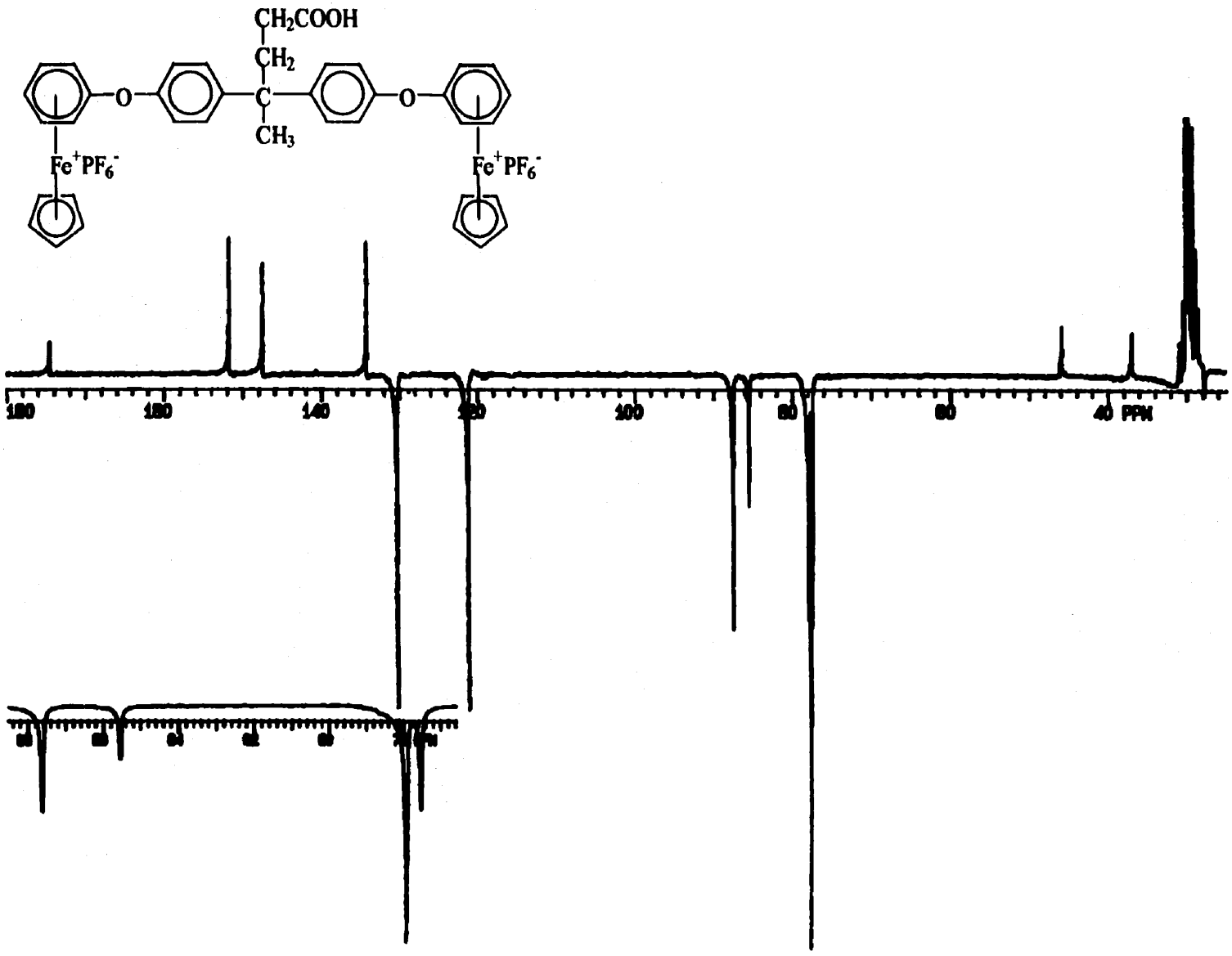

Figure 3.15: ^{13}C NMR spectrum of complex 7.

Table 3.8: Yield, IR and elemental analysis data for complexes **7** and **8**.

COMPLEX	PRODUCT YIELD	IR ABSORBANCES (cm^{-1})	CH ANALYSIS CALCULATED	CH ANALYSIS FOUND
7	1.591 g (82%)	1726 (CO)	C, 48.28; H, 3.74	---
8	1.787 g (86%)	1725 (CO)	C, 45.07; H, 3.30	C, 45.29; H, 3.26

Note: --- Denotes that CH analysis was not obtained.

Table 3.9: ^{1}H NMR data for bimetallic complexes **7** and **8**.

	δ (ppm) in acetone-d_6				
COMPLEX	ArH	$CpFe^+$-ArH	Cp	CH_2	CH_3
7	7.34 (d, 4H, J = 8.40) 7.49 (d, 4H, J = 8.80)	6.30 (t, 2H, J = 5.85) 6.39 (d, 4H, J = 6.40) 6.47 (t, 4H, J = 6.10)	5.25 (s, 10H)	2.14-2.22 (m, 2H) 2.50-2.58 (m, 2H)	1.76 (s, 3H)
8	7.33 (d, 4H, J = 8.06) 7.48 (d, 4H, J = 8.34)	6.50 (d, 4H, J = 6.59) 6.80 (d, 4H, J = 6.47)	5.37 (s, 10H)	2.12-2.20 (m, 2H) 2.40-2.50 (m, 2H)	1.75 (s, 3H)

Note: NMR spectra recorded at 200 MHz.
Coupling constants reported in hertz.

Table 3.10: ^{13}C NMR data for bimetallic complexes **7** and **8**.

δ (ppm) in acetone-d_6						
COMPLEX	quat. ArC	ArCH	quat. $CpFe^+$-ArC	$CpFe^+$-ArCH	Cp	OTHERS
7	147.60 151.87	121.25 130.37	134.27	77.52 85.54 87.62	77.92	27.75 (CH_3) 30.16 (CH_2) 37.09 (CH_2) 46.05* 174.62 (CO)
8	147.87 151.86	121.18 130.50	104.68 133.74	77.05 87.76	80.38	27.76 (CH_3) 37.14 (CH_2) 45.89 (CH_2) 46.21*

Note: NMR spectra recorded at 50 MHz.
* Denotes a quaternary carbon.

3.2.2.2 Preparation of Norbornenes Containing Two $CpFe^+$ moieties

The preparation of the bimetallic complexes containing free carboxylic acid groups allowed for a route to the isolation of norbornene monomers that contained two organoiron units within their structures. This was accomplished via an esterification reaction of a bimetallic species (**7** or **8**) with *exo,endo*-5-norbornene-2-methanol (**9**) in the presence of a coupling agent (dicyclohexylcarbodiimide, DCC), as illustrated in Scheme 3.11. The organometallic monomers **10** and **11** were isolated in good yields of 76 and 87 %, respectively, and fully characterized using NMR, FT-IR and CH analysis (Tables 3.11-3.14).

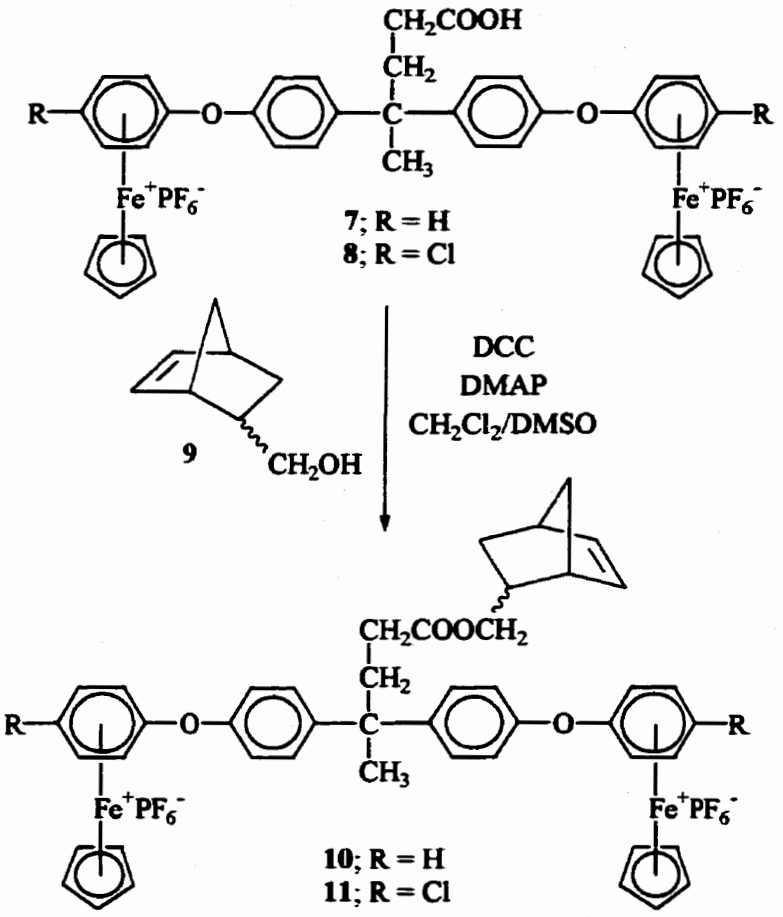

Scheme 3.11: Preparation of bimetallic norbornene monomers **10** and **11**.

The presence of the terminal chloro groups in the side chain of monomer **11** allowed for the extension of the aromatic bridges in a lateral manner via the formation of aromatic ether linkages. As outlined in Scheme 3.12, displacement of the chlorine atoms of monomer **11** was accomplished by its reaction with various phenolic compounds (**12a,b,c**) in the presence of a weak base. The resulting monomers (**13a,b,c**) were obtained in yields ranging from 85-89%, and as with the previous set of metallated monomers, their structural identification was accomplished using spectroscopy techniques and elemental analysis (Tables 3.11-3.14).

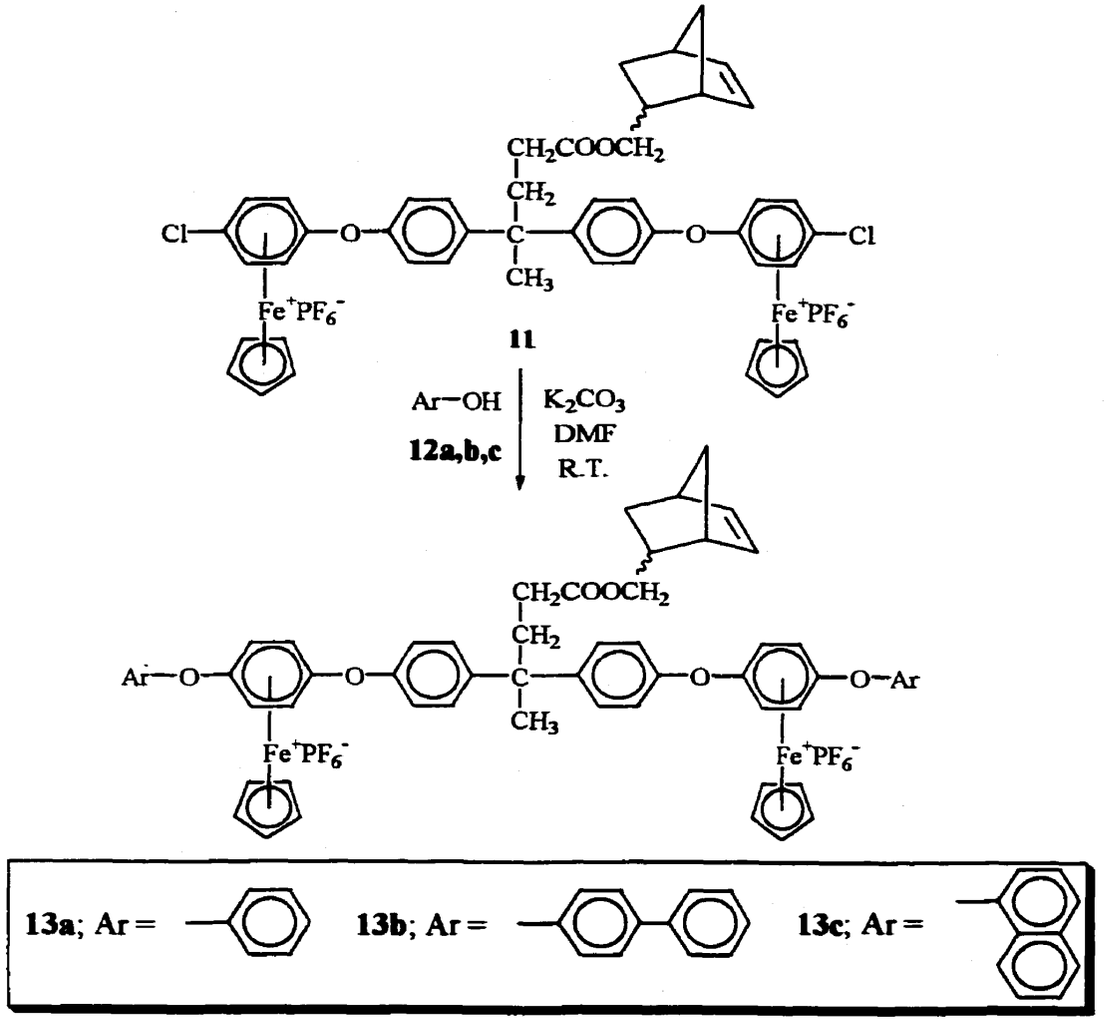

Scheme 3.12: Synthesis of bimetallic norbornenes with elongated side chains (**13a-c**).

Comparison of the NMR and FT-IR spectra for the bimetallic starting complexes 7 and 8) and the resulting monomers (**10**, **11**, **13a,b,c**) proved useful in determining if successful reaction had occurred. For example, the upfield region of the NMR spectra of the bimetallic complexes and their corresponding monomers showed striking differences as numerous new peaks representing the norbornene rings within the monomers' structures appeared. As well, peaks representing the olefinic carbons of the norbornene unit were found at lower fields in each monomer's spectrum that were lacking in the spectra of the starting complexes. Finally, evidence of successful formation of the ester linkages between the norbornene rings and the aromatic bridge was obtained upon observation of carbonyl resonances around 170 ppm in the ^{13}C NMR spectra of the monomers, as well as absorbances around 1725 cm^{-1} in their FT-IR spectra.

As with the norbornene monomers containing one $CpFe^+$ moiety in their structures (**5a-e**), two-dimensional NMR techniques were required to analyze the *exo,endo*-isomer mixtures of the diiron norbornene monomers (**10**, **11**, **13a,b,c**). In general, the method of analysis of the spectra was the same, as the proton and carbon resonances of the two classes of monomers followed analogous trends. For example, the uncomplexed and complexed aromatic protons resonated at similar chemical shifts, and the norbornene protons appeared within their expected regions. However, differences between 3 to 4 ppm in the ^1H NMR and 60 to 65 ppm in the ^{13}C NMR spectra were observed as a result of the aliphatic spacer in the bimetallic monomers' structures that was not found in the norbornenes containing one $CpFe^+$ moiety. Fortunately, these methylene protons could be used to help in the identification of the isomeric mixture of the norbornenes containing two $CpFe^+$ moieties.

The HH COSY NMR spectrum for monomer **13a** is provided in Figure 3.16 as a representative example. Assignment of the olefinic protons, H_6 and H_5 of the *endo* isomer to the two doublets of doublets resonating at 5.92 and 6.15 ppm was accomplished based on the strong coupling between them ($J_{5,6}$ = 5.56 Hz). The bridgehead protons, H_1 and H_4 were then identified via their expected correlations with the olefinic protons. H_1 was assigned to the broad singlet at 2.83 ppm, whereas H_4 was found slightly upfield at 2.79 ppm. The coupling between H_1 and H_2, which is exclusive to the *endo* isomer, was used to assign H_2 to the broad singlet resonating at 2.36 ppm. This assignment was confirmed via the correlation of the H_2 resonance with two peaks appearing further upfield in the spectrum at 1.8 and 0.5 ppm (Figure 3.17). These peaks represented the H_3 protons, where H_{3x} was assigned to the multiplet between 1.75-1.85 ppm, and H_{3n} appeared as a broad doublet resonating at 0.53 ppm. The chemical shift of H_2 was further verified as a result of its correlation with the two peaks representing the methylene protons directly attached to the norbornene ring (nor-CH_2O), as illustrated in Figure 3.17.[163] The chirality at C_2 caused the magnetic environments of the two methylene protons to be different, thus, one of the methylene protons appeared as a triplet (δ 3.62 ppm), while the other showed up as a doublet of doublets (δ 3.77 ppm). The H_7 bridge protons were identified via the strong coupling they exhibited with each other ($J_{7a,7s}$ = 9.20 Hz). H_{7a} resonated within the multiplet appearing between 1.24-1.28 ppm, whereas the doublet at 1.37 ppm represented H_{7s}.

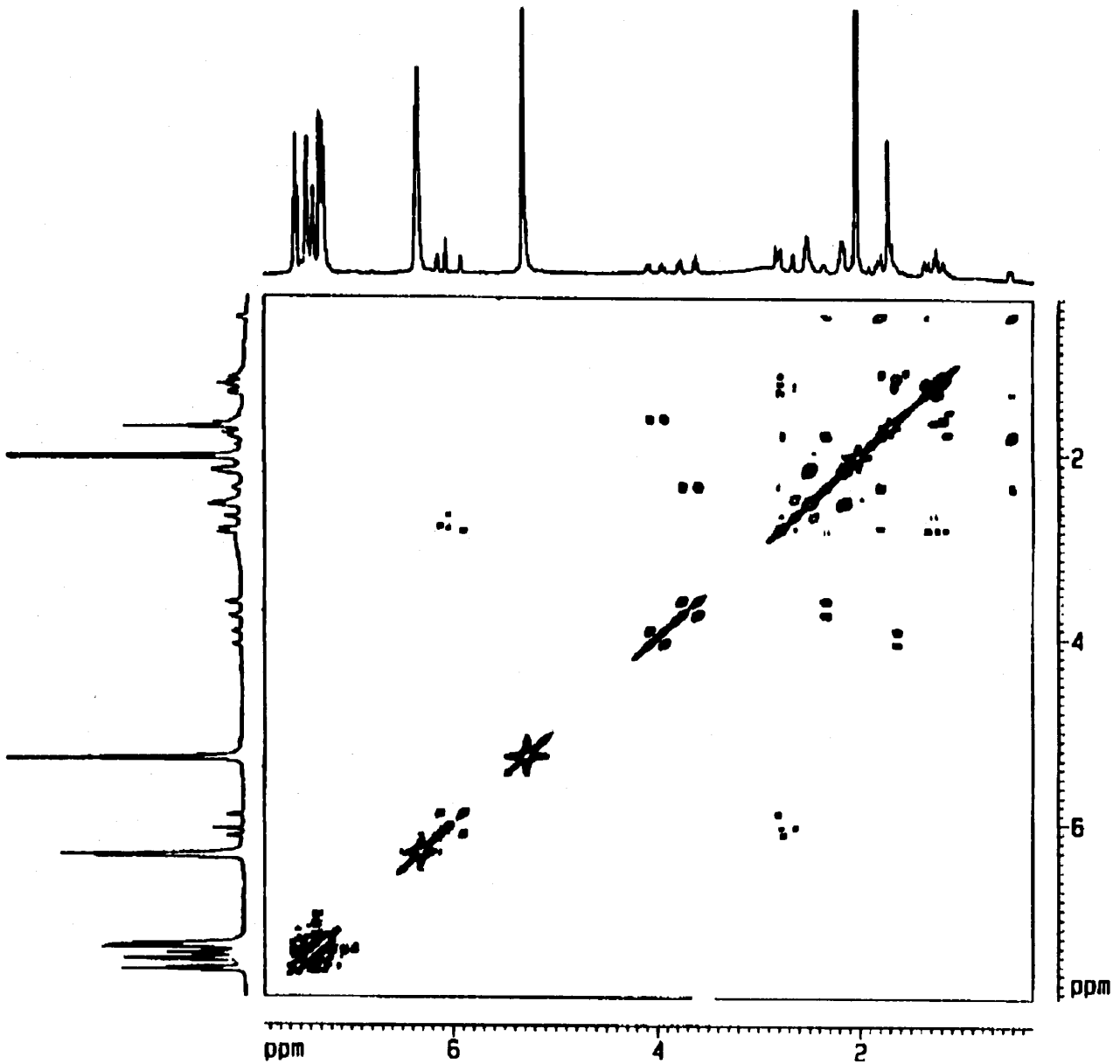

Figure 3.16: HH COSY NMR spectrum of monomer **13a**.

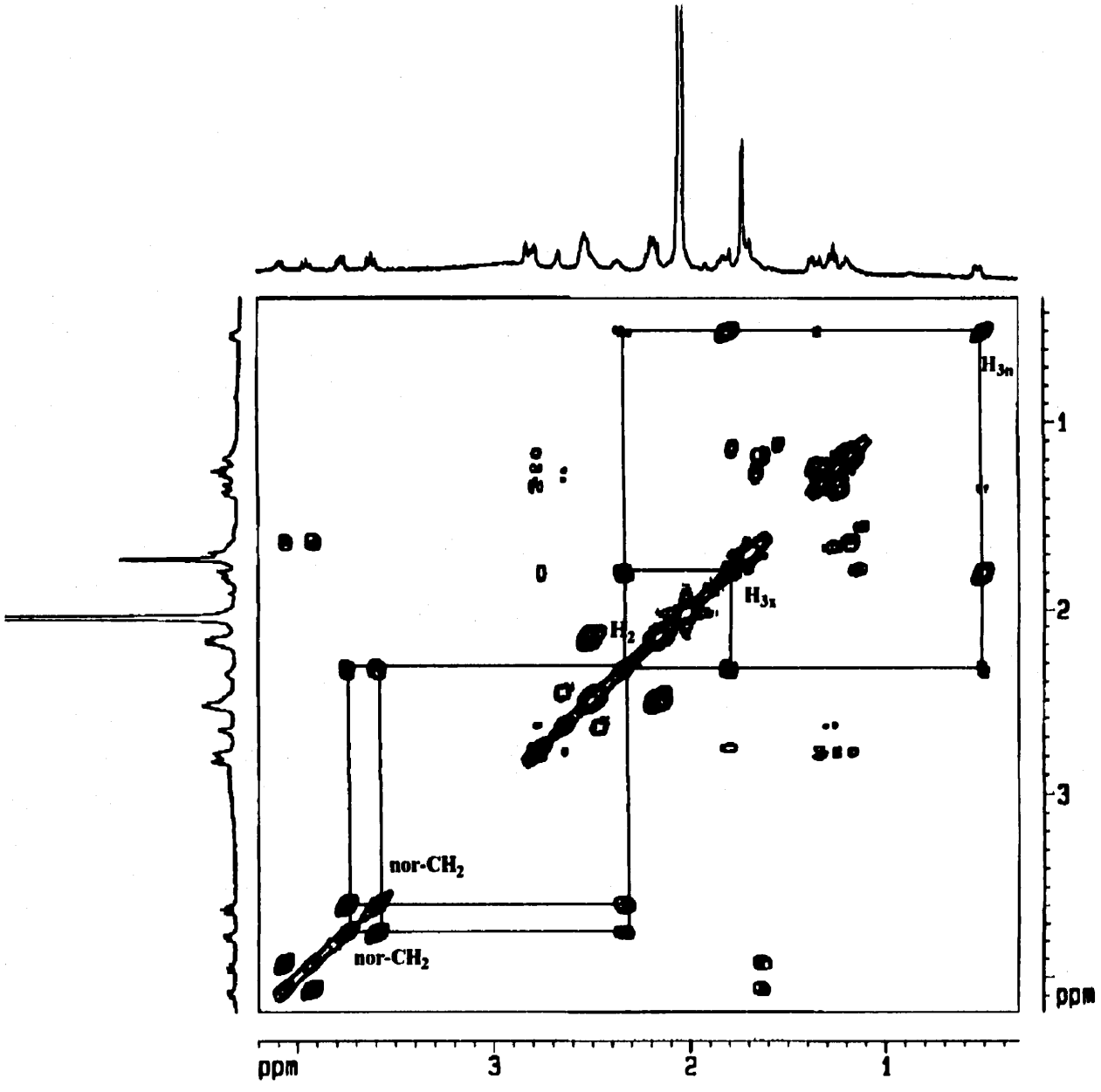

Figure 3.17: Proton assignments for the *endo* isomer of monomer **13a**.

The protons of the *exo* isomer were assigned in a similar manner, with H_6 and H_5 appearing as a multiplet at 6.7 ppm. The bridgehead protons H_1 and H_4 were both represented by broad singlets resonating at 2.66 and 2.80 ppm, respectively. Unlike the *endo* isomer, H_2 could not be assigned using H_1, as no coupling was observed between these protons, thus, H_2 was assigned based on its correlation with the H_3 protons and those of the methylene group attached to the norbornene ring (nor-CH_2O), as seen in Figure 3.18.[163] H_{3x} was identified as the multiplet resonating between 1.18-1.22 ppm, as it showed coupling with the bridgehead proton H_4. In contrast, H_{3n} (m, δ 1.75-1.85 ppm) did not show any correlation with H_4, and was solely identified using its coupling with H_{3x}. As in the *endo* isomer, the nor-CH_2O protons of the *exo* isomer appeared as a triplet and a doublet of doublets, however, they resonated further downfield at 3.95 and 4.09 ppm, respectively. Following the identification of these protons, H_2 was assigned to the broad singlet appearing at 1.69 ppm. Lastly, the bridge protons, H_{7a} and H_{7s} were assigned based on the large coupling they displayed ($J_{7a,7s}$ = 10.25 Hz). It was found that H_{7a} appeared within the multiplet resonating between 1.24 to 1.28 ppm, while H_{7s} appeared as a doublet at 1.34 ppm.

The remaining aliphatic protons within the aliphatic spacer of the monomer were assigned to the two doublet of doublets at 2.20 and 2.54 ppm. The 4 methylene protons appeared as doublets of doublets, and not simply doublets as would be expected, as a result of the isomerism of the norbornene ring. This isomerism caused the geminal protons of the methylenes to be chemical inequivalent and thus, couple differently with the protons attached to adjacent carbons. The protons of the methyl attached to the

quaternary carbon in the aromatic linkage appeared as a single resonance with a chemical shift equal to 1.73 ppm.

The residual peaks within the HH COSY NMR spectrum were assigned to the protons in the aromatic linkage of the monomer's side chain. The protons of the $CpFe^+$ moieties appeared as an intense singlet at 5.31 ppm. The protons of the *para*-substituted complexed aromatic rings gave rise to doublets resonating at 6.34 and 6.37 ppm, while, the uncomplexed aromatic protons originally present in the valeric acid nucleophile (**6**) were assigned to doublets appearing further upfield at 7.28 and 7.31 ppm. Lastly, the protons belonging to the two terminal phenyl rings appeared as a doublet and two triplets at lower fields ranging from 7.39-7.55 ppm.

Similar to the monometallic monomers, the CH COSY NMR spectra of the bimetallic monomers were used to verify the assignment of their proton resonances. Correlation of the olefinic carbon resonances with peaks appearing in the range of 5.9-6.2 ppm in the ^1H NMR spectrum verified that H_5 and H_6 of each isomer had been correctly identified. Correct assignment of the *exo* and *endo* nor-CH_2O protons was supported via their correlation with two peaks in the ^{13}C NMR spectrum that appeared at 68.90 and 68.22 ppm, respectively. It was expected that the proton resonances representing the nor-CH_2O protons of each isomer would correlate to a single peak within the ^{13}C NMR spectrum. This trend was also observed with the H_3/C_3 and H_7/C_7 relationships, which made their identification in the CH COSY NMR spectrum straightforward.

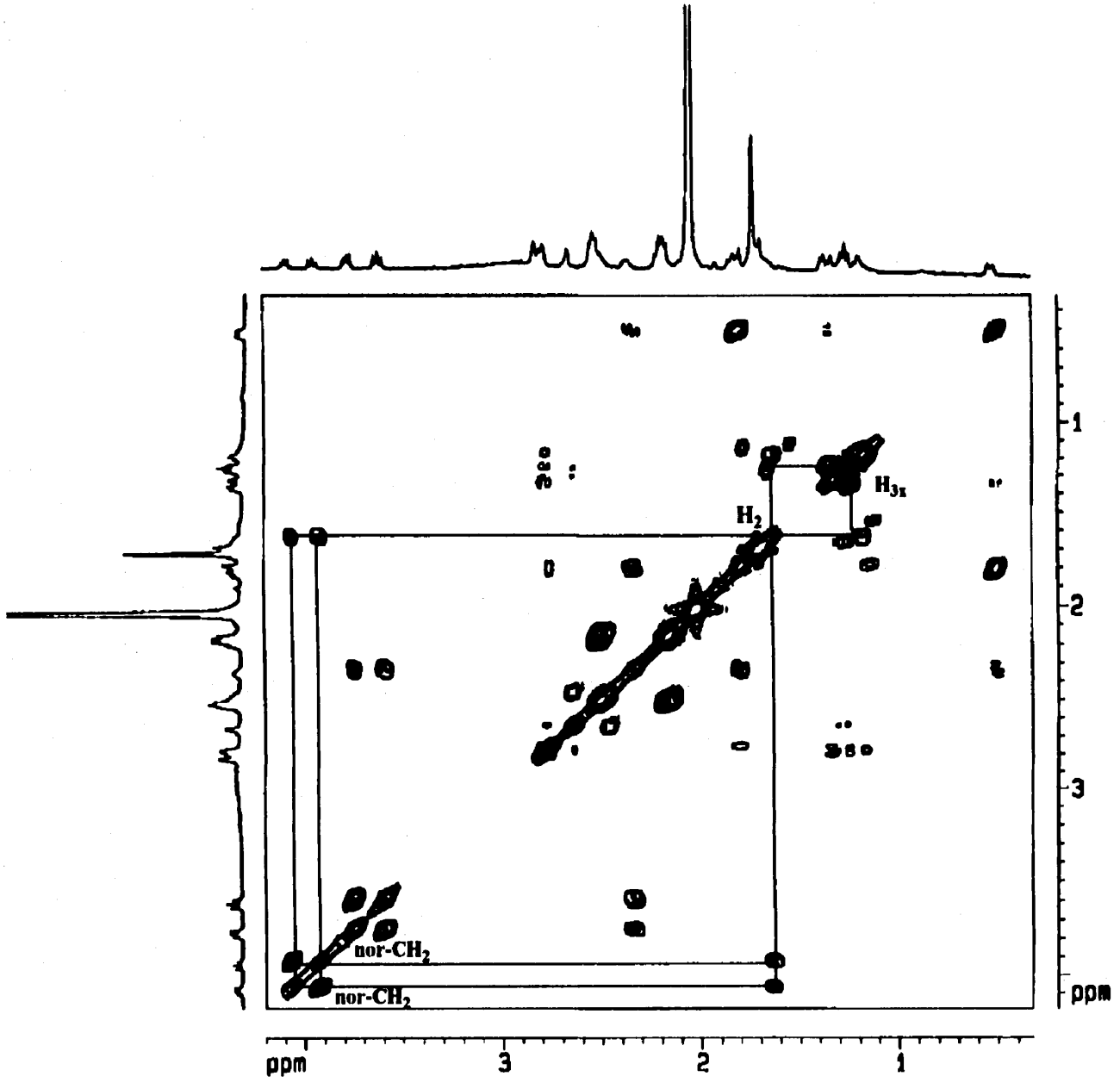

Figure 3.18: Proton assignments for the *exo* isomer of monomer **13a**.

Table 3.11: Yield, IR and elemental analysis data for bimetallic monomers **10, 11, 13a-b**.

MONOMER	PRODUCT YIELD	IR ABSORBANCES (cm^{-1})	CH ANALYSIS CALCULATED	CH ANALYSIS FOUND
10	1.636 g (76%)	1726 (CO)	C, 52.44; H, 4.31	---
11	1.993 g (87%)	1726 (CO)	C, 49.29; H, 3.87	C, 49.02; H, 3.71
13a	2.168 g (86%)	1726 (CO)	C, 56.21; H, 4.32	---
13b	2.515 g (89%)	1726 (CO)	C, 60.36; H, 4.42	---
13c	2.313 g (85%)	1726 (CO)	C, 59.14; H, 4.30	---

Note: --- Denotes that CH analysis was not obtained.

Table 3.12a: ^{1}H NMR data for bimetallic monomers **10**, **11** and **13a**.

δ (ppm) in acetone-d_6											
MONOMER		H_1	H_2	H_{3x}	H_{3n}	H_4	H_5	H_6	H_{7a}	H_{7s}	nor-CH_2
10	*endo*	2.84 (br s)	2.35 (br s)	1.82-1.86 (m)	0.53 (br d) $J_{3x,3n}$ = 11.00	2.79 (br s)	6.16 (dd) $J_{5,6}$ = 6.06 $J_{4,5}$ = 3.11	5.93 (dd) $J_{5,6}$ = 6.06 $J_{1,6}$ = 2.91	1.24 (br s)	1.36 (br s)	3.62 (t, 1H) J = 10.00 3.79 (dd, 1H) J = 10.70,6.70
	exo	2.67 (br s)	1.71 (br s)	1.18-1.20 (m)	1.82-1.86 (m)	2.80 (br s)	6.08 (br s)	6.08 (br s)	1.28 (br s)	1.33 (br s)	3.95 (t, 1H) J = 9.70 4.10 (dd, 1H) J = 11.00, 6.80
11~	*endo*	2.84 (br s)	2.37 (br s)	1.81-1.85 (m)	0.54 (br d) $J_{3x,3n}$ = 12.50	2.79 (br s)	6.15 (dd) $J_{5,6}$ = 5.55 $J_{4,5}$ = 2.76	5.93 (dd) $J_{5,6}$ = 5.55 $J_{1,6}$ = 2.61	1.25-1.29 (m)	1.38 (d) $J_{7a,7s}$ = 7.75	3.63 (t, 1H) J = 9.93 3.78 (dd, 1H) J = 11.08, 6.40
	exo	2.67 (br s)	1.71 (br s)	1.20-1.22 (m)	1.81-1.85 (m)	2.80 (br s)	6.07 (br s)	6.07 (br s)	1.25-1.29 (m)	1.35 (d) $J_{7a,7s}$ = 8.50	3.96 (t, 1H) J = 10.00 4.10 (dd, 1H) J = 10.75, 6.75
13a~	*endo*	2.83 (br s)	2.36 (br s)	1.75-1.85 (m)	0.53 (br d) $J_{3x,3n}$ = 10.50	2.79 (br s)	6.15 (dd) $J_{5,6}$ = 5.56 $J_{4,5}$ = 2.83	5.92 (dd) $J_{5,6}$= 5.56 $J_{1,6}$ = 2.55	1.24-1.28 (m)	1.37 (d) $J_{7a,7s}$ = 9.20	3.62 (t, 1H) J = 9.75 3.77 (dd, 1H) J = 10.60, 6.30
	exo	2.66 (br s)	1.69 (br s)	1.18-1.22 (m)	1.75-1.85 (m)	2.80 (br s)	6.07 (br s)	6.07 (br s	1.24-1.28 (m)	1.34 (d) $J_{7a,7s}$ = 10.25	3.95 (t, 1H) J = 9.80 4.09 (dd, 1H) J = 10.60, 6.50

Note: NMR spectra recorded at 500 (~) and 200 MHz.
Coupling constants reported in hertz.

Table 3.12b: ^{1}H NMR data for bimetallic monomers **13b** and **13c**.

MONOMER		δ (ppm) in acetone-d_6									
		H_1	H_2	H_{3x}	H_{3n}	H_4	H_5	H_6	H_{7a}	H_{7s}	nor-CH_2
13b	*endo*	2.82 (br s)	2.34 (br s)	1.81-1.84 (m)	0.51 (br d) $J_{3x,3n}$ = 10.80	2.78 (br s)	6.15 (dd) $J_{5,6}$ = 5.65 $J_{4,5}$ = 2.60	5.92 (dd) $J_{5,6}$= 5.65 $J_{1,6}$ = 2.50	1.21 (br s)	1.36 (br s)	3.61 (t, 1H) J = 10.00 3.77 (dd, 1H) J = 10.70,6.10
	exo	2.66 (br s)	1.63 (br s)	1.17-1.19 (m)	1.81-1.84 (m)	2.79 (br s)	6.06 (br s)	6.06 (br s)	1.26 (br s)	1.31 (br s)	3.94 (t, 1H) J = 10.60 4.09 (dd, 1H) J = 10.40,6.60
13c	*endo*	2.84 (br s)	2.37 (br s)	1.80-1.85 (m)	0.51 (br d) $J_{3x,3n}$ = 11.40	2.77 (br s)	6.14 (dd) $J_{5,6}$ = 6.88 $J_{4,5}$ = 4.22	5.91 (dd) $J_{5,6}$= 6.88 $J_{1,6}$ = 3.18	1.21 (br s)	1.38 (br s)	3.60 (t, 1H) J = 10.10 3.77 (dd, 1H) J = 10.90,7.10
	exo	2.65 (br s)	1.62 (br s)	1.16-1.18 (m)	1.80-1.85 (m)	2.79 (br s)	6.06 (br s)	6.06 (br s)	1.26 (br s)	1.31 (br s)	3.93 (t, 1H) J = 10.20 4.08 (dd, 1H) J = 10.50,6.50

Note: NMR spectra recorded at 500 (~) and 200 MHz.
Coupling constants reported in hertz.

Table 3.13: ^{1}H NMR data for bimetallic monomers **10, 11** and **13a-c**.

δ (ppm) in acetone-d_6				
MONOMER	ArH	$CpFe^+$-ArH	Cp	OTHERS
10	7.34 (d, 4H, *J* = 8.40) 7.49 (d, 4H, *J* = 8.40)	6.30 (t, 2H, *J* = 4.60) 6.37-6.50 (m, 8H)	5.25 (s, 10H)	1.75 (s, 3H, CH_3) 2.20 (dd, 2H, CH_2) *J* = 17.70, 5.70 2.54 (dd, 2H, CH_2) *J* = 16.70, 8.50
11~	7.32 (d, 4H, *J* = 8.05) 7.48 (d, 4H, *J* = 8.35)	6.50 (d, 4H, *J* = 5.40) 6.80 (d, 4H, *J* = 5.70)	5.36 (s, 10H)	1.74 (s, 3H, CH_3) 2.20 (dd, 2H, CH_2) *J* = 17.50, 8.28 2.55 (dd, 2H, CH_2) *J* = 14.65 Hz, 9.40
13a~	7.28 (d, 4H, *J* = 8.80) 7.31 (d, 4H, *J* = 7.70) 7.39 (t, 2H, *J* = 7.40) 7.45 (d, 4H, *J* = 8.80) 7.55 (t, 4H, *J* = 7.98)	6.34 (d, 4H, *J* = 6.40) 6.37 (d, 4H, *J* = 6.50)	5.31 (s, 10H)	1.73 (s, 3H, CH_3) 2.20 (dd, 2H, CH_2) *J* = 17.50, 8.23 2.54 (dd, 2H, CH_2) *J* = 14.65, 9.40
13b	7.68 (d, 4H, *J* = 7.60) 7.83 (d, 8H, *J* = 7.60) 7.40-7.52 (m, 14H)	6.40 (br s, 8H)	5.33 (s, 10H)	1.72 (s, 3H, CH_3) 2.15 (dd, 2H, CH_2) *J* = 18.0, 8.4 2.50 (br s, 2H, CH_2)
13c	7.30 (d, 4H, *J* = 8.00) 7.44 (d, 4H, *J* = 7.00) 7.61-7.65 (m, 6H) 7.93 (d, 4H, *J* = 8.00) 8.05 (br s, 4H)	6.40 (br s, 4H) 6.43 (br s, 4H)	5.35 (s, 10H)	1.72 (s, 3H, CH_3) 2.16 (br s, 2H, CH_2) 2.51 (dd, 2H, CH_2) *J* = 14.51, 6.91

Note: NMR spectra recorded at 500 (~) and 200 MHz.
Coupling constants reported in hertz.

Table 3.14a: ^{13}C NMR data for bimetallic monomers **10, 11** and **13a**.

δ (ppm) in acetone-d_6													
MONOMER		C_1	C_2	C_3	C_4	C_5	C_6	C_7	nor-CH_2	Cp	$CpFe^+$-ArCH	ArCH	OTHERS
10	*endo*	44.34	38.21	---	42.68	138.00	132.68	49.67	67.97	77.82	77.40 85.44 87.50 134.20*	121.18 130.29 147.48* 151.83*	27.72 (CH_3) ----- (CH_2) 37.02 (CH_2) 46.03* 173.35 (CO)
	exo	44.12	38.54	---	42.04	137.40	136.75	45.26	68.63				
11$^{\sim}$	*endo*	44.69	38.68	29.63	43.01	138.26	132.92	49.95	68.25	80.54	77.34 87.96 105.02* 133.98*	121.29 130.68 148.05* 152.31*	27.90 (CH_3) ----- (CH_2) 37.36 (CH_2) 46.45* 173.41 (CO)
	exo	44.49	38.94	---	42.37	137.68	137.01	45.53	68.93				
13a$^{\sim}$	*endo*	44.68	38.68	---	43.00	138.27	132.88	49.93	68.22	79.04	76.15 76.21 131.86*	121.03 121.36 127.29 130.53 131.66 147.64* 152.95* 154.75*	27.89 (CH_3) 30.77 (CH_2) 37.35 (CH_2) 46.36* 173.24 (CO)
	exo	44.47	38.94	---	42.35	137.69	136.98	45.51	68.90				

Note: NMR spectra recorded at 125 (~) and 50 MHz.
* Denotes a quaternary carbon.
--- Denotes a hidden peak.

Table 3.14b: ^{13}C NMR data for bimetallic monomers **13b** and **13c**.

δ (ppm) in acetone-d_6													
MONOMER		C_1	C_2	C_3	C_4	C_5	C_6	C_7	nor-CH_2	Cp	$CpFe^+$-ArCH	ArCH	OTHERS
13b	*endo*	44.07	37.98	---	42.44	137.81	132.45	49.48	67.80	78.54	75.35 75.54 130.80* 131.24*	121.39 127.22 128.14 129.49 139.06* 139.75* 147.07* 151.89* 153.44*	27.83 (CH_3) ----- (CH_2) 36.76 (CH_2) 45.63* 173.19 (CO)
	exo	43.89	38.23	---	41.82	137.17	136.51	45.11	68.49				
13c	*endo*	44.18	38.09	---	42.53	137.88	132.51	49.55	67.88	78.67	75.37 75.89 126.25* 131.33*	115.64 116.43 120.83 121.41 126.69 127.80 128.89 130.11 135.54* 147.18* 150.13* 151.99*	27.52 (CH_3) ----- (CH_2) 38.12 (CH_2) 45.75* 173.35 (CO)
	exo	43.98	38.34	---	41.92	137.24	136.58	45.15	68.55				

Note: NMR spectra recorded at 125 (~) and 50 MHz.
* Denotes a quaternary carbon.
--- Denotes a hidden peak.

3.2.3 Synthesis of Polynorbornenes with Organoiron Side Chains

Ring-opening metathesis polymerization (ROMP) of the cyclopentadienyliron-complexed norbornenes (**5a-e**, **10**, **11**, **13a-c**) was carried out in the presence of a highly tolerant ruthenium-based catalyst, bis(tricyclohexylphosphine)benzylidene ruthenium(IV) dichloride (Grubbs' Catalyst). The polymerization reactions were performed using a monomer/initiator ([M]/[I]) ratio of 20/1, and led to the isolation of polymeric species (**14a-e** and **15a-e**) in 63-87% yields (Schemes 3.13 and 3.14). The organoiron polymers displayed excellent solubility in organic solvents such as dimethylacetamide, dimethyl sulfoxide, and dimethylformamide due to the presence of the metallic moieties in the polymer's side chains.[36] In addition, the polynorbornenes with one $CpFe^+$ moiety in their terminal side chains (**14a-e**) were soluble in acetone and acetonitrile. The ability of these polymers to dissolve in less polar solvent systems was attributed to the fewer number of aromatic ether linkages in their side chains relative to the polynorbornenes with lateral side chains (**15a-e**). As well, the presence of flexible aliphatic groups within the side chains of polymers **14a-e** contributed to the increased solubility of the materials.[36]

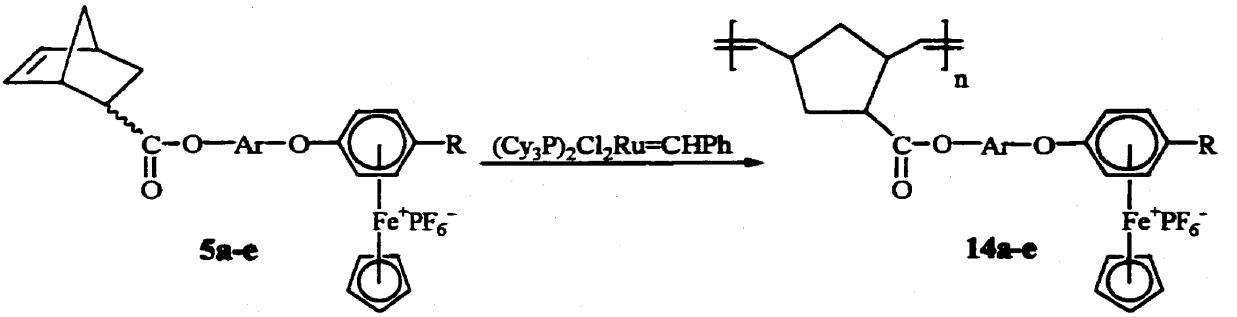

Polymers	R	Ar	Polymers	R	Ar
14a	H		14d	CH_3	
14b	CH_3				
14c	H		14e	H	

Scheme 3.13: Preparation of polynorbornenes with monometallic side chains (**14a-e**).

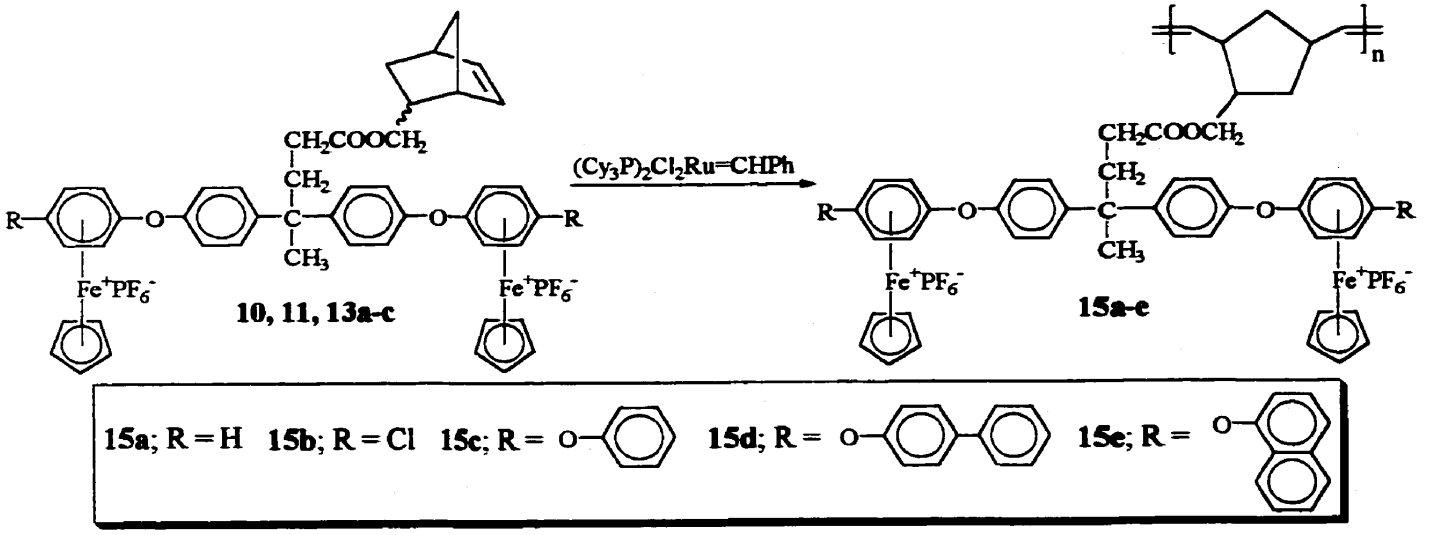

Scheme 3.14: Preparation of polynorbornenes with bimetallic side chains (**15a-e**).

NMR and IR spectroscopy were used to determine if successful polymerization of the organoiron monomers had occurred (Tables 3.15-3.18). In the polymers' spectra, the

absence of olefinic norbornene resonances between 5.9 and 6.3 ppm and the appearance of a set of peaks between 5.3 and 5.6 ppm, representing the double bonds in the polymer backbones, indicated that polymerization had taken place (Figure 3.19). The overall broadening of the peaks in the NMR spectra of the polymers, in comparison to the corresponding monomers also supported successful polymerization of the monomeric units. The presence of single Cp resonances between 5.1 and 5.3 ppm in the ^{1}H NMR spectra of the metallated polynorbornenes, as well as the presence of complexed aromatic peaks around 6.3 ppm, illustrated that the metallic moieties were retained during the polymerizations.

FT-IR also provided evidence that polymerization of the metallated monomers had been successful.[155,164-166] As observed in the ^{1}H NMR spectra, the peaks in the IR spectra of the polymers were much broader than those found in the monomers' spectra.[50] As well, the out-of-plane vibrations of the *cis* double bond in the norbornene rings (703-737 cm^{-1}) were lacking in the polymers' spectra, while peaks around 970 cm^{-1} that corresponded to out-of-plane =C-H vibrations of double bonds in the polynorbornene backbone were present. The fact that these absorbances appeared between 960 and 980 cm^{-1} indicated that the double bonds of the polymer backbone were of *trans* conformation.[164] The highly *trans* microstructure of the polymers was anticipated as it has previously been demonstrated that substituted polynorbornenes prepared using ruthenium-based catalysts often contain *trans* double bonds within their backbones.[8]

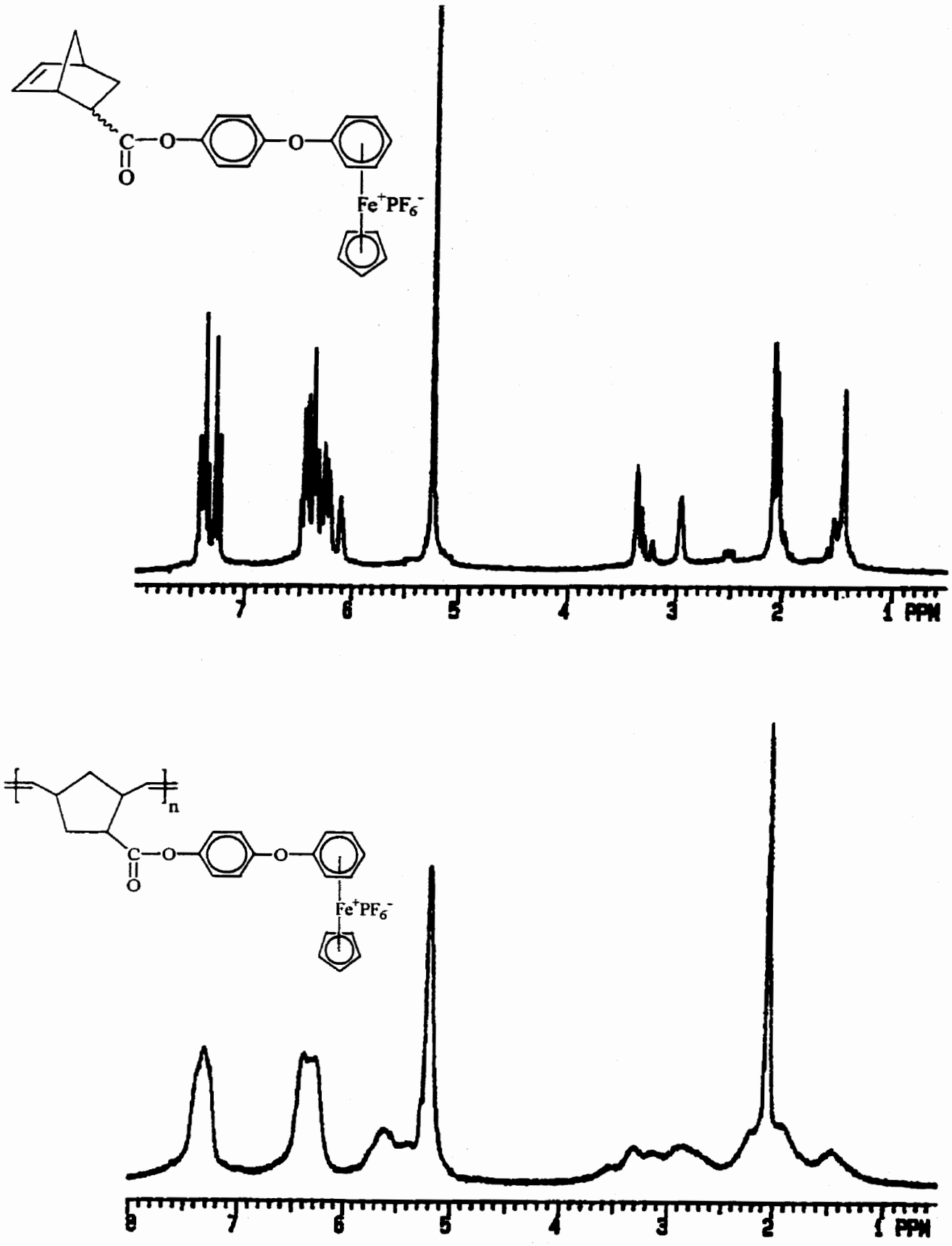

Figure 3.19: ^{1}H NMR spectra for monomer **5a** and polymer **14a**.

Table 3.15: Yield and IR data for organoiron polymers **14a-e**.

POLYMER	PRODUCT YIELD	IR ABSORBANCES (cm^{-1})
14a	0.2318 g (81%)	1754 (CO) 972 (*trans* =C-H out-of-plane)
14b	0.2140 g (87%)	1754 (CO) 972 (*trans* =C-H out-of-plane)
14c	0.2589 g (86%)	1753 (CO) 971 (*trans* =C-H out-of-plane)
14d	0.2712 g (77%)	1746 (CO) 971 (*trans* =C-H out-of-plane)
14e	0.3113 g (79%)	1746 (CO) 970 (*trans* =C-H out-of-plane)

Table 3.16: ^{1}H NMR data for organoiron polymers **14a-e**.

δ (ppm) in acetone-d_6						
POLYMER	RING H	CH_3	Cp	VINYL H	$CpFe^+$-ArH	ArH
14a	1.20-3.51 (broad peaks, 7H)	---	5.19 (s, 5H)	5.55 (br s, 2H)	6.28-6.32 (br m, 5H)	7.28 (br s, 4H)
14b	1.40-3.31 (broad peaks, 7H)	2.46 (br s, 3H)	5.16 (s, 5H)	5.48 (br s, 2H)	6.30 (br s, 4H)	7.31 (br s, 4H)
14c	1.38-3.44 (broad peaks, 7H)	1.68 (br s, 6H)	5.18 (s, 5H)	5.58 (br s, 2H)	6.39 (br d, 5H)	7.04 (br s, 2H) 7.22-7.37 (br m, 6H)
14d	1.39-3.48 (broad peaks, 7H)	1.68 (br s, 6H) 2.44 (br s, 3H)	5.14 (s, 5H)	5.54 (br s, 2H)	6.25 (br s, 4H)	7.02 (br s, 2H) 7.18-7.37 (br m, 6H)
14e	1.36-3.19 (broad peaks, 7H)	1.61 (br s, 6H) 1.66 (br s, 6H)	5.19 (s, 5H)	5.54 (br s, 2H)	6.33 (br d, 5H)	6.96 (br s, 2H) 7.16-7.21 (br m, 6H) 7.39 (br d, 4H)

Note: NMR spectra recorded at 200 MHz.

Table 3.17: Yield and IR data for organoiron polymers **15a-e.**

POLYMER	PRODUCT YIELD	IR ABSORBANCES (cm^{-1})
15a	0.3391 g (63%)	1727 (CO) 971 (*trans* =C-H out-of-plane)
15b	0.4982 g (87%)	1729 (CO) 971 (*trans* =C-H out-of-plane)
15c	0.4412 g (70%)	1727 (CO) --- (*trans* =C-H out-of-plane)
15d	0.5298 g (75%)	1729 (CO) 970 (*trans* =C-H out-of-plane)
15e	0.5014 g (72%)	1727 (CO) 971 (*trans* =C-H out-of-plane)

Note: ---Denotes a hidden peak.

Table 3.18: ^{1}H NMR data for organoiron polymers **15a-e**.

	δ (ppm) in acetone-d_6							
POLYMER	**RING H**	**CH_2 and CH_3**	**nor-CH_2 (*n*)**	**nor-CH_2 (*x*)**	**Cp**	**VINYL H**	**$CpFe^+$-ArH**	**ArH**
15a	1.14-2.48 (broad peaks, 7H)	1.14-2.48 (broad peaks, 7H)	3.86 (br s, 2H)	3.98 (br s, 2H)	5.17 (s, 10H)	5.36 (br s, 2H)	6.32 (br s, 10H)	7.36 (br d, 8H)
15b	1.20-2.48 (broad peaks, 7H)	1.20-2.48 (broad peaks, 7H)	3.86 (br s, 2H)	4.00 (br s, 2H)	5.31 (s, 10H)	5.35 (br s, 2H)	6.58 (br d, 8H)	7.36 (br d, 8H)
15c	0.87-2.89 (broad peaks, 7H)	0.87-2.89 (broad peaks, 7H)	3.86 (br s, 2H)	3.96 (br s, 2H)	5.24 (s, 10H)	5.37 (br s, 2H)	6.26 (br s, 8H)	7.27-7.50 (br m, 18H)
15d	0.87-2.85 (broad peaks, 7H)	0.87-2.85 (broad peaks, 7H)	3.82 (br s, 2H)	3.98 (br s, 2H)	5.22 (s, 10H)	5.34 (br s, 2H)	6.28 (br s, 8H)	7.39-7.74 (br m, 26H)
15e	0.84-2.87 (broad peaks, 7H)	0.84-2.87 (broad peaks, 7H)	3.79 (br s, 2H)	3.98 (br s, 2H)	5.23 (s, 10H)	5.36 (br s, 2H)	6.29 (br s, 8H)	7.23-8.00 (br m, 22H)

Note: NMR spectra recorded at 200 MHz.

The molecular weights of the organometallic polymers could not be directly measured using gel permeation chromatography (GPC), as the cationic metal moieties become trapped within the column matrix.[35,36] Therefore, prior to analysis, the metallic moieties were removed from polymers **14a-e** and **15a-e** using photolytic techniques, and their organic analogues **16a-e** and **17a-e**, were isolated (Schemes 3.15 and 3.16). Confirmation of successful removal of the metal moieties was obtained upon analysis of the NMR spectra of the demetallated polymers (Tables 3.19 and 3.20). Figure 3.20 shows the ^{1}H NMR spectra of polymer **15a** and its corresponding organic analogue, polymer **17a**. The demetallated polymer's spectrum lacked the strong singlet at 5.17 ppm, which represented the Cp hydrogens present in the organometallic polymer. The absence of this peak allowed for a clearer view of the broad singlet at 5.25 ppm, which corresponded to the olefinic hydrogens within the polymer backbone. A downfield shift of the complexed aromatic protons into the uncomplexed aromatic region around 7 ppm was also observed upon demetallation.

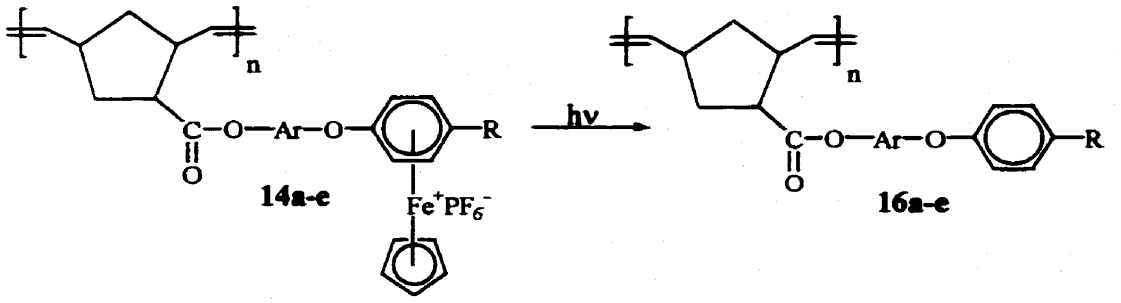

Polymers	R	Ar	Polymers	R	Ar
16a	H		16d	CH_3	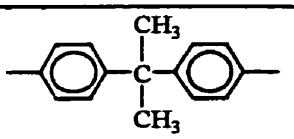
16b	CH_3	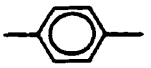			
16c	H	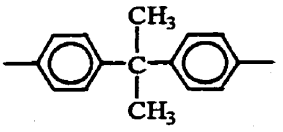	16e	H	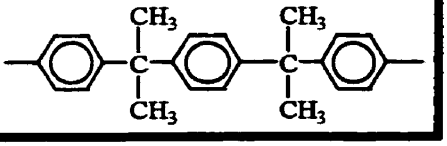

Scheme 3.15: Preparation of polynorbornenes with terminal side chains (**16a-e**).

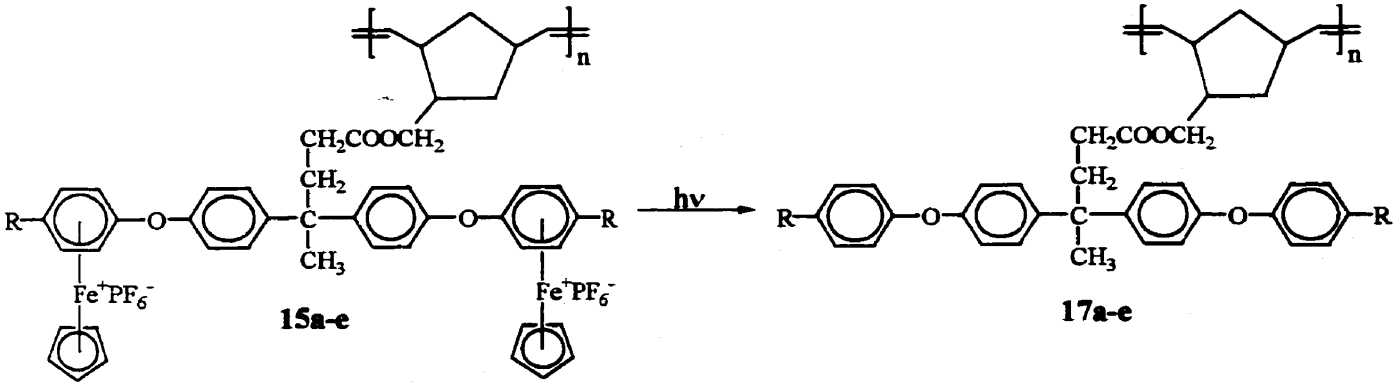

17a; R = H **17b**; R = Cl **17c**; R = 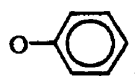 **17d**; R = 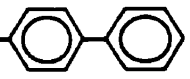 **17e**; R = 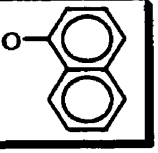

Scheme 3.16: Preparation of polynorbornenes with lateral side chains (**17a-e**).

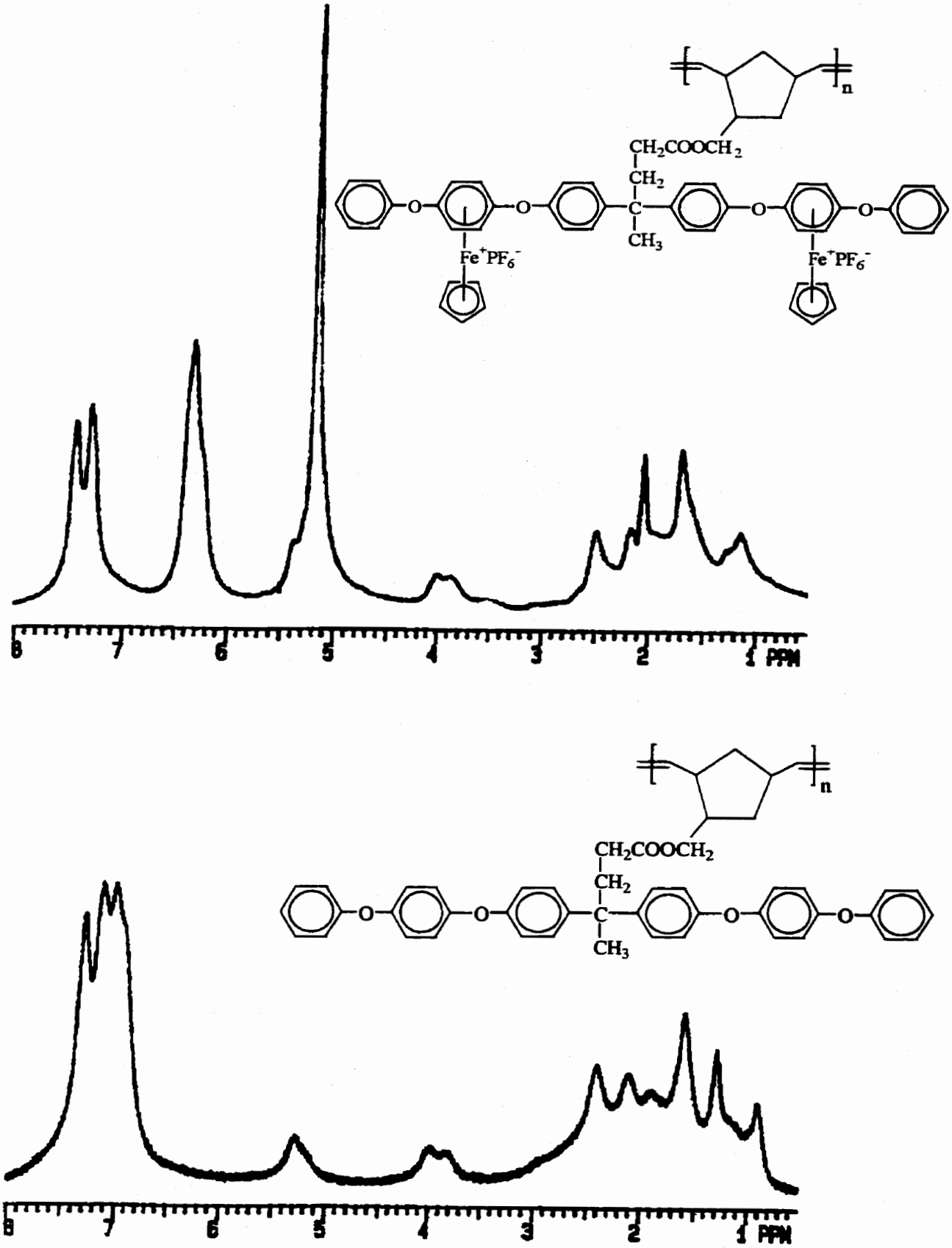

Figure 3.20: ^{1}H NMR spectra for polymers **15a** and **17a**.

Table 3.19: IR and ^{1}H NMR data for polynorbornenes **16a-e**.

		δ (ppm) in $CDCl_3$			
POLYMER	IR ABSORBANCES (cm^{-1})	RING H	CH_3	VINYL H	ArH
16a	1753 (CO) 971 (*trans* =C-H out-of-plane)	0.99-3.13 (broad peaks, 7H)	---	5.53 (br s, 2H)	6.97 (br s, 5H) 7.43 (br s, 4H)
16b	1753 (CO) 969 (*trans* =C-H out-of-plane)	1.37-3.48 (broad peaks, 7H)	2.32 (br s, 3H)	5.51 (br s, 2H)	6.92 (br s, 4H) 7.08 (br s, 4H)
16c	1753 (CO) 969 (*trans* =C-H out-of-plane)	1.21-3.32 (broad peaks, 7H)	1.63 (br s, 6H)	5.46 (br s, 2H)	6.86-7.25 (br m, 13H)
16d	1753 (CO) 969 (*trans* =C-H out-of-plane)	0.90-3.23 (broad peaks, 7H)	1.61 (br s, 6H) 2.28 (br s, 3H)	5.43 (br s, 2H)	6.81-7.23 (br m, 12H)
16e	1753 (CO) 969 (*trans* =C-H out-of-plane)	0.93-3.28 (broad peaks, 7H)	1.63 (br s, 6H) 2.26 (br s, 6H)	5.40 (br s, 2H)	6.88-7.12 (br m, 17H)

Note: NMR spectra recorded at 200 MHz.

Table 3.20: IR and ^{1}H NMR data for polynorbornenes **17a-e**.

		δ (ppm) in $CDCl_3$					
POLYMER	**IR ABSORBANCES (cm^{-1})**	**RING H**	**CH_2 and CH_3**	**nor-CH_2 (*n*)**	**nor-CH_2 (*x*)**	**VINYL H**	**ArH**
17a	1729 (CO) 970 (*trans* =C-H out-of-plane)	0.89-2.40 (br peaks, 7H)	0.89-2.40 (br peaks, 7H)	3.81 (br s, 2H)	3.98 (br s, 2H)	5.25 (br s, 2H)	7.04 (br d, 18H)
17b	1727 (CO) 970 (*trans* =C-H out-of-plane)	1.59-2.66 (br peaks, 7H)	1.59-2.66 (br peaks, 7H)	3.91 (br s, 2H)	3.83 (br s, 2H)	5.29 (br s, 2H)	6.62-7.27 (br m, 16H)
17c	1729 (CO) 971 (*trans* =C-H out-of-plane)	1.27-2.99 (br peaks, 7H)	1.27-2.99 (br peaks, 7H)	3.78 (br s, 2H)	3.97 (br s, 2H)	5.24 (br s, 2H)	6.95 (br s, 26H)
17d	1728 (CO) 971 (*trans* =C-H out-of-plane)	1.26-3.54 (br peaks, 7H)	1.26-3.54 (br peaks, 7H)	3.96 (br s, 2H)	4.14 (br s, 2H)	5.25 (br s, 2H)	6.96-8.06 (br m, 34H)
17e	1726 (CO) --- (*trans* =C-H out-of-plane)	1.16-2.37 (br peaks, 7H)	1.16-2.37 (br peaks, 7H)	3.81 (br s, 2H)	3.96 (br s, 2H)	5.25 (br s, 2H)	6.96-8.21 (br m, 30H)

Note: NMR spectra recorded at 200 MHz.
--- Denotes hidden peak.

Once the degrees of polymerization (DP) for the organic polymers (**15a-e** and **17a-e**) were calculated using GPC, an approximate value for the weight-average molecular weight (Mw) of the corresponding organometallic polymers was determined. This was accomplished using the DP of the organic polymer and the formula weight of the repeating unit of the corresponding metallated polymer. The number-average molecular weight (Mn) of the organometallic polymer could then be calculated using the polydispersity index (PDI) of the sample and the predicted Mw of the organometallic polymer. The values for all of the organometallic and organic polymers are found in Tables 3.21 and 3.22. It was found that the Mw for the organometallic polymers were in the range of 20,000 to 48,400 with polydispersity indices (PDI's) between 1.24 and 2.01. As well, the average number of repeating units for polynorbornenes containing one metal moiety was calculated to be 35, while the polynorbornenes with two metal moieties had an average DP of 27.

The thermal properties of the polynorbornenes were investigated using thermogravimetric analysis (TGA) and differential scanning calorimetry (DSC) (Tables 3.23 and 3.24). All of the organoiron polynorbornenes showed two weight loss steps in their TGA thermograms, with the first weight loss occurring between 220 and 230°C. It has previously been established that this is the temperature range in which the metal moieties cleave from the polymer's side chains.[36] The second weight loss steps, which occurred at much higher temperatures, represented decomposition of the backbones of the polymers. It was found that the polynorbornenes with terminal side chains containing one $CpFe^+$ moiety (**14a-e**) displayed decomposition temperatures in the range of 388-402°C (Table 3.23). Upon demetallation, their corresponding organic polymers (**16a-e**)

displayed decomposition temperatures that were consistent with those of the organoiron polymers (Table 3.25). This phenomenon can be observed in Figure 3.21, which shows the TGA curves for polymers **14a** and **16a**.

The polynorbornenes with extended lateral side chains that contained two $CpFe^+$ moieties, decomposed at higher temperatures relative to the polynorbornenes with terminal side chains (Tables 3.24 and 3.26). This trend was attributed to the increased number of aromatic ethers within the structures of the polymers, as it has been previously shown that the incorporation of aromatic ethers into the side chains of polynorbornenes leads to an increase in their thermal stability.[37] Figure 3.22 shows a comparison of the TGA curves for polymer **14a** and **15d**. It can be seen that the first weight loss steps, which represents the loss of the metal moieties occurred at approximately the same temperature in both curves, however, the polymer decomposition temperatures were very different. Degradation of polymer **14a**, which contains two aromatic rings within its side chains occurred at 402°C, while polymer **15d**, which has eight aromatic rings in its side chains did not begin to decompose until 431°C. In general, an increase in the polymers' thermal stabilities was observed as the number of aromatic units within their side chains increased.

DSC was performed to determine the glass transition temperatures (T_g's) of the substituted polynorbornenes. Analysis of polymers **16a-e** showed that the polynorbornenes with terminal side chains displayed T_g values between 59 and 81°C (Table 3.25), while the polynorbornenes with lateral side chains exhibited T_g values in the range of 69-92°C (Table 3.26). An assessment of the DSC curves for a series of substituted polynorbornenes are shown in Figure 3.23. A comparison of the DSC curves

for polymer **17a** and **17d** showed that increasing the number of aromatic ether units in the side chains led to an increase in the resulting polymer's T_g value. As well, it can be seen that the incorporation of chlorine atoms into the side chains led to a dramatic increase in the T_g of the material (**17b**). This occurred because the presence of the polar halogen atoms within the polymer's side chains caused a decrease in their mobility, and thus more energy was needed to bring about a phase change in the polymer.[1]

3.3 Summary

This work demonstrated that two classes of polynorbornenes containing cationic iron moieties within their side chains could be prepared via ring-opening metathesis polymerization in the presence of a ruthenium-based catalyst. Molecular weight analysis of the polymers showed that the polynorbornenes with terminal side chains had average chain lengths of 35 units, while the lengths of the polymers with lateral side chains were approximately 27 units. Overall, all of the organometallic polymers demonstrated excellent solubility and thermal properties. Furthermore, thermal analysis of the polynorbornenes showed the thermal stability of the polymers could be increased via the incorporation of halogen atoms or aromatic ether units into their side chains.

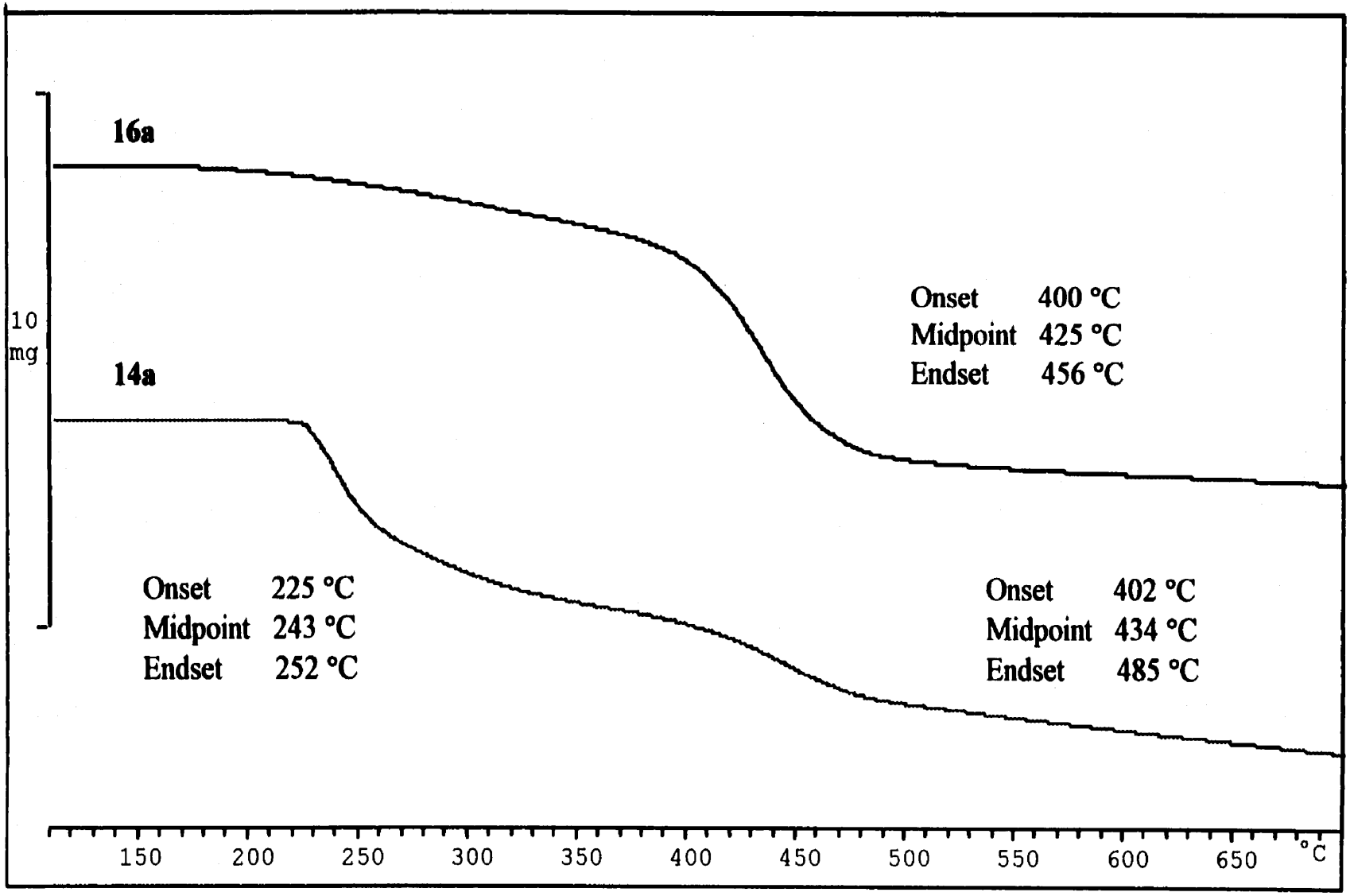

Figure 3.21: TGA thermogram of polymers **14a** and **16a**.

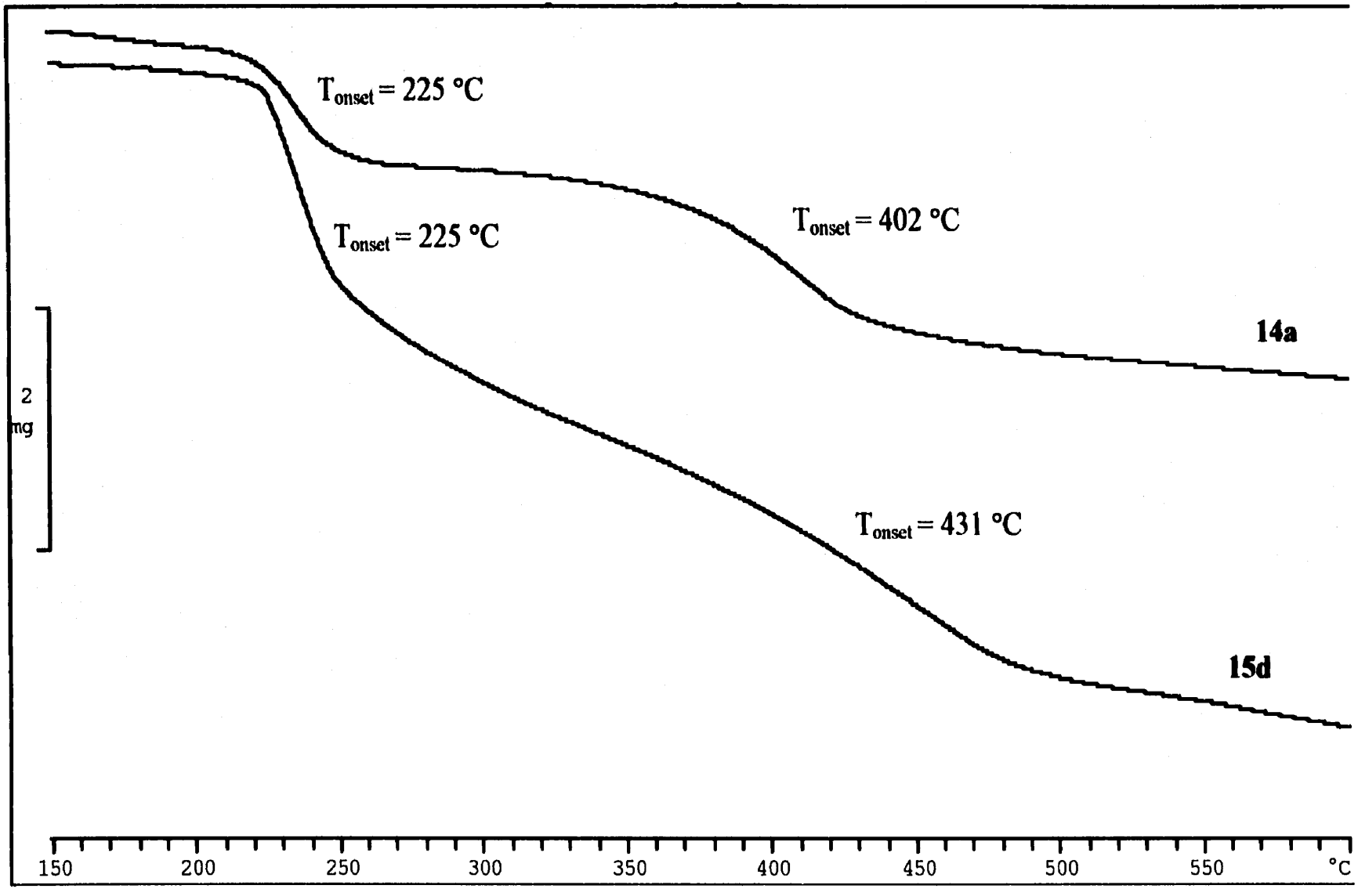

Figure 3.22: TGA thermogram of polymers **14a** and **15d**.

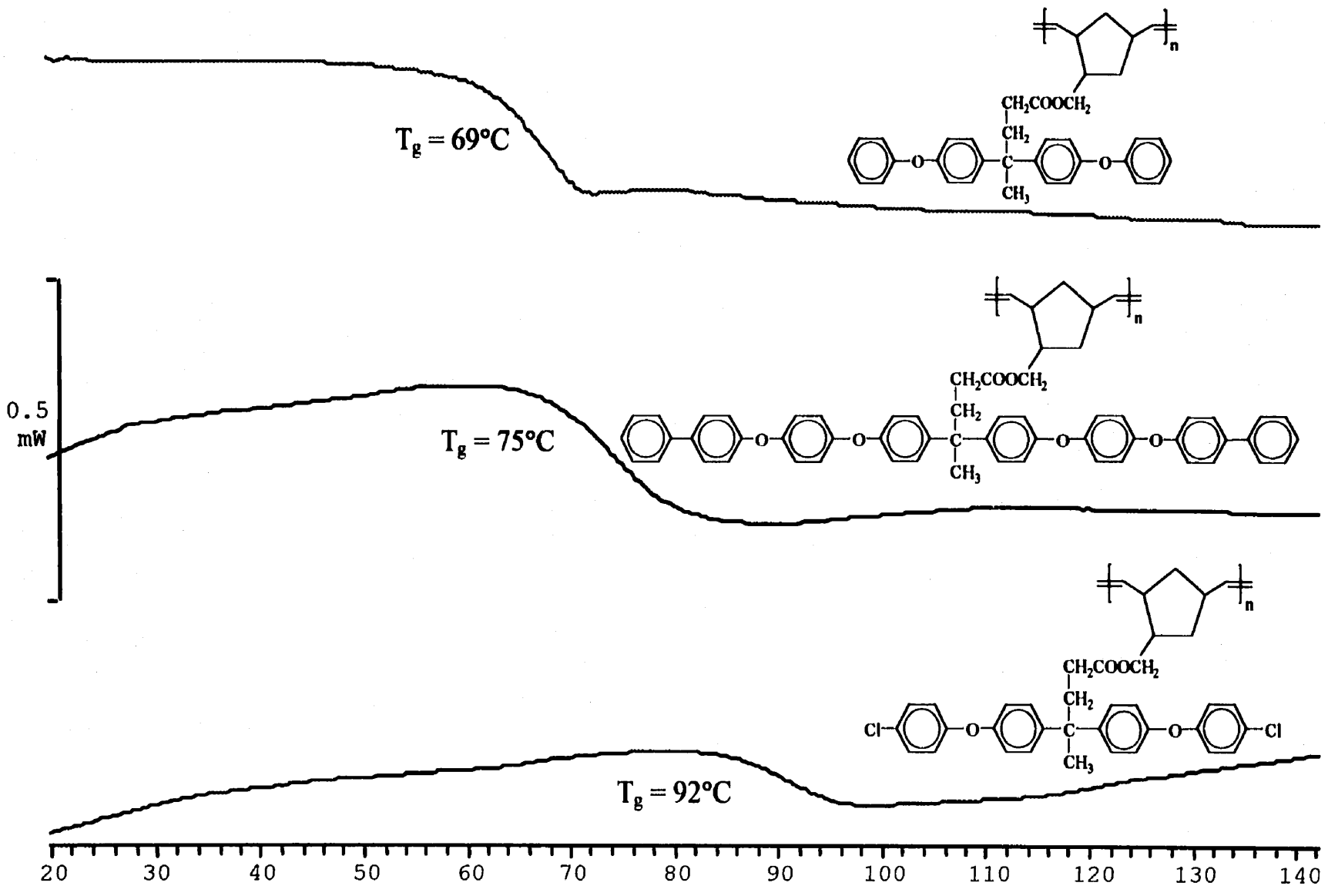

Figure 3.23: DSC thermogram of polymers **17a**, **17b** and **17d**.

Table 3.21: GPC data for polynorbornenes **14a-e** and **16a-e**.

POLYMER	Mw	Mn	PDI	DP
14a	22,900	14,700	1.56	40
14b	21,100	15,700	1.34	36
14c	20,000	15,800	1.27	29
14d	21,900	17,700	1.24	31
14e	21,800	16,500	1.32	27
16a	14,800	9,500	1.56	40
16b	11,600	8,600	1.34	36
16c	12,300	9,700	1.27	29
16d	13,400	10,800	1.24	31
16e	14,400	10,900	1.32	27

Note: Mw = weight-average molecular weight.
Mn = number-average molecular weight.
PDI = polydispersity index.
DP = degree of polymerization.

Table 3.22: GPC data for polynorbornenes **15a-e** and **17a-e**.

POLYMER	Mw	Mn	PDI	DP
15a	48,400	27,400	1.77	45
15b	24,000	11,900	2.01	21
15c	31,500	16,900	1.86	25
15d	29,700	18,000	1.65	21
15e	32,700	19,700	1.66	24
17a	24,600	13,900	1.77	45
17b	12,800	6,100	2.01	21
17c	17,800	9,500	1.86	25
17d	18,200	11,000	1.65	21
17e	20,300	12,200	1.66	24

Note: Mw = weight-average molecular weight.
Mn = number-average molecular weight.
PDI = polydispersity index.
DP = degree of polymerization.

Table 3.23: TGA data for organoiron polymers **14a-e**.

POLYMER	ONSET (°C)	MIDPOINT (°C)	ENDSET (°C)	% WT LOSS	ONSET (°C)	MIDPOINT (°C)	ENDSET (°C)	% WT LOSS
14a	225	244	252	25	402	434	485	64
14b	228	236	243	16	398	434	471	60
14c	224	241	252	17	392	420	466	39
14d	234	247	257	21	388	421	456	34
14e	231	242	251	15	393	423	454	49

Table 3.24: TGA data for organoiron polymers **15a-e**.

POLYMER	ONSET (°C)	MIDPOINT (°C)	ENDSET (°C)	% WT LOSS	ONSET (°C)	MIDPOINT (°C)	ENDSET (°C)	% WT LOSS
15a	224	238	251	20	368	409	461	33
15b	220	235	248	17	380	414	449	28
15c	222	235	248	22	419	445	473	35
15d	227	241	254	26	431	467	518	49
15e	227	239	250	18	431	460	496	31

Table 3.25: TGA and DSC data for polynorbornenes **16a-e**.

POLYMER	ONSET (°C)	MIDPOINT (°C)	ENDSET (°C)	% WT LOSS	T_g (°C)
16a	400	425	456	46	78
16b	400	422	442	50	78
16c	402	428	460	56	81
16d	398	414	430	51	59
16e	402	424	442	57	59

Note: T_g = glass transition temperature.

Table 3.26: TGA and DSC data for polynorbornenes **17a-e**.

POLYMER	ONSET (°C)	MIDPOINT (°C)	ENDSET (°C)	% WT LOSS	T_g (°C)
17a	406	433	462	66	69
17b	382	417	447	50	92
17c	478	489	510	45	76
17d	431	476	528	43	76
17e	431	463	520	47	75

Note: T_g = glass transition temperature.

3.4 Experimental

3.4.1 General Methods

^{1}H and ^{13}C NMR spectra were recorded at 200 and 50 MHz, respectively, on a Varian Gemini 200 NMR spectrometer and at 500 and 125 MHz on a Bruker 500 spectrometer, with chemical shifts referenced to the solvent residues and coupling constants reported in hertz. Infrared spectra were recorded on a Bomem, Hartmann & Braun FT-IR spectrophotometer as KBr pellets or using NaCl plates. Elemental analyses were preformed at the University of Saskatchewan and Guelph Chemical Laboratories Ltd. Molecular weights and molecular weight distributions were determined using gel permeation chromatography at 35°C, using a BL-gel mixed D column (Phenomenex) equipped with a CH-30 column heater (Eppendorf) and a PL-DCU data collection unit (Polymer Laboratories). $CHCl_3$ was used as the mobile phase at flow rates of 0.7 mL/min, and the column was calibrated versus polystyrene standards. Thermogravimetric analysis was performed on a Mettler-Toledo TGA/SDTA851^{e} at heating rates of 20°C/min under a steady stream of nitrogen (50 mL/min). Differential scanning calorimetry was performed on a Mettler DSC821^{e} at heating rates of 20°C/min under nitrogen (50 mL/min), and the glass transition temperatures (Tg's) are reported at the midpoint for the second heating.

3.4.2 Starting Materials

Anhydrous aluminum chloride, aluminum powder, ferrocene, chlorobenzene, 4-chlorotoluene, 1,4-dichlorobenzene, ammonium hexafluorophosphate, hydroquinone, bisphenol-A, bisphenol-P, 4,4'-bis(4-hydroxyphenyl)valeric acid, phenol, 4-phenylphenol, 1-naphthol, *exo,endo*-5-norbornene-2-carboxylic acid, *exo,endo*-5-

norbornene-2-methanol, dimethylaminopyridine (DMAP), dicyclohexylcarbodiimide (DCC), potassium carbonate and bis(tricyclohexylphosphine)benzylidene ruthenium(IV) dichloride are commercially available and were used as received. All solvents (reagent grade) were used without further purification except for dichloromethane, hexane and pyridine. These solvents were dried over $CaCl_2$ or CaH_2, distilled and stored over 4-Å molecular sieves prior to their use.

The chloroarene complexes (**1a-c**) used in the syntheses, were prepared according to previously reported methodologies.[51,52] As well, the monometallic starting complexes **3a** and **3b** have been previously prepared and fully characterized.[34]

3.4.3 Synthesis of Monometallic and Bimetallic Starting Materials

(i) Monometallic starting materials (complexes 3c-e). In a 50 mL round bottom flask, η^6-chlorobenzene-η^5-cyclopentadienyliron hexafluorophosphate (**1a**) or η^6-4-chlorotoluene-η^5-cyclopentadienyliron hexafluorophosphate (**1b**) (2-4 mmol) was combined with an 8 fold excess of the appropriate dinucleophile, K_2CO_3 (5 mmol, 0.6911 g) and a 4:1 mixture of THF:DMF. The solution was stirred for 6 hours at 65°C under a nitrogen atmosphere, and then poured into 10% (v/v) HCl, to which NH_4PF_6 was added. The organometallic product was then extracted from the water layer using dichloromethane, washed with several portions of distilled water, dried over $MgSO_4$, gravity filtered and the solvent removed under reduced pressure. The crude product was then precipitated into diethyl ether to remove the excess nucleophile and isolated as an orange-brown oil.

(ii) Bimetallic starting material (complex 7). In a 50 mL round bottom flask, η^6-chlorobenzene-η^5-cyclopentadienyliron hexafluorophosphate (**1a**) and 4'-bis(4-

hydroxyphenyl)valeric acid (**6**) were combined in a 2:1 molar ratio with an 2.5 fold excess of K_2CO_3 and dissolved in 15 mL of DMF. The reaction was stirred under a nitrogen atmosphere for 24 h at 65 °C. The yellow-brown solution was then poured into 10% (v/v) HCl, to which NH_4PF_6 was added. This caused the precipitation of the organometallic product as a yellow solid, which was collected by suction filtration, washed with several portions of distilled water and allowed to dry. After this time, a small amount of diethyl ether was used to wash any remaining nucleophile from the product.

(iii) Bimetallic starting material with terminal chlorine atoms (complex 8). In a 50 mL round bottom flask, a 2:1 molar ratio of η^6-1,4-dichlorobenzene-η^5-cyclopentadienyliron hexafluorophosphate (**1c**) and 4'-bis(4-hydroxyphenyl)valeric acid (**6**) were combined with an 2.5 fold excess of K_2CO_3 and dissolved in 15 mL of DMF. The resulting mixture was stirred under a nitrogen atmosphere for 16 h at room temperature, after which time it was worked-up using the procedure outline in section **3.4.3(ii)**.

3.4.4 Isolation of Organoiron Monomers

(i) Norbornenes containing one $CpFe^+$ moiety (monomers 5a-e). In a 25 mL round bottom flask, the organoiron complex (**3a-e**, 2 mmol) was dissolved in 5 mL of dichloromethane. To this, a three-fold excess of DCC and *exo,endo*-5-norbornene-2-carboxylic acid were added, followed by 5 mL of dichloromethane and 10 drops of pyridine. The brown solution was allowed to stir for 24 hours under a nitrogen atmosphere. After this time, the pale yellow mixture was gravity filtered and the solvent removed under reduced pressure. The resulting brown oil was dissolved in acetone and precipitated into diethyl ether.

(ii) Norbornenes containing two $CpFe^+$ moieties (monomers 10 and 11). In a 25 ml round bottom flask, complex 7 or **8** (2 mmol), *endo,exo*-5-norbornene-2-methanol (**9**) (6 mmol, 0.73 mL) and DMAP (6 mmol, 0.7330 g) were cooled to 0°C under a nitrogen atmosphere in 5 mL of a 3:1 dichloromethane:DMSO solution. To this solution, DCC (6 mmol, 1.238 g) dissolved in 5 mL of 3:1 dichloromethane:DMSO was added, and the mixture was stirred for 24 h under a nitrogen atmosphere. The resulting solution was hydrolyzed in 50 mL of ice water, to which NH_4PF_6 was added. The product was then extracted with dichloromethane, washed with brine, dried over $MgSO_4$ and the solvent removed under reduced pressure. The crude product was dissolved in acetone, precipitated into diethyl ether, and the resulting yellow solid collected by suction filtration.

(iii) "Capped" norbornenes containing Two $CpFe^+$ moieties (monomers 13a-c). In a 50 mL round bottom flask, **11** (1.00 mmol, 1.145 g), a three fold excess of the appropriate phenolic compound (**12a-c**) and K_2CO_3 (5.00 mmol, 0.691 g) were dissolved in 15 mL of DMF and reacted under a nitrogen atmosphere for 16 h. The procedure outlined in section **3.4.3*(ii)*** was then carried out to allow for successful isolation of the corresponding monomers.

3.4.5 Preparation of Substituted Polynorbornenes

(i) Ring-opening metathesis polymerizations (polymers 14a-e and 15a-e). In a 10 mL round bottom flask, the metallated monomer (**5a-e**, **10**, **11**, **13a-c**) and 0.5 mL of distilled dichloromethane for every 100 mg of monomer were combined and stirred under a nitrogen atmosphere. In a second flask, the catalyst ([M]/[I] = 20/1) was dissolved in an equivalent amount of dichloromethane and also purged with N_2. The catalyst solution

was then added dropwise to the stirring monomer solution at which time a black sticky solid began to collect on the sides and bottom of the flask. The reaction was allowed to stir for 1-4 h during which time more solid formed. The polymerization was then terminated by the addition of ethyl vinyl ether, and stirred for 15-30 min. The crude polymer was washed with dichloromethane to remove any remaining monomer, dissolved in acetone or acetonitrile and precipitated into a 3:1 water:methanol mixture containing NH_4PF_6. The purified polymer was then collected via suction filtration as a yellow or brown solid.

(ii) Photolytic Demetallation (polymers 16a-e and 17a-e). In a 50 mL centrifuge tube, the metallated polymer (**14a-e, 16a-e**) and 40 mL of a 3:1 CH_2Cl_2:acetonitrile solution were combined. If the organometallic polymer was not completely soluble as was observed for some of the polymers containing many aromatic ether linkages (**15a-e**), a small amount of DMF was added to the mixture. The polymer solution was then irradiated with UV light for 4-6 hours, after which time the solvent was removed under reduced pressure. The residue was dissolved in chloroform, washed with several portions of distilled water, dried over $MgSO_4$, gravity filtered and the solvent removed using a rotary evaporator. The crude product was dissolved in a minimal amount of chloroform and precipitated into hexane. The resulting white solid was collected via suction filtration and allowed to further dry.

4.0 References

1. G. Odian, *Principles of Polymerization*, 3rd ed.; John Wiley & Sons, INC.: New York, 1991.

2. L. H. Sperling, *Introduction to Physical Polymer Science*, 3rd ed.; John Wiley & Sons, INC.: New York, 2001.

3. M. P. Stevens, *Polymer Chemistry: An Introduction*, Oxford University Press: New York, 1999.

4. D. J. Brunelle, *Ring-opening Polymerization: Mechanisms, Catalysis Structure, Utility*, Hanser: New York, 1993.

5. K. Matyjaszewski, Ed.; *Controlled Living/Radical Polymerization: Progress in ATRP, NMP and RAFT*, ACS Symposium Series 768, American Chemical Society: Washington, 2000.

6. Y. Ding, A. R. Hlil, A. S. Hay, E. Tsuchida, K. Miyatake *Macromolecules* **1999**, 32, 315-321.

7. Y.-F. Wang, K. P. Chan, A. S. Hay *React. Funct. Polym.* **1996**, 30, 205-227.

8. K. J. Ivin, J. C. Mol, *Olefin Metathesis and Metathesis Polymerization*, Academic Press: San Diego, 1997.

9. V. Dragutan, R. Streck, *Catalytic Polymerization of Cycloolefins: Ionic, Ziegler-Natta and Ring-Opening Metathesis Polymerization*, Elsevier: Amsterdam, 2000.

10. H. S. Eleuterio, U.S. Patent 3,074,918, 1957.

11. K. J. Ivin, T. Saegusa, "Cycloalkenes and Bicycloalkenes" in *Ring-opening Polymerization*, Elsevier: London, 1984; vol. 1, Chapter 3.

12. W. L. Truett, D. R. Johnson, I. M. Robinson, B. A. Montague *J. Am. Chem. Soc.* **1960**, 82, 2337.

13. D. S. Breslow, "Metathesis Polymerization" in *Prog. Polym. Sci.* **1993**, 18, 1141-1195.

14. A. S. Abd-El-Aziz, D. C. Schriemer, C. R. de Denus *Organometallics* **1994**, 13, 374-384.

15. R. J. Cotter *Engineering Plastics: A Handbook of Polyarylethers*, Gordon and Breach Publishers: Basel, 1995.

16. A. A. Moroz, M. S. Shvartsberg *Russ. Chem. Rev.* **1974**, 43, 679.

17. R. N. Johnson, A. G. Farnham, R. A. Clendinning, W. F. Hale, C. N. Merriam *J. Polym. Sci.: Part A-1* **1967**, 5, 2375-2398.

18. H. R. Kricheldorf, C. Jurgens *Eur. Polym. J.* **1993**, 7, 903-908.

19. Z. Y. Wang, L. Suzzarini *Macromolecules* **1996**, 29, 1073-1075.

20. S. M. MacKinnon, Z. Y. Wang *Macromolecules* **1998**, 31, 7970-7972.

21. Y. Meng, I. A. Abu-Yousef, A. R. Hlil, A. S. Hay *Macromolecules* **2000**, 9185-9191.

22. F. A. Carey, R. J. Sundberg *Advanced Organic Chemistry: Part B: Reactions and Synthesis*; 3rd ed., Plenum Press: New York, 1990.

23. E. Buncel, R. Y. Moir,A. R. Norris, A.-P. Chartrousse *Can. J. Chem.* **1981**, 59, 2470-2474.

24. R. D. Pike, D. A. Sweigart *Coord. Chem. Rev.* **1999**, 187, 183-222.

25. A. S. Abd-El-Aziz, E. K. Todd *Polymer News* **2001**, 26, 5-13.

26. P. C. Gomes, E. J. S. Vichi, P. J. S. Moran, A. F. Neto, M. L. Maroso, J. Miller *Organometallic* **1996**, 15, 3198-3203.

27. A. C. Knipe, S. J. McGuiness, W. E. Watts *J. Chem. Soc. Chem. Commun.* **1979**, 842-843.

28. A. C. Knipe, S. J. McGuiness, W. E. Watts *J. Chem. Soc. Perkin Trans. II* **1981**, 193-200.

29. R. G. Sutherland *J. Organomet. Chem. Lib.* **1977**, 3, 311-342.

30. D. Astruc *Top. Curr. Chem.* **1991**, 160, 47-95.

31. A. J. Pearson, *Iron Compounds in Organic Synthesis*, Academic Press Limited: San Diego, 1994.

32. A. S. Abd-El-Aziz, S. Bernardin *Chem. Rev.* **2000**, 219-267.

33. A. S. Abd-El-Aziz, K. M. Epp, C. R. de Denus, G. Fisher-Smith *Organometallics* **1994**, 13, 2299-2308.

34. A. S. Abd-El-Aziz, C. R. de Denus, M. J. Zaworotko, L. R. MacGillivray *J. Chem. Soc. Dalton Trans.* **1995**, 3375-3393.

35. A. S. Abd-El-Aziz, E. K. Todd, K. M. Epp *J. Inorg. Organomet. Polym.* **1998**, 8, 127-133.

36. A. S. Abd-El-Aziz, E. K. Todd, G. Z. Ma, *J. Polym. Sci. Part A: Polym. Chem.* **2001**, 39, 1216-1231.

37. A. S. Abd-El-Aziz, A. L. Edel, L. J. May, K. M. Epp,H. M. Hutton *Can. J. Chem.* **1999**, 77, 1797-1809.

38. A. S. Abd-El-Aziz, L. J. May, A. L. Edel *Macromol. Rapid Commun.* **2000**, 21, 598-602.

39. A. S. Abd-El-Aziz, C. R. de Denus, M. J. Zaworotko, C. V. Krishnamohan Sharma *Chem. Commun.* **1998**, 265-266.

40. A. S. Abd-El-Aziz, C. R. deDenus, E. K. Todd, S. A. Bernardin *Macromolecules* **2000**, 33, 5000-5005.

41. A. J. Pearson, A. M. Gelormini *Macromolecules* **1994**, 27, 3675-3677.

42. A. J. Pearson, A. M. Gelormini *J. Org. Chem.* **1994**, 59, 4561-4570.

43. A. J. Pearson, A. M. Gelormini *J. Org. Chem.* **1995**, 60, 281-284.

44. A. J. Pearson, L. Sun *J. Polym. Sci. Part A: Polym. Chem.* **1997**, 35, 447-453.

45. T. H. Coffield, V. Sandel, R. D Closson *J. Am. Chem. Soc.* **1957**, 79, 5826.

46. T. H. Coffield, R. D Closson U.S. Patent 3,130,214.

47. A. N. Nesmeyanov, N. A. Vol'kenau, I. N. Bolesova *Dokl. Akad. Nauk SSSR* **1963**, 149, 615-618.

48. A. N. Nesmeyanov, N. A. Vol'kenau, I. N. Bolesova *Tetrahedron Lett.* **1963**, 25, 1725-1729.

49. A. N. Nesmeyanov, N. A. Vol'kenau, E. I. Sirotkina, V. V. Deryabin *Dokl. Akad. Nauk SSSR.* **1967**, 177, 1110-1112.

50. E. I. Sirotkina, A. N. Nesmeyanov, N. A. Vol'kenau *Izves Akad. Nauk SSSR.* **1969**, (7), 1524-1529.

51. I. U. Khand, P. L. Pauson, W. F. Watts *J. Chem. Soc. C.* **1968**, 2257-2260.

52. I. U. Khand, P. L. Pauson, W. F. Watts *J. Chem. Soc. C.* **1968**, 2261-2265.

53. A. N. Nesmeyanov, N. A. Vol'kenau, I. N. Bolesova *Dokl. Akad. Nauk SSSR* **1967**, 175, 606-609.

54. D. A. Skoog, J. J. Leary, *Principles of Instrumental Analysis*, 4th ed.; Saunders College Publishers: Fort Worth, 1992.

55. J. M. Hornback, *Organic Chemistry*, Brooks/Cole Publishing Company: Pacific Grove, 1998.

56. R. M. Silverstien, G. C. Bassler, T. C. Morrill, *Spectrometric Identification of Organic Compounds*, 5th ed.; John Wiley & Sons, INC.: New York, 1991.

57. A. E. Derome, *Modern NMR Techniques for Chemistry Reseach*, Pergamon Press: Oxford, 1987; vol. 6.

58. C. J. Pedersen *J. Am. Chem. Soc.* **1967**, 89, 7017-7036.

59. C. J. Pedersen *Angew. Chem. Int. Ed. Engl.* **1988**, 27, 1021-1027.

60. B. Dietrich, P. Viout, J.-M. Lehn *Macrocyclic Chemistry, Aspects of Organic and Inorganic Supramolecular Chemistry*; VCH: Weinheim, 1993.

61. J.-M. Lenh *Supramolecular Chemistry, Concepts and Prespectives*; VCH: Weinheim, 1995.

62. D. J. Cram, T. Kaneda, G. M. Lein, R. C. Helgeson *J. C. S. Chem. Comm.* **1979**, 948-950.

63. D. J. Cram *Angew. Chem. Int. Ed. Engl.* **1988**, 27, 1009-1020.

64. J.-M. Lehn *Angew. Chem. Int. Ed. Engl.* **1988**, 27, 89-112.

65. D. E. Kime, J. K. Norymberski *J. Chem. Soc. Perkin Trans. I* **1977**, 1048-1052.

66. G. Montaudo, F. Bottino, E. Trivellone *J. Org. Chem.* **1972**, 37, 504-505.

67. P. A. Lehmann *Tehtrahedron* **1974**, 30, 727-733.

68. M. J. Mullins, E. P. Woo, D. J. Murray, M. T. Bishop *Chemtech* **1993**, 25-28.

69. H. M. Colquhoun, D. F. Lewis, R. A. Fairman, I. Baxter, D. J. Williams *J. Mater. Chem.* **1997**, 7, 1-3.

70. P. Hodge, H. M. Colquhoun, D. J. Williams *Chem. Indust.* **1998** (5) 162-167.

71. A. J. Hall, P. Hodge *React. and Funct. Polym.* **1999**, 41, 133-139.

72. H. W. Gibson, D. S. Nagvekar, D. Xie *J. Org. Chem.* **1997**, 62, 7503-7506.

73. L. Rossa, F. Vogtle, In *Topics in Current Chemistry*; F. L. Boschke, Ed.; Springer-Verlag: Berlin, vol. 113, 1983; Chapter 1.

74. D. Xie, Q. Ji, H. W. Gibson *Macromolecules* **1997**, 30, 4814-4827.

75. M. J. Mullins, E. P. Woo, C. C. Chen, D. J. Murray, M. T. Bishop, K. E. Balon *Polym. Prepr. Am. Chem. Soc. Div. Polym. Chem.* **1991**, 32 (2), 174-175.

76. M. J. Mullins, R. Galvan, M. T. Bishop, E. P. Woo, D. B. Gorman, T. A. Chamberlin *Polym. Prepr. Am. Chem. Soc. Div. Polym. Chem.* **1992**, 33 (1), 414-415.

77. J. A. Cella, J. J. Talley, J. M. Fukuyama *Polym. Prepr. Am. Chem. Soc. Div. Polym. Chem.* **1989**, 30 (2), 581-582.

78. J. M. Fukuyama U.S. Patent 110893, 1992.

79. D. J. Brunelle, T. L. Guggenheim, J. A. Cella, T. L. Evans, L. P. Fontana, G. R. Faler, J. M. Fukuyama, E. P. Boden, J. D. Rich, T. G. Shannon, S. J. McCormick, P. J. McDermott, A. M. Colley, J. W. Guiles U.S. Patent 4980453, 1990.

80. D. J. Brunelle, E. P. Boden, T. G. Shannon *J. Am. Chem. Soc.* **1990**, 112, 2399-2404.

81. D. J. Brunelle, T. G. Shannon *Macromolecules* **1991**, 24, 3035-3044.

82. D. J. Brunelle, M. F. Garbauskas, *Macromolecules* **1993**, 26, 2724-2729.

83. Y.-F. Wang, M. Paventi, A. S. Hay *Polym. Prepr. Am. Chem. Soc. Div. Polym. Chem.* **1995**, 36, 128-129.

84. K. P. Chan, Y.-F. Wang, A. S. Hay *Polym. Prepr. Am. Chem. Soc. Div. Polym. Chem.* **1995**, 36, 132-133.

85. K. P. Chan, Y.-F. Wang, A. S. Hay *Macromolecules* **1995**, 28, 653-655.

86. Y.-F. Wang, A. S. Hay, X. L. Hronowski, R. Cotter. *Macromolecules* **1995**, 28, 6705-6717.

87. Y.-F. Wang,K. P. Chan, A. S. Hay *Macromolecules* **1995**, 28, 6371-6374.

88. Y.-F. Wang, K. P. Chan, A. S. Hay *Macromolecules* **1996**, 29, 3717-3726.

89. Y. Ding, A. S. Hay *Macromolecules* **1996**, 29, 6386-6392.

90. Y. Ding, A. S. Hay *Macromolecules* **1996**, 29, 3090-3095.

91. K. Miyatake, Y. Yoshirio, K. Yamamoto, E. Tsuchida, A. S. Hay *Macromolecules* **1997**, 30, 4502-4503.

92. Y.-F. Wang, A. S. Hay *Macromolecules* **1997**, 30, 182-193.

93. Y. Ding, A. S. Hay *Macromolecules* **1997**, 30, 2527-2531.

94. E. Tsuchida, K. Miyatake, K. Yamamoto, A. S. Hay *Macromolecules* **1998**, 31, 6469-6475.

95. I. Baxter, H. M. Colquhoun, P. Hodge, F. H. Kohnke, D. J. Williams *Chem. Commun.* **1998**, 283-284.

96. I. Baxter, H. M. Colquhoun, P. Hodge, F. H. Kohnke, D. J. Williams *Chem. Commun.* **1998**, 1991-1992.

97. D. Xie, H. W. Gibson *Polym. Prepr. Am. Chem. Soc. Div. Polym. Sci.* **1994**, 35 (1), 401.

98. D. Xie, H. W. Gibson *Macromol. Chem. Phys.* **1996**, 197, 2133-2148.

99. H. M. Colquhoun, C. C. Dudman, M. Thomas, C. A. O'Mahoney, D. J. Williams *J. Chem. Soc. Chem. Commun.* **1990**, 336-339.

100. C. Baldoli, P. D. Buttero, S. Maiorana, P. Antonio *J. Chem. Soc., Chem. Commun.* **1985**, 1181-1182.

101. K. J. Odell, E. M. Hyde, B. L. Shaw, I. Shepherd *J. Organomet. Chem.* **1979**, 103-114.

102. R. Kramer *Angew. Chem. Int. Ed. Engl.* **1996**, 35, 1197-1199.

103. J. W. Janetka, D. H. Rich, *J. Am. Chem. Soc.* **1995**, 117, 10585-10586.

104. J. W. Janetka, D. H. Rich *J. Am. Chem. Soc.* **1997**, 119, 6488-6495.

105. P. Comba, A. Faith, A. Kuhner, B. Nuber *J. Chem. Soc., Dalton Trans.* **1997**, 1889-1898.

106. A. S. Abd-El-Aziz, C. R. de Denus, M. J. Zaworotko,C. V. K. Sharma *Chem. Commun.* **1998**, 265-266.

107. C. E. Anson, C. S. Creaser, G. R. Stephenson *J. Chem. Soc., Chem. Commun.* **1994**, 2175-2176.

108. C. Chen, H. Zhou, Y. Chen, Z. Jiang, Z. Wu, W. Zhang *Polym. Prepr. Am. Chem. Soc. Div. Polym. Chem.* **1999**, 40 (1), 143-144.

109. C. R. deDenus, Ph. D. Thesis, University of Manitoba, Manitoba, 1997.

110. E. E. Boros, C. W. Andrews, A. O. Davis *J. Org. Chem.* **1996**, 61, 2553-2555.

111. M. F. Teasley, B. S. Hsiao *Macromolecules* **1996**, 29, 6432-6441.

112. H. M. Colquhoun, D. J. Williams *Macromolecules* **1996**, 29, 3311-3314.

113. H. M. Colquhoun, L. G. Sestiaa, M. G. Zolotukhin, D. J. Williams *Macromolecules* **2000**, 33, 8907-8909.

114. H. Jiang, T. Chen, S. Bo, J. Xu *Polymer* **1998**, 24, 6079-6083.

115. P. L. Anelli, P. R. Ashton, R. Ballardini, V. Balzani, M. Delgado, M. T. Gandolfi, T. T. Goodnow, A. E. Kaifer, D. Philp, M. Pietraszkiewicz, L. Prodi, M. V. Reddington, A. M. Z. Slaswin, N. Spencer, J. F. Stoddart, C. Vicent, D. J. Williams *J. Am. Chem. Soc.* **1992**, 114, 193-218.

116. J. S. Murdzek, R. R. Schrock *Organometallics* **1987**, 6, 1373-1374.

117. G. C. Bazan, E. Khosravi, R. R. Schrock, W. J. Feast, V. C. Gibson, M. B. O'Regan, J. K. Thomas, W. M. Davis *J. Am. Chem. Soc.* **1990**, 112, 8378-8387.

118. G. C. Bazan, R. R. Schrock, H.-N. Cho, V. C. Gibson *Macromolecules* **1991**, 24, 4495-4502.

119. G. C. Bazan, J. H. Oskam, H.-N. Cho, L. Y. Park, R. R. Schrock *J. Am. Chem. Soc.* **1991**, 113, 6899-6907.

120. Z. Komiya, R. R. Schrock *Macromolecules* **1993**, 26, 1393-1401.

121. J.-K. Lee, R. R. Schrock, D. R. Baigent, R. H. Friend *Macromolecules* **1995**, 28, 1966-1971.

122. T. J. Boyd, R. R. Schrock *Macromolecules* **1999**, 32, 6608-6618.

123. B. M. Novak, R. H. Grubbs *J. Am. Chem. Soc.* **1988**, 110, 7542-7543.

124. B. M. Novak, R. H. Grubbs *J. Am. Chem. Soc.* **1988**, 110, 960-961.

125. S. T. Nguyen, L. K. Johnson, R. H. Grubbs *J. Am. Chem. Soc.* **1992**, 114, 3974-3975.

126. G. C. Fu, S. T. Nguyen, R. H. Grubbs *J. Am. Chem. Soc.* **1993**, 115, 9856-9857.

127. P. Schwab, M. B. France, J. W. Ziller, R. H. Grubbs *Angew. Chem. Int. Ed. Engl.* **1995**, 34, 2039-2041.

128. R. H. Grubbs, S. Chang *Tetrahedron* **1998**, 54, 4413-4450.

129. T. J. Boyd, Y. Geerts, J.-K. Lee, D. E. Fogg, G. G. Lavoie, R. R. Schrock, M. F. Rubner *Macromolecules* **1997**, 30, 3553-3559.

130. M. A. Tlenkopatchev, S. Fomine, L. Fomina, R. Gavino, T. Ogawa *Polym. J.* **1997**, 29, 622-625.

131. A. Laschewsky, W. Schulz-Hanke *Makromol. Chem. Rapid Commun.* **1993**, 14, 683-691.

132. C. Fraser, R. H. Grubbs *Macromolecules* **1995**, 28, 7248-7255.

133. H. D. Maynard, S. Y. Okada, R. H. Grubbs *Macromolecules* **2000**, 33, 6239-6248.

134. H. D. Maynard, S. Y. Okada, R. H. Grubbs *J. Am. Chem. Soc.* **2001**, 123, 1275-1279.

135. M. Weck, B. Mohr, B. R. Maughon, R. H. Grubbs *Macromolecules* **1997**, 30, 6430-6437.

136. M. Ungerank, B. Winkler, E. Eder, F. Stelzer *Macromol. Chem. Phys.* **1995**, 196, 3623-3641.

137. B. Winkler, M. Ungerank, F. Stelzer *Macromol. Chem. Phys.* **1996**, 197, 2343-2357.

138. F. Stelzer *Pure Appl. Chem.* **1996**, A33, 941-952.

138. M. Ungerank, B. Winkler, E. Eder, F. Stelzer *Macromol. Chem. Phys.* **1997**, 198, 1391-1410.

140. C. Pugh *Macromol. Symp.* **1994**, 77, 325-337.

141. C. Pugh, J. Dharin, S. V. Arehart *Macromolecules* **1997**, 30, 4520-4532.

142. C. Pugh, J. Shao, J. J. Ge, S. Z. D. Cheng *Macromolecules* **1998**, 31, 1779-1790.

143. C. Pugh, J.-Y. Bae, J. Dharia, J. J. Ge, S. Z. D. Cheng *Macromolecules* **1998**, 31, 5188-5200.

144. G.-H. Kim, C. Pugh, S. Z. D. Cheng *Macromolecules* **2000**, 33, 8983-8991.

145. D. Albagli, G. C. Bazan, M. S. Wrighton, R. R. Schrock *J. Am. Chem. Soc.* **1992**, 114, 4150.

146. D. Albagli, G. C. Bazan, R. R. Schrock, M. S. Wrighton, *J. Am. Chem. Soc.* **1993**, 115, 7328.

147. H. R. Allcock, W. R. Laredo, C. R. deDenus, J. P. Taylor *Macromolecules* **1999**, 32, 7719-7725.

148. H. R. Allcock, W. R. Laredo, E. C. Kellam, R. V. Morford *Macromolecules* **2001**, 34, 787-794.

149. C. U. Pittman, M. D. Rausch *Pure Appl. Chem.* **1986**, 58, 617.

150. P. Nguyen, P. Gomez-Elipe, I. Manners *Chem. Rev.* **1999**, 99, 1515.

151. S. Wizel, S. Margel, A. Gedanken, T. C. Rojas, A. Fernandz, R. J. Prozorov *J. Mater. Res.* **1999**, 14, 3913.

152. A. B. Moustafa, A. Faizalla, B. M. Adb El Hady *J. Appl. Polym. Sci.* **1998**, 67, 637.

153. A. S. Abd-El-Aziz, C. R. de Denus, K. M. Epp, S. Smith, R. J. Jaeger, D. T. Pierce *Can. J. Chem.* **1996**, 74, 650.

154. J.-L. Fillaut, D. Astruc *New. J. Chem.* **1996**, 20, 945.

155. R. Madan, R. C. Anand, I. K. Varma *J. Polym. Sci. Part A: Polym. Sci.* **1997**, 35, 2917-2924.

156. R. R. Fraser *Can. J. Chem.* **1962**, 40, 78-84.

157. J. I. Musher *Mol. Phys.* **1963**, 6, 93-100.

158. K. L. Williamson *J. Am. Chem. Soc.* **1963**, 85, 516-519.

159. P. Laszlo, P. von Rague Schleyer *J. Am. Chem. Soc.* **1963**, 85, 2709-2712.

160. P. Laszlo, P. von Rague Schleyer *J. Am. Chem. Soc.* **1964**, 86, 1171-1179.

161. E. W. C. Wong, C. C. Lee *Can. J. Chem.* **1964**, 42, 1245-1249.

162. E. I. Snyder, B. Franzus *J. Am. Chem. Soc.* **1964**, 86, 1166-1170.

163. J. Fisher, M. J. Gradwell *Magn. Reson. Chem.* **1991**, 29, 1068-1069.

164. W. J. Feast, L. A. Shahada *Eur. Polym. J.* **1991**, 27, 27-33.

165. W. Apichatachutapan, L. J. Mathias *J. Appl. Polym. Sci.* **1998**, 67, 183-190.

166. F. Cataldo *Polym. Int.* **1994**, 34, 49-57.

Appendices A and B

Appendix A: X-ray crystallography data for macrocycle **6a**.

Crystal data and structure refinements.

Empirical formula	C37 H24 O5	
Formula weight	548.56	
Temperature	223(2) K	
Wavelength	0.71073 Å	
Crystal system	Monoclinic	
Space group	C2/c	
Unit cell dimensions	a = 17.0378(18) Å	α= 90°.
	b = 20.176(2) Å	β= 120.543(2)°.
	c = 9.0714(10) Å	γ = 90°.
Volume	2685.6(5) Å^3	
Z	4	
Density (calculated)	1.357 Mg/m^3	
Absorption coefficient	0.090 mm^{-1}	
F(000)	1144	
Crystal size	.2 x .3 x .3 mm^3	
Theta range for data collection	1.72 to 26.50°.	
Index ranges	-19<=h<=21, -25<=k<=25, -11<=l<=5	
Reflections collected	7654	
Independent reflections	2771 [R(int) = 0.0254]	
Completeness to theta = 26.50	99.0 %	
Absorption correction	None	
Refinement method	Full-matrix least-squares on F^2	
Data / restraints / parameters	2771 / 0 / 192	
Goodness-of-fit on F^2	1.068	
Final R indices [I>2sigma(I)]	R1 = 0.0383, wR2 = 0.0988	
R indices (all data)	R1 = 0.0463, wR2 = 0.1034	
Extinction coefficient	0.0029(5)	
Largest diff. peak and hole	0.272 and -0.205 e.Å^{-3}	

Atomic coordinates ($x10^4$) and equivalent isotropic displacement parameters (A^2x10^{-3}).

	x	y	z	U(eq)
O(1)	0	4952(1)	-2500	52(1)
O(2)	2924(1)	3231(1)	3472(1)	44(1)
O(3)	2415(1)	871(1)	3580(1)	47(1)
C(1)	0	4345(1)	-2500	34(1)
C(11)	721(1)	3987(1)	-964(2)	30(1)
C(12)	1043(1)	3358(1)	-1009(2)	33(1)
C(13)	1761(1)	3076(1)	448(2)	35(1)
C(14)	2160(1)	3427(1)	1974(2)	33(1)
C(15)	1843(1)	4053(1)	2056(2)	35(1)
C(16)	1133(1)	4330(1)	596(2)	33(1)
C(21)	3210(1)	2578(1)	3851(2)	35(1)
C(22)	2617(1)	2048(1)	3399(2)	37(1)
C(23)	2983(1)	1420(1)	3975(2)	36(1)
C(24)	3909(1)	1322(1)	5012(2)	38(1)
C(25)	4483(1)	1863(1)	5441(2)	38(1)
C(26)	4144(1)	2491(1)	4862(2)	38(1)
C(31)	1733(1)	823(1)	1859(2)	39(1)
C(32)	1960(1)	691(1)	631(2)	46(1)
C(33)	1279(1)	645(1)	-1069(2)	44(1)
C(34)	362(1)	732(1)	-1580(2)	36(1)
C(35)	158(1)	839(1)	-292(2)	45(1)
C(36)	835(1)	883(1)	1416(2)	46(1)

Note: U(eq) is defined as one third of the trace of the orthogonalized Uij tensor.

Bond lengths (Å).

O(1)-C(1)	1.225(2)
O(2)-C(14)	1.3780(14)
O(2)-C(21)	1.3860(15)
O(3)-C(23)	1.3917(16)
O(3)-C(31)	1.3978(16)
C(1)-C(11)#1	1.4937(15)
C(1)-C(11)	1.4937(15)
C(11)-C(12)	1.3924(17)
C(11)-C(16)	1.4012(17)
C(12)-C(13)	1.3872(17)
C(13)-C(14)	1.3879(18)
C(14)-C(15)	1.3901(18)
C(15)-C(16)	1.3786(17)
C(21)-C(22)	1.3825(18)
C(21)-C(26)	1.3854(18)
C(22)-C(23)	1.3918(18)
C(23)-C(24)	1.3798(18)
C(24)-C(25)	1.384(2)
C(25)-C(26)	1.3820(18)
C(31)-C(36)	1.375(2)
C(31)-C(32)	1.378(2)
C(32)-C(33)	1.383(2)
C(33)-C(34)	1.3975(19)
C(34)-C(35)	1.394(2)
C(34)-C(34)#1	1.488(3)
C(35)-C(36)	1.387(2)

Note: Symmetry transformations used to generate equivalent atoms.

Bond angles (Deg).

C(14)-O(2)-C(21)	123.66(10)
C(23)-O(3)-C(31)	114.70(10)
O(1)-C(1)-C(11)#1	118.87(7)
O(1)-C(1)-C(11)	118.87(7)
C(11)#1-C(1)-C(11)	122.25(15)
C(12)-C(11)-C(16)	118.49(11)
C(12)-C(11)-C(1)	124.21(11)
C(16)-C(11)-C(1)	117.17(11)
C(13)-C(12)-C(11)	121.08(11)
C(12)-C(13)-C(14)	119.25(11)
O(2)-C(14)-C(13)	125.13(11)
O(2)-C(14)-C(15)	113.98(11)
C(13)-C(14)-C(15)	120.70(11)
C(16)-C(15)-C(14)	119.48(12)
C(15)-C(16)-C(11)	120.99(12)
C(22)-C(21)-C(26)	121.27(12)
C(22)-C(21)-O(2)	123.34(12)
C(26)-C(21)-O(2)	115.13(11)
C(21)-C(22)-C(23)	118.19(12)
C(24)-C(23)-O(3)	117.80(11)
C(24)-C(23)-C(22)	121.70(12)
O(3)-C(23)-C(22)	120.43(12)
C(23)-C(24)-C(25)	118.61(12)
C(26)-C(25)-C(24)	121.15(12)
C(25)-C(26)-C(21)	119.05(12)
C(36)-C(31)-C(32)	120.54(13)
C(36)-C(31)-O(3)	119.37(13)
C(32)-C(31)-O(3)	120.05(13)
C(31)-C(32)-C(33)	119.56(14)
C(32)-C(33)-C(34)	121.60(14)
C(35)-C(34)-C(33)	117.03(13)
C(35)-C(34)-C(34)#1	121.57(15)
C(33)-C(34)-C(34)#1	121.38(16)
C(36)-C(35)-C(34)	121.76(14)
C(31)-C(36)-C(35)	119.41(14)

Anisotropic displacement parameters (A^2x10^{-3}).

	U^{11}	U^{22}	U^{33}	U^{23}	U^{13}	U^{12}
O(1)	64(1)	26(1)	39(1)	0	7(1)	0
O(2)	43(1)	31(1)	38(1)	0(1)	6(1)	4(1)
O(3)	52(1)	38(1)	36(1)	7(1)	12(1)	-6(1)
C(1)	38(1)	28(1)	32(1)	0	16(1)	0
C(11)	32(1)	29(1)	30(1)	1(1)	16(1)	-2(1)
C(12)	39(1)	31(1)	30(1)	-2(1)	18(1)	0(1)
C(13)	40(1)	30(1)	37(1)	0(1)	21(1)	5(1)
C(14)	32(1)	32(1)	32(1)	4(1)	13(1)	0(1)
C(15)	40(1)	30(1)	30(1)	-3(1)	15(1)	-3(1)
C(16)	39(1)	25(1)	35(1)	0(1)	18(1)	1(1)
C(21)	40(1)	31(1)	28(1)	1(1)	14(1)	5(1)
C(22)	33(1)	37(1)	32(1)	4(1)	11(1)	4(1)
C(23)	44(1)	32(1)	28(1)	2(1)	15(1)	-1(1)
C(24)	45(1)	36(1)	27(1)	4(1)	15(1)	10(1)
C(25)	35(1)	46(1)	26(1)	1(1)	11(1)	7(1)
C(26)	37(1)	40(1)	29(1)	-2(1)	12(1)	-2(1)
C(31)	42(1)	29(1)	36(1)	3(1)	13(1)	-2(1)
C(32)	36(1)	51(1)	46(1)	1(1)	17(1)	-1(1)
C(33)	39(1)	50(1)	43(1)	-4(1)	21(1)	-2(1)
C(34)	37(1)	27(1)	40(1)	0(1)	17(1)	-1(1)
C(35)	39(1)	49(1)	46(1)	0(1)	21(1)	4(1)
C(36)	50(1)	51(1)	41(1)	-1(1)	24(1)	3(1)

Note: The anisotropic displacement factor exponent takes the form: $-2\pi^2 [h^2 a^{*2} U11 + ... + 2 h k a^{*2} b^* U12]$

Hydrogen coordinates ($x10^{-4}$) and isotropic displacement parameters ($A^2 \times 10^{-3}$).

	x	y	z	U(eq)
H(12A)	770	3120	-2044	39
H(13A)	1975	2651	401	42
H(15A)	2109	4285	3099	42
H(16A)	922	4755	648	40
H(22A)	1984	2110	2722	44
H(24A)	4144	896	5419	45
H(25A)	5116	1802	6139	45
H(26A)	4540	2855	5150	45
H(32A)	2573	633	946	55
H(33A)	1437	553	-1901	53
H(35A)	-455	883	-590	54
H(36A)	682	954	2263	55

Appendix B: X-ray crystallography data for macrocycle **6b**.

Crystal data and structure refinements.

Empirical formula	C36 H24 O6 S
Formula weight	584.61
Temperature	293(2) K
Wavelength	0.71073 A
Crystal system, space group	Monoclinic, P2(1)/c
Unit cell dimensions	a = 10.1746(5) A alpha = 90 deg. b = 29.2615(15) A beta = 110.0030(10) deg. c = 10.1746(5) A gamma = 90 deg.
Volume	2844.5(2) A^3
Z, Calculated density	4, 1.365 Mg/m^3
Absorption coefficient	0.163 mm^-1
F(000)	1216
Crystal size	0.35 x 0.20 x 0.15 mm
Theta range for data collection	6.82 to 26.37 deg.
Limiting indices	-12<=h<=11, -36<=k<=28, -12<=l<=12
Reflections collected / unique	15649 / 5654 [R(int) = 0.0531]
Completeness to theta = 26.37	97.0 %
Refinement method	Full-matrix least-squares on F^2
Data / restraints / parameters	5654 / 0 / 388
Goodness-of-fit on F^2	1.036
Final R indices [I>2sigma(I)]	R1 = 0.0486, wR2 = 0.1047
R indices (all data)	R1 = 0.0796, wR2 = 0.1167
Largest diff. peak and hole	0.391 and -0.439 e.A^-3

Atomic coordinates ($x10^4$) and equivalent isotropic displacement parameters (A^2x10^{-3}).

	x	y	z	U(eq)
S(1)	5053(1)	1037(1)	982(1)	34(1)
O(1)	4906(1)	915(1)	2292(1)	42(1)
O(2)	6412(1)	1055(1)	850(2)	42(1)
O(3)	3061(2)	2935(1)	-176(2)	49(1)
O(4)	-1684(1)	3078(1)	-254(2)	49(1)
O(5)	-3094(1)	-55(1)	-4054(1)	40(1)
O(6)	1798(1)	-295(1)	-3221(1)	37(1)
C(1)	4313(2)	1586(1)	544(2)	32(1)
C(2)	3432(2)	1762(1)	1201(2)	39(1)
C(3)	2963(2)	2207(1)	969(2)	41(1)
C(4)	3389(2)	2479(1)	67(2)	36(1)
C(5)	4255(2)	2304(1)	-603(2)	38(1)
C(6)	4715(2)	1860(1)	-370(2)	37(1)
C(7)	2062(2)	3135(1)	318(2)	39(1)
C(8)	693(2)	2981(1)	-196(2)	39(1)
C(9)	-284(2)	3202(1)	231(2)	39(1)
C(10)	82(2)	3569(1)	1136(2)	47(1)
C(11)	1456(2)	3716(1)	1613(2)	53(1)
C(12)	2462(2)	3496(1)	1217(2)	47(1)
C(13)	-1975(2)	2632(1)	-750(2)	40(1)
C(14)	-1468(2)	2265(1)	119(2)	49(1)
C(15)	-1736(2)	1828(1)	-399(2)	45(1)
C(16)	-2515(2)	1739(1)	-1798(2)	33(1)
C(17)	-3065(2)	2120(1)	-2632(2)	44(1)
C(18)	-2805(2)	2562(1)	-2114(2)	45(1)
C(19)	-2725(2)	1267(1)	-2367(2)	32(1)
C(20)	-3612(2)	1166(1)	-3717(2)	42(1)
C(21)	-3723(2)	729(1)	-4271(2)	42(1)
C(22)	-2946(2)	382(1)	-3468(2)	33(1)
C(23)	-2095(2)	467(1)	-2113(2)	42(1)
C(24)	-1984(2)	903(1)	-1579(2)	42(1)
C(25)	-1910(2)	-332(1)	-3635(2)	32(1)
C(26)	-636(2)	-165(1)	-3638(2)	33(1)
C(27)	504(2)	-455(1)	-3206(2)	32(1)
C(28)	400(2)	-899(1)	-2813(2)	37(1)
C(29)	-893(2)	-1056(1)	-2855(2)	41(1)
C(30)	-2055(2)	-774(1)	-3254(2)	35(1)
C(31)	2493(2)	20(1)	-2228(2)	31(1)
C(32)	2090(2)	138(1)	-1101(2)	40(1)
C(33)	2865(2)	454(1)	-136(2)	38(1)
C(34)	4043(2)	650(1)	-295(2)	31(1)
C(35)	4444(2)	527(1)	-1423(2)	34(1)
C(36)	3674(2)	213(1)	-2386(2)	36(1)

Note: U(eq) is defined as one third of the trace of the orthogonalized Uij tensor.

Bond lengths (Å).

S(1)-O(2)	1.4346(13)
S(1)-O(1)	1.4366(14)
S(1)-C(34)	1.7621(19)
S(1)-C(1)	1.7649(19)
O(3)-C(4)	1.375(2)
O(3)-C(7)	1.407(2)
O(4)-C(9)	1.387(2)
O(4)-C(13)	1.393(2)
O(5)-C(25)	1.392(2)
O(5)-C(22)	1.395(2)
O(6)-C(31)	1.373(2)
O(6)-C(27)	1.402(2)
C(1)-C(2)	1.387(3)
C(1)-C(6)	1.391(3)
C(2)-C(3)	1.379(3)
C(3)-C(4)	1.391(3)
C(4)-C(5)	1.383(3)
C(5)-C(6)	1.375(3)
C(7)-C(12)	1.363(3)
C(7)-C(8)	1.385(3)
C(8)-C(9)	1.375(3)
C(9)-C(10)	1.381(3)
C(10)-C(11)	1.382(3)
C(11)-C(12)	1.381(3)
C(13)-C(18)	1.371(3)
C(13)-C(14)	1.375(3)
C(14)-C(15)	1.372(3)
C(15)-C(16)	1.397(3)
C(16)-C(17)	1.396(3)
C(16)-C(19)	1.483(3)
C(17)-C(18)	1.387(3)
C(19)-C(24)	1.390(3)
C(19)-C(20)	1.393(3)
C(20)-C(21)	1.384(3)
C(21)-C(22)	1.373(3)
C(22)-C(23)	1.377(3)
C(23)-C(24)	1.377(3)
C(25)-C(30)	1.372(3)
C(25)-C(26)	1.386(3)
C(26)-C(27)	1.382(3)
C(27)-C(28)	1.374(3)
C(28)-C(29)	1.380(3)
C(29)-C(30)	1.385(3)
C(31)-C(36)	1.386(3)
C(31)-C(32)	1.386(3)
C(32)-C(33)	1.382(3)
C(33)-C(34)	1.388(3)
C(34)-C(35)	1.391(3)
C(35)-C(36)	1.375(3)

Note: Symmetry transformations used to generate equivalent atoms.

Bond angles (Deg).

O(2)-S(1)-O(1)	120.42(9)
O(2)-S(1)-C(34)	107.04(9)
O(1)-S(1)-C(34)	107.78(9)
O(2)-S(1)-C(1)	106.48(8)
O(1)-S(1)-C(1)	106.74(9)
C(34)-S(1)-C(1)	107.83(9)
C(4)-O(3)-C(7)	120.01(15)
C(9)-O(4)-C(13)	115.98(15)
C(25)-O(5)-C(22)	116.45(14)
C(31)-O(6)-C(27)	117.66(14)
C(2)-C(1)-C(6)	119.62(18)
C(2)-C(1)-S(1)	120.48(15)
C(6)-C(1)-S(1)	119.64(15)
C(3)-C(2)-C(1)	120.80(18)
C(2)-C(3)-C(4)	118.93(19)
O(3)-C(4)-C(5)	115.20(17)
O(3)-C(4)-C(3)	124.09(18)
C(5)-C(4)-C(3)	120.64(18)
C(6)-C(5)-C(4)	120.08(18)
C(5)-C(6)-C(1)	119.93(18)
C(12)-C(7)-C(8)	122.4(2)
C(12)-C(7)-O(3)	118.39(18)
C(8)-C(7)-O(3)	119.04(18)
C(9)-C(8)-C(7)	117.99(19)
C(8)-C(9)-C(10)	121.18(19)
C(8)-C(9)-O(4)	122.05(18)
C(10)-C(9)-O(4)	116.74(18)
C(9)-C(10)-C(11)	119.0(2)
C(12)-C(11)-C(10)	120.9(2)
C(7)-C(12)-C(11)	118.4(2)
C(18)-C(13)-C(14)	120.02(19)
C(18)-C(13)-O(4)	119.19(19)
C(14)-C(13)-O(4)	120.77(19)
C(15)-C(14)-C(13)	119.9(2)
C(14)-C(15)-C(16)	122.3(2)
C(17)-C(16)-C(15)	116.13(18)
C(17)-C(16)-C(19)	122.03(17)
C(15)-C(16)-C(19)	121.83(18)
C(18)-C(17)-C(16)	121.87(19)
C(13)-C(18)-C(17)	119.68(19)
C(24)-C(19)-C(20)	116.52(18)
C(24)-C(19)-C(16)	120.65(17)
C(20)-C(19)-C(16)	122.77(17)
C(21)-C(20)-C(19)	122.18(18)
C(22)-C(21)-C(20)	119.38(18)
C(21)-C(22)-C(23)	119.99(18)
C(21)-C(22)-O(5)	117.83(16)
C(23)-C(22)-O(5)	122.14(17)
C(22)-C(23)-C(24)	120.05(18)
C(23)-C(24)-C(19)	121.83(18)
C(30)-C(25)-C(26)	121.49(18)
C(30)-C(25)-O(5)	118.03(17)
C(26)-C(25)-O(5)	120.46(17)
C(27)-C(26)-C(25)	117.91(18)
C(28)-C(27)-C(26)	122.18(18)
C(28)-C(27)-O(6)	118.99(17)
C(26)-C(27)-O(6)	118.78(17)
C(27)-C(28)-C(29)	118.27(18)
C(28)-C(29)-C(30)	121.27(19)
C(25)-C(30)-C(29)	118.84(19)
O(6)-C(31)-C(36)	115.86(17)
O(6)-C(31)-C(32)	123.54(17)
C(36)-C(31)-C(32)	120.58(18)
C(33)-C(32)-C(31)	119.72(18)
C(32)-C(33)-C(34)	119.91(18)
C(33)-C(34)-C(35)	119.88(17)
C(33)-C(34)-S(1)	119.24(15)
C(35)-C(34)-S(1)	120.83(14)
C(36)-C(35)-C(34)	120.30(17)
C(35)-C(36)-C(31)	119.60(18)

Anisotropic displacement parameters (A^2x10^{-3}).

	U11	U22	U33	U23	U13	U12
S(1)	26(1)	40(1)	34(1)	-1(1)	7(1)	1(1)
O(1)	41(1)	51(1)	31(1)	3(1)	8(1)	1(1)
O(2)	22(1)	51(1)	51(1)	-5(1)	10(1)	0(1)
O(3)	46(1)	39(1)	71(1)	7(1)	32(1)	3(1)
O(4)	36(1)	38(1)	75(1)	-11(1)	20(1)	-3(1)
O(5)	32(1)	40(1)	44(1)	-4(1)	7(1)	3(1)
O(6)	31(1)	43(1)	40(1)	-7(1)	15(1)	-5(1)
C(1)	27(1)	36(1)	34(1)	-3(1)	9(1)	-4(1)
C(2)	41(1)	40(1)	43(1)	4(1)	21(1)	0(1)
C(3)	43(1)	43(1)	46(1)	0(1)	25(1)	2(1)
C(4)	31(1)	35(1)	40(1)	1(1)	12(1)	-2(1)
C(5)	37(1)	45(1)	36(1)	7(1)	15(1)	-2(1)
C(6)	30(1)	50(1)	34(1)	-2(1)	14(1)	1(1)
C(7)	39(1)	36(1)	47(1)	5(1)	19(1)	3(1)
C(8)	42(1)	33(1)	42(1)	-3(1)	17(1)	-1(1)
C(9)	37(1)	33(1)	47(1)	-1(1)	15(1)	-3(1)
C(10)	50(1)	45(1)	52(1)	-11(1)	24(1)	-2(1)
C(11)	57(2)	48(1)	54(1)	-18(1)	18(1)	-11(1)
C(12)	38(1)	48(1)	51(1)	-4(1)	9(1)	-8(1)
C(13)	33(1)	36(1)	54(1)	-5(1)	19(1)	-3(1)
C(14)	49(1)	47(1)	43(1)	-4(1)	5(1)	-8(1)
C(15)	49(1)	39(1)	42(1)	5(1)	8(1)	-5(1)
C(16)	26(1)	38(1)	38(1)	0(1)	14(1)	-1(1)
C(17)	46(1)	44(1)	37(1)	0(1)	8(1)	7(1)
C(18)	48(1)	38(1)	50(1)	4(1)	16(1)	11(1)
C(19)	28(1)	37(1)	34(1)	2(1)	15(1)	1(1)
C(20)	36(1)	40(1)	44(1)	6(1)	3(1)	6(1)
C(21)	33(1)	45(1)	37(1)	-2(1)	-3(1)	0(1)
C(22)	30(1)	36(1)	35(1)	-2(1)	14(1)	1(1)
C(23)	53(1)	41(1)	30(1)	6(1)	10(1)	13(1)
C(24)	48(1)	45(1)	28(1)	-1(1)	9(1)	6(1)
C(25)	31(1)	38(1)	25(1)	-3(1)	7(1)	3(1)
C(26)	38(1)	32(1)	30(1)	-1(1)	11(1)	-1(1)
C(27)	31(1)	36(1)	29(1)	-6(1)	10(1)	-3(1)
C(28)	34(1)	37(1)	35(1)	-1(1)	6(1)	3(1)
C(29)	44(1)	32(1)	43(1)	2(1)	11(1)	-2(1)
C(30)	33(1)	38(1)	34(1)	-5(1)	10(1)	-5(1)
C(31)	29(1)	31(1)	32(1)	2(1)	8(1)	3(1)
C(32)	36(1)	50(1)	37(1)	-2(1)	16(1)	-10(1)
C(33)	38(1)	49(1)	33(1)	-4(1)	17(1)	-6(1)
C(34)	27(1)	33(1)	31(1)	2(1)	8(1)	2(1)
C(35)	28(1)	37(1)	42(1)	3(1)	16(1)	2(1)
C(36)	34(1)	40(1)	38(1)	-2(1)	19(1)	1(1)

Note: The anisotropic displacement factor exponent takes the form: $-2\pi^2 [h^2 a^{*2} U11 + ... + 2 h k a^{*2} b^* U12]$

Hydrogen coordinates ($x10^{-4}$) and isotropic displacement parameters ($A^2 \times 10^{-3}$).

	x	y	z	U(eq)
H(2)	3155	1578	1804	47
H(3)	2370	2324	1410	50
H(5)	4526	2488	-1212	46
H(6)	5295	1742	-823	45
H(8)	443	2735	-812	47
H(10)	-587	3716	1420	56
H(11)	1707	3966	2210	64
H(12)	3389	3591	1555	57
H(14)	-945	2312	1056	59
H(15)	-1388	1583	203	54
H(17)	-3623	2076	-3561	53
H(18)	-3191	2810	-2690	54
H(20)	-4148	1399	-4265	51
H(21)	-4318	672	-5179	50
H(23)	-1594	229	-1558	51
H(24)	-1397	956	-665	50
H(26)	-551	132	-3923	40
H(28)	1180	-1089	-2526	44
H(29)	-986	-1358	-2611	49
H(30)	-2918	-882	-3263	42
H(32)	1302	5	-996	48
H(33)	2596	535	620	46
H(35)	5237	657	-1526	41
H(36)	3943	131	-3140	43